Estimating the Dynamic Characteristics of Road Vehicles Using Vibration Response Data

Daniel Thomas Ainalis B.Eng. (Hons)

College of Engineering and Science, Victoria University

Submitted in fulfilment of the requirements for the degree of Doctor of Philosophy

November 2014

Supervisors:

Associate Professor Vincent Rouillard

Associate Professor Michael Sek

ABSTRACT

A developed and well-maintained road network is imperative for the distribution of freight in the modern world. During transportation, both passengers and products are subjected to dynamic motion due to the irregular nature of pavement surfaces. This dynamic interaction is difficult to accurately predict due to the random and nonstationary nature of pavements and the complicated (and often nonlinear) dynamic characteristics of vehicles. Accurately characterising the dynamic motion generated by vehicles during transport would provide significant benefits to numerous fields. One field of interest is in the development of protective packaging systems to prevent, or minimise, product damage occurring during the distribution phase. Often, the level of packaging used is far greater than required, resulting in excessive waste which is of significant environmental concern. Another is in evaluating the performance of heavy vehicles to prevent and minimise pavement damage. As a heavy vehicle passes over a pavement, dynamic forces are exerted onto the pavement and induce damage, resulting in rougher roads. The maximum allowable loads of heavy vehicles is constantly increasing, further emphasising the importance of designing suspension systems which are considered road-friendly. For both fields it is important to establish accurate estimates of the dynamic characteristics, namely the Frequency Response Function (FRF), of vehicles.

Numerous experimental methods are currently available to estimate the dynamic characteristics of road vehicles. While each of the various methods has their own advantages and disadvantages, no critical evaluation of their accuracy and repeatability has been undertaken. To evaluate the various methods and eliminate complexities associated with multi-wheel vehicles, a single-wheeled prototype vehicle was designed and commissioned. There are two configurations of the idealised vehicle, one with the factory-fitted shock absorber and the second with a custom-designed, nominally linear shock absorber. Both configurations were subjected to a variety of response-only (transient) and excitation-response methods to estimate the dynamic characteristics. There is inconsistency in the estimated dynamic characteristics of the vehicle between the various methods and the true FRF is not known. Furthermore, all these approaches require the vehicle is taken out of operation.

The main focus of this thesis is on the development of two experimental techniques to analyse the vertical vibration acceleration response of a vehicle during normal operation (in-service). The first experimental technique is based on two principal assumptions; the first is that the excitation function (pavement) takes the form of the ISO 8608 spectral model and the second assumption is that the vehicle's frequency response does not vary for a change in operating speed. The response of a vehicle travelling at two distinct constant operating speeds can be used to estimate not only the dynamic characteristics of the vehicle, but also the spectral properties of the pavement (using the ISO 8608 spectral model). The second technique is based on establishing the random decrement signature from the response data, from which the dynamic characteristics of the sprung mass (Hilbert Domain) or the vehicle's FRF (Frequency Domain) can be estimated. An experimental investigation was undertaken to determine the optimal parameters for establishing the random decrement signature for both approaches.

The first series of in-service experiments, undertaken using an idealised, Single-Wheeled Experimental Vehicle (SWEV) travelling at three different nominally constant operating speeds, were aimed at evaluating the first experimental technique. The results from this series of in-service experiments were inconclusive due to a lack of knowledge of the actual pavement profile that the SWEV travelled over during each run. To remedy this, the SWEV was instrumented as an inertial profilometer and a second series of in-service experiments were undertaken over two different routes at three nominally constant operating speeds.

The results revealed that the spectral approach analysis technique is not able to accurately estimate the spectral exponent of the pavement, and therefore the FRF of the vehicle. This is due to the technique's sensitivity to variations in both the measured excitation and response spectra. The two random decrement approaches were used to establish the vehicle dynamic characteristics, yielding reasonable estimates in comparison with the actual measured FRFs. An investigation was also undertaken into the length of vibration record required to estimate the dynamic characteristics of the vehicle. Finally, one random decrement approach (Hilbert Domain) was used to analyse the response of two transport vehicles (heavy and light truck) during operation. The method based on the random decrement technique is promising to estimate the dynamic characteristics of vehicles, however is limited to the sprung mass mode.

STUDENT DECLARATION

"I, Daniel Thomas Ainalis, declare that the PhD thesis entitled 'Estimating the Dynamic Characteristics of Road Vehicles Using Vibration Response Data' is no more than 100,000 words in length including quotes and exclusive of tables, figures, appendices, bibliography, references and footnotes. This thesis contains no material that has been submitted previously, in whole or in part, for the award of any other academic degree or diploma. Except where otherwise indicated, this thesis is my own work."

Signature: **Date:** 19/11/2014

ACKNOWLEDGEMENTS

First and foremost, I would like to extend my deepest gratitude to my principal supervisor, Associate Professor Vincent Rouillard, for his knowledge, support, guidance and encouragement throughout the course of this thesis. I would also like to express my warm thanks to my associate supervisor, Associate Professor Michael Sek, for his support, guidance and assistance.

A special thank you goes to Mr Michael Long for his enormous assistance throughout the course of my PhD. Michael was responsible for the initial design of the idealised vehicle and spent many late nights accompanying me during the in-service experiments.

I would also like to thank the technical staff from Victoria University, in particular Mr Laszlo Kovacs for developing the power-unit used during the in-service experiments.

My gratitude also extends to the International Association of Packaging Research Institutes for awarding me a scholarship to spend six months at another member institution continuing my research.

I am very thankful to Mr Javier Zabaleta and all of his staff at the ITENE Packaging, Transport and Logistics Research Institute for allowing me to spend six months as a visiting research fellow (as part of my scholarship) there and making me feel at home in a place so far away.

In particular I would like to thank Dr Manuel Garcia-Romeu-Martinez for all of his assistance and support in the organisation of the in-service experiments undertaken during my stay.

I would also like to thank Dr Matthew Lamb for his support and advice throughout my studies.

Thanks to Mr Richard Wix from the ARRB for kindly providing pavement elevation profiles.

Finally, I would like to thank my parents for their love and support; words cannot describe how grateful I am to you both.

LIST OF PUBLICATIONS AND AWARDS

PUBLICATIONS

Ainalis, D., Rouillard, V. & Sek, M. 2012, *Evaluation of Experimental Techniques for Establishing Vehicle Suspension Characteristics*, Proceedings of the 7th Australian Congress on Applied Mechanics, Adelaide, Australia, 9-12th Dec.

Ainalis, D., Rouillard, V. & Sek, M. 2013, *Estimating the Dynamic Characteristics of Vehicles Using Only In-Service Response Data*, Proceedings of the 26th IAPRI Symposium on Packaging, Espoo, Finland, 10-13th Jun.

Ainalis, D., Rouillard V. & Sek, M. 2014, *Issues with Combining Road Elevation Spectral Models and Vehicle Vibration Response to Estimate Vehicle Dynamic Characteristics*, Journal of Packaging Technology and Science, DOI: 10.1002/pts.2101.

Ainalis, D., Rouillard V. & Sek, M. 2014, *Issues with the Experimental Characterisation of Automotive Shock Absorbers for Vehicle Dynamic Simulations*, Proceedings of the 8th Australian Congress on Applied Mechanics, Melbourne, Australia, 23rd-26th Nov.

AWARDS

IAPRI Research Scholarship for Student Exchange (IAPRI Research Scholar), 2012 – 2013.

TABLE OF CONTENTS

LIST OF FIGURES

NOMENCLATURE

ABBREVIATIONS

2DoF	2 Degree-of-Freedom
AASHO	American Association of State Highway Officials
AC	Asphalt Concrete
APC	Australian Packaging Covenant
ASTM	American Society for Testing and Materials
CEU	Council of the European Union
DFT	Discrete Fourier Transform
DLC	Dynamic Load Coefficient
DoTaRS	Department of Transport and Regional Services
DIVINE	Dynamic Interaction between Vehicles and Infrastructure Experiment
ESALs	Equivalent Standard Axle Loads
EU	European Union
EURF	European Union Road Federation
FT	Fourier Transform
FFT	Fast Fourier Transform
FRA	Frequency Response Analyser
FRF	Frequency Response Function
IMECH	Institution of Mechanical Engineers
IRTU	International Road Transport Union
ISO	International Organisation for Standardisation
ISTA	International Safe Transit Association
MISO	Multiple-Input-Single-Output
MSE	Mean Squared Error
NPCC	National Packaging Covenant Council
OECD	Organisation for Economic Co-operation and Development
PCA	Packaging Council of Australia

PCC	Portland Concrete Cement
PDF	Probability Density Function
PP	Peak Picking
PSD	Power Spectral Density
RD	Random Decrement
rms	root-mean-square
SDoF	Single Degree-of-Freedom
S/N	Signal to Noise ratio
SWEV	Single-Wheeled Experimental Vehicle
SWEV-A	SWEV with factory-fitted shock absorber
SWEV-B	SWEV with nominally-linear shock absorber
VSB11	Vehicle Standards Bulletin 11
UK	United Kingdom
USA	United States of America
U.S. DoT	United States Department of Transport
WPO	World Packaging Organisation

ROMAN SYMBOLS

$*$	Convolution
$\boldsymbol{a_c}$	Arbitrary parameter
$\boldsymbol{a(t)}$	Complex analytical signal
$\boldsymbol{A(t)}$	Envelope of the analytical signal $a(t)$
$\boldsymbol{A_1}$	Amplitude of the first peak of the free decay
$\boldsymbol{A_2}$	Amplitude of the second peak of the free decay
$\boldsymbol{c_c}$	Critical damping coefficient
$\boldsymbol{c_s}$	Suspension damping coefficient
$\boldsymbol{c_t}$	Tyre damping coefficient
$\boldsymbol{C}$	Amplitude of roughness constant
$\boldsymbol{C_1}$	Amplitude of roughness constant in specified frequency band

C_2	Amplitude of roughness constant in specified frequency band
C_3	Amplitude of roughness constant in specified frequency band
D_{xx}	Auto random decrement
e	Euler's number
$E(f)$	Excitation spectrum
f	Frequency
f_1	Half-power point lower frequency
f_2	Half-power point upper frequency
f_d	Damped natural frequency
f_n	Natural frequency
f_{res}	Resonant frequency
f_{sd}	Sprung mass mode damped natural frequency
f_{sn}	Sprung mass mode natural frequency
$G(n)$	Generalised PSD function
$G(n_0)$	Roughness constant
$\mathrm{G_d}$	Pavement elevation PSD function (spatial frequency)
$\mathrm{G_x}$	Pavement elevation PSD function (temporal frequency)
$\mathrm{G_{\ddot{x}}}$	Pavement elevation acceleration PSD function (temporal frequency)
$G_{Ex}(f)$	Excitation PSD function
$G_{Re}(f)$	Response PSD function
$h(\tau)$	Impulse response function
$H(f)$	Frequency Response Function
$H_1(f)$	Frequency Response Function variant
$H_2(f)$	Frequency Response Function variant
i	Random decrement trigger index
j	$\sqrt{-1}$
k	Integer
k_c	Constant
k_s	Suspension stiffness of a quarter car

k_t	Tyre stiffness of a quarter car
$ln[\,]$	Natural logarithm of [ ]
m	Number of successive oscillations between selected peaks
m_p	Arbitrarily chosen integer
m_s	Sprung mass of a quarter car
m_u	Unsprung mass of a quarter car
n	Spatial frequency
n_1	Spatial frequency discontinuity frequency
n_a	Spatial frequency lower cut-off value
n_b	Spatial frequency upper cut-off value
n_0	Discontinuity spatial frequency
N	Number of points
N_D	Number of independent averages
N_{RD}	Random decrement signature averages
p	Constant
P	Vehicle static load
P_0	Reference static load
q	Constant
r	Frequency ratio, $r = f/f_n$
r^2	Coefficient of determination
$\mathrm{R}_{\ddot{\mathrm{x}}}(f)_v$	Acceleration Response PSD function at speed v
$\mathrm{R}_{\ddot{\mathrm{x}}_1}$	Acceleration Response PSD function at speed v_1
$\mathrm{R}_{\ddot{\mathrm{x}}_2}$	Acceleration Response PSD function at speed v_2
S_f	Sampling frequency
S_V	Vehicle operating speed
t	Time
t_i	Random decrement trigger start time
$T(f)$	Transmissibility Frequency Response Function
$T(f)_{v_1}$	Transmissibility of a quarter car travelling at a speed v_1

$\boldsymbol{T(f)_{v_2}}$	Transmissibility FRF of a quarter car travelling at a speed v_2
$\boldsymbol{T_r}$	Temporal resolution
$\boldsymbol{T_{sr}}$	Sub-record length
$\boldsymbol{u}$	Base displacement excitation
$\boldsymbol{\dot{u}}$	Base velocity excitation
$\boldsymbol{v}$	Vehicle operating speed
$\boldsymbol{v_1}$	Vehicle operating speed
$\boldsymbol{v_2}$	Vehicle operating speed
$\boldsymbol{w}$	Spectral exponent
$\boldsymbol{w_1}$	Spectral exponent of the first band
$\boldsymbol{w_2}$	Spectral exponent of the second band
$\boldsymbol{w_3}$	Spectral exponent of the third band
$\boldsymbol{X}$	Amplitude
$\boldsymbol{x}$	General signal
$\boldsymbol{x(t)}$	General analytical signal
$\boldsymbol{\tilde{x}(t)}$	Hilbert Transform of a signal
$\boldsymbol{\ddot{x}}$	Acceleration signal
$\boldsymbol{x_1}$	Amplitude of the first peak of the free decay
$\boldsymbol{x_c}$	Arbitrary parameter
$\boldsymbol{x_{m+1}}$	Amplitude of the next peak of the free decay
$\boldsymbol{X(f)}$	Fourier transform of $x(t)$
$\boldsymbol{y(t)}$	Response of a system
$\boldsymbol{Y(f)}$	Response spectrum
$\boldsymbol{z_s}$	Sprung mass vertical displacement of a quarter car
$\boldsymbol{\dot{z}_s}$	Sprung mass vertical velocity of a quarter car
$\boldsymbol{\ddot{z}_s}$	Sprung mass vertical acceleration of a quarter car
$\boldsymbol{z_u}$	Unsprung mass vertical displacement of a quarter car
$\boldsymbol{\dot{z}_u}$	Unprung mass vertical velocity of a quarter car
$\boldsymbol{\ddot{z}_u}$	Unsprung mass vertical acceleration of a quarter car

GREEK SYMBOLS

α	Dimensionless constant
β	Integer
γ^2	Coherence
δ	Logarithmic decrement
Δf	Frequency resolution
Δt	Time increment
ε_r	Spectral uncertainty
ζ	Damping ratio
ζ_s	Sprung mass mode damping ratio (quarter car)
$H[\,]$	Hilbert Transform of [ ]
μ	Mean
π	Constant ratio of a circle’s circumference to its diameter
σ	Standard deviation
τ	Sample time between two measured points
τ_w	Duration of random decrement signature window
$\phi(t)$	Instantaneous phase
ω_0	Instantaneous natural frequency in radians per second
ω_d	Damped natural frequency in radians per second
ω_n	Natural frequency in radians per second

Chapter 1

INTRODUCTION

A developed and well-maintained road network is imperative for the distribution of freight in the modern world. During transportation, both passengers and products are subjected to dynamic motion due to the irregular nature of pavement surfaces. This dynamic interaction is difficult to accurately predict due to the random and nonstationary nature of pavements and the complicated (and often nonlinear) dynamic characteristics of vehicles. Accurately characterising the dynamic motion generated by vehicles during transport would provide significant benefits to numerous fields.

One field of interest is in the development of protective packaging systems to prevent, or minimise, product damage occurring during the distribution phase. Often, the level of packaging used is far greater than required, resulting in excessive waste which is of significant environmental concern. Another is in evaluating the performance of heavy vehicles to prevent and minimise pavement damage. As a heavy vehicle passes over a pavement, dynamic forces are exerted onto the pavement and induce damage, resulting in rougher roads. The maximum allowable loads of heavy vehicles is constantly increasing, further emphasising the importance of designing suspension systems which are considered road-friendly. For both fields it is important to establish accurate estimates of the dynamic characteristics, namely the Frequency Response Function (FRF), of vehicles.

This thesis is focused on the development and validation of a practical technique to estimate the dynamic characteristics of road vehicles, namely the Frequency Response Function (FRF), using only in-service vibration response data. Currently, various methods are available to estimate the dynamic characteristics and are separated into two broad categories; response-only (transient) and excitation-response methods. There are numerous drawbacks associated with both types of approaches, such as cost and relevance. Furthermore, these approaches all require the vehicle to be removed from operation. The development of a practical method to estimate the dynamic characteristics using only response data measured during a vehicle's normal operation would offer significant benefits to numerous industries.

Chapter 2 describes the background and impetus of the research undertaken in this thesis, primarily focused on the optimisation of protective packaging for products during transportation. The significance of vehicle ride quality and the use of protective packaging systems to prevent product damage are explained. The optimisation of protective packaging systems by simulating transportation vibration in the laboratory is also discussed. A history of quantifying pavement deterioration due to the passage of heavy vehicles, focused on establishing the road-friendliness of heavy vehicles, is presented.

Chapter 3 presents a comprehensive literature review related to vehicle-road interaction. The Chapter is divided into three main sections. The first section discusses the fundamental quarter car model commonly used in vehicle dynamic simulations and its dynamic characteristics. The second section of the literature review is focused on the nature of longitudinal pavement profiles and the development of various spectral models used to approximate them. A brief investigation into the statistical nature of longitudinal pavement profiles is also discussed. The third section describes the various experimental approaches and analysis techniques used to estimate the dynamic characteristics of vehicles. The section is separated into the three different categories; response-only (transient), excitation-response and in-service response methods.

Chapter 4 presents the principal hypothesis of the research and is supported by a number of sub-hypotheses. Chapter 5 describes the methodology of the research to be undertaken in this thesis. First, the design and configuration of an idealised, single-wheeled vehicle to validate the various experimental approaches is described. The general methodology to critically evaluate the current methods used to estimate the dynamic characteristics of vehicles (to determine the true FRF of the vehicle) is outlined, focusing on both response-only (transient) and excitation-response methods. The methodology for the in-service experiments is also presented and discusses important considerations that must be made, such as the selection of suitable roads for testing.

Chapter 6 presents an experimental evaluation of the various approaches currently available to estimate the dynamic characteristics of vehicles and determine the true FRF, if it exists, of the idealised vehicle. Both response-only (transient) and excitation-response methods are evaluated and compared using the prototype vehicle.

Chapter 7 is focused on the development and methodology of two analytical techniques to estimate the dynamic characteristics of vehicles using only in-service response data. The first approach is based on the fact that the transmissibility FRF of a quarter car vehicle tends towards one at low frequencies. Combining an assumed spectral function to represent the road elevation profile with the vibration response data, the approach aims to estimate both the dynamic characteristics of the vehicle and the road spectral properties. The second analytical method uses the random decrement technique to obtain the random decrement signature from the response of the vehicle, from which the dynamic characteristics may be estimated. The random decrement technique can be used to estimate the sprung mass mode dynamic characteristics or the FRF directly from the signature. An experimental evaluation to ascertain the optimum parameters of the random decrement signature for the estimation of the dynamic characteristics for both approaches is also presented.

Chapter 8 presents the results from a series of in-service experiments using the idealised vehicle. The first series of experiments were undertaken using the idealised vehicle; however inconsistencies were found and ultimately required the actual profile travelled by the vehicle to be known. The second series of in-service experiments were undertaken with the idealised vehicle instrumented as an inertial profilometer. An investigation into the minimum length of road required to obtain a sufficient estimate of the dynamic characteristics was undertaken using a Monte Carlo simulation. The Chapter closes with the estimation of the dynamic characteristics of in-service response data measured from two transport vehicles during normal operation.

Chapter 9 concludes the thesis by outlining the main outcomes of the research and identifies future work that may be undertaken.

Chapter 2

BACKGROUND

When a vehicle travels on a road at speed, a complex dynamic interaction occurs between uneven road surfaces (pavements), the vehicle itself and anything that is being transported by the vehicle. The dynamic motion experienced by vehicles, and hence passengers or payloads (consisting of goods or equipment), during transportation is identified as shocks and vibration. This interaction, rendered more complex by the random and nonstationary nature of uneven pavement surfaces and the complicated (and often nonlinear) dynamic characteristics of vehicles, is difficult to accurately predict. The vertical vibratory motion vehicles experience during transit is the cause of the most significant shocks and vibration and is of particular interest (Gillespie 1985). Modern road vehicles experience a broad spectrum of vibration due to the high speeds they are capable of travelling at (Gillespie 1992b, p. 125).

A consequence of this complex interaction is the occurrence of product damage during transport. While the implementation of single-use protective packaging systems is aimed at preventing product damage, it poses a significant challenge for engineers to provide adequate product protection against a broad range of conditions using the minimum amount of packaging possible. Another principal consequence of this dynamic interaction is the generation of dynamic loads due to the vibration of heavy vehicles during operation. These dynamic loads generated are induced into pavements and cause damage. As a pavement deteriorates over time due to the passage of heavy vehicles, the level of roughness of the road is increased and in turn results in greater dynamic loads exerted onto the pavement.

A sophisticated and well-maintained road network capable of transporting freight and other products is essential for developed economies. The Australian road network, for example, consists of over 812,000 km of various pavement types including freeways, highways, arterials and local urban and rural roads (Austroads 2005). Of this figure, only 341,448 km of the roads in Australia are paved (U.S. DoT 2010). The principal mode of freight distribution in Australia is road transport, with an increase in the total domestic freight distributed by road from 28.7 billion tonne-kilometres in 1972-73 to 156.2 billion tonne-kilometres in 2002-03 (Austroads 2005). It is expected that the total freight to be transported in Australia will double over the next two decades from the 2002-03 estimates.

The United States of America (USA) possesses the world's largest freight transportation network, with the public road network alone spanning more than 6,465,000 km (U.S. DoT 2010). Of this extensive road network, 4,209,835 km of roads are paved (U.S. DoT 2010). In 2007, the dominant mode utilised to distribute freight in the USA was road transport with an annual total of 2,290.3 billion tonnes per kilometre (U.S. DoT 2008). While the United Kingdom (UK) has a significantly smaller road network of 398,366 km in comparison to the USA and Australia, the entire public road network is paved (U.S. DoT 2010). From 2009 to 2010, the UK saw an increase of 11 % in the amount freight distributed, totalling 139 billion tonne kilometres (Department for Transport 2011).

Extensive paved public road networks are also a common feature in many major European countries such as France (951,500 km), Germany (644,480 km), Italy (487,700 km) and Spain (681,224 km) (U.S. DoT 2010). The total road network of the twenty-seven member countries of the European Union (EU) contained over 5,000,000 km of roads of varying types in 2006 (EURF 2009). Between 1995 and 2007, the transport of freight via road has increased by 43.9 % in the EU (EURF 2009). Furthermore, the transport of freight distributed via road within the EU has increased steadily over the years to 1,927 billion tonne kilometres in 2007 (EURF 2009). China is experiencing rapid economic growth and development. The Chinese road industry, since the 1990s, has experienced one of the fastest periods of development in history (IRTU 2009). In 2008, the Chinese road network consisted of over 3,700,000 km of public roads, of which 60,300 km were expressways (IRTU 2009). An illustration of the rapid growth is the amount of freight distributed in 2007, totalling 1,135.5 billion tonnes per kilometre, which more than doubled in the following year with an estimated 3,286.8 billion tonnes per kilometre of freight distributed in 2008 (IRTU 2009).

Such significant increases in the amount of freight distributed via roads inevitably places significant strain on the road network and performance of transport vehicles by causing pavement damage and increasing the level of roughness of pavement surfaces. It is important that the design, construction and on-going maintenance of the road network ensures the pavement is able to reduce unnecessary excitation due to increased roughness (as best as is feasible). To cope with the increase in freight distribution, there is an initiative to reward heavy vehicles whose suspensions are deemed to minimise the dynamic loads induced onto pavements, also known as road-friendly vehicles, to operate with increased mass limits. The suspension systems of heavy vehicles are designed for many purposes, including but not limited to supporting the vehicle and load, maintaining equal load distribution, preventing the wheels from leaving the pavement where possible through sufficient axle articulation and also isolating the body of the vehicle from vibration (OECD 1992). The ability of a suspension system to isolate vibration is critical to reduce vehicle maintenance, ensure adequate ride quality for passenger and driver comfort and also to minimise noise, ground vibration and impact loads on pavements (OECD 1992).

Another significant consequence of a rough ride is the potential for product or equipment damage to occur during transport. To alleviate this, protective packaging is used to ensure that the shipment reaches its destination undamaged. There is a constant conflict between the environmental and commercial demands to minimise the amount of protective packaging used and the ability of the protective packaging system to adequately prevent damage from occurring to the product (PCA 2005). The trend to reduce the amount of protective packaging not only allows for the distribution of greater quantities of freight per single journey, but also minimises the environmental impacts associated with packaging waste, posing significant issues for product, vehicle and pavement damage if not dealt with appropriately. The effects of vibration on products during shipment can be manifested in many ways, such as loosening of closures, scuffing of containers, bruising of fruit, cracking of printed circuit boards, fractures in component leads, fuses unseating, fatigue failure, compression failure and powdering of tablets amongst other effects (Caldicott 1991). In underdeveloped countries, products are often transported via poorly maintained roads, leading to constant vibration that generates further bruising and damage (IMechE 2013).

Understanding the complex dynamic interaction between vehicles, pavements and payloads is important to a number of applications and industries, such as ride quality and protective packaging (for packaging optimisation), the minimisation of pavement damage caused by heavy vehicles and also the effect of repeated vibration on the vehicle's health (suspension properties). The significance of each of these issues will be discussed in the following sections.

2.1 VEHICLE RIDE QUALITY AND PROTECTIVE PACKAGING

Ride quality is concerned with the measurement and control of the level of shocks and vibration to which vehicle occupants, equipment and payloads are subjected to during transport. There are three contributing factors to assess ride quality: the vehicle's suspension system, the pavement surface (and other excitations such as driveline and engine vibration) and the subject's tolerance to these shocks and vibration (Gillespie 1992b, p. 126). Gillespie (1992b, p. 125) stated that the vibration experienced by a vehicle can be separated into two categories; 1) rigid-body ride vibration, which is between 0 – 25 Hz and 2) noise, in the frequency bandwidth of 25 – 20,000 Hz. Although Gillespie identifies a large bandwidth as only noise, this frequency band also contains structural vibration due to pavement irregularities and engine-borne vibration. A sustained rough ride is usually attributed to a rough surface or an inadequate suspension system and some studies have found there is evidence of a possible link between low frequency vibration and driver and passenger fatigue (Mabbot *et al.* 2001). The response acceleration of a vehicle, often expressed in the form of a Power Spectral Density (PSD) function, can be used to establish the vehicle's ride quality. The response PSD function is related to the excitation (pavement) PSD function via the transmissibility FRF of the vehicle under consideration. The transmissibility FRF acts as a weighting factor to the excitation (Gillespie & Sayers 1981).

For passenger vehicles, the ride quality is concerned with isolating the vibration introduced by irregular pavements through the use of an adequate suspension system designed for passenger comfort (Gillespie & Sayers 1981). The ride quality of heavy vehicles is important for not only passenger comfort, but also to prevent payload damage during transport. The suspension systems of heavy vehicles are subject to a compromise between asymmetric damping to achieve an optimum balance between ride quality and road-friendliness (Woodrooffe 1995). While the suspension systems of passenger vehicles are tuned for payload changes within a small range (often for an additional load of one to five passengers), the payloads transported by heavy vehicles may be up two or three times heavier than the vehicle's tare. This highlights the difficulty in tuning the suspension system of a heavy vehicle for a considerable range of loading configurations (payload masses).

2.1.1 Protective Packaging and the Environment

Protective packaging systems have existed for centuries in some form, however during the second half of the twentieth century their use swiftly increased, particularly in industrialised and developed countries (PCA 2005). As society began to move from small group self-sufficiency, it became necessary to handle, transport and store products, leading to damage as the products were unable to adequately withstand such conditions (Goodwin & Young 2010, p. 1). Packaging systems are now essential to all modern commerce to ensure the product is secure, safe and clean while preventing damage, spillage and spoilage from occurring (PCA 2005). There are three broad categories of packaging:

1) Primary packaging (consumer packaging) is the packaging used as one sales unit to the final user.
2) Secondary packaging (grouped packaging) is the packaging system used to group the primary packages together.
3) Tertiary packaging (transport packaging) is designed to prevent damage of a large quantity of individual or grouped packages during transportation and handling.

In 2004, the global packaging industry was estimated to have turned over approximately US$485 billion globally, with around US$460 billion due to packaging container sales and the remaining US$25 billion from machinery sales (WPO 2008). The total packaging consumption estimates in 2003 for North America, Europe and Japan was approximately US$308 billion, while the rest of the world consumed the remaining US$177 billion (WPO 2008). In 2003, the largest market for packaging was North America which consumed a combined total of US$132 billion, with the USA accounting for the vast majority with sales of US$113 billion (WPO 2008). If the rest of the world, particularly developing nations with large populations such as China and India, increased their consumption of packaging to rates similar to North America, Europe and Japan then the total consumption of world packaging would drastically increase.

In recent years, the environmental impacts of protective packaging have come under increased scrutiny (PCA 2005). While increased transport of freight rewards economies, there are environmental implications if sustainable approaches to all phases of packaging (from design and development to usage and disposal) are not undertaken. Around the world, there are an increasing number of governments placing mandates on the recycling rates of protective packaging systems (PCA 2005). In Australia, the expected target recycling rate of packaging will be 70 % by 2015, with the recycling rate in 2011 at 63 % (APC 2011). The environmental impact of the use of packaging materials has also been subject to enquiry, with some packaging materials (such as expanded polystyrene) prohibited by local governments (Reck 1990). In recent times, there has been an increased focus on using sustainable packaging materials to improve the recycling rate (NPCC 2010).

In light of these concerns the Council of the European Union (CEU) outlined, under directive 94/62/EC (amended by directive 2005/20/EC), the principal strategy for the management of packaging waste to "as a first priority, preventing the production of packaging waste and, as additional fundamental principles, at reusing packaging, at recycling and other forms of recovering packaging waste and, hence, at reducing the final disposal of such waste" (1994). There have also been further measures through legislation to reduce packaging waste disposal by placing responsibility on the manufacturers to reduce the amount of packaging used (Eichstädt *et al.* 1999).

The National Packaging Covenant Council (NPCC) introduced a series of five-year Australian Packaging Covenants (APC) in 1999, 2005 and 2010 as an agreement between supply chains and governments to minimise the environmental impacts associated with consumer packaging in Australia. The NPCC outlined three main objectives under the APC (2011):

1) To design more efficient (volume) and recyclable packaging.
2) To improve recovery and recycling of packaging from consumers.
3) To assume responsibility to reduce the occurrence and impact of waste due to packaging.

These objectives are to be met using a number of approaches including the design of packaging using sustainable packaging guidelines, improving the national recycling rate of packaging and increasing the allocation of materials reprocessed for packaging (APC 2011). Reducing the level of protective packaging below what is required would result in under-packaging of the product or equipment and is often identified as damage in the product. Conversely, it is far more difficult to identify if a product is over-packaged. A study undertaken in 1991 in the EU found that the hidden costs associated with over-packaging were estimated at a value of €130 billion per year (Ostergaard 1991). These hidden costs of over-packaging are due to factors such as increased traffic, pollution, disposal and antedated pavement deterioration. These statistics indicate the strong need to engineer protective packaging systems to minimise the consumption of materials while ensuring that the shocks and vibration experienced during transportation do not cause equipment and product damage, not to mention minimising the various environmental impacts associated with over-packaging.

2.1.2 Protective Packaging Optimisation

In broad terms, there are three possible approaches to develop the optimum protective packaging solution. The first approach is to improve the robustness of the actual product; the second is to optimise the design or level of the protective packaging, or the severity of the distribution hazards associated with the transportation of the product may be reduced (Goodwin & Young 2010, p. 143). Establishing the optimum level of protective packaging involves a compromise between the costs associated with environmental impacts, damaged products and production of the packaging system. One of the most widely accepted methods for the development of optimised package-product systems is the Six-Step Method (Root 1997), defined as follows:

1) Evaluate and quantify distribution hazards.
2) Determine product robustness (or its fragility).
3) Increase product robustness.
4) Characterise protective packaging material.
5) Design protective packaging system.
6) Test and validate the package-product system against synthesised distribution hazards.

Figure 2-1 demonstrates the importance of having the optimum package-product system to sufficiently prevent the expected hazards from causing damage. The method also encourages that product robustness be a factor in the optimisation process, not only the protective packaging system. This is highlighted in the fourth case presented, where an increase in the product's robustness results in a reduced amount of protective packaging required.

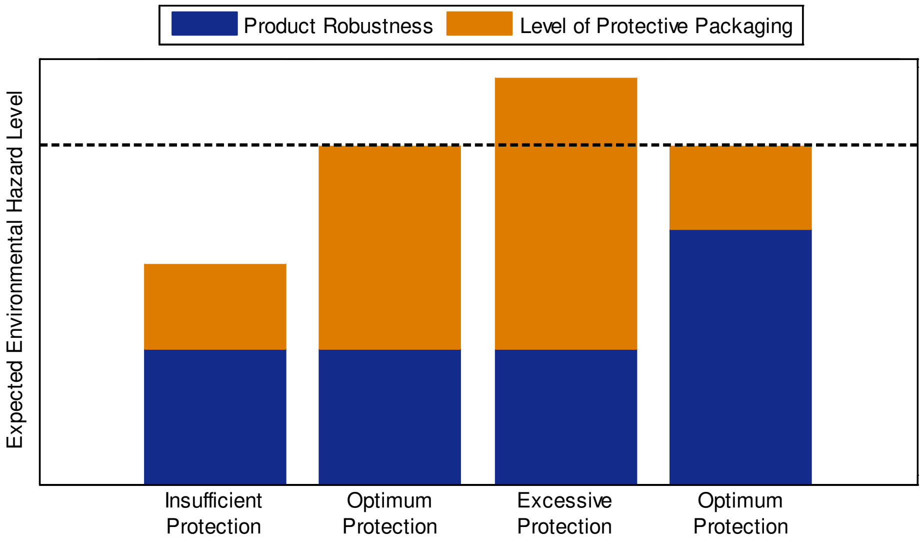

Figure 2-1: An illustrative example of various product-packaging systems (robustness and level of packaging) against the level of environmental hazards expected.

The Six-Step Method is also guided by economic considerations that control the design of both products and packages for distribution handling, illustrated in *Figure 2-2*. The optimum level occurs when the combined lowest cost of the three factors are achieved, indicating the potential economic and environmental considerations that must be taken into account when designing products and protective packaging systems. In order to ensure protective packaging systems are well engineered and use the optimal level of packaging for a given product, it is imperative to understand and accurately predict the complex relationship between road vehicles and irregular pavements. During transport, vehicles are subjected to broadband random vibration and only statistical representations are able to adequately describe the interaction.

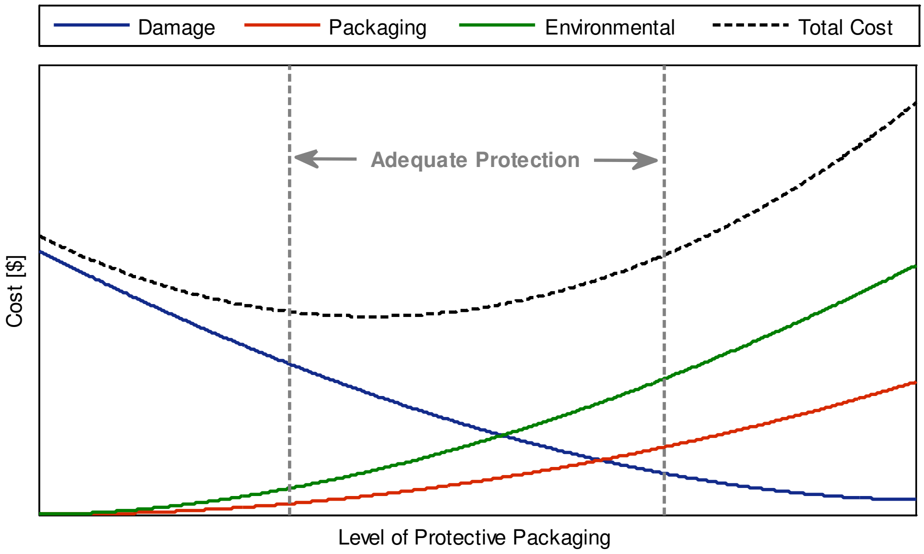

Figure 2-2: An illustrative economic cost function for product and package optimisation.

2.1.3 Validating Protective Packaging by Simulation

As the volume of products transported by road continues to rapidly increase, it is becoming increasingly important to use sufficient levels of protective packaging to protect products from road vehicle vibration during transport. The significant costs associated with inadequate or excess packaging further reinforce the need to develop improved approaches for the optimisation of product-packaging systems to prevent damage during transportation. Evaluating various protective packaging systems through actual trial shipments is impractical and expensive, leading to testing in the laboratory as an increasingly valid and widely implemented alternative (Sek 2001).

Prior to the 1980s, the use of vibration tables for random vibration testing was impractical and extraordinarily expensive. The first machines used for the simulation of transportation vibration were known as transportation simulators and consisted of one or more mechanically-driven eccentric cams (Kipp 2008). While these systems were accepted as an industry standard, the use of fixed-displacement, circular-synchronous motion provides a repetitive shock and poorly represents the vibration experienced during transport (Kipp 2008). In the early 1980s random vibration, based on measured PSD functions, became a practical choice for testing product-package systems and this trend has continued to the present day. The current practice to evaluate the effectiveness of protective packaging systems dictates that prototypes are subjected to simulated random vibration using a programmable vibration controller and shaker system. There are two approaches currently in-use for the laboratory simulation of the transport environment:

1) Employ the use of generic PSD functions provided by several organisations or standards.
2) Undertake a series of measurements to gather typical response data for specific vehicles and routes and compute the PSD functions and root-mean-square (rms) levels.

The current practice (method 1) makes use of generic PSD functions, created by combining or averaging the response PSD function from various vehicle types and routes (ASTM 2009). A more complex approach, though still using generic spectra, developed by the International Safe Transit Association (ISTA) provides an alternative testing procedure known as ISTA Project 4AB (ISTA 2009). These practices outlined by organisations such as the American Society for Testing and Materials (ASTM) and ISTA use average test severities that are based on time compression. In recent times, the effectiveness of these approaches as a tool to optimise protective packaging systems has been brought into question, notably by Charles (1993), Rouillard and Sek (2000) and Shires (2011). While these test standards are far quicker and easier to undertake, they are generally conservative and often lead to over-packaging of the product (Rouillard 2008).

The second approach (method 2), involving the measurement of various vehicle and route combinations, provides a more accurate representation of the transport environment than the generic spectra. The major drawback of the second approach is that significant time and resources are required to collect and analyse the data. The extensive resources required to undertake such measurements are particularly prohibitive for small volumes of a product, often resulting in the use of generic spectra due to their cost-effectiveness. *Figure 2-3* presents a comparison between the typical spectra for both the generic and measured response approaches and highlights the lack of complexity of the generic spectra in comparison to actual measured response spectra.

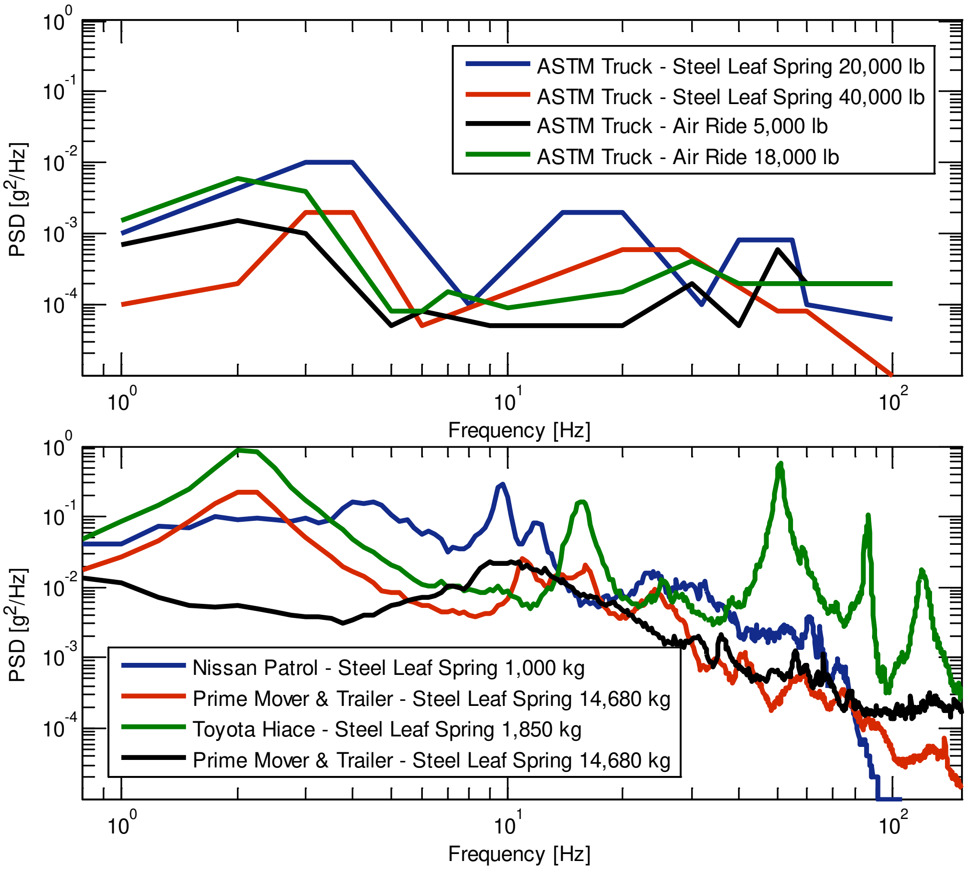

Figure 2-3: A comparison of the generic (top) and measured (bottom) PSD functions of the vertical sprung mass acceleration used for laboratory simulation (Rouillard & Sek 2013).

Rouillard and Sek (2013) proposed an affordable alternative approach to synthesise realistic road vehicle vibration without the need to repeatedly collect vibration response data for each vehicle-route combination. The approach requires knowledge of the road roughness properties, vehicle FRF and the trip schedule (speed and route length information). These three components are combined to generate a test schedule to simulate the expected vibration (in terms of the rms and PSD function) generated during transport. The method, outlined in *Figure 2-4*, uses a combination of pavement types and vehicle speeds, resulting in different target rms and PSD distributions throughout the test and notably, this method does not involve the use of time compression (Rouillard & Sek 2013).

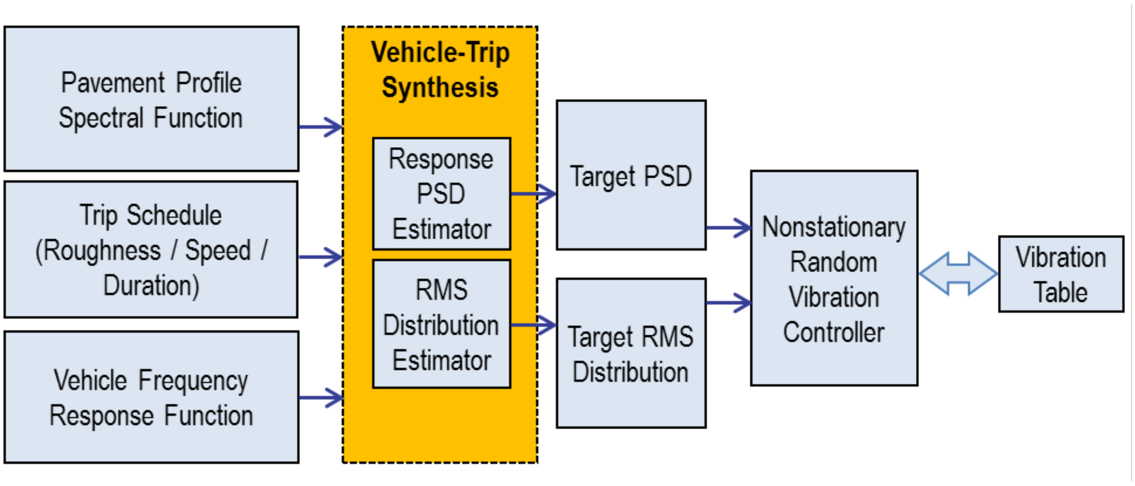

Figure 2-4: Outline of the technique to synthesise response vibration for a particular vehicle-route combination.

Despite the availability of the three required components, the various vehicle FRFs that are currently available are all based on idealised quarter car models, shown in *Figure 2-5*. While the user is able to select a vehicle FRF type that approximates their vehicle, these models still do not provide an accurate representation of the actual vehicle being used. A viable alternative to produce realistic transportation vibration for simulation without the measurement of significant amounts of data exists, however there remains difficulty for the user to select the FRF of their vehicle from the various idealised models available. Instead of using these generic FRFs, an improved approach would be to estimate the actual FRF of the user's vehicle to improve the simulation of transportation vibration.

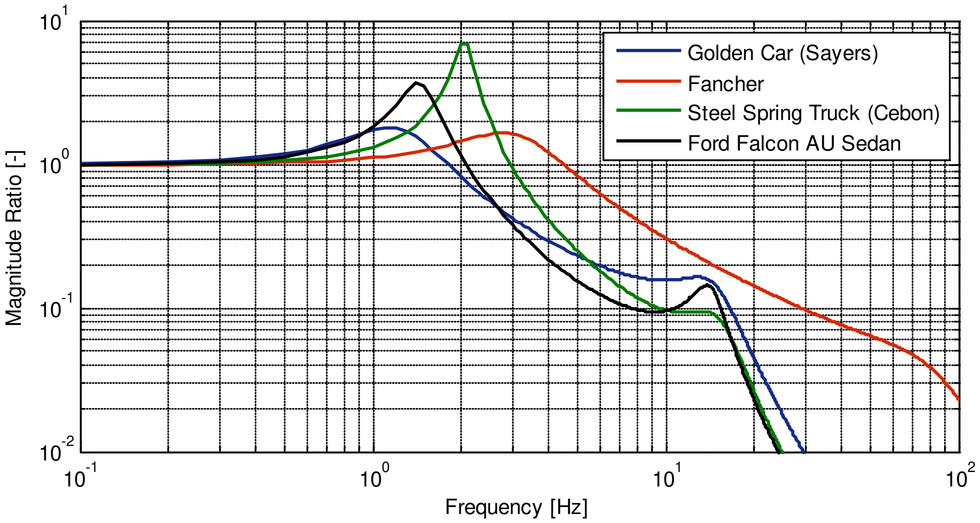

Figure 2-5: The transmissibility FRFs of typical numerical quarter car models, reproduced from Rouillard and Sek (2013).

2.2 ROAD-FRIENDLINESS AND PAVEMENT DAMAGE

Another consequence of the complex interaction between vehicles and roads is pavement deterioration. The occurrence of pavement deterioration has long been a significant issue in many developed countries where road networks are used to transport increasingly large volumes of freight for a single vehicle. The predicted increases in the volume of freight inevitably leads to an increase in the dynamic loads exerted onto pavements. There exists a great amount of literature concerned with understanding the cause and mechanisms of pavement damage.

Road-friendliness is the ability of a vehicle, or suspension system, to reduce the dynamic loads induced onto pavements during transportation as much as possible. A road-friendly vehicle is one that will, "to the greatest extent possible, isolate the vehicle from road unevenness so that dynamic wheel loading is minimised for given static loads" (OECD 1998). It is also important that a road-friendly suspension system is able to perform well on both smooth and rough pavements (OECD 1998). This requires knowledge of the entire interaction, including pavement composition, vehicle dynamic characteristics and the dynamic loads induced onto pavements (Cebon 1999, p. 508). For a long period of time, engineers have sought for a single relationship between the dynamic forces induced by a vehicle and the deterioration of pavements.

A large-scale study conducted during 1958-60 by the American Association of State Highway Officials (AASHO), who enlisted the US Army Corps to drive two-hundred vehicles over six custom test tracks in Ottawa, Illinois (AASHO 1962a; AASHO 1962b). The total mileage completed by AASHO during this two-year period equated to 17 million vehicle-miles. The analysis of the data collected from these experiments found the decrease in pavement condition caused by a single axle of a heavy vehicle was proportional to the fourth-power of its static load (Cebon 1999, pp. 9-10). These results finally yielded the relationship that pavement engineers had been seeking, known as the fourth-power law. The fourth-power law, shown in Equation 2-1, enabled the dramatic simplification in estimating the dynamic tyre forces induced by various vehicles in traffic, where all vehicles could now be defined in terms of their Equivalent Standard Axle Loads (ESALs) (Cebon 1999, p. 10).

$$No.\ ESALs = \left(\frac{P}{P_0}\right)^4 \tag{2-1}$$

where P is the static load and P_0 is generally 80 kN.

The validity of the fourth-power law has been questioned by numerous authors, particularly the variation in the value of the exponent due to a number of factors including diverse pavement types, suspensions, axle configurations, traffic volume and tyre sizes, among others (Cebon 1999, p. 10). Despite the criticism, the use of ESALs and the fourth-power law still hold significant influence for economic and political decision-making (Cebon 1999, p. 10). The CEU (1996) outlined the requirements for road-friendly suspensions (or equivalent to air suspension) under directive 92/7/EEC, later amended by 96/53/EC, as:

1) The sprung mass must have a natural frequency no higher than 2.0 Hz.
2) The damping ratio of the suspension system must be more than 0.20 during operation.
3) The damping ratio of the suspension system, with all shock absorbers removed or ineffective, must be no more than 0.50.
4) For multiple axle groupings, the static load-sharing between each axle must be within 5 %.

The Department of Transport and Regional Services (DoTaRS) in Australia use the same guidelines and test methods to determine road-friendliness as the CEU, outlined under the Vehicle Standards Bulletin 11 (VSB11) (2004). Heavy vehicles equipped with a road-friendly suspension system are permitted to operate with increased mass limits. The next major study, overseen by the Organisation for Economic Co-operation and Development (OECD), was the Dynamic Interaction between Vehicles and Infrastructure Experiment (DIVINE) (1998). This worldwide study, with active participation from seventeen member countries of the OECD, was separated into six main elements outlined in *Table 2-A*.

Table 2-A: The six research elements of DIVINE and the leading organisations of each element (OECD 1998).

No.	Research Element	Research Element Leader	Country
1	Accelerated dynamic pavements tests	Technical Research Centre of Finland, Federal Highway Administration	Finland, USA
2	Pavement primary response testing	Federal Highway Administration	USA
3	Road simulator testing	National Research Council	Canada
4	Computer simulation of heavy vehicle dynamics	Netherlands Organisation for Applied Scientific Research	Netherlands
5	Spatial repeatability of dynamic loads	French Institute of Science and Technology for Transport	France
6	Bridge dynamic loads	Swiss Federal Laboratories for Materials Science and Technology	Switzerland

Road-friendliness was further investigated and examined in DIVINE, with emphasis on the comparison between steel and air suspension systems fitted to heavy vehicles (namely trucks). One of the key findings of this study was that heavy vehicles with air suspension generally exhibit lower dynamic loads, expressed as the rms dynamic tyre force divided by the static force, commonly known as the Dynamic Load Coefficient (DLC), compared to common steel-leaf spring suspension systems. Previous studies discovered the most important factors for road-friendly suspensions are low sprung mass natural frequency, by means of low spring stiffness and reduced coulomb damping (friction), along with adequate viscous damping of the suspension system (OECD 1998).

The study also examined the relationship between the dynamic characteristics of a vehicle (namely the sprung mass natural frequency and the damping ratio of the suspension system) and the DLC. The study observed that a "strong relationship exists between the sprung mass frequency and DLC" (OECD 1998). The viscous damping was also found to exhibit significant influence on the DLC, i.e. as the viscous damping decreases, the DLC increases rapidly (OECD 1998). Some key recommendations from the DIVINE study were that the sprung mass natural frequency, outlined under CEU directive 96/53/EC, be reduced from 2.0 Hz to 1.5 Hz and interestingly noted that suspension damping ratios above 0.20 yield "diminishing benefits" (OECD 1998). Ideally, the dampers should be replaced once they fall below 0.20, however significant reductions in the road-friendliness of heavy vehicles may not occur until the dampers fall below 0.10 – 0.15 (OECD 1998). One shortcoming of the DIVINE study was the lack of attention given to the payload conditions of the various heavy vehicles. As heavy vehicles are often equipped with a trailer (which may be loaded with a wide variety of products), it is difficult to control and account for the variation in the payload being transported. Considering that the sprung mass natural frequency of a vehicle is also a function of the payload mass, variations in the dynamic characteristics are to be expected and may alter the system from its original configuration.

In order to effectively apply these recommendations, the dynamic characteristics of the sprung mass (or the FRF) of heavy vehicles must be established. Numerous techniques exist to estimate these dynamic characteristics; however they have not been evaluated to determine their accuracy and repeatability. A method to accurately estimate the FRF of a vehicle during normal operation is important to establish whether a heavy vehicle may be considered road-friendly.

2.3 VEHICLE AND SUSPENSION HEALTH MONITORING

Another consideration is the fatigue of vehicle and suspension components throughout its operational life. An ineffective or inadequate suspension system leads to poor ride quality and an increase in pavement damage. The two most important suspension parameters of vehicle ride have been identified as the sprung mass natural frequency and the damping ratio of the suspension system. Sweatman *et al.* (2000) identified the shock absorber as the most critical component “whose wear is likely to erode suspension road friendliness in-service” and is also the most difficult component to assess. A survey conducted by Blanksby *et al.* (2006) on the Hume Highway showed that at least one of the requirements for road-friendly suspensions outlined under the VSB11 was not met by more than half of the heavy vehicles inspected. A change in the sprung mass natural frequency (provided the payload remains constant) is a result of deterioration in the stiffness of the suspension system, while a change in the level of damping (concerned with reduction in the critical damping) is due to a decline in the performance of the shock absorbers. This provides yet another need for determining the FRF of a vehicle in order to monitor the health of a vehicle or suspension system. As the vehicle’s FRF would have to be established multiple times throughout its lifecycle, it is ideal if the approach is not only accurate but also practical and cost-effective.

Chapter 3

LITERATURE REVIEW

The previous Chapter highlights the importance of establishing accurate estimates of the dynamic characteristics of road vehicles. The literature review presented herein investigates the vehicle-road interaction with particular attention to estimating the dynamic characteristics of road vehicles. An investigation of the fundamental quarter car model commonly used in vehicle dynamic simulations is presented. The nature of longitudinal pavement profiles is then examined in detail, focusing on their analysis, implementation and implications relating to vehicle dynamics. A history of the various spectral models used to approximate longitudinal pavement profiles and their statistical nature is also presented. Also included in the Chapter is a thorough discussion of the various experimental methods that are currently used to estimate the dynamic characteristics of road vehicles, including response-only (transient), excitation-response and in-service response methods.

3.1 VEHICLE DYNAMIC CHARACTERISTICS

This section discusses the dynamic characteristics of the fundamental quarter car model and the significance of the model in understanding the dynamics of real vehicles. The quarter car is a 2 Degree-of-Freedom (2DoF) system commonly used in the simulation of vehicle dynamics. The model is designed to represent one quarter of a vehicle and consists of six independent parameters; the sprung and unsprung masses (m_s and m_u) and the stiffness and damping of the suspension system (k_s and c_s) and tyre (k_t and c_t). The excitation to the quarter car occurs via a vertical input to the tyre, usually a road elevation profile (where the displacement is u and the slope of the displacement is $\dot{u}$). An illustration of the 2DoF quarter car model is presented in *Figure 3-1*.

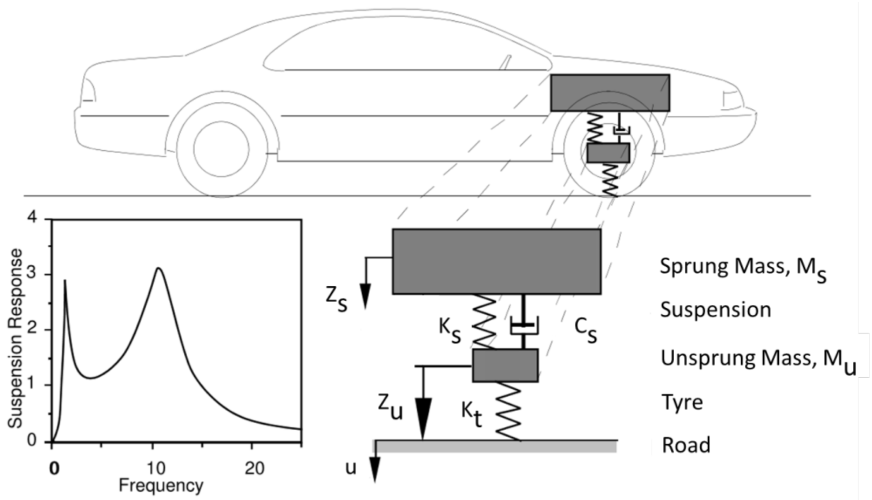

Figure 3-1: Schematic of the quarter car model (without tyre damping), reproduced from Gillespie (1992a).

The equations of motion for the sprung and unsprung masses (including the damping of the tyre) are given in Equations 3-1 and 3-2, respectively.

$$m_s\ddot{z}_s = -k_s\left(z_s - z_u\right) - c_s\left(\dot{z}_s - \dot{z}_u\right) \tag{3-1}$$

$$m_u\ddot{z}_u = k_s\left(z_s - z_u\right) + c_s\left(\dot{z}_s - \dot{z}_u\right) - k_t\left(z_u - u\right) - c_t\left(\dot{z}_u - \dot{u}\right) \tag{3-2}$$

where the acceleration, velocity and displacement of the sprung mass are represented as $\ddot{z}_s$, $\dot{z}_s$ and z_s and $\ddot{z}_u$, $\dot{z}_u$ and z_u for the unsprung mass. The sprung and unsprung masses are m_s and m_u, the stiffness and damping of the suspension system are k_s and c_s and the stiffness and damping of the tyre are k_t and c_t.

There are some important assumptions that are often made when using the quarter car model. One is that the damping in the system (shock absorbers) is viscous (and does not take into account friction or other damping within the shock absorber). Also, in most models it is assumed that the tyre is always in contact with the base (or road); however in practice and particularly at high frequencies this is not always the case (Jazar 2009, p. 933). For a 2DoF system the modes are coupled, however in many cases the dynamic forces generated by the unsprung mass mode are insignificant in comparison to the sprung mass mode. It is common in vehicle dynamics for the sprung mass mode to be the main focus and approximated as a Single Degree-of-Freedom (SDoF) system, with the simplified equations outlined herein. From the quarter car model several important relationships can be used to estimate the dynamic characteristics. Firstly, the natural frequency of the sprung mass, f_{sn}, is established via the following relationship:

$$f_{sn} = \frac{1}{2\pi}\sqrt{\frac{k_s}{m_s}} \tag{3-3}$$

The critical damping coefficient of the suspension system, c_c, is dependent upon the sprung mass and the stiffness of the suspension, and is defined as:

$$c_c = 2\sqrt{k_s m_s} \tag{3-4}$$

The damping ratio of the suspension system, ζ_s, is the dimensionless ratio of the damping coefficient and the critical damping and defined as:

$$\zeta_s = \frac{c_s}{c_c} \tag{3-5}$$

The damped natural frequency of the sprung mass, f_{sd}, can then be established using the natural frequency and the damping ratio by the following relationship:

$$f_{sd} = f_{sn}\sqrt{1-\zeta_s^2} \tag{3-6}$$

From Equation 3-6, it is evident that as the damping of the suspension system is increased the damped natural frequency of the sprung mass is reduced. In practice, the six parameters of the quarter car model are rarely known and it is considerably more practical to estimate the sprung mass natural frequency and damping ratio using experimental methods rather than estimating each of the individual parameters. To establish the FRF of a quarter car, the irregular pavement elevation profile and the acceleration response of the sprung or unsprung mass must be measured (or known). The FRF is used to describe the dynamic characteristics of the vehicle, or how the sprung (or unsprung) mass mode responds with respect to frequency.

When the excitation and response are measured with the same motion (e.g. acceleration), a special case FRF is obtained known as the transmissibility FRF. The magnitude of the transmissibility is the dimensionless "ratio of response amplitude to excitation amplitude" of a system and is also known as the transfer function or gain (Gillespie 1985). The dynamic characteristics may be established from the transmissibility through various methods. Furthermore, if the dynamic characteristics and the sprung and unsprung masses are known, the remaining parameters of the model may be established. For many applications in vehicle dynamics the response of the sprung mass is of primary interest. For a vehicle with linear characteristics (idealised), the response PSD function, $G_{Re}(f)$, can be obtained by weighting the road excitation PSD function, $G_{Ex}(f)$, with the vehicle's transmissibility squared, $T^2(f)$, shown in Equation 3-7 and illustrated in *Figure 3-2*.

$$G_{\mathrm{Re}}(f) = T^2(f)G_{Ex}(f) \tag{3-7}$$

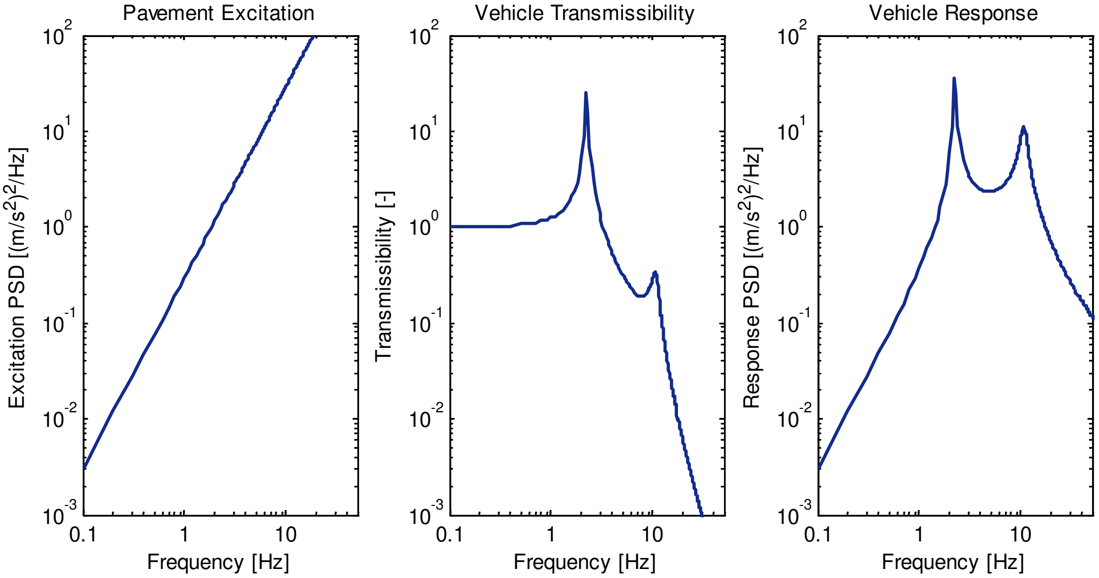

Figure 3-2: A pavement excitation spectrum (left) combined with the transmissibility squared (middle) produces the response spectrum of the vehicle-road combination (right).

Depending on the values selected for the parameters of the quarter car model, it is able to represent a variety of different vehicle types from passenger cars to light transport vehicles and even heavy vehicles. For example, Prem (1987) outlined parameters to create a “quarter truck model,” while Cebon (1999, pp. 67-68) described a quarter car model that is “broadly representative of single axle truck suspensions in current highway use.” One limitation of the quarter car model is that it is only useful for the investigation of the vertical vibratory motion of vehicles. To simulate other degrees of freedom of vehicles, such as pitch and roll, more intricate models are required. Complete passenger vehicles, heavy vehicles and even truck-trailer combinations can be created using elaborate numerical models (Cebon 1999, pp. 91-106).

3.1.1 Parameter Influence on the Dynamic Characteristics

Despite the quarter car’s inability to provide a true representation of a complete vehicle, the model is important to explain how each parameter influences the dynamic characteristics and is applicable to more complex vehicles. The sprung mass consists of the rigid body of the vehicle, including any passengers or cargo. The sprung mass is where the ride quality is assessed and the damped frequency is measured to evaluate whether heavy vehicles qualify as road-friendly. Equation 3-3 reveals that any increase in the sprung mass will result in a decrease of its natural frequency. The sprung mass also has an influence on the damping ratio via the level of critical damping in the suspension system. Equation 3-4 and Equation 3-5 illustrate that any increase in the sprung mass will raise the critical damping level; effectively reducing the damping ratio of the suspension system. The unsprung mass consists of anything not supported by the suspension system, such as the axle and other components for the wheels (Gillespie 1985). At the resonant frequency of the unsprung mass a phenomenon known as axle hop occurs. When axle hop occurs, the tyre begins to bounce and if the damping of the suspension system is not sufficiently great then the tyre may lose contact with the pavement (Jazar 2009, p. 933).

The suspension system, in its simplest form, consists of a spring and a hydraulic damper, or shock absorber, and connects the wheels to the body to allow for relative motion (Jazar 2009, p. 455). The primary function of the suspension system is to perform two conflicting roles: to support the body of the vehicle at a constant height to minimise vibration while also maintaining a constant load to the pavement through the tyre without any delay (Popp & Schiehlen 2010, p. 291). These conflicting roles pose a challenge to the design of an effective suspension system; it must somehow overcome the compromise between good ride quality and minimising pavement damage (Woodrooffe 1995).

The spring of the suspension system allows vibration to occur in the vehicle's sprung mass, preventing the vehicle occupants or products being directly subjected to the irregular pavement. As shown in Equation 3-3, the stiffness of the suspension system will affect the sprung mass natural frequency, where an increase in stiffness will increase the sprung mass natural frequency. The damping of the suspension system acts to reduce vibration induced via the irregular pavement. The damping ratio is also dependent upon the sprung mass and stiffness of the suspension system (via the critical damping). It is important to note that these effects are only valid provided the suspension system is linear; it is widely noted that vehicle suspension systems are often nonlinear. The various issues and difficulties associated with estimating the dynamic characteristics of nonlinear vehicles are discussed in the following section on experimental techniques to estimate the dynamic characteristics of road vehicles.

The tyre is integral for a vehicle as it is the only component that is in contact with the road. A vehicle is able to "maneuver only by longitudinal, vertical and lateral force systems generated under the tyres" by Jazar (2009, p. 95). The tyre acts as both a spring and a damper; however the damping of the tyre is often neglected in quarter car models as the damping coefficient is relatively small in comparison to the damping of the suspension system (Jazar 2009, p. 932). Furthermore, in numerical simulations the pavement elevation is differentiated which introduces further errors into the simulation and is another factor to support the omission of the tyre's damping.

Gillespie and Karamihas (1994) noted that "variations in tyre inflation pressure affect pavement damage by changing the size of the contact patch and the vertical tyre stiffness." Correct inflation of the tyre is essential for "optimum performance, safety and fuel economy" and provides optimum surface contact with the pavement (Jazar 2009, p. 124). Over-inflation of the tyre increases the pressure, which in turn increases the stiffness and reduces the surface contact area to the pavement, diminishing the "ride comfort and generates vibration" (Jazar 2009, pp. 124-125). While under-inflation also reduces the tyre-road contact area, it leads to "an overloaded tyre that operates at high deflection with a low fuel economy, and low handling" (Jazar 2009, p. 124).

Cebon (1999, p. 24) described the effect of tyres enveloping the short wavelengths of road roughness "of the order of the tyre contact length." The envelopment acts to filter the effect of the short wavelengths of the road. This phenomenon is not relevant at "normal highway speeds" as the short wavelengths correspond to high frequencies that do not influence the suspension system (Cebon 1999, p. 24). Imperfections in the manufacturing of the tyres and wheel assembly may transmit additional vibration to the axle, introducing another source of excitation in the vehicle (Gillespie 1985). Some typical examples of imperfections in the tyre and wheel assembly include dimensional variations of the tyre, mass imbalance and non-uniform tyre stiffness (Gillespie 1985).

Wheelbase filtering, while irrelevant to the quarter car, is an important occurrence in normal (multi-wheeled) vehicles travelling over uneven pavements. Due to two or more wheels travelling along the same longitudinal path, nodes occur in the vehicle's frequency response (Gillespie 1985). These nodes occur at frequencies equal to the speed divided by half the wheelbase length and odd multiples thereafter (Gillespie 1985). The effect of this on the vertical vibration (bounce) depends on the wheelbase length of the vehicle; for short to medium wheelbases the response is attenuated at high speed (Gillespie 1985). For vehicles with long wheelbases, the nodes are "proportionally higher" and the excitation (via the road) decreases by a "speed-squared relationship" due to wheelbase filtering (Gillespie 1985).

3.2 NATURE OF LONGITUDINAL PAVEMENT PROFILES

As discussed in the background (Chapter 2), understanding and predicting the transportation vibration environment requires knowledge of all aspects of the interaction, from the product(s) or passenger(s), the vehicle and the pavement. It is practically and economically impossible to construct a pavement surface devoid of roughness, therefore the principal cause of dynamic motion in road vehicles is the irregular nature of pavement topography. Pavement surface roughness, as a whole, is defined by the ASTM (2005) as "the deviations of a surface from a true planar surface with characteristic dimensions that affect vehicle dynamics, ride quality, dynamic loads, and drainage, for example, longitudinal profile, transverse profile, and cross slope." The main shortcoming of this definition from the standard is the lack of a method to quantify the road roughness (Sayers & Karamihas 1998, p. 37). Gillespie (1985) suggested that the main excitation induced in road vehicles by an irregular pavement occurs in the vertical vibratory motion and so only longitudinal pavement profiles (which induce vertical vibratory motion in vehicles) are investigated in this section. Sayers and Karamihas (1998, p. 9) described the four main categories of interest for the measurement of longitudinal pavement profiles:

1) Road network condition monitoring.
2) Evaluating the quality of new or repaired pavements.
3) Identifying deterioration in sections of pavements (to determine appropriate remedies).
4) Studying the condition of pavements for research purposes.

While it is practically impossible to measure the true profile of a pavemen, the motivation for obtaining the profile in the first place determines how the measurement should be made. It is also essential to select the appropriate wavelengths of interest prior to the measurement of a profile. One of the earliest devices used to measure the longitudinal elevation profiles was the rod and level (Sayers & Karamihas 1998, p. 3). Further developments in profilometer technology continued to rely on the use of hand-moved equipment. While these approaches were reliable, they were cumbersome to undertake and required significant time to measure extensive lengths of road (Robson & Dodds 1976). In the 1960s, General Motors unveiled the first high-speed inertial profilometer capable of obtaining profile measurements in a similar manner to a rod and level in significantly less time (Sayers & Karamihas 1998, p. 6). These devices do not measure the true elevation profile, but are designed to obtain the same statistical values of the true profile (Sayers & Karamihas 1998, p. 10).

3.2.1 Spectral Models of Longitudinal Pavement Profiles

The elevation of longitudinal pavement profiles are generally found to be “broad-band random” and as such are suitably described by the elevation profile itself or a statistical representation, the most useful description being the PSD function (Gillespie 1985). In fact, the initial impetus for obtaining the PSD function of longitudinal pavements was for their “usefulness in vehicle dynamics” (Andren 2006). The process of recreating an identical pavement profile for analysis and simulation is practically unfeasible; it is easier to replicate a profile that has the same statistical characteristics. The spectral characterisation of longitudinal, single-track pavement profiles is able to provide detailed roughness information at specific longitudinal wavelengths (Mann *et al.* 1997) and can also illustrate any periodic irregularities present in the road profile (Delanne & Pereira 2001). A spectral description of a longitudinal pavement profile is valuable to numerous industries, including vehicle and component design and for the prediction of road-vehicle interaction (Kropac & Mucka 2008). The pavement elevation PSD function of the pavement profile is considered to be “indispensable” for applications in vehicle dynamics (Kropac & Mucka 2009a).

The PSD function is not entirely useful in some applications, such as in the management of the serviceability of pavements (Delanne & Pereira 2001). Those concerned with the design, construction and maintenance of road surfaces often use a single-number index to provide an adequate evaluation of the pavement (Kropac & Mucka 2004). Of all the single-number indices used to evaluate longitudinal pavement profiles, the International Roughness Index is the most widely used. While other indices exist and are commonly used, these single-number indicators are unable to provide sufficient information for use in applications relating to vehicle dynamics

(Kropac & Mucka 2004). Another limitation of the PSD function is the inability to locate local defects in a pavement, unless of course the defect is periodic (Delanne & Pereira 2001). A transient event such as a pothole would not be identified from the PSD function of the pavement. The PSD function also assumes that the signal is stationary and Gaussian, making it unable to account for nonstationary due to variations in the pavement roughness along the profile. One of the earliest uses of a spectral function to describe the longitudinal roughness of aircraft runways was by Houbolt *et al.* (1955) and continued in Houbolt (1962), where an approximated displacement PSD function in the spatial frequency domain, n, was proposed (Equation 3-8).

$$G(n) = C(2\pi n)^{-2} \tag{3-8}$$

La Barre *et al.* (1969) commissioned the use of a profile measurement vehicle and measured a series of fifty-four roads throughout the UK and Europe. The analysis of these profiles found the displacement PSD functions generally conformed to the model suggested by Houbolt (1962) in Equation 3-8. Vogel (1965) found that the spectral shape of road profiles are generally independent of the road type, instead they are a function of the rms level (roughness). Macaulay (1963) suggested the use of a piecewise spectrum over different wavelengths to represent longitudinal road profiles:

$$G(n) = \begin{cases} Cn^{-w_1}, \ 0.011 \le n \le 0.328 \\ Cn^{-w_2}, \ 0.328 \le n \end{cases} \tag{3-9}$$

where Macualay (1963) recommended the exponents to be w_1 = 2.5 and w_2 = 1.5.

Dodds and Robson (1973) also advocated the use of a piecewise spectral density function:

$$G(n) = \begin{cases} G(n_0)\left(\dfrac{n}{n_0}\right)^{-w_1}, \ n \le n_0 \\ G(n_0)\left(\dfrac{n}{n_0}\right)^{-w_2}, \ n \ge n_0 \end{cases} \tag{3-10}$$

where the discontinuity spatial frequency is $n_0 = \dfrac{1}{2\pi}$.

The authors also stated that the spectral function approaches unity as the wavenumber decreases (towards the value of the roughness constant) and conversely, as the wavenumber increases, the spectrum approaches zero (Dodds & Robson 1973). For the two spectral exponents, w_1 and w_2, Dodds and Robson (1973) used the fifty-four road spectra obtained by La Barre *et al.* (1969) and calculated the mean and standard deviation for the various roads. The mean values for w_1 were 1.945, 2.050 and 2.280 with the respective standard deviations of 0.464, 0.487 and 0.534 for various road classifications (motorway, principal roads and minor roads). For the same road classifications, the mean values of w_2 were 1.360, 1.440 and 1.428, while the standard deviations were 0.221, 0.266 and 0.263, respectively.

Kamash and Robson (1977) investigated the implications of assuming that road surfaces are homogeneous and isotropic. This means that the statistical properties of a homogeneous random surface are independent of coordinate translation, while the statistical properties of an isotropic random surface are independent of coordinate rotations (Heath 1987). For isotropy to be a valid assumption, limits for the possible range of wavelengths must be specified. Kamash and Robson (1977) described a spectral model that would satisfy the requirements of isotropy as:

$$G(n) = \begin{cases} C, n_a \geq |n| \\ C.n^{-w_1}, n_a \leq |n| \leq n_0 \\ C.n^{-w_2}, n_0 \leq |n| \leq n_b \\ 0, n_b < |n| \end{cases} \tag{3-11}$$

where n_a and n_b are the lower and upper wavenumbers of interest and depend on the application of the spectral model.

The model described in Equation 3-11 was further refined by Kamash and Robson (1978), with the following spectral function also satisfying the conditions of isotropy:

$$G(n) = \begin{cases} Cn_a^{-w}, & 0 \leq n \leq n_a \\ Cn^{-w}, & n_a \leq n \leq n_b \\ 0, & n_b < n \end{cases} \tag{3-12}$$

where the value of the spectral exponent, w, is recommended to be 2.5.

Kamash and Robson (1978) stated that the wavenumbers n_a and n_b in Equation 3-12 are "not simply the limits of the range of wavenumber known to be relevant in the actual response analysis," but that they should be selected to verify that the "derived direct and cross-spectra are valid over this wavenumber range." The authors also discussed the appropriate range of the exponent, w, to be within 2.0 – 3.0 and used a value of 2.5 in their analysis. Kamash and Robson (1978) suggested that, for vehicle response analysis, a range of 0.01 – 10 c/m is appropriate. Robson (1979) contended that since the use of a spectral function is only an approximation of the actual road spectral density, it is acceptable to use a generalised, single-slope spectrum of the form described in Equation 3-13.

$$G(n) = C|n|^{-w} \tag{3-13}$$

where the value of the exponent, w, was recommended by the author to be 2.5.

In 1982, the International Organisation for Standardisation (ISO) outlined a standard spectral model for the measurements of road profile data using the piecewise model proposed by Dodds and Robson (1973) in Equation 3-10. The values of the exponents w_1 and w_2 were specified as 2.0 and 1.5, respectively. Gillespie (1985) developed an average PSD function of a vehicle's left and right wheel tracks to describe the road using a single model:

$$G(n) = C\left(1 + \left(\frac{x_c}{n}\right)^2\right)n^{-2} \tag{3-14}$$

where C and x_c are parameters that are dependent on the pavement type. For example, a flexible pavement has values of C = 1.25×10^{-6} and x_c = 0.164.

Sayers (1986) introduced a generalised spectral model based on Houbolt's (1962) model, in Equation 3-8, to deal with a greater range of wavelengths of interest by using this model as a piecewise function if required:

$$G(n) = C(2\pi n)^{-\alpha} \tag{3-15}$$

Sayers (1986) suggested that using the spectral model in Equation 3-15 would improve the fit applied to pavement elevation data, and that Houbolt's (1962) model is "a special case." Sayers (1986) also devised an alternative PSD model comprising three components:

$$G(n) = C_1(2\pi n)^{-4} + C_2(2\pi n)^{-2} + C_3 \tag{3-16}$$

where C_1 is a coefficient calculated using the acceleration PSD between 0.003 – 0.050 c/m, C_2 is the overall roughness coefficient of the mean value of the slope PSD between 0.08 – 0.50 c/m and subtracted from the PSD over all wavelengths to keep only the residual roughness and C_3 is determined from the displacement PSD between 0.7 – 3.0 c/m.

Marcondes *et al.* (1991) examined twenty typical 306 m sections of longitudinal pavement profiles in Michigan near Lansing. The various pavements were new and old Portland Concrete Cement (PCC) pavements and a combination of Asphalt Concrete (AC) and PCC pavements. Due to "peculiarities in the form of concentrated roughness" the authors suggested the use of a new spectral model to deal with a greater range of spatial frequencies of the form:

$$G(n) = \begin{cases} C_1 e^{-k_c n^p} & , n_1 \geq n \\ C_2(n-n_0)^q & , n_1 \leq n \end{cases} \tag{3-17}$$

where C_1 and C_2 are constant roughness amplitudes, n_1 is the discontinuity frequency (chosen by inspection) and k_c, p and q are constants.

Xu *et al.* (1992) proposed a spectral model based on the standard deviation and an arbitrary parameter, a_c, with a flat spectrum in the region of n = 0:

$$G(n) = \frac{\sigma^2}{2a_c\sqrt{\pi}} e^{\left(\frac{-n^2}{4a_c^2}\right)} \tag{3-18}$$

To validate the spectral model in Equation 3-18, Xu *et al.* (1992) conducted a series of measurements over ten different 300 m sections of road and found that the proposed spectral model agrees well with the actual PSD estimates. In 1995, the ISO released standard 8608 detailing the process of measuring and describing longitudinal road profile elevation data. For single-track longitudinal elevation profiles, the ISO recommend that the displacement PSD is presented in a log-log scale, with the proposed model outlined under ISO 8608:

$$G(n) = G(n_0)\left(\frac{n}{n_0}\right)^{-w} \tag{3-19}$$

where the spectral exponent, w, is recommended to be 2.0.

Under this standard model, a series of road grades, or classifications, from very good (A) to unclassified (F, G and H) are defined by the ISO (1995) and presented in *Figure 3-3*. The ISO (1995) specified the range of spatial frequencies of interest to be between 0.01 – 10 c/m. The standard road spectrum is equivalent to brown noise in the displacement domain, white noise in the velocity domain and violet noise in the acceleration domain.

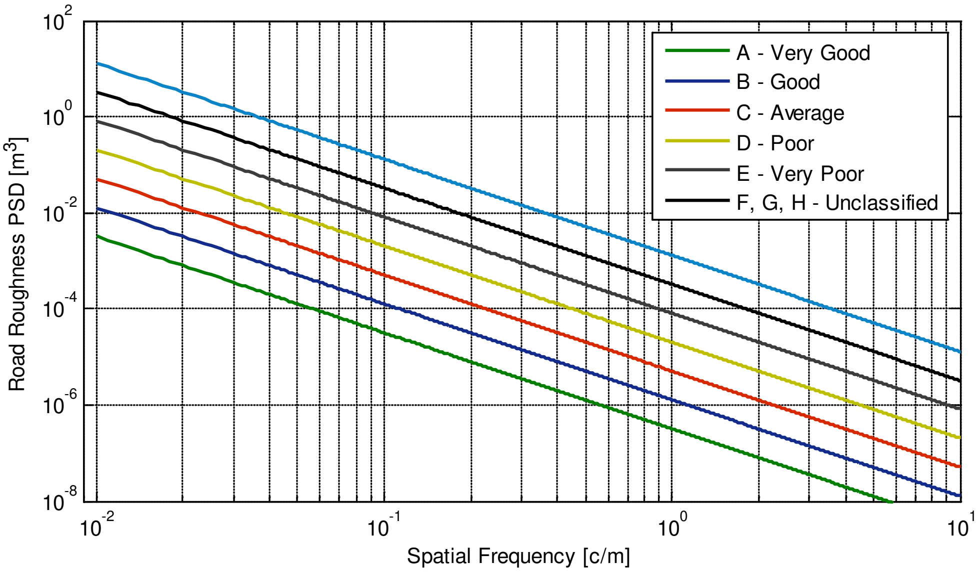

Figure 3-3: The ISO (1995) standard 8608 road classification guide.

Andren (2006) provided a comprehensive review of the various spectral models that have been used to characterise longitudinal pavement profiles and discussed the two split approximation that is supposedly well-known but no earlier references describing the model exist. A previous reference was found to reveal that the two-split, or three-band model, was first used in France in the 1970s (Kropac & Mucka 2008) and has the form:

$$G(n) = \begin{cases} C.n^{-w_1}, 0 \le n \le n_a \\ C.n^{-w_2}, n_a \le n \le n_b \\ C.n^{-w_3}, n_b \le n \le \infty \end{cases} \tag{3-20}$$

where n_a and n_b are the selected breakpoints of interest to split the model and are given by Andren (2006) as 0.21 c/m and 1.22 c/m.

Andren (2006) briefly discussed defining appropriate discontinuity frequencies; however the author's final selection was determined by which discontinuity frequencies would produce the lowest total least-square error based on the PSD elevation functions of the entire Swedish road network. In general, the various spectral models all adhere to a simple relationship where the spectral amplitude is inversely proportional to the spatial frequency to the power of the exponent, given in Equation 3-21 (Kamash & Robson 1977).

$$G(n) \propto n^{-w} \tag{3-21}$$

Equation 3-21 affirms that, generally, the shape of a pavement spectral model is independent of the road type; instead they are a function of the rms level (or overall roughness). Rouillard *et al.* (1996) studied 2.35 km of "typical road surface elevation data" and found the road elevation PSD functions retained their general shape and only shifted up or down due to varying roughness. Bruscella (1997) examined 415 km of road elevation data from Victoria, Australia, and further confirmed that the shape of the PSD function is generally independent of road type, rather a function of the rms level (roughness). Further confirmation of this has been provided by a number of authors (notably Vogel 1965; Dodds & Robson 1973; Heath 1988; Xu *et al.* 1992).

Kropac and Mucka (2004) suggested an alternative PSD model based on work by Dodds and Robson (1973), similar to the two-split approximation in Equation 3-20, which separates the spectrum into three distinct wavelength bands: long, medium and short wavelengths. This spectral model can be used to identify whether the pavement elevation PSD deviates from the standard model (Kropac & Mucka 2004). This approximation was further investigated by

Kropac and Mucka in 2008; finding that the three wavelength bands is only required when “the PSD course is very irregular.” This implies that a one or two band spectral model should be sufficient to describe the majority of roads that are well maintained.

3.2.2 Variation in the Spectral Exponent

The literature review of the nature of longitudinal pavement profiles thus far indicates there exists much conjecture and debate over the appropriate value of the spectral exponent, w, for single-band spectral models. The validity of using the standard value of 2.0 for the exponent, as described under ISO standard 8608, has been disputed by numerous authors claiming that the value will vary depending on the road. Accurately establishing the correct value of the spectral exponent reveals significant information about the unevenness of the longitudinal profile. It can divulge the types of wavelengths that are prominent in the road, for example when the exponent is greater than 2.0 the long wavelengths are more pronounced, while if the exponent is less than 2.0 then short wavelengths feature more prominently in the profile (Kropac & Mucka 2009b).

Mucka (2004) investigated the influence of two spectral models on the relative dynamic tyre forces of a numerical quarter car. The first model, for comparison, was the current standard model as suggested by ISO 8608 (1995), while the second was the same model proposed by Dodds and Robson (1973) in Equation 3-10, separated into long and short wavelength bands. The second model varied the values and combinations of the two exponents from 1.5 to 2.5 in steps of 0.25. The results found that small variations in the exponent (between 1.9 and 2.1) had little influence on the relative dynamic tyre forces (less than 5 % difference from the standard model). The variation in the short wavelength exponent was found to have a marginal effect on the dynamic tyre forces compared to the exponent for the long wavelengths (Mucka 2004).

Mucka and Kropac (2004) found that if homogeneity is a valid assumption, then averaging sections of up to 500 m are recommended, while if the assumption is invalid (or transient events are present) then each section length should be within 50 – 100 m. Nonstationary, or transient events, are often of a much shorter duration. For example, Bruscella *et al.* (1999) was able to identify a “bump” within a 0.5 m section of road. The three-band spectral model, separated into long, medium and short wavelengths can be used to identify whether the PSD of actual pavement profiles deviate from the standard model (Mucka & Kropac 2004). Andren (2006) analysed the entire Swedish road network using the standard spectral model (ISO 1995) and found the spectral exponent, w, may vary from 1.5 to 3.0. Further to this, Andren (2006) also undertook a comparative study of four PSD models (ISO 1995; Sayers 1986, Dodds 1973 and two split) using pavement profile data of the entire Swedish road network. The evaluation was based on the least square error of the fits and Andren (2006) found the ISO standard model to perform the worst, while the two split was the best of the four techniques.

Mucka and Granlund (2012) investigated the character of old highway lanes in Sweden and fitted three different spectral models; the standard single-band (ISO), two-band and three-band models. The authors found that the two-band spectral model provided the best fit of the three. Further investigation was undertaken by Mucka (2012), who agreed the use of a two-band spectral model was the most appropriate. Two of the conclusions by Mucka (2012) from this work were that the improvement over the standard ISO model compared to the two-band model was in the region of approximately 30 %, with the mean error decreasing by 6 % and 14 % when using the two and three-band models, respectively. While the three-band model was also investigated; Mucka (2012) stated that the medium waveband was "too coarse," and the exponents in the long and medium wavebands "differ only slightly."

Kropac and Mucka (2008) investigated the use of three spectral models over 25,800 longitudinal pavement profiles in the USA and Canada. Two common pavement types were evaluated; AC and PCC. The models investigated were the ISO 8608 standard model, the piecewise model proposed by Dodds and Robson (1973) separated into long and short wavelength bands and the third model was based on the two-split approximation (Andren 2006) separated into long, medium and short wavelength bands. The results of the evaluation highlight the variation in estimates of the spectral exponent and are presented in *Table 3-A*. Rouillard and Sek (2010b) conducted a series of in-service, constant-speed experiments using a small transport vehicle and found the value of the exponent, w, cannot always be assumed to be 2.0. Mucka (2012) evaluated the ISO 8608 single-band approximation and the two and three-band spectral models, finding the two and three-band models superior to the single-band ISO model.

Table 3-A: The estimated mean and standard deviation of the spectral exponent(s) for two pavement types using the single, two and three band spectral models (Kropac & Mucka 2008).

	Standard	**Two-Band**		**Three-Band**		
Pavement Type	w	w_1	w_2	w_1	w_2	w_3
AC Pavement						
Mean	2.475	3.222	2.090	2.935	3.156	2.154
Standard Deviation	0.417	0.600	0.566	0.782	0.839	0.684
PCC Pavement						
Mean	2.479	2.434	2.377	2.314	2.802	2.326
Standard Deviation	0.314	0.723	0.451	0.864	0.825	0.555

3.2.3 Assumptions of Isotropy and Stationarity

There has been considerable interest in investigating the assumption that longitudinal pavement profiles are isotropic and stationary. The valid estimation of the PSD function of a pavement profile requires the random process to be stationary and have a Gaussian distribution. In order to characterise a complete road surface, a significant amount of elevation data (from multiple wheel paths) is required; a laborious approach, to say the least. To simplify this approach, Dodds and Robson (1973) examined the possibility of assuming road surfaces to be homogeneous and isotropic to allow the use of a single PSD function to describe an entire road surface. The authors investigated a small sample of three different road classifications (motorway, principal and minor roads) and found the assumption of isotropy and homogeneity to be reasonable. It was suggested by Bendat and Piersol (2000) that although the majority of "the random data of interest in practice is nonstationary ... it is often possible to force the data to be at least piecewise stationary for measurement and analysis purposes." Rouillard *et al.* (1996) found the elevation rms varies over a road and that the process "should not be treated as stationary," however for simulation purposes the road may be treated in stationary sections where the rms level does not excessively vary.

Robson and Dodds (1975/76) acknowledged that while pavements are nonstationary in nature, finite sections of a profile can each be considered to be stationary. Nonstationarity of a pavement is manifested as "large and sustained variations" in the rms level (Rouillard & Sek 2002). Nonstationary events in pavements are usually considered as "statistically uncommon events," comprising of occurrences outside $\pm 3\sigma$ (Bruscella *et al.* 1999) and are typically due to transient events such as potholes or train tracks. It is imperative that any transient events are removed from the elevation profile and considered separately (Dodds & Robson 1973). Cebon and Newland (1983) continued to advance the isotropic assumption by simulating an entire road surface from a single track profile using a two-dimensional Discrete Fourier Transform (DFT). Heath (1988; 1989) investigated the assumption of isotropy and found it to be applicable for smooth roads, but not for rough roads. Heath (1989) also found that roads are rarely completely homogeneous and isotropic; however sections of road can be considered stationary.

Bogsjo (2007) investigated two models using a numerical front-half car over 20 Swedish roads with longitudinal pavement elevation data for both the left and right wheel tracks (totalling 520 km in length). The first model proposed was an isotropic Gaussian model that was found to be inaccurate; while the second model assumed the left and right wheel paths are "statistically equivalent" and resulted in a more accurate representation of the profiles (Bogsjo 2007). Kropac and Mucka (2008) found the difference between the right and left wheel tracks for a number of roads in the USA to be negligible, providing further agreement that isotropy is a valid assumption. Chemistruck *et al.* (2009) acknowledged that, in general, smooth roads tend to be stationary, while rough roads are not. Generally, the shorter the pavement profile sections are, the more likely they are to be stationary (Chemistruck *et al.* 2009).

3.2.4 Statistical Nature of Longitudinal Pavement Profiles

To adequately characterise a road profile for use in vehicle dynamics and simulation, a PSD function alone is insufficient (Rouillard & Sek 2010a). As mentioned, the basis of the PSD approach relies on the pavement elevation data to be Gaussian. The statistical distribution of the pavement profile, usually described in the form of the Probability Density Function (PDF), is required to ensure a complete understanding of the profile. The PDF is useful for a number of fields including transportation and pavement maintenance (Rouillard *et al.* 2000).

As pointed out by Rouillard and Sek (2010a), the PSD function illustrates “the average magnitude for each frequency band within the spectrum” and is unable to offer “information on time-variant parameters such as possible variations in amplitude or the time at which these variations occur.” If the profile is a realisation of a random, stationary process with a Gaussian distribution, such limitations of the PSD are irrelevant (Rouillard & Sek 2010a). This simplifies the simulation of road profiles enormously, as most random vibration controllers are designed to synthesise random, Gaussian processes. When dealing with non-Gaussian distributions, the skewness and kurtosis are the two parameters primarily used to evaluate deviation of the distribution from the standard Gaussian. The skewness is a measure of the asymmetric nature of the distribution, while the kurtosis indicates the ‘peakedness’ of the distribution. For a Gaussian distribution, the values of the skewness and kurtosis are zero and three, respectively.

Extensive analyses of longitudinal pavement profiles in various countries have shown they are random in nature with a Gaussian distribution, provided that transient events are excluded (Cebon 1999, p. 21). However, Heath (1989) found the distribution of typical road surfaces may deviate from the Gaussian. This was further confirmed by Rouillard *et al.* (1996) and Bruscella *et al.* (1999). Moreover, Rouillard *et al.* (1996) discovered the distributions of individual pavement sections within a single track profile differ, making it difficult to advocate treating pavements as a Gaussian or narrow-band process.

Bruscella (1997) investigated the statistical distributions of 415 km of road profile data from Victoria, Australia, and found them to exhibit "significant" non-Gaussian properties, with a large number of events occurring outside the standard range of ± 3σ, which was also acknowledged by Mucka (2004). A typical road profile measured in metropolitan Victoria, Australia, with a non-Gaussian distribution is shown in *Figure 3-4*.

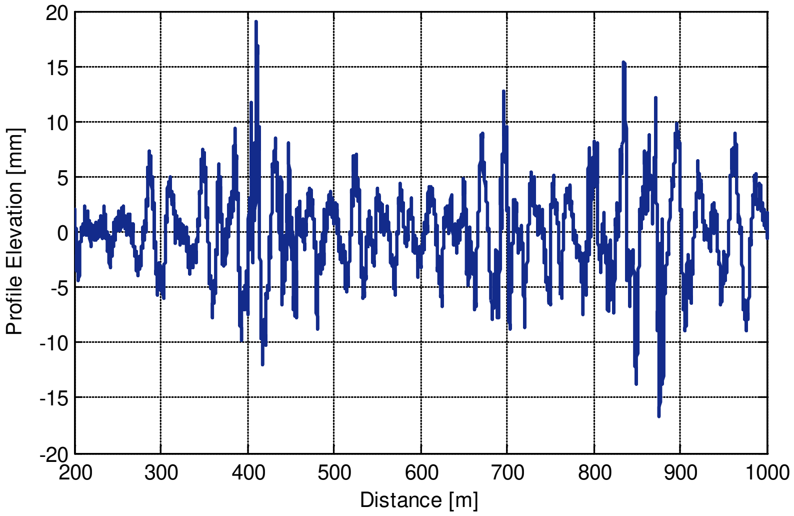

Figure 3-4: A sample of a typical pavement profile elevation (left) and the statistical distribution of the same profile with the best Gaussian fit (right). Elevation data details: Princes Highway East, 22.85 km length, from Bruscella (1997).

Bruscella *et al.* (1999) used the double derivative of the pavement elevation to establish the spatial acceleration of the pavement for analysis. The spatial acceleration of the pavement profile is well suited for use in vehicle simulations and is able to identify transient events more easily (Bruscella *et al.* 1999). Bruscella *et al.* (1999) analysed a series of typical pavements from Victoria, Australia, using the moving rms and moving crest factor of the spatial acceleration. The moving rms was used to determine the nonstationary nature of the pavement, while the moving crest factor was used to identify transient events, which corresponded to high kurtosis values.

It was also suggested that transient events may be less prevalent in rougher roads as they are a function of the rms level (Bruscella *et al.* 1999). Rouillard *et al.* (1999) discovered that the kurtosis is inversely related to the roughness of the road; such that the kurtosis will decrease as the roughness increases. The skewness of the distribution was found to be insignificant, with little variation between roads (Bruscella 1997). The insignificance of the skewness was further confirmed by Kropac and Mucka (2008). A typical pavement profile presented in terms of spatial acceleration, moving rms and moving crest factor is presented in *Figure 3-5*.

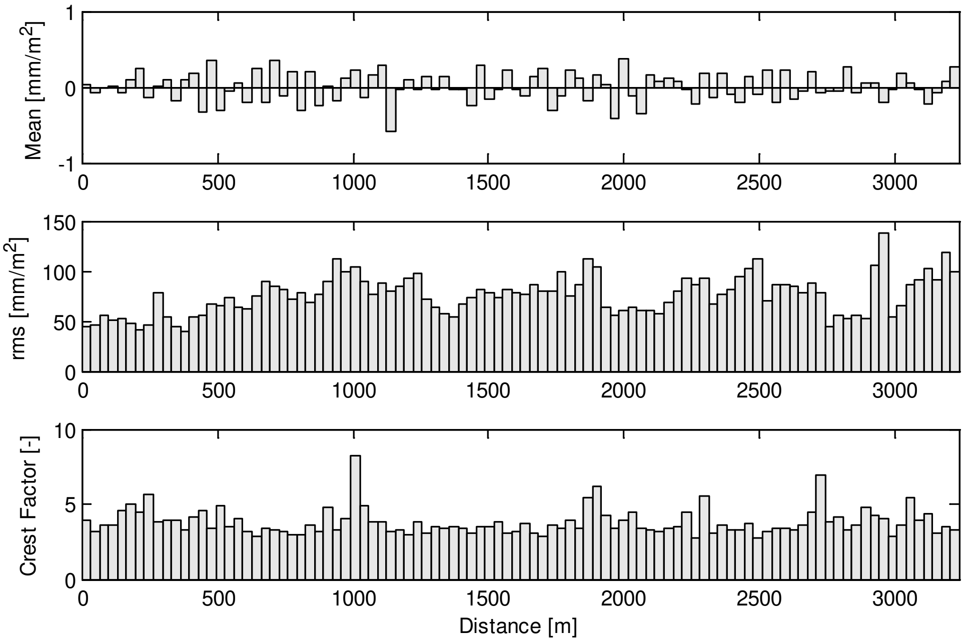

Figure 3-5: The moving statistics for the spatial acceleration of a typical road; mean (top), rms (middle) and crest factor (bottom) for a moving window width of 33 m with 0 % overlap. Elevation data details: Princes Highway East, 22.85 km length, from Bruscella (1997).

Rouillard *et al.* (2000) presented an alternative approach to characterise the profile of a pavement by individually evaluating the statistical distributions (PDF) of the rms and transient levels. The authors put forward an approach to describe the longitudinal pavement elevation profile using nine different parameters. Rouillard and Sek (2002) investigated the use of an offset Rayleigh distribution to characterise the spatial acceleration of pavement profiles free of transient events. The authors also applied an offset Rayleigh distribution to characterise the transient density. The PDFs of the spatial acceleration rms for typical smooth and rough pavements with the best-fitting offset Rayleigh distribution are presented in *Figure 3-6*.

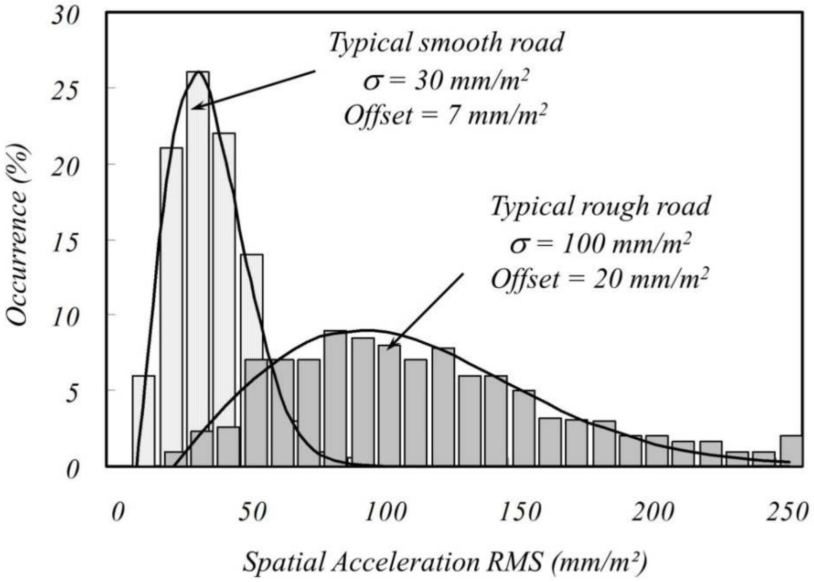

Figure 3-6: The PDFs of the spatial acceleration rms for typical smooth and rough pavements, from Rouillard and Sek (2002).

Chaika *et al.* (2004) evaluated two pavements from a USA Army test course for Gaussianity and stationarity. The two pavements investigated were a Belgian Block surface; an artificial course constructed of bricks and a Perryman3 course which "emulates the characteristics" of off-road travel, shown in *Figure 3-7*. These pavements are not very common in modern countries and are considered to be an extreme transport environment. The Belgian Block surface was found to be nonstationary, while tests for Gaussianity revealed less than half of the sections may be considered non-Gaussian (4/11 sections). On the other hand, the Perryman3 surface is "very rough" and is both nonstationary and non-Gaussian.

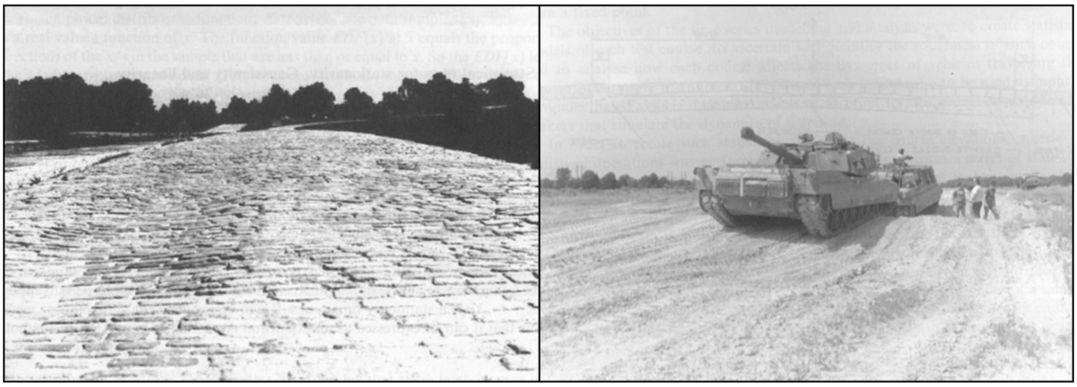

Figure 3-7: Photographs of the Belgian Block (left) and Perryman3 (right) courses, from Chaika *et al.* (2004).

Rouillard (2009) found that nonstationary and non-Gaussian pavement profiles (using three roads in Victoria, Australia) may be modelled as a series of piecewise Gaussian random processes with different rms levels and durations for each section. Rouillard (2009) also developed a novel technique to decompose pavement profiles into a series of Gaussian sections with varying dose levels. Mucka and Granlund (2012) analysed two sets of road elevation data from a highway in Sweden that was in poor condition and then repaired. The PDFs established from the old and repaired wheel paths, while similar in nature, were both found to deviate from the Gaussian. When investigating the nature of longitudinal pavement profiles, the statistical nature is another aspect that must be examined, particularly if the road is very rough.

3.3 ESTIMATING VEHICLE DYNAMIC CHARACTERISTICS

The dynamic characteristics of road vehicles, specifically the sprung mass mode natural frequency and the damping ratio, can be established using various experimental methods. The two most common approaches for establishing the dynamic characteristics of vehicles are:

1) Induce the vehicle to vibrate by means of a suitable obstacle or disturbance and measure the resulting decaying free vibration, which is analysed to extract the damped natural frequency and damping ratio.
2) Subject the vehicle to a known broad-band excitation over a range of frequencies and measure the excitation and response simultaneously to compute the FRF, from which the natural frequency and damping ratio may be obtained by curve-fitting.

Some of the literature examined in this section is concerned with the estimation of the dynamic characteristics of road vehicles in order to assess its road-friendliness. In order to accurately determine the road-friendliness of a vehicle, Cebon (1999, p. 508) contends that a vehicle must travel over a standard test road at various constant speeds in order to measure the distribution of damage induced onto the pavement. The author, however, acknowledges that conducting these experiments is not always possible or feasible. An easier approach outlined by the CEU (1996) is to establish the sprung mass frequency and compare equivalency to heavy vehicles with air suspension.

As discussed in the background (Chapter 2), when evaluating the road-friendliness of a vehicle the emphasis is on estimating the sprung mass frequency and damping ratio of the suspension system. Establishing the FRF allows for estimates of not only the sprung (and unsprung) mass natural frequency and damping ratio of the suspension to be obtained, but also other salient dynamic characteristics of the vehicle provided the sprung and unsprung masses are known.

The FRF is useful for a number of other applications related to vehicle dynamics and the transportation of products or equipment. An important consideration to make when estimating the dynamic characteristics of road vehicles is whether to test the entire vehicle or solely the suspension system. De Pont (1999) investigated this using a simple linear dynamic model, finding that while whole vehicle effects influenced the suspension response significantly, they change depending on the operating conditions, leading the author to state that assessing a vehicle in a particular configuration is of "no more use than a suspension-by-suspension assessment."

LeBlanc (1995) also investigated the proposition of assessing whole vehicles or suspension systems, addressing three key occurrences: wheelbase-filtering, suspension cross-coupling and spatial repeatability. LeBlanc (1995) stated that suspension assessment is "far more practical" and is not affected by wheelbase filtering or suspension cross-coupling; however if spatial repeatability is a valid consideration then the whole vehicle will need to be assessed. The CEU (1996) test methods for evaluating road-friendliness are designed to assess the entire vehicle. Some previously noted difficulties encountered during heavy vehicle suspension testing include standardising the temperature and spring deflection and also applying a simultaneous excitation to all axles (OECD 1992).

This section presents a state-of-the-art review of the various experimental methods used to establish the dynamic characteristics of unmodified road vehicles, with an emphasis on estimating the FRF and the sprung mass natural frequency and damping ratio of the suspension system. This section of the literature review is limited to approaches used to test unmodified vehicles. The various techniques used to analyse the measured data are also discussed. It should be noted that the literature review will not investigate other techniques used to determine the performance of vehicles, such as the dynamic tyre forces or the primary pavement response due to the passage of vehicles.

3.3.1 Response-Only (Transient) Techniques

In order to provide a series of easily accessible approaches to estimate the dynamic characteristics of vehicles, the CEU (1996) outlined a number of experimental methods to induce a transient excitation into a vehicle, allowing the subsequent response to be measured and analysed to determine the sprung mass frequency and suspension damping ratio. The principal benefit of such approaches is the ability to undertake testing at non-specific locations. The CEU directive (and subsequently the VSB11 in Australia which is based on this directive) is designed to assess a heavy vehicle's suspension system for equivalency to air suspensions. De Pont (1992) criticised the assumption made from these directives (CEU 1996; DoTaRS 2004) that air suspensions are the most road-friendly, as it stifles any innovations in suspension design by penalising any other suspension system, regardless of its performance.

3.3.1.1 Experimental Methods

The CEU (1996) outlined three methods to evaluate the road-friendliness of heavy vehicles by subjecting them to transient excitations and analysing the response. The first is the ramp test, where a vehicle is driven at low speed (5 ± 1 km/h) over a specified ramp (with a drop of 80 mm at the end of the ramp) to induce a step excitation on the vehicle and the resulting response is analysed. The next test, known as the pull down test, involves forcing the vehicle down until it is loaded to approximately one-and-a-half times the maximum static load, suddenly released and the resulting oscillations analysed. The final test outlined is the lift and drop test, where the chassis of the vehicle is raised 80 mm above the driving axle, then suddenly released and analysing the resulting response.

Sweatman *et al.* (1994) devised a transient step excitation method where a vehicle is placed on blocks, begins to crawl forward and as soon as the vehicle departs the upper surface, the blocks are simultaneously removed (the blocks have ropes fitted on the side). Despite reasonable response data obtained, the authors acknowledged that the technique is not suitable for general suspension assessment. The main difficulties encountered were due to the complex procedure requiring the coordination of many people to remove the blocks from under the vehicle and also involves a great deal of time and effort to obtain "usable data" (Sweatman *et al.* 1994). The sprung mass acceleration, suspension displacement and wheel forces were measured and compared, with the authors noting that there is a much larger variation in the estimates of the damping ratio compared to the sprung mass frequency.

Woodroffe (1996) used a four-post shaker to simulate a number of test methods in order to investigate the road-friendliness of a trailer with various suspension types (rigid trailing arm air suspension, four spring steel leaf suspension and a rubber walking beam suspension). A simultaneous axle drop test, where the four-posts of the shaker are displaced down by 80 mm, is considered by Woodroffe (1996) to be “a valid test for compliance” with the CEU directive. The results of this test revealed a clear distinction between the mechanical and air suspended sprung mass frequency and damping, however it was noted that there was “considerable variation” in the estimated damping ratios (Woodroffe 1996). The ramp test was replicated by sequentially dropping the axles of the trailer to simulate the test at a speed of 5 km/h. The results of the sequential axle drop test did not yield results that were “as clear and consistent as the simultaneous drop test” (Woodroffe 1996). While the sprung mass frequency estimates were in agreement between the sequential and simultaneous axle drop tests, the damping ratio estimates were not in good agreement (Woodroffe 1996). The author also attempted to drop a single-axle only; but the response of the air suspension from this test was “not readily distinguishable.”

Milliken *et al.* (2001) described the design and implementation of an apparatus to raise all axles of a heavy vehicle to a specified height (48, 80 and 112 mm), drop the vehicle whilst measuring the displacement response using a string potentiometer. The response was analysed using the DFT to determine the sprung mass frequency, while the damping ratio was obtained first using a weighted least squares linear fit on the logarithm of the displacement, then a modified version of the logarithmic decrement method. Milliken *et al.* (2001) encountered numerous difficulties with this test, some of which include the significant duration required to set up the apparatus, issues with the simultaneous release of the platforms and some issues with the use of the string potentiometer to measure the displacement. The authors found that the different drop heights did not generate “significantly different results.” It was also shown that the repeatability of the tests were within ± 7 % and ± 18 % for the damped natural frequency and damping ratio estimates, respectively. Milliken *et al.* (2001) acknowledged that while the apparatus is not portable, it may be installed at a permanent test facility and vehicles could be tested “within an hour.”

Davis and Sack (2004) devised a test to excite an air suspended heavy vehicle (prime mover) with an impulse by driving it at low speed (approximately 5 km/h) across a fixed pipe. The pipe used in the test was 50 mm in diameter; however no recommendation was made as to the most suitable diameter of pipe (nor was another diameter used). Results from the pipe test show the presence of the subsequent axles (2nd, 3rd and 4th) travelling over the pipe, emphasising the difficulty in obtaining uncontaminated estimates of the response from a single axle. Davis and Sack (2004) also conducted a modified version of the ramp test, with a drop height of 65 mm instead of 80 mm due to the convenience of having a drop between the warehouse slabs at the test site. The response data analysed by the authors was the measured air pressure in the high-pressure air lines of the suspension converted to excursions of mass (40 kg incremental excursions). Only the damping ratio was estimated from these tests using the logarithmic decrement. The modified ramp test yielded a response signal that was unable to produce meaningful results in terms of the sprung mass frequency. A heavy vehicle testing rig designed to reproduce the CEU drop test was commissioned by Sweatman, where the vehicle is driven onto a platform and suddenly released (although no direct references exist detailing the testing platform). The testing platform was used to evaluate heavy vehicle suspension systems travelling on the Hume Highway in New South Wales, Australia (Blanksby *et al.* 2006).

The validity of the CEU and other equivalent transient test methods have been scrutinised by many authors. Cole and Cebon (1991) found that a numerical simulation of the three CEU methods produced similar results for a nonlinear heavy vehicle (for two combinations: with a trailer and then a lumped mass on the rear axle of the vehicle). The authors then investigated the amplitude of excitation by reducing the ramp height from 80 mm to 20 mm and found that the reduced drop height resulted in an increase in the sprung mass frequency estimates. Cole and Cebon (1991) explained that this increase is due to the “nonlinear, hysteretic characteristics” that are common in steel leaf springs. Further to the issues described by Cole and Cebon (1991), Woodroffe (1996) also investigated the effect of the ramp height drop and discovered that “in general, the experiments found that the damping ratio decreased with increased drop height.” This would also have an effect on the modified ramp test undertaken by Davis and Sack (2004).

As has been noted throughout the various test methods discussed, there clearly exists greater difficulty in establishing estimates of the damping ratio of the suspension system than the sprung mass frequency (Woodroffe 1996; OECD 1998). Woodroffe (1996) stated that there is difficulty in establishing the road-friendliness when trucks are coupled with a trailer and that this interaction “must be eliminated to accurately assess the performance of a particular suspension.” Cole and Cebon (1991) noted a prominent flaw in the CEU directive in regards to the lack of specification about the loading of the heavy vehicle during the tests, with the authors noting that attaching a trailer does influence the estimates. The validity of the approach undertaken by the CEU was further scrutinised by Cole and Cebon (1991), stating that no known relationship exists between the dynamic characteristics of a vehicle’s suspension system and the subsequent damage induced onto roads. The approach is aimed at determining equivalency to air suspensions, which are considered to be road-friendly (Cole & Cebon 1991). The authors concluded by remarking it is “not clear why the CEU legislators have concentrated on encouraging the use of equivalent air suspensions.”

Gillespie (1985) noted that, for a quarter car model subjected to a smooth and rough road, the sprung mass mode frequency is reduced for the rough road compared to the smooth road. The author suggested this may be due to the greater suspension deflections occurring during travel over the rough road than on the smooth road; “thus it is often observed that some trucks ride better on rough roads than on smooth roads.” De Pont (1999) argued that the CEU tests can be “quite severe and may not reflect the behaviour on roads of good to moderate roughness, which are primarily the ones in need of protection.” Cebon (1993) described another issue with the CEU approach for establishing the sprung mass frequency, namely that during operation “many different natural modes of vibration contribute” and will be dependent upon the speed of the vehicle. Cebon (1993) states “there is no reason to believe that a particular transient input will excite the natural mode(s) that dominate the generation of dynamic tyre forces under highway conditions.”

Several publications since Cole and Cebon (1991) have investigated the relationship between the sprung mass mode frequency and the dynamic tyres forces generated by heavy vehicles. A common approach to describing the dynamic tyre forces was proposed by Sweatman (1983), where the root-mean-squared dynamic tyre force divided by the static force, known as the Dynamic Load Coefficient (DLC), is used. The OECD (1998), using a numerical simulation, found that a “strong relationship exists between the sprung mass frequency and DLC.” *Figure 3-8* shows the relationship between the DLC and the sprung mass frequency for a vehicle with a suspension damping ratio of 0.20.

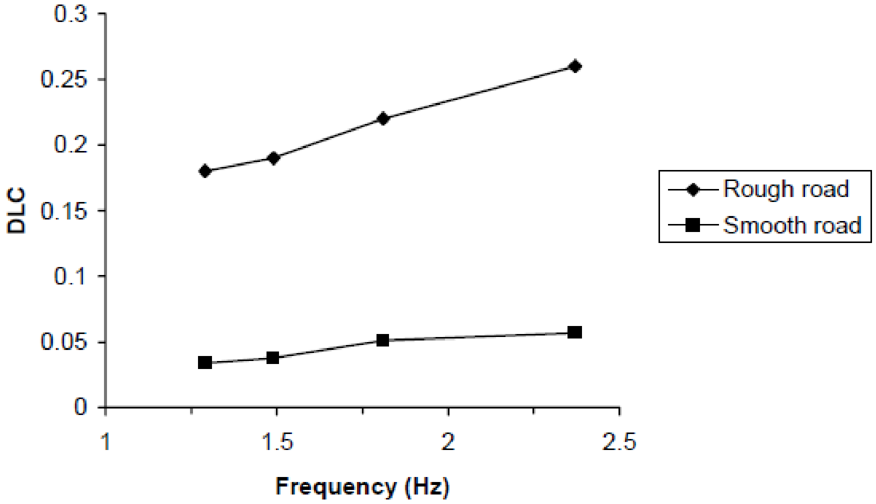

Figure 3-8: The relationship between the sprung mass mode frequency and the DLC for a vehicle with a suspension damping ratio of 0.20, from OECD (1998).

3.3.1.2 Analysis Techniques

The experimental methods described all attempt to induce a transient excitation into the vehicle to elicit a free vibration response that is then analysed to estimate the sprung mass mode damped natural frequency and damping ratio. The CEU (1996) recommends that a heavy vehicle be instrumented with a vertical displacement transducer during the experiments to measure the decaying vibration response. Although any instrument that is able to measure dynamic motion (displacement, velocity and acceleration) can be used, it is beneficial to measure the acceleration as is not a relative quantity. The sprung mass damped natural frequency, according to the CEU (1996), can be determined via "the time interval between the first and second compression peaks." Instead of using only two compression peaks, the elapsed time for as many successive oscillations that are measured may be used to establish the damped natural frequency. The CEU approach only uses a small amount of the measured data, so an alternative method to analyse the data is to compute the Fourier Transform (FT) of the free response of the vehicle. The FT converts a signal from the time domain to the frequency domain by decomposing the signal into a series of superpositioned sinusoidal and co-sinusoidal waves. The FT of a continuous signal is given in Equation 3-22 (Bendat & Piersol 2000, p. 403).

$$X(f)=\int_{-\infty}^{\infty} x(t)e^{-j2\pi ft}\,dt \tag{3-22}$$

When dealing with signals that are discretely sampled and have a finite duration, the FT is not applicable. The DFT is instead used and is given in Equation 3-23 (Bendat & Piersol 2000, p. 404).

$$X(f_k)=\sum_{n=0}^{N-1} x(n\Delta t)e^{\frac{-j2\pi k}{N}}\,dt \qquad k=0,1,2,\ldots,N-1 \tag{3-23}$$

note that the results are valid only up to the Nyquist frequency ($k = N/2$).

Each coefficient of the DFT is spaced by a factor of Δf, known as the frequency resolution, which is determined using the relationship described in Equation 3-24 (Bendat & Piersol 2000, p. 404).

$$\Delta f=\frac{1}{N\Delta t}=\frac{S_f}{N}=\frac{1}{T_r} \tag{3-24}$$

Transposing Equation 3-24 yields a clearer relationship between the temporal and frequency resolutions, shown in Equation 3-25.

$$\Delta f \; T_r = 1 \tag{3-25}$$

Interestingly, this relationship in Equation 3-25 follows Heisenberg's uncertainty principle, where the frequency resolution and the duration of the signal under analysis are limited by each other. In order to obtain a finer frequency resolution, the duration of the signal must be increased. In order to efficiently determine the frequency components from the DFT, the Fast Fourier Transform (FFT) was developed. The most widely-used method was established by Cooley and Tukey (1965), which is a special case of the general FFT algorithm specifically designed to be implemented using binary digital computers. An advantage in processing is gained when the number of points used in the FFT follows the relationship outlined in Equation 3-26.

$$N = 2^{m_p} \tag{3-26}$$

where N is the number of points in the FFT and m_p is an arbitrarily chosen integer.

Another benefit of the FFT is that the phase information of the signal is retained, allowing for the signal to be transformed between the time and frequency domains (Randall 1987, p. 147). A detailed description of the Cooley-Tukey FFT algorithm can be found in Cooley and Tukey (1965) and Bendat and Piersol (2000, pp. 405-413). When measuring any signal, the sampling frequency, at a minimum, must be set to at least twice the expected natural frequency of the system according to Shannon's Sampling Theorem (Randall 1987, pp. 29-30). Also, the response signal should always be inspected to identify whether the effects of other modes of vibration are present. If this is the case then appropriate filtering should be applied in order to isolate the sprung mass of the vehicle. The entire duration of the data can be used, or a smaller section of the response can be selected for analysis. It is important to remember that the temporal resolution is inversely proportional to the spectral resolution and so the longer the duration, the better. This will, of course, also be limited by the vehicle's ability to reduce the oscillations (damping ratio of the suspension) and the level of excitation applied.

A common issue associated with Fourier analysis is spectral leakage, however, since these response-only (transient) methods can be measured with a zero-value start and end, it is not necessary to apply a windowing function to the response. One difficulty with the response-only (transient) methods is the limited scope for increasing the duration of the signal by recording for a longer time to increase the frequency resolution. To overcome this, an alternative method may be implemented to increase the length of data available for analysis. Zero-padding is a technique that attempts to artificially increase the spectral resolution by appending a sequence of zeros to the end of the signal under analysis. The purpose of zero-padding is to provide an "appearance of a spectrum with higher resolution" by increasing the number of frequency points within a spectrum (Semmlow 2005, pp. 96-97). Weeks (2007, pp. 202–203) provides a detailed mathematical justification of zero-padding.

Once the response spectrum of the vehicle is established, the Peak Picking (PP) method is the most commonly used technique to establish the damped natural frequency of the system by simply identifying the frequency location of the maximum amplitude (He & Fu 2001, p.163). This process is not always straightforward to undertake; particularly when modes of vibration are closely spaced it can become difficult to detect each mode (Alam *et al.* 2009). In order to establish the natural frequency from the damped natural frequency, the damping ratio must first be determined. Two common approaches to estimate the damping ratio using transient response data are discussed; the logarithmic decrement or the instantaneous magnitude envelope. The logarithmic decrement is a common analysis technique that is used to estimate the damping ratio from the free vibration response of a system. The logarithmic decrement, δ, is a representation of the "rate at which the amplitude of a free-damped vibration decreases," and is given in Equation 3-27 (Rao 2005, p. 146).

$$\delta = \frac{1}{m}\ln\left(\frac{x_1}{x_{m+1}}\right) \tag{3-27}$$

Once the value of the logarithmic decrement has been determined it is then used to establish the damping ratiom, shown in Equation 3-28 (Rao 2005, p. 147).

$$\zeta = \frac{\delta}{\sqrt{(2\pi)^2 + \delta^2}} \tag{3-28}$$

A linear approximation of the logarithmic decrement may be used that is considered valid for low levels of damping, given in Equation 3-29 (Rao 2005, p. 147).

$$\zeta \cong \frac{\delta}{2\pi} \tag{3-29}$$

The CEU (1996) states that the damping ratio can be obtained using the "amplitude ratio" of the successive peaks, which is based on the approximation of the logarithmic decrement from Equation 3-29, shown in Equation 3-30.

$$\zeta = \frac{1}{2\pi}\ln\left(\frac{A_1}{A_2}\right) \tag{3-30}$$

A comparison of the actual and approximated relationships between the logarithmic decrement and the damping ratio (Equations 3-28 and 3-29, respectively) is presented in *Figure 3-9*, along with the calculated error between the actual and approximated estimates of damping ratio.

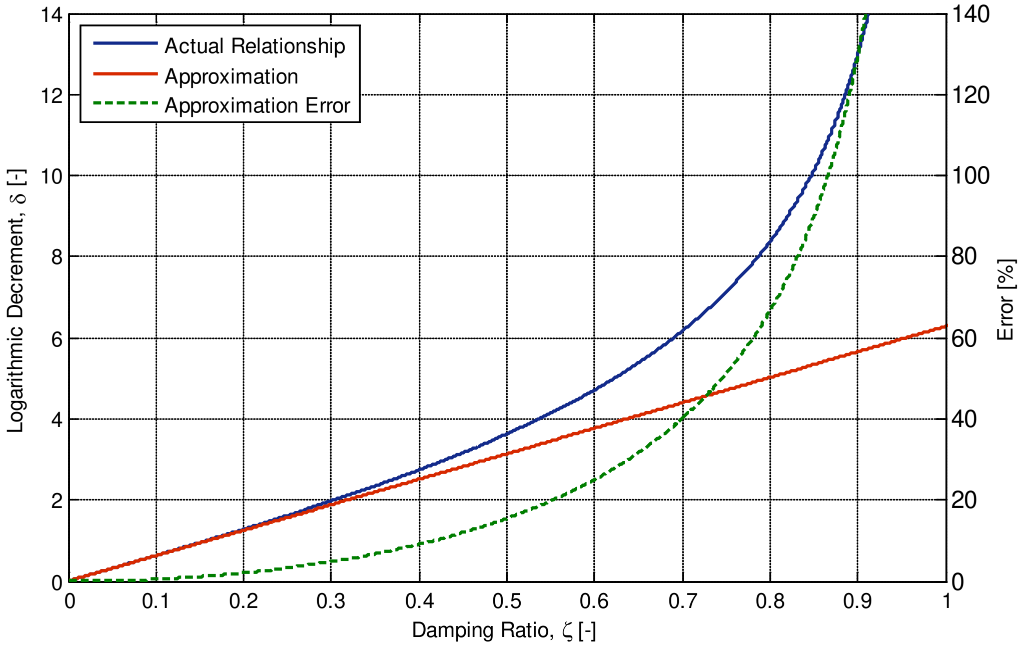

Figure 3-9: The relationship between the damping ratio and the logarithmic decrement (blue) and the linear approximation used by the CEU (red), along with the error between the actual and approximated relationships (green). Note the different vertical axes on either side.

As mentioned, Rao (2005, p. 147) specified that the use of the linear approximation is for low levels of damping (when $\zeta << 1$). By visual observation, there is no discernable difference at low levels of damping until around 0.35 – 0.40. The use of the linear approximation will result in significantly incorrect calculations for damping ratios above 0.30. While this remains unlikely for vehicles, it may cause concern when estimating vehicles whose suspension systems are particularly highly damped or when the hydraulic dampers have been removed from the vehicle.

An alternative approach to estimate the damping ratio is the Hilbert envelope technique, which makes use of the entire measured decayed response signal. For a real-valued time signal, $x(t)$, its Hilbert Transform is defined in Equation 3-31 (Thrane 1984; Bendat &Piersol 2000, p. 518).

$$\mathrm{H}\left[x(t)\right]=\tilde{x}(t)=\int_{-\infty}^{\infty}\frac{x(\tau)}{\pi(t-\tau)}=\frac{1}{\pi}x(t)*\frac{1}{t} \tag{3-31}$$

where the * denotes convolution.

Unlike the FT, the Hilbert Transform does not transform between domains but instead assigns a complementary imaginary component to a given real part (or vice versa) of a signal by shifting each component by a quarter of a period (90° phase shift) (Feldman 2011, pp. 92-93). This phase shift creates a complex analytic signal, $a(t)$, given in Equation 3-32.

$$a(t)=A(t)e^{j\phi(t)}=x(t)+j\tilde{x}(t) \tag{3-32}$$

The FT of which is *A(f) = X(f) + sign(f)X(f)*. The analytical envelope, $A(t)$, and the instantaneous phase, $\phi(t)$, of the analytical signal can then be established via Equations 3-33 and 3-34, respectively.

$$A(t)=\sqrt{x^2(t)+\tilde{x}^2(t)} \tag{3-33}$$

$$\phi(t)=\arctan\left(\frac{\tilde{x}(t)}{x(t)}\right) \tag{3-34}$$

For a detailed mathematical explanation of the Hilbert Transform, see Thrane (1984). The instantaneous natural frequency of the system, ω_0, is determined using Equation 3-35.

$$\omega_0(t)=\frac{d\phi(t)}{dt} \tag{3-35}$$

To estimate the damping ratio of an SDoF system, the envelope of the analytic signal is used, given in Equation 3-36 (Rao 2005, p. 143).

$$A(t) = X e^{-\zeta\omega_n t} \tag{3-36}$$

If the natural logarithm is taken of both sides of Equation 3-36, then Equation 3-37 is obtained.

$$\ln\left(A(t)\right) = \ln\left(X\right) - \zeta\omega_n t \tag{3-37}$$

By differentiating Equation 3-37 with respect to time, Equation 3-38 is established.

$$\frac{d}{dt}\left(\ln\left(A(t)\right)\right) = -\zeta\omega_n \tag{3-38}$$

Equation 3-39 is obtained by substituting the relationship between the damped natural frequency and natural frequency from Equation 3-6 into Equation 3-38.

$$\frac{d}{dt}\left(\ln\left(A(t)\right)\right) = -\zeta\frac{\omega_d}{\sqrt{1-\zeta^2}} \tag{3-39}$$

Finally, by rearranging the relationship in terms of the damping ratio Equation 3-40 is obtained.

$$\zeta = \pm\sqrt{\frac{\left(\frac{d}{dt}\left(\ln\left(A(t)\right)\right)\right)^2}{{\omega_d}^2 + \left(\frac{d}{dt}\left(\ln\left(A(t)\right)\right)\right)^2}} \tag{3-40}$$

note that since $\zeta > 0$, any negative solution is ignored.

The natural frequency of the system may then be calculated from Equation 3-6 using the estimated values of the damped natural frequency and damping ratio.

3.3.2 Excitation-Response Techniques

The second category of approaches that can be used to estimate the dynamic characteristics of vehicles are known as excitation-response techniques. These techniques are able to establish not just the dynamic characteristics of vehicles, but also the FRF as both the excitation and response are simultaneously measured. The following section describes the various excitation-response experimental methods and analysis procedures that are available to establish the dynamic characteristics of road vehicles.

3.3.2.1 Experimental Methods

One of the most common approaches to establish the FRF is to place or mount the system onto a suitable vibration table and subject it to a known excitation. There are four main types of vibration testing: resonance search, vibratory impact, swept-sine and random vibration (Caldicott 1991). The resonance search and vibratory impact tests are not considered to be relevant to this thesis and so will not be discussed further. For road vehicles, this is usually undertaken with vibration tables that are configured to provide the necessary vertical motion at the wheels. Modern vibration controllers allow the user to specify any spectral shape (and level) to excite the table. The excitation produced by these controllers is normally-distributed (Gaussian) and both the excitation and the system's response are simultaneously measured to compute the FRF using Fourier analysis.

There are numerous approaches that may be implemented to excite a system using a sinusoidal excitation. The classical method to measure the FRF is to use a stepped-sine excitation, where the system is excited by a series of discrete sinusoids of fixed amplitude and frequency (Ewins 1995, p. 143). The excitation is stepped "from one discrete value to another in such a way as to provide the necessary density of points on the frequency response plot" (Ewins 1995, p. 143). This approach can be one of the slowest to undertake and depends on the time required for the system to settle before a new frequency can be selected (Ewins 1995, p. 143). Furthermore, the time to undertake this test is also dependent on how many discrete frequencies are chosen for measurement. Ewins (1995, p. 144) suggested that around resonance, the frequency interval should be spaced finely and outside the region greater frequency intervals can be used. Ewins (1995, pp. 143-144) also described some causes of unwanted transients contaminating the response once a new frequency has been selected, such as the speed at which the changeover from one frequency to the next is made, if the frequency is close to the system's natural frequency and also if the damping of the system is quite small. The presence of transients during a stepped-sine test usually warrants attention only when the damping ratio of the system is very small (Ewins 1995, p. 144).

A slow sine-sweep is another commonly-used excitation for establishing the FRF of a system, involving the use of a vibration controller (sweep oscillator) to provide a sinusoidal command signal whose frequency is "varied slowly but continuously through the range of interest" (Ewins 1995, pp. 144-145). Ewins (1995, pp. 145-147) discussed the various sweep rates that can be set and the different types of sweeps that may be used, such as linear or logarithmic, and noted that if care is not exercised when selecting the sweep rate (i.e. the rate is too slow or too fast) then a distorted FRF may be obtained. Sine-chirp is another excitation that can be used, which essentially is "a fast sweep from low to high frequency within one sample interval of the analyser" (Avitabile 1999). The sine-chirp has a short duration due to the fast sweep through the frequency range and, according to Ewins (1995, p. 157) it allows for "the possibility of greater control of both amplitude and frequency content of the input."

Quinn and Zable (1966) used a stepped-sine excitation over a range of relevant frequencies to establish the transfer function of a vehicle. Woodrooffe (1996) used a four-post shaker and subjected various heavy vehicle trailer configurations (different suspensions) to constant displacement, in-phase and out-of-phase (lead and trailing axles excited 180° out-of-phase) sine-sweeps between 0.5 – 20 Hz. Various displacement amplitudes were used (1, 2, 3, 4, 6 and 8 mm) and the rate of change was 5 Hz per minute (Woodrooffe 1996). The results indicated the in-phase 1 mm constant displacement obtained the best results in identifying the sprung and unsprung natural frequencies, while the out-of-phase experiments were unable to obtain these frequencies.

The OECD (1998) described the same approach to Woodrooffe (1996) as being a suitable test to determine the dynamic characteristics of heavy vehicles, notably the sprung and unsprung masses. In assessing the performance of road-friendly suspensions, Sweatman *et al.* (2000) described the use of a vibration shaker to perform a sine-sweep test from 0 – 25 Hz to excite a vehicle. The OECD (1998) declared that while "constant amplitude sinusoidal sweep excitation shows promise as a suspension test, work is still needed to define appropriate criteria for suspension road-friendliness using this test." The use of a sine-sweep excitation was once considered an "easier and cheaper" approach compared to random vibration excitation for testing (Caldicott 1991). However, reduction in the cost of instrumentation and computing combined with increased experience and understanding of random vibration testing and its more realistic representation of the environment has led to its increasing use as a valid alternative (Caldicott 1991).

For random vibration testing, band-limited white noise (acceleration) is most commonly used and applies equal energy at all frequencies within the specified frequency bandwidth. Spectral descriptions of road profiles, used to drive vibration shakers, are well established and are able to be directly applied to frequency-domain simulations of vehicle response (Cebon 1999, p. 28). The standard spectral description of an average road profile is outlined by the ISO under standard 8608 (1995). Another alternative is to use a measured pavement elevation profile. Woodroffe (1996) used a four-post shaker to excite a heavy vehicle with a trailer using three actual measured road profiles and three synthetic road profiles representing "generic good, average and poor roads" based on the ISO standard 8608 (1995). The results from both sets of data "compare favourably" however the dynamic axle loads during these tests were found to be higher than expected, believed to be caused by the truck-trailer interaction (Woodroffe 1996).

Establishing an accurate FRF using random vibration testing relies on good coherence. Low coherency may occur due to transducer issues, a highly nonlinear system or uncorrelated inputs to the system such as engine vibration (Sayers 1988). Rouillard (2002) investigated various excitation signals as applied to nonlinear cushioning systems and found significant differences in the system FRF, which was attributed primarily to the nonlinear character of the material under investigation. The suspension systems of vehicles are often highly nonlinear, further complicating the issue of estimating the dynamic characteristics (Cebon 1999, p. 511). De Pont (1999) also pointed out that vehicle suspensions are nonlinear and as a result the response is dependent on the level of excitation and some frequency shifting may occur. Rouillard and Sek (2010) showed that, for a small transport vehicle, the shape (white, violet and brown acceleration spectra – see Appendix A for a full description of the colours of noise) and level of the excitation PSD function had no significant effect on the estimated FRF. The authors did not attempt to establish the level or type of nonlinearity (if any) in the vehicle.

The major benefit of the use of vibration shakers is the ability to recreate the environment more realistically as opposed to the transient (response-only) techniques. However, the impracticality of measuring the FRF of heavy vehicles is a significant limitation of such shaker tests. Woodroffe (1996) recognized that the high capital involved in acquiring such systems capable of testing heavy vehicles is a major limiting factor in their use. Another limitation of vibration shakers is that they must remain in a fixed location; they are not able to be easily transported for testing in multiple locations.

3.3.2.2 Analysis Techniques

Various analytical methods are available to establish the transmissibility FRF (and dynamic characteristics) of an SDoF system when excited by either random or sinusoidal vibration and the excitation and response are simultaneously measured. The various methods used to compute the FRF from the measured excitation and response data are discussed, along with any considerations that must be made. As the FRF is the ratio of the response to the excitation, it is important to consider what is measured. Depending on the application, it may be of interest to measure the excitation force and the response acceleration, or the excitation displacement and the response acceleration may require measurement. For this thesis, the most relevant FRF to use is the transmissibility FRF which is obtained when the excitation and response are measured using the same units of motion.

This section describes the process to analyse the data obtained when exciting a system using random vibration. Establishing the FRF of the system depends on the method of excitation used, for example random vibration requires a different analysis approach compared to a sine (or swept-sine) excitation. Considering a constant-parameter linear system, the dynamic characteristics can be defined by an impulse response function, $h(\tau)$, described in terms of the response of the system, $y(t)$, at any time due to a unit impulse excitation applied at a time τ before, shown in Equation 3-41 (Bendat & Piersol 2000, p. 29).

$$y(t) = \int_{-\infty}^{\infty} h(\tau)\,x(t-\tau)\,d\tau \tag{3-41}$$

While the impulse response function is able to establish the dynamic characteristics in the time domain, it is also possible to establish them in the frequency domain via the FRF. To establish the FRF of a system, the FT of the impulse response function is computed, shown in Equation 3-42 (Bendat & Piersol 2000, p. 31).

$$H(f) = \int_{0}^{\infty} h(\tau)\,e^{-j2\pi f\tau}\,d\tau \tag{3-42}$$

If, instead, the FT is taken of both sides of Equation 3-41, the FRF can be established in terms of the excitation, $E(f)$, and response, $Y(f)$, shown in Equation 3-43.

$$Y(f) = H(f)E(f) \tag{3-43}$$

Finally, rearranging Equation 3-43 yields the FRF in terms of the ratio of the excitation and response, presented in Equation 3-44.

$$H(f) = \frac{Y(f)}{E(f)} \tag{3-44}$$

In some cases, it may be beneficial to modify the FRF from the general relationship specified in Equation 3-44. Randall (1987, p. 240) describes two variations that can be implemented to calculate the FRF using convolution. The first FRF, denoted as $H_1(f)$, is obtained by multiplying both the numerator and denominator of Equation 3-44 by the complex conjugate of the excitation, presented in Equation 3-45.

$$H_1(f) = \frac{Y(f)}{E(f)} . \frac{E^*(f)}{E^*(f)} \tag{3-45}$$

Randall (1987, p.24) stated that the second variation, $H_2(f)$, is obtained by multiplying both the numerator and denominator in Equation 3-44 by the complex conjugate of the response, shown in Equation 3-46.

$$H_2(f) = \frac{Y(f)}{E(f)} . \frac{Y^*(f)}{Y^*(f)} \tag{3-46}$$

Randall (1987, p. 241-247) discussed the two variations of the FRF and stated that $H_1(f)$ is better for minimising the effect of extraneous noise in the measurements, while $H_2(f)$ is best used to minimise the effect of spectral leakage.

The ratio of these two FRFs is always equal to the coherence, shown in Equation 3-47 (Randall 1987, p. 240).

$$\gamma^2 = \frac{H_1(f)}{H_2(f)} = \frac{\left|G_{EY}(f)\right|^2}{G_{EE}(f)G_{YY}(f)} \tag{3-47}$$

where $G_{EY}(f)$ is the single-sided cross spectrum and $G_{EE}(f)$ and $G_{YY}(f)$ are the single-sided autospectra of the excitation and response, respectively.

Various analysis parameters must be carefully considered when establishing the FRF of a system. As the FRF is established using the FFT (the DFT and FFT are discussed in detail in the previous section on response-only (transient) analysis techniques), a number of considerations must be made before the measurements are undertaken.

Spectral averaging is often implemented when establishing the FRF in order to reduce the influence of noise and other effects and so, when dealing with random excitation, the excitation and response of a system should be measured for an extended period of time. Spectral averaging is used to minimise the statistical uncertainty inherent in random data. The spectral uncertainty or error, ε_r, is equal to the inverse of the square root of the number of distinct spectral averages, N_d, provided in Equation 3-48 (Bendat & Piersol 2000, pp. 306-308).

$$\varepsilon_r = \frac{1}{\sqrt{N_d}} \tag{3-48}$$

The original relationship between the temporal and frequency resolutions, previously outlined in Equation 3-24, does not take into account spectral averaging. With the introduction of spectral averaging, the temporal resolution is now dependent upon the duration of each average, also known as the sub-record length, T_{sr}, and the number of independent averages, given in Equation 3-49.

$$T_r = N_d\, T_{sr} \tag{3-49}$$

Substituting the sub-record length into Equation 3-49, the following relationship for the frequency resolution with spectral averaging is obtained, shown in Equation 3-50.

$$\Delta f = \frac{N_d}{T_r} = \frac{1}{T_r \varepsilon_r^{\,2}} \tag{3-50}$$

As discussed briefly in the response-only (transient) analysis techniques section, the use of windowing is important to minimise spectral leakage. Spectral leakage is a consequence of taking a finite section of a time-history coupled with the assumption of periodicity. A "practical solution" to this issue is the use of windowing (Ewins 1995, p. 137). Using the DFT and applying no windowing function to the signal prior to analysis is akin to applying a rectangular window which possesses a value of one (unity) across the duration (Randall 1987, p. 157). This rectangular window possess large side lobes in the DFT and allows for power to leak at frequencies well separated from the main lobe into adjacent bands (Randall 1987, p. 155). This leakage of power may cause significant distortions in the estimated frequency spectrum. The role of windowing (also known as time-history tapering) is to eliminate any discontinuities at the ends of each sub-record and reduce side lobe leakage. While various windows are available for use, the Hanning window is the most common and Randall (1987, p. 157) considered it to be "an excellent general purpose window." The process of windowing reduces the overall magnitude in each spectrum and requires a multiplication factor to restore this loss.

Two additional enhancement techniques can also be implemented to improve the FRF estimates obtained; zero-padding the data and overlapping of spectral averages. The requirement to maintain a fine temporal resolution by increasing the sub-record length will result in a decreased number of averages, increasing the spectral uncertainty of the estimates. Overlapping of averages seeks to provide an increased number of averages without increasing the duration required for analysis. Each data record is divided into equal segments that overlap one another, rather than dividing the records into independent segments. The role of overlapped averages, in a statistical sense, retrieves most of the information lost due to windowing (Randall 1987, p. 175; Bendat & Piersol 2000, p. 430). Randall (1987, p. 175) stated that "overlaps greater than 50 % generally give a more uniform overall weighting function, but no appreciable improvement in statistical error." A numerical and experimental study undertaken by Lamb *et al.* (2010) found that the use of zero-padding and overlapped spectral averages improves the modal parameter extraction results.

The following section describes the various analysis procedures and considerations required for establishing the FRF of a system when excited by a sine-based excitation. While the same relationship is used (Equation 3-44), it should be noted that as sine-based excitations will satisfy the periodicity requirement of the FFT, no spectral leakage will occur as long as complete cycles are used and there is no need to apply a windowing function to the excitation and response data. An alternative approach that can be used is to determine the ratio of the peak acceleration (or rms) of the excitation and response at each frequency. This involves subjecting the system to a series of discrete sinusoidal excitations at various frequencies. The peak or rms ratio at each discrete frequency is combined to construct the transmissibility FRF of the vehicle at all the selected excitation frequencies during the test. This technique can be rather time-consuming and cumbersome, particularly if the controller is manually operated and a fine frequency resolution is required. Sweatman *et al.* (2000) suggested that when a swept-sine excitation is applied to a vehicle the phase spectrum can be analysed to determine the level of damping in the suspension system whereas the adhesion spectrum (the adhesion is the ratio of the minimum dynamic tyre force at a given frequency to the static weight of the vehicle) can be used to determine the frequencies of the sprung and unsprung masses.

There are three common analysers that are used to establish the magnitude and phase from the excitation and response from a sine-based test. The first analyser is a tracking filter, which is a (generally analogue) device used to generate the FRF of a system subjected to a slow sine-sweep excitation. The oscillator (or controller) used to generate the sine-sweep is coupled with a set of narrowband filters, through which the transducer signals are passed, and the centre frequency of the filters are continuously adjusted in order to match the current frequency of the excitation (Ewins 1995, p. 128). The tracking filter is able to establish both the magnitude and phase of the component of each of the transducer signals related to the actual excitation source (Ewins 1995, p. 129).

The second analyser, the Frequency Response Analyser (FRA), is different to tracking filters in that the processing is performed digitally. The command signal (sine wave at the desired frequency) is digitally generated within the FRA and output through a digital-to-analogue converter (Ewins 1995, p. 129). Within the FRA, the excitation and response signals are digitised and correlated numerically with the outgoing signal (digitally generated) to eliminate all the components in the incoming signals that are not at the frequency of the sine wave (Ewins 1995, p. 129). The advantage of using an FRA over a tracking filter is that both channels are treated in exactly the same way; there is no need to tune the two tracking filters to obtain accurate data (Ewins 1995, p. 129).

As with many similar instruments, the measurement of the FRAs can be improved by performing the correlation over a longer duration (Ewins 1995, p. 130). The third analyser that may be implemented is a spectrum analyser, which is significantly different than the FRA (Ewins 1995, p. 130). Unlike the FRA, the spectrum analyser simultaneously measures all the frequency components in a complex time-varying signal (Ewins 1995, p. 130). The spectrum analyser, which can be digital or analogue, will produce a spectrum with the relative magnitudes of the range of frequencies present in the signal (Ewins 1995, p. 130). The digital spectrum analyser is commonly in use today and uses the DFT to obtain many important properties of signals, including establishing the FRF of the system.

Once the FRF of the system has been established, numerous techniques are available for the extraction of the dynamic characteristics of the system, namely the natural frequency and damping ratio of the first mode. Two common approaches to estimating the dynamic characteristics are discussed. The simplest approach is to use the PP method to estimate the natural frequency of the system by identifying the location of the maximum amplitude of the FRF (He & Fu 2001, p. 163). To estimate the damping ratio, the half-power bandwidth method can be used. This method uses the half-power points of the FRF, located at either side of the resonance (f_{res}) amplitude at frequencies f_1 and f_2, divided by the square-root of two, shown in Equation 3-51 (Bendat & Piersol 2000, p. 37).

$$\left|H(f_1)\right|^2 = \left|H(f_2)\right|^2 = \frac{1}{2}\left|H(f_{res})\right|^2 \tag{3-51}$$

Once the half-power point frequencies have been established, the damping ratio can be approximated via Equation 3-52 (Bendat & Piersol 2000, p. 37). It is important to recognise that this is only an approximation and is limited to systems with “light damping” (Bendat & Piersol 2000, p. 37). Once the damping ratio has been established, the natural frequency can be found using Equation 3-6.

$$\zeta \approx \frac{f_2 - f_1}{2f_{res}} \tag{3-52}$$

where the relationship is valid for $\zeta \leq 0.1$.

The second approach to establish the dynamic characteristics is to apply a curve-fit to the transmissibility FRF. The magnitude and phase of the transmissibility FRF of an SDoF system is presented in Equation 3-53 and Equation 3-54, respectively (Rao 2005, p. 240).

$$T(f)=\sqrt{\frac{1+(2\zeta r)^2}{(1-r^2)^2+(2\zeta r)^2}} \tag{3-53}$$

$$\phi(f)=\arctan\left(\frac{2\zeta r^3}{1+(4\zeta-1)r^2}\right) \tag{3-54}$$

where the frequency ratio is $= f/f_n$.

The magnitude of the transmissibility FRF (Equation 3-53) is of significant interest, as it may be used to provide a curve-fit (via least-squares regression) to extract the sprung mass mode natural frequency and damping ratio. The data that is used for the curve-fit must be selected by the user beforehand, as not all of the data provided by the FRF is relevant for modal parameter estimation. The region of resonance is almost always selected, whether by manual selection or by using a set number of points either side of the maximum magnitude of the transmissibility FRF (Ewins 1995, p. 190). For the estimation of the modal parameters of the system via curve-fitting, it is recommended that no fewer than six data points be used (Ewins 1995, p. 190).

3.3.3 In-Service Response Techniques

The response-only (transient) and excitation-response techniques are the two most common types of approaches used to estimate the dynamic characteristics of road vehicles. One of the key criticisms of the response-only (transient) methods is that they do not attempt to determine the dynamic characteristics of a vehicle under real in-service conditions (Cebon 1999, p. 511). As for the excitation-response methods, particularly for heavy vehicles, they are limited to the few locations where suitable (i.e. large) vibration tables exist. There exists great motivation for research into measuring and analysing the response of a vehicle during normal operation to estimate the dynamic characteristics.

3.3.3.1 Experimental Methods and Analysis Techniques

It is well known that a linear system has a directly proportional relationship between the excitation and the response (Equation 3-7). Houbolt (1955) applied this relationship to the taxiing of aeroplanes, making a further assumption that if the transmissibility is independent of the speed of the plane; then the speed will be linearly proportional to the response spectrum. Houbolt (1955) suggested the mean-squared response will therefore be linearly proportional to the velocity, and tests undertaken using a Boeing B-29 aeroplane at various constant speeds exhibited a linear relationship up to taxiing speeds of around 50 mph. Over time, this relationship has been examined by a number of authors in the field of vehicle dynamics, notably Gillespie (1985) and Sayers (1988). Dodds and Robson (1975) acknowledged that since the components of vehicles are generally nonlinear, calculating the output spectrum using Equation 3-7 will establish "an average linearised" spectrum which will approximate "that which would be measured in service."

For in-service experimental testing, as the length of the test section (road) increases, the statistical reliability of the estimate also increases (Quinn & Zable 1966). It can be difficult to locate a road that is long enough without the presence of various factors that will disrupt the in-service measurement of constant speed testing. One common factor is that the flow of traffic may prevent the test vehicle from travelling at a constant speed. Other issues, such as steep ascents or descents, traffic lights and sharp turns, among other factors, may also prevent the vehicle from travelling at a constant speed. This highlights the benefits of using a purpose-built test track, where vehicles are able to travel at constant speed without interruption and can reduce the nonstationary component of the dynamic response.

Virchis and Robson (1971) developed a simple linear spring-mass-damper model with similar dynamic characteristics to a Sunbeam Imp vehicle and investigated the effect of the change in constant speed on the dynamic characteristics. The authors found that the deviations of the mean-square response values were "not large" which suggests that such nonstationary effects may be neglected. Quinn and Zable (1966) attempted to determine the dynamic tyre force PSD function using the differential air pressure. The vehicle was driven over a section of pavement at various constant operating speeds; while the nonlinear characteristics of the vehicle influenced the relationship, the results indicated that there was only a slight change in the response spectrum between operating speeds of 40, 50 and 60 mph (Quinn & Zable 1966).

Marcondes (1990) proposed an experimental approach to estimating the acceleration levels in truck-semitrailer beds using a combination of in-service response data and measured profile elevations. A truck-semitrailer combination (with 6 and 4 wheels, respectively) was used to undertake the in-service experiments, while the vibration acceleration was measured in the trailer bed above the axles. A profilometer was used to establish the pavement profiles for twenty highway sections in Michigan, USA. To calibrate the approach, Marcondes (1990) measured the pavement elevation profiles and computed the PSD function of each pavement; then measured the acceleration of the trailer bed while travelling at three constant speeds (45, 52 and 60 mph) to establish the transmissibility.

The transmissibilities established for the selected pavements illustrate the significant nonlinear behaviour of the vehicle; with variation between each speed travelled over a single pavement observed. The author then developed a model to predict the acceleration PSD functions of the truck bed at two constant speeds (55 and 60 mph) using the transmissibility obtained at an operating speed of 52 mph. Although the author states that the predicted acceleration PSD functions are "very close to the actual values" there is considerable variation between the predicted and actual estimates, including frequency shifting, particularly at low frequencies (Marcondes 1990). A sample of the predicted and obtained acceleration PSD functions for two pavement sections are shown in *Figure 3-10.*

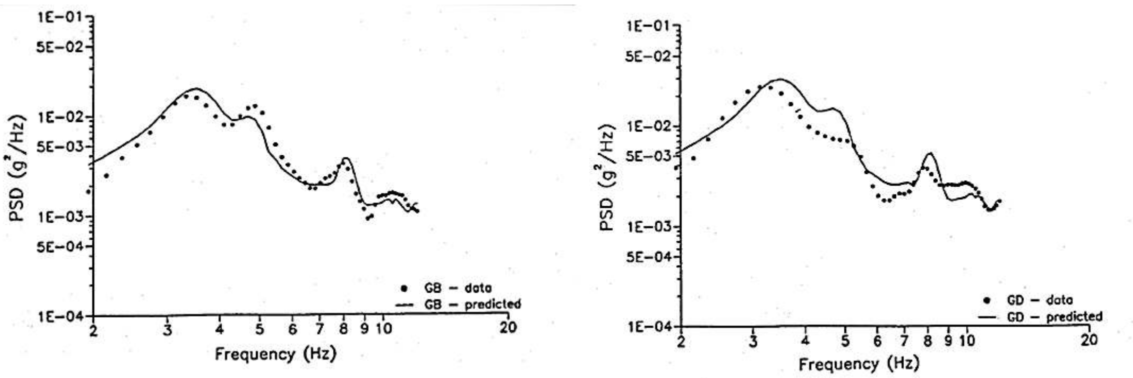

Figure 5.11 Predicted and obtained PSD acceleration for section VGB.

Figure 5.13 Predicted and obtained PSD acceleration for section VGD.

Figure 3-10: The predicted and obtained acceleration PSDs for two different pavement sections, from Marcondes (1990).

Davis and Sack (2004) conducted a small number of in-service experiments by driving a semi-trailer over a number of suburban roads with a system to record the suspension airbag pressure. The instrument used in the study was originally designed for static applications as made evident by the slow response and poor resolution of the signal and is not suitable for measuring the dynamic response of vehicles. The vehicle speed during the in-service experiments is stated as being up to 60 km/h, suggesting that the vehicle was not travelling at a constant speed during the experiments. The resulting frequency responses presented do not provide any useful information despite some optimistic conclusions from the authors.

Davis *et al.* (2007) performed a similar series of experiments as those by Davis and Sack (2004), except in this case an accelerometer was mounted onto the chassis of the vehicle to measure the vibration response. The authors conducted a series of in-service experiments over “typical, uneven road sections,” with various vehicles at speeds ranging between 40 – 90 km/h. The application of Fourier analysis to the random vibration responses appears to be flawed making it impossible to draw meaningful conclusions about the location of peaks (natural frequencies), let alone the damping ratios. In the papers, the authors do not provide the specific location or accurate description of the roads, merely an elementary indication of the pavement roughness. Another issue with the experiments is the lack of repeatability; the operating speeds of the vehicles vary during the experiments and it is therefore impossible to attempt to replicate them. Furthermore, the authors do not disclose a sound scientific basis for these in-service road tests; only the assumption that by “driving the combination on some normal, uneven suburban roads” it was “hoped that this would apply a random signal” to the vehicle (Davis & Sack 2004).

Gonzalez *et al.* (2008) proposed that the PSD of a longitudinal pavement profile could be obtained using only the vertical response acceleration of a vehicle, based on Equation 3-7. The outcome the authors were seeking was to determine the classification of the road as described in ISO standard 8608 (1995). A numerical model of a half car (side car) was developed and the vertical acceleration was measured at the front and rear axles and at the body. The transfer function was obtained by combining the measured profile with the acceleration measurements (for each of the front and rear axles and the body). The effect of travelling at different constant speeds was also investigated by Gonzalez *et al.* (2008), finding the speed to have an influence on the estimated PSD – the authors recommend that transfer functions be established for a range of speeds (in steps of 5 km/h) to provide “sufficient accuracy.”

The profiles were then artificially contaminated with noise, with the results indicating that as the Signal to Noise (S/N) ratio increases, the accuracy decreases at lower spatial frequencies for estimating the road profile. The authors further commented that “the influence of S/N on the high spatial frequency components of the spectra is not so important, and once the frequencies are above 0.1 c/m, the road class is generally accurately predicted regardless of the noise level.” When randomly generated noise was introduced into the acceleration measurements, it was found that the low spatial frequency components were overestimated. Also, the results found that the body accelerations are "as accurate as axle acceleration data" (Gonzalez *et al.* 2008).

Rouillard and Sek (2010b) proposed that an estimate of a vehicle's operational FRF can be established using only in-service vibration response data, provided the road profile can be represented by an appropriate spectral function. The authors assumed that, over sufficient distances, the average spectral shape of the road profile approaches a brown spectrum in displacement as defined in ISO standard 8608 (1995). If a vehicle travelled over the same road at two different nominally constant speeds, provided the vehicle is linear during operation, the dynamic characteristics and the spectral exponent of the road may be determined. Rouillard and Sek (2010b) proposed this relationship, based on Equation 3-7, in Equation 3-55.

$$\sqrt{\frac{R_{\ddot{x}}(f)_{v_1}}{G_{\ddot{x}}(f)_{v_1}}} = \sqrt{\frac{R_{\ddot{x}}(f)_{v_2}}{G_{\ddot{x}}(f)_{v_2}}} \qquad (3\text{-}55)$$

where the acceleration response PSD function at constant speed v is $R_{\ddot{x}}(f)_v$.

Multiple experiments using a small transport vehicle travelling at various constant speeds over a long country road (approximately 40 km) showed that the use of a standard value of 2.0 for the spectral exponent, w, did not yield the best agreement between the predicted vehicle FRF and the FRF measured using broad-band excitation on a vibration table. One of the issues encountered by the authors was the presence of an "unidentified response spectral peak" within 25 – 30 Hz. Rouillard and Sek (2010b) concluded that the approach is promising, however further work is required to establish the technique for a variety of experimental vehicles and roads, to quantify the effects of vehicle speed and suspension type, to investigate the influence of the record length on the response PSD function and to assess whether the spectral exponent actually tends towards two as the length of the road increases.

As with the analysis techniques for excitation-response and response-only (transient) data, the PP method can also be used to estimate the damped natural frequency of the system from the autospectrum of the in-service response data. From the response autospectrum, the occurrence of peaks can generally be assumed to be due to either the excitation spectrum or the response of the system (Bendat & Piersol 1980, p. 181). For broad-band random excitation, it is generally assumed that the excitation spectrum will not include any significant peaks or troughs within the relevant frequency bandwidth. The major limitation of these approaches is that estimating the damping ratio is “uncertain or impossible” using only in-service response data (Alam *et al.* 2009).

3.3.3.2 Random Decrement Technique

Out of the numerous approaches investigated, the random decrement technique was initially investigated due to its relevance for the estimation of the dynamic characteristics of a system using only response data. It has often been used to establish the modal parameters of large structures such as bridges or buildings and originally for evaluating structural components in the aeronautical industry, where measuring the excitation is impossible or very difficult. In vehicle dynamics it is difficult to measure the excitation applied via the pavement, requiring the use of specialised instrumentation. This inability to easily measure the excitation applied to a vehicle demonstrates the motivation that exists to investigate the use of alternative analysis techniques to establish the dynamic characteristics of a vehicle using only in-service response data.

The random decrement technique was developed by Henry Cole during the late 1960s and early 1970s to identify failure in aerospace structures using only in-service response data (Cole 1968; Cole 1973). Cole’s (1968) initial motivation for the development of the random decrement technique was due to the difficulty in measuring the excitation during wind tunnel testing of aeronautical structural components. Cole (1968) initially attempted to establish the PSD function of the response and used the half-power bandwidth method to establish the damping ratio, but the results were found “to have large variance.” Furthermore, establishing the PSD function of the response does not reveal whether the system is nonlinear and requires the input to be measured (Cole 1968). Common analysis techniques such as establishing the PSD function are “very dependent on the input” and so an increase in the excitation level may cause a change in the level of damping or natural frequency of the system (Cole 1973).

By analysing the response using the random decrement technique, the “normal operation of the structure under test is not interrupted” and the excitation is not required (Ibrahim *et al.* 1996). The random decrement signature has an appearance “similar to the autocorrelation,” however it possesses properties which are suitable for use as “a failure detector.” The first property being that it has a constant amplitude which “represents a calibrated displacement of the structure” and maintains the level independent of the excitation (Cole 1973). The auto random decrement function, D_{xx}, for single-channel measurements is shown in Equation 3-56.

$$D_{xx} = \frac{1}{N_{RD}} \sum_{i=1}^{N_{RD}} x\left(t_i + \tau_w\right) \middle| x\left(t_i\right) \tag{3-56}$$

Analysis of a system's response via multiple channel measurements using the random decrement technique is also possible. The cross random decrement function, as investigated by Ibrahim and Mikulcik (1977), defines a trigger for a single response channel and all the sections to be averaged are obtained from various measurement locations depending on the system. The cross random decrement function is particularly useful for establishing the mode shapes of structures or other systems and will not be further discussed.The random decrement signature obtained is "an estimate of the step response of a system and is obtained by averaging sections of the system time response in a particular way such that the components due to random and velocity inputs tend to zero as the number of averages increases" (Siviter & Pollard 1985).

Figure 3-11 demonstrates how the random decrement technique works to average each signature obtained (via a pre-determined trigger level) from the in-service response data until the influence of the excitation is cancelled out. After sufficient averaging, the influence of the excitation is cancelled out and the remaining random decrement signature is related to the free vibration decay of the system with an initial step displacement (Cole 1973). For a detailed mathematical description of the random decrement technique, see Vandiver *et al.* (1982).

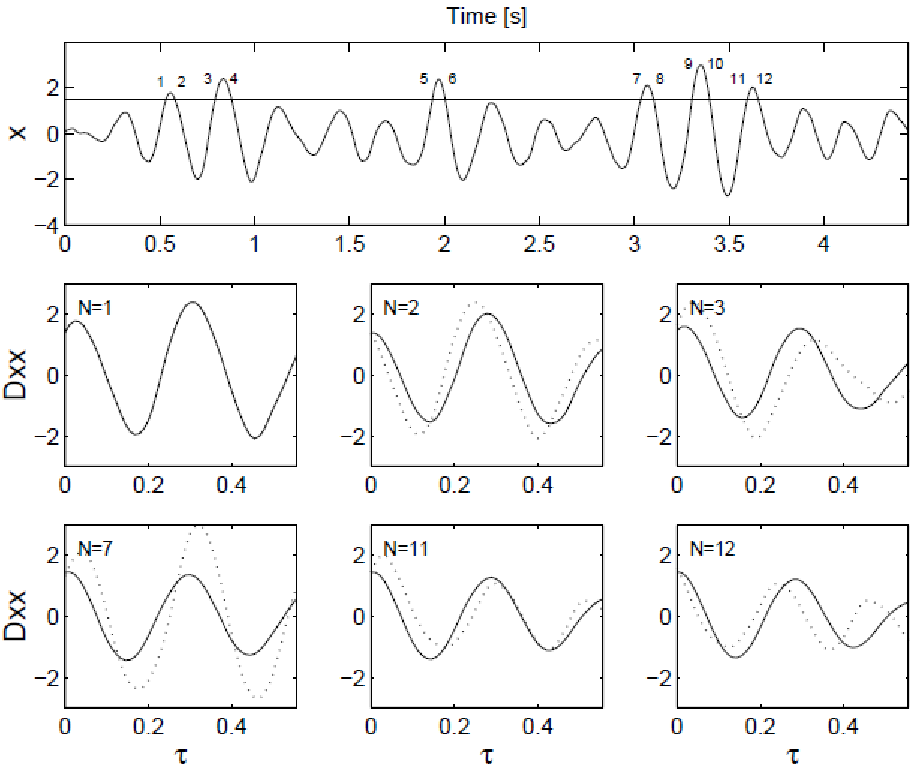

Figure 3-11: A random signal with a preselected trigger level (top) and the averaged sections of the random decrement technique (solid lines: random decrement signature, dashed lines: current time segment obtained), from Asmussen (1997).

Once the random decrement signature has been obtained, the dynamic characteristics of the system may be obtained using the same analysis techniques for response-only (transient) methods. Several authors have used these same analysis techniques to estimate the dynamic characteristics, for instance Elshafey *et al.* (2009) measured the time between two successive peaks of a cycle to provide an estimate of the damped natural frequency. To estimate the damping of the system, several authors have suggested the use of the logarithmic decrement technique (Cole 1973; Kijewski & Kareem 2000).

Cole (1973) noted that, like the FFT, aliasing also affects the random decrement technique and so it is important to select a suitable sampling rate when measuring the response. Cole (1973) noted that for "failure detection" the sampling frequency must be at least twice the natural frequency (as stated by Shannon's Sampling Theorem), while for establishing the damping ratio sixteen-times the natural frequency is "desirable to define the signature adequately." Another option would be to choose a new trigger level in order to reduce the estimation time if this is an issue. Another limitation of the random decrement technique is bias due to high levels of damping. Asmussen (1997) investigated this bias effect due to high damping and found the best way to reduce bias is to select a much higher sampling rate. The random decrement signatures may also become highly biased if the user decides to omit some of the detected trigger points (and hence omit some averages) to reduce the computational time. Asmussen (1997) stated that it was "very difficult to exclude some of the triggering points without introducing bias" and recommended to avoid this. One benefit of the random decrement technique is that the decay towards zero "should eliminate the leakage problem" common with standard spectral analysis (Brincker & Asmussen 1997).

In practice, a plethora of trigger level conditions are available to establish the random decrement signature. Only some of the most common trigger level conditions are described. The original triggering condition used by Cole (1968; 1973) was the level crossing condition, where the trigger begins once the signal is equal to a predetermined value. Asmussen (1997) evaluated three trigger level conditions using a simulated 2DoF system excited with Gaussian white noise. The three trigger conditions examined were the level crossing, local extremum and positive point triggering conditions. The local extremum triggering condition begins trigger once a local extreme is found within the predetermined trigger level, while the positive point trigger begins when any value of the signal is greater than zero. The positive point triggering condition can be modified to use a smaller bandwidth if required. Asmussen (1997) found that the positive point triggering condition produces the most accurate estimates of the modal parameters compared to the level crossing and local extremum triggering conditions.

Asmussen and Brincker (1996) investigated the effect of using a trigger level at local extremes (extrema) and also at zero-crossings, finding the local extreme condition to be the most reliable. The triggering condition will directly influence the number of averages that will be obtained to establish the random decrement signature, with Kijewski and Kareem (2000) finding that the estimates of the dynamic characteristics are best when the random decrement signature comprises 200 averages and the first 5 cycles of the signature are used. Cole (1973) stated that 500 averages are suitable to obtain an "accurate signature," while Chang (1975) recommended that 2,000 averages should be used.

Vandiver *et al.* (1982) stated that for a linear, time invariant system excited by a zero-mean, stationary and Gaussian random process the random decrement signature is proportional to the autocorrelation function; however the autocorrelation function itself is not, in general, proportional to the free vibration decay (Vandiver *et al.* 1982). The special case which allows the free vibration decay from a determined initial displacement to be obtained is when the system is excited by stationary and Gaussian white noise (Vandiver *et al.* 1982). However, for an excitation that has a band limited spectrum the results are to a "sufficient accuracy equivalent to the response to white noise" (Vandiver *et al.* 1982).

Ibrahim (1980) investigated the effect of various excitation functions in the form of seven PSD shapes ranging from white noise, ramps, triangular and sine waves, along with other shapes of input force on the random decrement. The author found the accuracy of the non-white-noise input forces are "as good as the accuracy in the white-noise case." The condition of requiring white-noise is not necessary; however the excitations were stationary, zero-mean random signals (Ibrahim 1980). Kijewski and Kareem (2000) investigated the effect of nonstationarity on an SDoF oscillator. The authors noted that the stationary sections of Gaussian samples are "incapable of averaging out the variance of the isolated samples." The authors concluded that "the variance of estimates will be far greater than idealised theory would predict" due to the presence of nonstationary sections.

Siviter and Pollard (1985) undertook a numerical and experimental investigation using the random decrement to establish the dynamic characteristics of railway vehicles. The estimates of the frequency and damping of a simple numerical model yielded were good, although the damping ratios were slightly underestimated. Brincker and Asmussen (1997) performed a comparative study of the random decrement and PSD analysis techniques to establish the FRF of a three-span laboratory bridge model subjected to white noise. The results showed the estimated frequencies from the various mode shapes matched well between the two techniques; however the random decrement technique generally slightly underestimated the damping ratios.

Asmussen and Brincker (1996) investigated the use of the random decrement technique and performing FFT analysis of the signature in comparison with a pure FFT analysis on a simulated Three Degree-of-Freedom system. The results indicate that the random decrement technique coupled with the FFT on the resulting signature is “more reliable” than simply using the FFT (Asmussen & Brincker 1996).

3.4 LITERATURE REVIEW SUMMARY

The literature review presented a broad investigation of vehicle-pavement interaction, focused on experimentally estimating the dynamic characteristics of road vehicles. A commonly used numerical model for the simulation of vehicle dynamics is the quarter car model, consisting of a sprung and unsprung mass, a suspension system (spring and damper) and a tyre (spring and sometimes a damper). When suitable parameters are set for the quarter car model, it can provide a representation of a real vehicle and is useful in understanding the role each component performs within a vehicle and their influence on the dynamic characteristics.

Longitudinal pavement elevation profiles are characterised by broad-band random vibration. One useful approach for pavement elevation profile analysis is to establish the PSD function, particularly for vehicle dynamics. Since the 1950s many authors have proposed numerous spectral models to approximate the pavement elevation spectra. The most common model, outlined by the ISO, takes the form of a linear relationship in logarithmic scales and has only two unknowns; a roughness constant that translates the spectrum vertically and a spectral exponent which determines the slope of the spectrum and is recommended to be 2.0. Despite this, many authors have questioned and criticised the use of the standard value of the spectral exponent and the approximation. Alternative models have been developed, often comprising multiple bands with differing spectral exponents across specific wavelengths and generally provide an improved fit of the measured pavement elevation spectra over the standard approximation.

The shape of the spectral model of pavement elevation profiles is generally independent of the road type; rather it is a function of the rms level. The rms level often varies along a pavement and therefore the process cannot always be treated as stationary, however for simulation purposes a pavement profile may be considered as a series of finite stationary sections. In general, the smoother a pavement profile is (lack of roughness), the more likely the elevation is stationary in nature. If the pavement profile is nonstationary, this will result in the assumption of isotropy to be invalid. Isotropy is an important assumption when measuring pavement elevation profiles. If the assumption of isotropy is valid, then only one path along the road requires measurement in order to characterise the entire surface.

Nonstationary, or transient, events often occur outside three-times the standard deviation and include artefacts such as potholes or train tracks. These artefacts must be excluded from the analysis of a longitudinal pavement profile. The statistical distribution is also required in order to adequately characterise a pavement profile. The use of a PSD function for analysis depends on the pavement elevation profile to be Gaussian by nature. Analysis of pavement profiles has shown that while some pavement profiles possess a Gaussian distribution, others can vary significantly from the Gaussian. Even sections within a single road elevation profile can differ, leading to difficulty in advocating the approach of treating pavement profiles as a Gaussian process. Over even a single road, a vehicle may be subjected to nonstationary vibration in the form of varying rms and possibly a non-Gaussian statistical distribution; not to mention the occurrence of transient events. These variations in the type and level of vibration, coupled with the nonlinear and complex nature of vehicles, may result in a nonstationary, non-Gaussian response.

Various experimental techniques can be used to estimate the dynamic characteristics of road vehicles. The first category, known as response-only (transient) techniques, is a relatively cheap and straightforward approach for estimating the dynamic characteristics of the sprung mass mode (natural frequency and damping ratio). The most prevalent methods are those outlined by the CEU to evaluate the road-friendliness of heavy vehicles. There are, however, numerous issues associated with these experimental methods which have been discussed by various authors. One notable issue raised is that these methods are only focused on establishing equivalency to air suspensions and do not directly assess a vehicle’s ability to reduce the dynamic loading applied to pavements.

Excitation-response methods are another series of experimental methods that involve establishing the FRF of a vehicle by placing it on a suitable vibration table, subjecting it to a pre-determined excitation and simultaneously measuring the excitation and response. The most common type of excitation function used for characterising vehicles was swept-sine; however recent developments in computing and an improved understanding of the distribution environment have brought random vibration testing to the fore as a more realistic test. Establishing the FRF of the vehicle enables not only the sprung mass natural frequency and suspension damping ratio to be obtained but also the dynamic characteristics of the unsprung mass. One prohibiting factor associated with vibration tables is the cost and maintenance of suitable large-scale tables to support and excite heavy vehicles.

The final category is in-service response methods, which aim to estimate the dynamic characteristics of vehicles using only response data obtained during operation (driving over a road). It is well known that the response of a vehicle with linear characteristics is related to the excitation via its transmissibility FRF. Several authors have used this relationship to estimate the FRF of a vehicle using only in-service response data. While many authors have had limited success, one promising approach was described by Rouillard and Sek (2010b). The authors proposed an experimental technique that assumes the excitation spectrum takes the form of the ISO 8608 standard and measured the in-service response of a light transport vehicle and its FRF using a servo-hydraulic vibration table. The initial results showed that the use of the standard value of the spectral exponent of 2.0 does not provide the best match with the FRFs obtained using a servo-hydraulic vibration table.

The random decrement technique was found another promising technique that may be used to analyse in-service response data. The technique is used when the excitation applied to the system is impossible or difficult to measure. A series of signatures are obtained from the measured response, which depend on the set trigger level and type. Each of the signatures are averaged together and eventually the influence of the excitation is cancelled out and the resulting random decrement signature is an estimate of the impulse response of the system. Once the random decrement signature has been obtained, common analysis techniques (such as those used for the response-only (transient) methods) may be used to estimate the dynamic characteristics of the system. Several researchers have published literature using the random decrement technique to estimate the dynamic characters for various civil engineering structures; however no literature has been discovered applying the technique to vehicles. There is some promising work using only in-service response data, however further research and development is required to validate its use as a viable alternative.

The wide range of experimental techniques that have been adopted to estimate the dynamic characteristics of road vehicles, shown in the literature, have not been evaluated to establish their accuracy, repeatability or validity. Furthermore, no comparative study has been undertaken to investigate the difference in the estimated dynamic characteristics between the various methods. For instance, no study has shown the established dynamic characteristics using response-only (transient) methods will be the same as those from the excitation-response methods. The majority of the literature is focused on evaluating the performance of vehicle shock absorbers and determining only the damped natural frequency of the sprung mass mode, since these are considered the most important factors for identifying road-friendly suspension systems. While both the response-only (transient) and excitation-response techniques may be valid, they require the vehicle to be mobilised and taken out of operation for a period of time and there is reluctance for these tests to occur. Furthermore, they are often only tested for one particular set of conditions (i.e. payload). An alternative method that does not require the vehicle to be mobilised, by which the dynamic characteristics of the vehicle can be estimated during normal operation, would be of great benefit to the industry as a whole.

Chapter 4

HYPOTHESIS

The principal hypothesis of this thesis is that estimates of the dynamic characteristics of road vehicles, namely the transmissibility FRF, can be obtained using only in-service vertical vibration response data from a vehicle travelling at a nominally constant operating speed.

Two distinct techniques to analyse the in-service response data will be considered:

1) The first technique (the spectral approach) uses the standard spectral model of road profiles combined with the average vibration response spectrum to compute the vehicle's FRF.

2) The second approach is based on the application of the random decrement technique. Once the random decrement signature has been established from the measured response data, the FRF and associated vehicle dynamic characteristics are estimated using Fourier and Hilbert Transform analysis techniques.

4.1 SUB-HYPOTHESES

There are three further sub-hypotheses that will also be considered:

1) The dynamic characteristics estimated using either the response-only (transient) or excitation-response methods are not consistent and do not agree with the true, or actual, FRF of a vehicle during normal operation.
2) The longitudinal pavement elevation profile of any pavement approaches the standard model as described in ISO 8608 as the pavement length increases.
3) The entire length of a pavement is not required to establish an accurate estimate of the dynamic characteristics using the two analysis techniques, provided the road is not significantly nonstationary.

Chapter 5

METHODOLOGY

The literature review has shown that while some preliminary research has been undertaken, no reliable and easy-to-use method exists for accurately determining the dynamic characteristics (FRF) of road vehicles using only in-service response data. Furthermore, the current methods available to estimate the dynamic characteristics each have their own significant limitations and have not been comparatively evaluated.

To undertake the comparative evaluation and validate the in-service analysis techniques, an idealised vehicle must be developed. The broad approach to be taken in this research is to:

1) Develop and configure a physical idealised vehicle.
2) Experimentally establish and compare estimates of the transmissibility FRF of the idealised vehicle using existing laboratory techniques.
3) Drive the idealised vehicle over a range of selected roads under various conditions (namely speed) and use the measured response data to predict the true FRF of the vehicle and compare these estimates with the laboratory experiments.

5.1 IDEALISED VEHICLE DEVELOPMENT AND CONFIGURATION

There are a number of reasons why undertaking the research with a standard road vehicle is not appropriate. These include: drive-train noise, wheel imbalance and Multiple-Input Single-Output (MISO) effects due to the excitation being applied via multiple wheels. In order to undertake a series of critical evaluation and in-service experiments, an idealised physical quarter vehicle must be developed. As a physical quarter car, the vehicle should be designed to have a single wheel-spring-shock and exhibit realistic dynamic characteristics.

- The vehicle is to be towed using any capable vehicle.

The tow bar must be sufficiently long enough to minimise the pitch motion and stiff enough to prevent torsion to ensure the vehicle remains upright. Conversely, the tow bar must not be too long such that it is difficult to maneuver with the towing vehicle through public streets.

- The suspension system of the vehicle must be interchangeable.

The components of the suspension system should be able to be changed with relative ease to allow for different vehicle configurations (i.e. different shock absorbers and springs).

- The vehicle should be able to support varied mass loading configurations.

A frame to support additional mass loading allows for another option to easily vary the dynamic characteristics of the vehicle.

5.2 LABORATORY-BASED EXPERIMENTAL METHODOLOGY

To critically evaluate and compare the various techniques currently available to estimate the dynamic characteristics of the sprung mass mode of the different configurations of the idealised vehicle, a series of laboratory experiments are to be undertaken.

1) Response-only (transient) methods (outlined by the CEU).

For the response-only (transient) experiments, the idealised vehicle is instrumented to measure the sprung mass acceleration and subjected to the three tests outlined by the CEU (1996). The measured response requires analysis to estimate the dynamic characteristics. It is expected that there will be noise and the effects of other modes (such as the motion of the unsprung mass) present in the measured response, therefore the response of the sprung mass will be isolated using appropriate filtering. The filtered response data is analysed using the FFT and the PP method to estimate the damped natural frequency of the sprung mass mode. The damping ratio is estimated by computing the instantaneous magnitude envelope using the Hilbert Transform. Finally, the sprung mass natural frequency is estimated using the damped natural frequency and the damping ratio (Equation 3-6).

2) Excitation-response methods (random vibration excitation).

The excitation-response experiments require a suitable vibration table to subject the vehicle to a predefined excitation by inducing vertical motion at the wheels, while the sprung mass acceleration of the idealised vehicle and the excitation acceleration of the vibration table are simultaneously measured. While sinusoidal-based excitations were once used, a significantly improved representation of the distribution environment is provided by subjecting the vehicle to random vibration. Two spectral shapes will be used for the evaluation. One spectral shape is acceleration band-limited white noise, which excites the vehicle with equal level at all frequencies within the specified bandwidth. The other spectral shape is acceleration band-limited violet noise, which corresponds to the PSD model adopted under ISO standard 8608 (1995) to approximate the excitation of longitudinal pavement profiles (Equation 3-19). During the tests, the temperature of the shock absorber must be monitored to ensure the starting temperature is same for each test. Once the excitation and response data have been measured, the FRF of the vehicle is then established (Equation 3-44). To extract the sprung mass natural frequency and damping ratio from the FRF, a least-squares regression curve-fit of the transmissibility magnitude of an SDoF system is applied (Equation 3-53).

5.3 IN-SERVICE EXPERIMENTAL METHODOLOGY

The second stage of the research is focused on a series of in-service experiments, where the idealised vehicle is driven along a selected route at different nominally constant operating speeds. One of the most important considerations is to identify a suitable road to undertake the in-service experiments. The most significant criterion is to undertake the measurements only while the vehicle is travelling at the desired nominal constant speed. Maintaining constant speed is not only dependent on the driver, but also on the road being devoid of stop signs, traffic lights, large ascents or descents, sharp turns, roundabouts and other hazards that may require the driver to slow down or stop the vehicle. Furthermore, it is desirable to undertake the experiments while the traffic on the road is very light, as other vehicles on the road may force the driver to slow down or stop.

The speed limit of the road must remain constant, or at least the slowest permitted speed on the road must be the same as the selected operating speed. Another consideration is the length of the road; the longer the road is, the better chance the excitation spectrum will approach the spectral model outlined under ISO standard 8608 (1995). It is also important that the selected road is fairly uneven so as to induce a reasonable level of excitation into the vehicle across a broad range of frequencies.

Once an appropriate road has been identified, the vehicle is instrumented to measure the vertical vibration acceleration of the sprung mass (body) and driven over a series of roads at various nominally constant operating speeds. The vehicle is then driven out to the location near the beginning of the selected route. The driver begins driving along the route and once the vehicle reaches the desired operating speed the measurement of the sprung mass acceleration vibration may begin. Throughout the experiment, the driver must ensure that the nominally constant operating speed is maintained. Once the vehicle approaches the end of the route, the measurement is stopped and the driver may begin to slow the vehicle down. The driver then turns the vehicle around safely where possible and the process is repeated for the return length of the road at the same constant operating speed. This may be repeated for as many different operating speeds as is desired.

Once the various measurements have been undertaken, the measured vibration response of the vehicle is analysed using two experimental approaches. The first approach relies on the assumption that the excitation may be assumed using a predetermined spectral function, while the second approach is based on the use of the random decrement technique. Both of these experimental techniques are described in detail in Chapter 7. The first series of in-service experiments will be undertaken using the idealised vehicle, where it will be towed along the selected routes using a light transport vehicle. As a final phase of the in-service experiments, once the analytical techniques have been validated using the idealised vehicle, a series of in-service experiments using various road vehicles will be undertaken and their response analysed.

Chapter 6

CRITICAL EVALUATION OF EXISTING METHODS TO ESTIMATE VEHICLE DYNAMIC CHARACTERISTICS

Prior to the development of a new technique using only in-service response data, the various methods currently in-use must be critically evaluated to determine which method obtains the best estimates of the true dynamic characteristics of vehicles (if it exists). There have been no studies undertaken to critically evaluate and compare the response-only (transient) and excitation-response methods. This Chapter is focused on critically evaluating the various experimental methods to estimate the dynamic characteristics (and whether a single true estimate of the dynamic characteristics exist) using the idealised custom-designed vehicle. There are two configurations of the idealised vehicle and both were experimentally evaluated for a series of response-only (transient) and excitation-response methods.

It is important to establish the true dynamic characteristics of a vehicle to not only provide a comparison for the in-service experiments, which are the main focus of this thesis, but also to establish any nonlinear behaviour in the vehicle. The idealised vehicle, the development of which is described in this Chapter, is used to evaluate the three response-only (transient) methods outlined by the CEU (1996) and two different spectral shapes (random vibration) at various rms intensities for the excitation-response methods. The dynamic characteristics of the vehicle's sprung mass mode were estimated from each of the experimental methods and evaluated for their accuracy and repeatability. They are also used to assess the vehicle for any nonlinear behaviour and investigate the effect of various excitation types and levels on the dynamic characteristics of the vehicle.

6.1 EXPERIMENTAL PROCEDURE

The two configurations of the idealised vehicle were subjected to the various experimental methods currently used to estimate the dynamic characteristics of vehicles. The two categories of experimental approaches that were evaluated are the response-only (transient) and excitation-response methods.

6.1.1 Idealised Vehicle Development and Configuration

In order to undertake the critical evaluation and the in-service experiments, an idealised quarter car vehicle, known as the Single-Wheeled Experimental Vehicle (SWEV), was designed and commissioned to test and validate the currently available methods and the proposed methods using in-service response data. Constructed from a demonstration model Honda CBR 125R, the rear section was adapted to maintain the original factory-fitted shock absorber, spring and wheel and was fitted with a custom-designed tow bar. The SWEV is a towable system which has a frame located above the fairings to support dead weights, allowing the dynamic characteristics of the vehicle to be varied by adjusting the (sprung) mass loading. A conceptual illustration and photograph of the SWEV is presented in *Figure 6-1*.

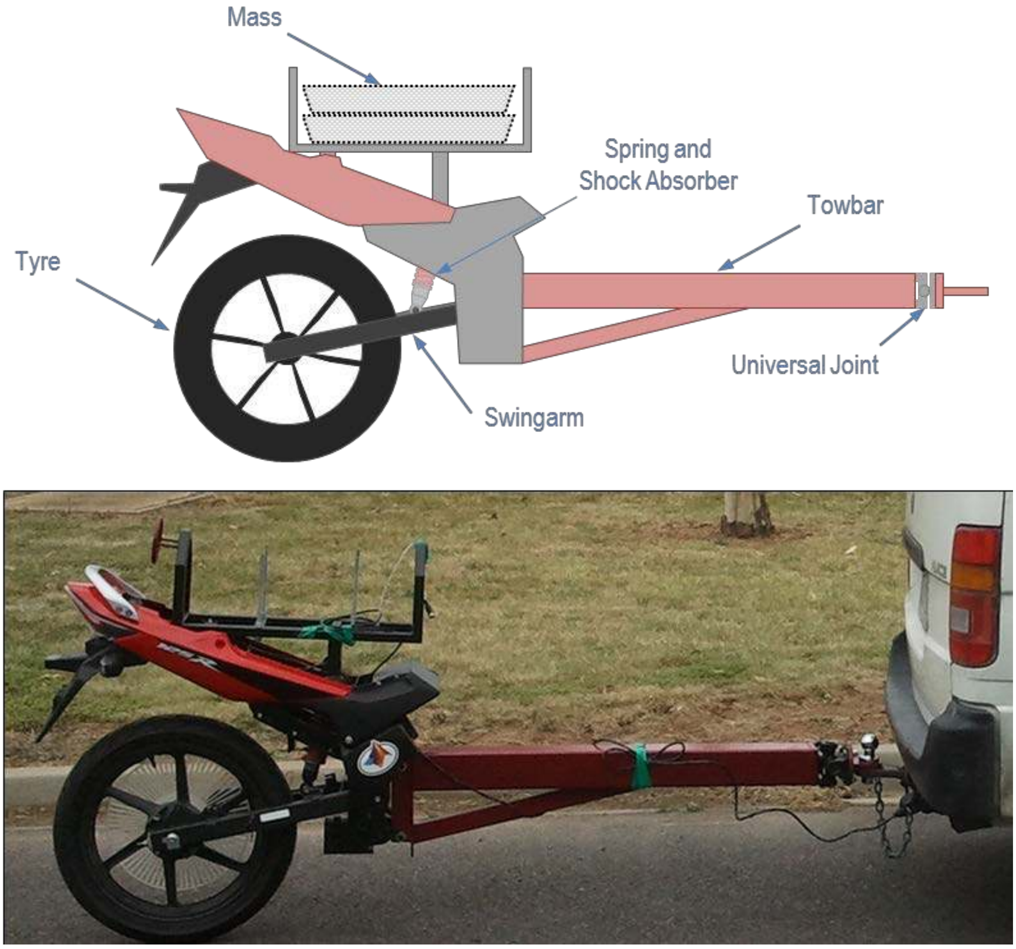

Figure 6-1: Conceptual illustration (top) and photograph (below) of the idealised physical quarter car (SWEV).

Another consideration made prior to the commissioning of the SWEV was for the ability to change the components of the suspension system due to the notoriously nonlinear nature of automotive shock absorbers. A preliminary investigation revealed that the original factory-fitted shock absorber exhibited significant nonlinear characteristics, and so an alternative shock absorber with nominally linear characteristics was commissioned. This resulted in two configurations of the SWEV; the first configuration is known as the SWEV-A and has the original factory-fitted shock absorber. The second configuration, the SWEV-B, has the custom-designed shock absorber with a nominally constant damping coefficient of 2,000 Ns/m that is intended to be velocity-invariant.

The spring remains the same between the two configurations and is mounted onto the shock absorber, so it was important to ensure that the second shock absorber has the same geometrical specifications as those of the factory-fitted shock absorber in order to fit to the original spring and vehicle mounts. For the series of critical evaluation experiments presented in this Chapter, both configurations of the SWEV were loaded with 100 kg of dead weight at the sprung mass.

6.1.2 Response-Only (Transient) Methods

The response-only (transient) methods all attempt to induce the vehicle with a transient excitation in order to measure the free-response vibration for analysis. This is achieved by applying and swiftly releasing a load to the vehicle, or driving over a suitable geometric obstacle. Both configurations of the SWEV were subjected to the three methods outlined by the CEU (1996). These methods are specifically designed for heavy vehicles, and so two of the tests required modification due to the physical limitations of the SWEV. The SWEV was instrumented with an accelerometer to measure the acceleration response of the sprung mass with a sampling frequency of 1,000 Hz. Each of the three test methods were repeated three times to investigate the consistency of the estimates of the dynamic characteristics.

1) Push and Release Test.

CEU Method: The push and release test requires the application of one-and-a-half times the vehicle's maximum static load before immediate release.

Adapted Approach: Because the method is suited to heavy vehicles, it is not applicable to the SWEV, requiring the applied load to be modified. Suitably large static loads were applied in order to induce the vehicle to vibrate upon release (300 N and 600 N).

2) Lift and Release Test.

CEU Method: The lift and release test requires the body of the vehicle to be raised 80 mm above the chassis and then swiftly released.

Adapted Approach: The sprung mass of the SWEV was not able to be raised 80 mm above the chassis; instead the vehicle was raised to its maximum allowable height of 25 mm without causing the tyre to leave the ground.

3) Ramp Test.

CEU Method: The vehicle is driven at a speed of 5 ± 1 km/h over a ramp as per the dimensions specified in the CEU directive (80 mm drop at the end of the ramp). The ramp is designed to have a relatively long lead up to minimise any vibration generated in the vehicle prior to the step down off the ramp.

Adapted Approach: The ramp test was undertaken using the exact specifications outlined under the CEU directive (80 mm drop).

Once the subsequent decaying free vibration of the SWEV's sprung mass was measured, they were analysed to establish the sprung mass dynamic characteristics. The response data was filtered to isolate the sprung mass mode (Low-Pass Filter: Butterworth 5th order, cut-off frequency of 5 Hz). The filtered response data was then analysed using the FFT (with zero-padding of sixteen-times the sub-record length) to estimate the damped natural frequency, while the instantaneous magnitude envelope was established (using the Hilbert Transform) to estimate the damping ratio of the suspension system. When using the Hilbert Transform to estimate the damping ratio, there is a level of subjectivity on the operator to select the appropriate section of the envelope for analysis and so three independent estimates of the curve-fit bandwidth were obtained for each test run.

6.1.3 Excitation-Response Methods

The excitation-response experiments use a suitable vibration table to subject the vehicle to a predefined excitation spectrum (inducing vertical motion at the wheels) whilst simultaneously measuring the excitation and response, from which the vehicle's FRF is established. This experimental method was achieved through the use of an in-ground servo-hydraulic vibration test system driven by a programmable vibration controller. The SWEV was placed onto a vibration table and the tow bar was mounted onto a stand fixed to the ground. Two accelerometers were used to measure the excitation (at the table) and the response of the sprung mass. The experimental arrangement of the excitation-response experiments using the SWEV is shown in *Figure 6-2*.

The excitation of the table and the response of the sprung mass for each experiment were simultaneously measured with a sampling rate of 1,000 Hz for a duration of 410 seconds (where possible) to provide a sufficient number of independent averages of the FRF. The first spectral function used was acceleration band-limited white noise (frequency range: 0.7 – 50 Hz) at three rms intensities of 1.00, 2.00 and 3.00 m/s^2. The second PSD function used was acceleration band-limited violet noise, which corresponds to the ISO 8608 spectral model (frequency range: 0.5 – 50 Hz), at three rms intensities of 3.00, 6.00 and 9.00 m/s^2. The vibration controller was set with a crest factor limit of four (producing normally-distributed vibration limited to ± 4 standard deviations). Before and after each experiment, the temperature of the shock absorber was measured and no significant change in temperature was encountered (less than 1 °C).

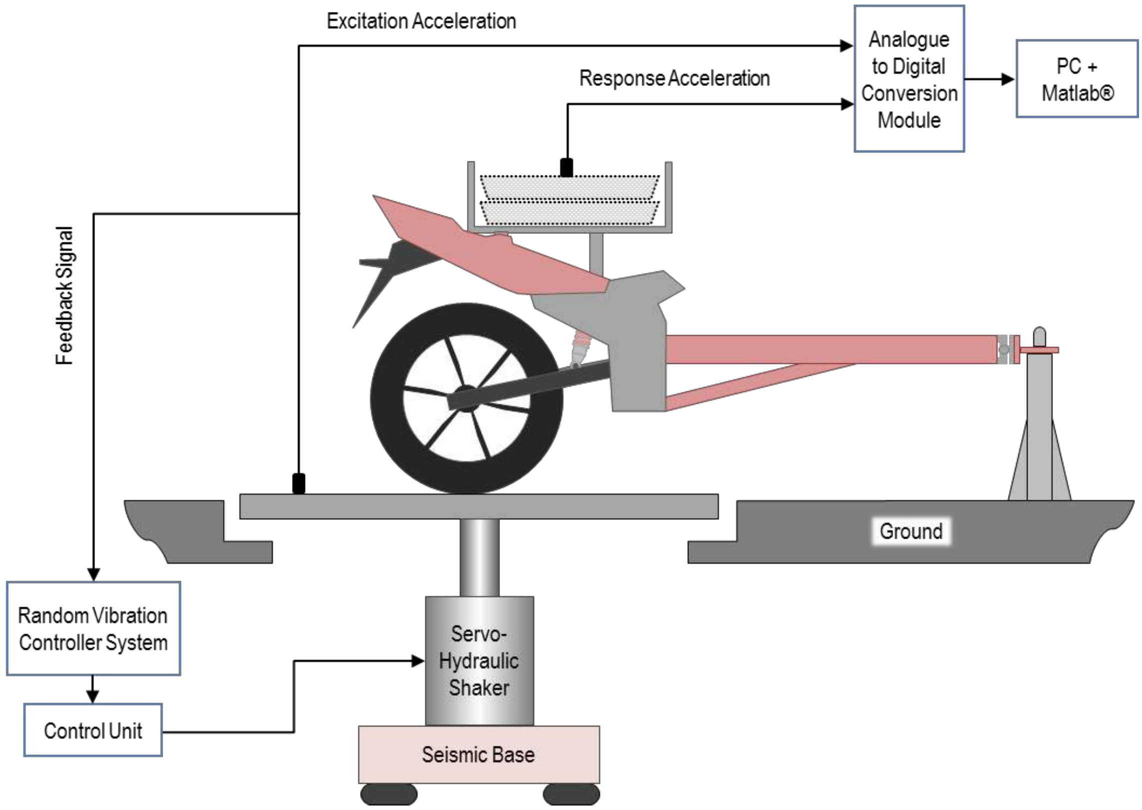

Figure 6-2: The experimental arrangement of the excitation-response experiments.

The measured excitation and response data were analysed using the FFT with a sub-record length of 10 seconds (frequency resolution, Δf = 0.10 Hz) and 41 independent averages, unless stated otherwise, to establish the transmissibility FRF, $H_1(f)$ (Equation 3-45). A Hanning window was also applied, along with 50 % overlapping of averages. It is important to note that since windowing is used, a loss in power occurs and so a correction factor was applied to compensate. Once the transmissibility FRF of the vehicle was established, the sprung mass' natural frequency and damping ratio were extracted using a least-squares regression curve-fit to the magnitude transmissibility FRF of an SDoF system (Equation 3-53).

In addition, the statistical distribution (PDF) of the excitation and response for each experiment were determined. As modern vibration controllers produce stationary, Gaussian random vibration, if the vehicle is linear, the statistical distribution of the response will also be Gaussian. This may be used to provide further indication of any nonlinear characteristic in either configuration of the SWEV. Prior to establishing the PDF of the normalised acceleration rms of the excitation and response data, a low-pass filter was applied to remove the influence of noise outside of the relevant frequency bandwidth (Low-Pass Filter: Butterworth 4th order, cut-off frequency of 60 Hz) and a total of 100 bins were used to calculate the PDFs.

6.2 EXPERIMENTAL RESULTS

This section presents the experimental results for the SWEV-A and SWEV-B configurations, loaded with 100 kg of dead weight, subjected to the response-only (transient) and excitation-response methods.

6.2.1 Response-Only (Transient) Methods

The results from the various response-only (transient) methods using both configurations of the SWEV are described in this section. Typical examples of the filtered time response and Hilbert envelope from the response-only methods are presented in *Figure 6-3* and *Figure 6-4* for the SWEV-A and SWEV-B, respectively.

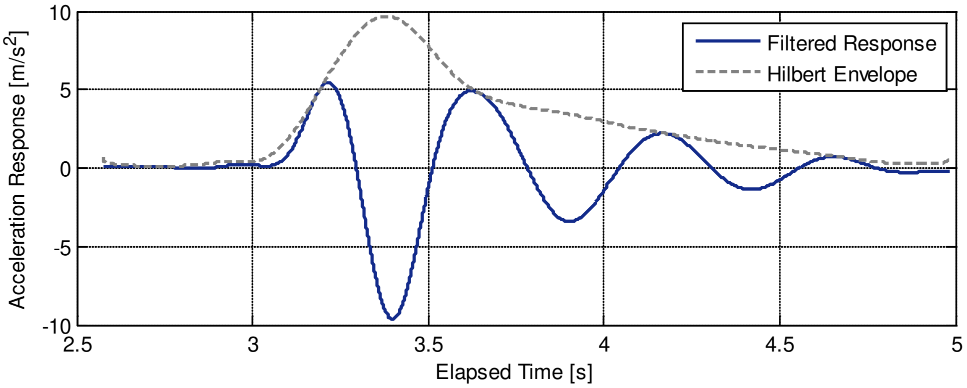

Figure 6-3: Typical filtered time response of the SWEV-A from the ramp test (run 3) and the Hilbert envelope (Low-Pass Filter: Butterworth 5th order, cut-off frequency of 5 Hz).

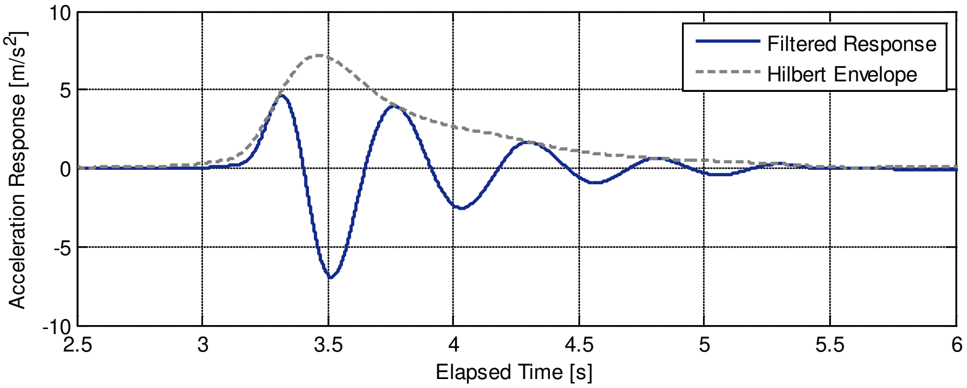

Figure 6-4: Typical filtered time response of the SWEV-B from the ramp test (run 2) and the Hilbert envelope (Low-Pass Filter: Butterworth 5th order, cut-off frequency of 5 Hz).

From the measured response, the resulting magnitude spectra and Hilbert envelopes were determined and used to estimate the damped natural frequency and damping ratio, respectively. A typical example of the magnitude spectrum and Hilbert envelope obtained are presented for the SWEV-A in *Figure 6-5* and for the SWEV-B in *Figure 6-6*.

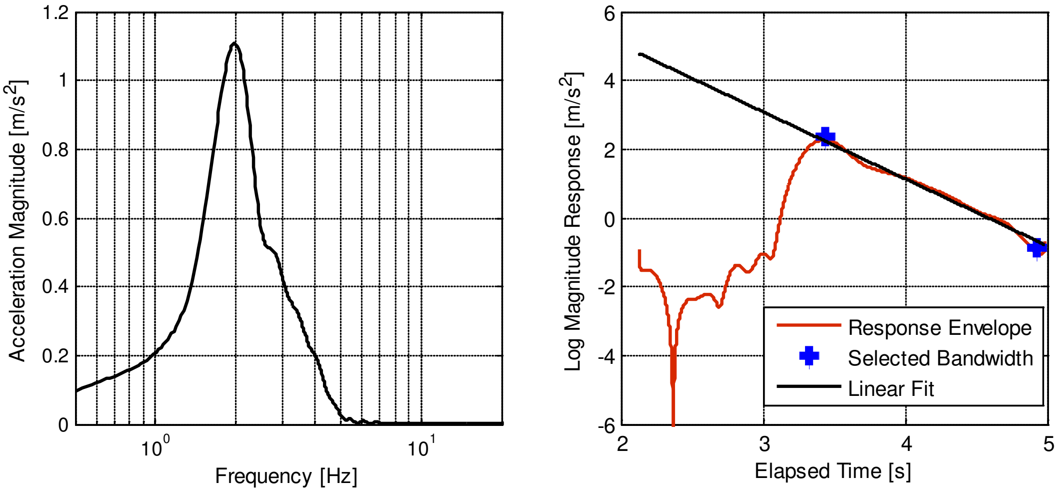

Figure 6-5: Magnitude spectrum (left) and Hilbert envelope (right) established from run 3 of the ramp test for the SWEV-A.

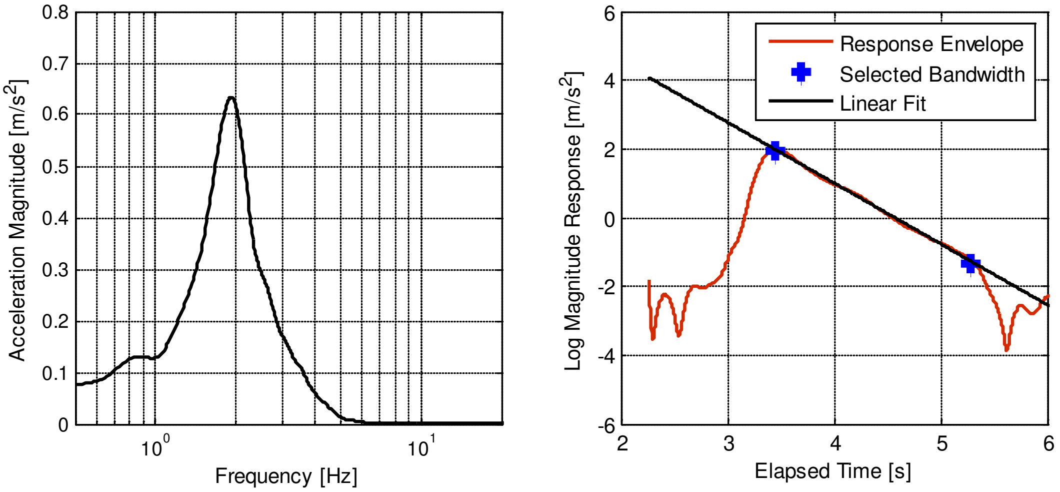

Figure 6-6: Magnitude spectrum (left) and Hilbert envelope (right) established from run 2 of the ramp test for the SWEV-B.

The dynamic characteristics of the sprung mass for both SWEV-A and SWEV-B were estimated and are presented in *Table 6-A* and *Table 6-B*, respectively. It is important to note that due to the use of zero-padding, the spectral resolution is artificially increased and so the sprung mass natural frequency can be selected using a much finer frequency resolution.

Table 6-A: Estimated sprung mass dynamic characteristics from the various response-only methods for the SWEV-A configuration. Note that the range is estimated from three damping ratio estimates of the same run (Δf at least 0.05 Hz).

	Sprung Mass Frequency		**Damping Ratio, ζ_s**	
Test Method	**f_{sd} [Hz]**	**f_{sn} [Hz]**	**Mean [-]**	**Range [-]**
Ramp Test (80 mm Drop) Run 1	2.00	2.02	0.154	0.003
Ramp Test (80 mm Drop) Run 2	2.02	2.05	0.160	0.002
Ramp Test (80 mm Drop) Run 3	2.01	2.04	0.158	0.011
Ramp Average	**2.01**	**2.04**	**0.157**	**0.005**
Lift and Release Test (25 mm) Run 1	2.08	2.15	0.248	0.014
Lift and Release Test (25 mm) Run 2	2.10	2.17	0.248	0.012
Lift and Release Test (25 mm) Run 2	2.11	2.19	0.261	0.014
Lift and Release Average	**2.10**	**2.17**	**0.252**	**0.013**
Push and Release Test (300 N) Run 1	2.05	2.09	0.200	0.011
Push and Release Test (300 N) Run 2	2.06	2.11	0.210	0.008
Push and Release Test (300 N) Run 3	2.05	2.10	0.218	0.021
Push and Release (300 N) Average	**2.05**	**2.10**	**0.209**	**0.013**
Push and Release Test (600 N) Run 1	2.03	2.08	0.226	0.005
Push and Release Test (600 N) Run 2	2.02	2.07	0.218	0.009
Push and Release Test (600 N) Run 3	2.01	2.05	0.194	0.009
Push and Release (600 N) Average	**2.02**	**2.07**	**0.213**	**0.008**

Table 6-B: Estimated sprung mass dynamic characteristics from the various response-only methods for the SWEV-B configuration. Note that the range is estimated from three damping ratio estimates of the same run (Δf at least 0.05 Hz).

	Sprung Mass Frequency		**Damping Ratio, ζ**	
Test Method	f_{sd} **[Hz]**	f_{sn} **[Hz]**	**Mean [-]**	**Range [-]**
Ramp Test (80 mm Drop) Run 1	1.95	1.97	0.143	0.001
Ramp Test (80 mm Drop) Run 2	1.95	1.97	0.143	0.000
Ramp Test (80 mm Drop) Run 3	1.94	1.96	0.145	0.002
Ramp Average	**1.95**	**1.97**	**0.144**	**0.001**
Lift and Release Test (25 mm) Run 1	2.01	2.04	0.162	0.005
Lift and Release Test (25 mm) Run 2	2.00	2.03	0.157	0.004
Lift and Release Test (25 mm) Run 2	2.01	2.03	0.152	0.002
Lift and Release Average	**2.01**	**2.03**	**0.157**	**0.004**
Push and Release Test (300 N) Run 1	2.02	2.04	0.144	0.004
Push and Release Test (300 N) Run 2	2.01	2.03	0.154	0.004
Push and Release Test (300 N) Run 3	2.03	2.05	0.154	0.006
Push and Release (300 N) Average	**2.02**	**2.04**	**0.151**	**0.005**
Push and Release Test (600 N) Run 1	1.98	2.00	0.149	0.005
Push and Release Test (600 N) Run 2	1.97	1.99	0.147	0.004
Push and Release Test (600 N) Run 3	1.98	2.00	0.150	0.002
Push and Release (600 N) Average	**1.98**	**2.00**	**0.149**	**0.004**

For the SWEV-A, the obtained estimates of the sprung mass damped natural frequency are reasonably consistent, with the total range between all the estimates approximately 0.10 Hz. The lift and release test was found to, on average, provide higher estimates of the damped natural frequency compared to the other methods. The damped natural frequency estimates of the sprung mass of SWEV-B for each run of the test methods are slightly more consistent than those estimated for the SWEV-A configuration, with a variation between each run of the test methods of 0.01 Hz (except the between the runs of the push and release 300 N test, which varies by 0.02 Hz). The range between all estimates of the SWEV-B damped natural frequency is reduced in comparison to the SWEV-A at 0.07 Hz.

There is variation between the estimates of the suspension damping ratio of the SWEV-A for the various test methods. The ramp test had the lowest estimates of the damping ratio, while the lift and release test had the highest estimated damping ratio (range of 0.100 between the two test methods). The various test methods are fairly consistent, with minor variation between each run. The ramp test provided the most consistent estimates (range of 0.005), while both the lift and release and push and release (300 N) tests were found to have the least consistent estimates between runs (both had a range of 0.013).

The variation in the estimated damping ratios of the SWEV-B was considerably reduced between the test methods. The lowest and highest estimated damping ratios were obtained from the ramp and the lift and release tests, respectively (range of 0.013 between the two test methods). The consistency of the damping ratio estimates (between the different runs) improved considerably for the SWEV-B. The most consistent estimates of the damping ratio were obtained from the ramp test (range of 0.001), while the push and release test (300 N) yielded the least consistent estimates (average range of 0.005). The estimated dynamic characteristics are, overall, far more consistent for the SWEV-B than the SWEV-A configuration, due to the introduction of the custom-made nominally linear shock absorber.

6.2.2 Excitation-Response Methods

Both configurations of the SWEV were placed, one at a time, onto a large-scale vibration table and subjected to various random vibration excitations. For the various spectra and rms intensities, the nominal (set by the operator) and the actual (measured) rms values during the tests for both the SWEV-A and SWEV-B are given in *Table 6-C*. It should be noted that some issues were encountered when using the vibration controller during the band-limited white noise 3.00 m/s^2 rms test, where only 19 and 20 independent averages of the FRF were obtained for the SWEV-A and SWEV-B, respectively.

Table 6-C: Nominal and actual excitation rms levels for the SWEV-A and SWEV-B configurations from the excitation-response experiments.

	Nominal rms	**Actual rms**		
	Acceleration	**Acceleration**	**Velocity**	**Displacement**
Spectral Shape	**[m/s^2]**	**[m/s^2]**	**[m/s]**	**[mm]**
SWEV-A Configuration				
White Noise	1.00	0.97	0.03	3.48
White Noise	2.00	1.95	0.06	7.01
White Noise	3.00	3.03	0.10	10.80
Violet Noise	3.00	2.85	0.02	0.84
Violet Noise	6.00	6.19	0.04	1.72
Violet Noise	9.00	9.10	0.06	2.54
SWEV-B Configuration				
White Noise	1.00	0.93	0.03	3.85
White Noise	2.00	1.92	0.06	6.95
White Noise	3.00	2.97	0.10	11.00
Violet Noise	3.00	2.88	0.02	0.86
Violet Noise	6.00	5.98	0.04	1.70
Violet Noise	9.00	8.97	0.06	2.61

The established FRFs for both configurations of the SWEV are presented in *Figure 6-7* for the white noise excitation and *Figure 6-8* for the violet noise excitation.

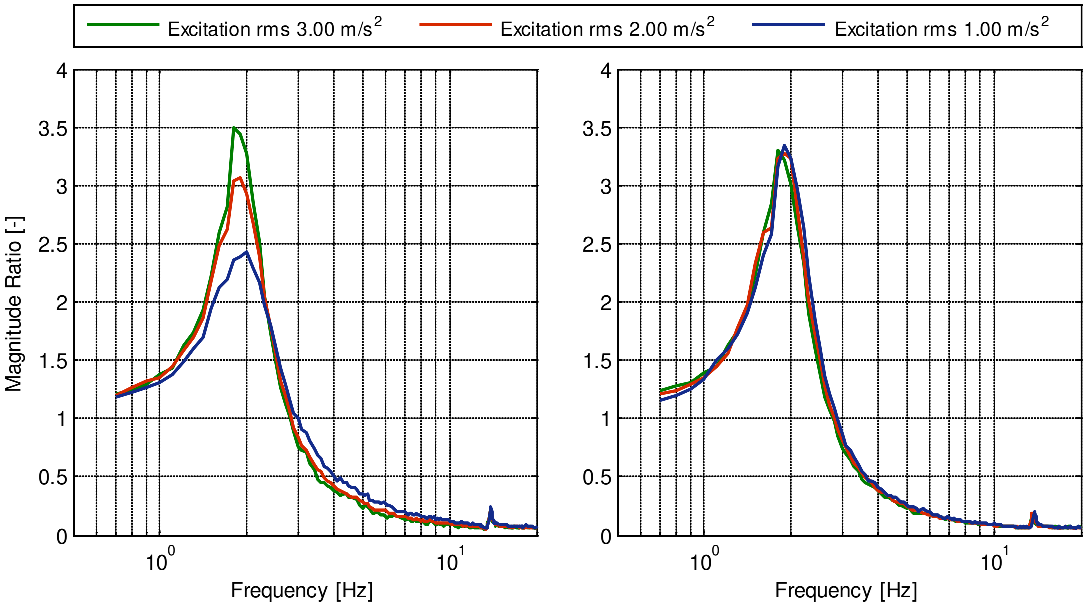

Figure 6-7: The estimated FRFs of the SWEV-A (left) and SWEV-B (right) subjected to acceleration band-limited white noise at various rms intensities (Δf = 0.10 Hz).

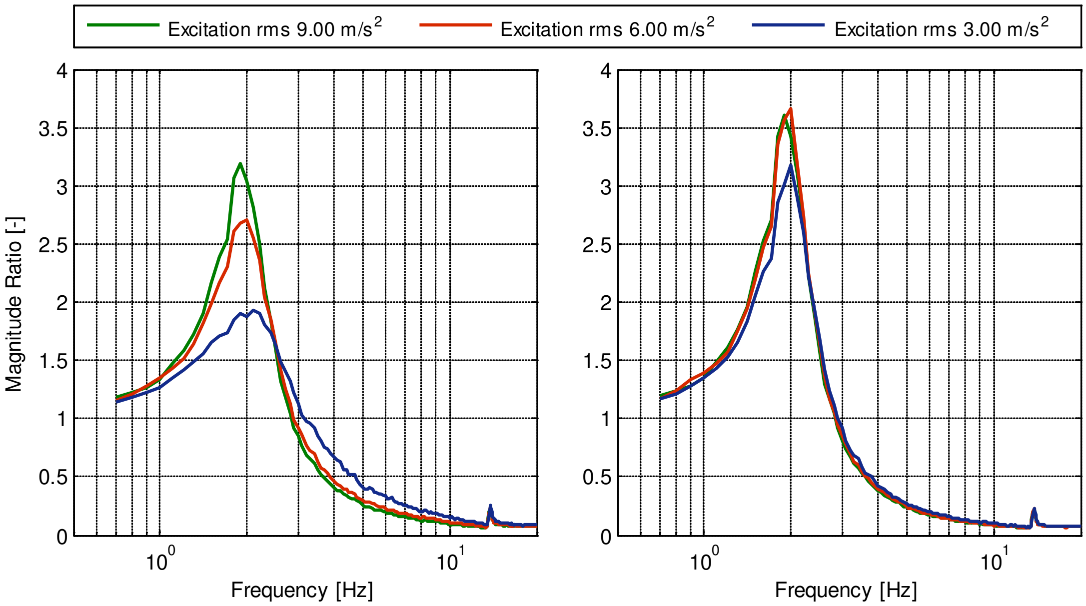

Figure 6-8: The estimated FRFs of the SWEV-A (left) and SWEV-B (right) subjected to acceleration band-limited violet noise at various rms intensities (Δf = 0.10 Hz).

From both series of established FRFs of the SWEV-A, the damping ratio is clearly dependent on the type and level of excitation applied and there is also a slight shift in the main resonance of the sprung mass mode at low excitation levels (rms intensities). The FRFs of the SWEV-B configuration, with its nominally linear shock absorber, exhibit no significant variation in either the natural frequency or damping ratio of the sprung mass mode. The only estimated FRF of the SWEV-B that is noticeably different is the violet noise excitation at an rms level of 3.00 m/s^2.

This was also observed with the SWEV-A and is likely due to the relatively low level of dynamic motion induced into the vehicle during the test (see *Table 6-C*). The estimated values of the sprung mass natural frequency and suspension damping ratio for both configurations of the SWEV were established via curve-fitting from the excitation-response test methods and are presented in *Table 6-D*.

Table 6-D: Estimated dynamic characteristics of the SWEV-A and SWEV-B sprung mass from the excitation-response experiments.

Excitation Type	**Independent Averages**	**Natural Frequency f_{sn} [Hz]**	**Damping Ratio ζ_s [-]**
SWEV-A Configuration			
White Noise rms 1.00 m/s^2	41	2.06	0.228
White Noise rms 2.00 m/s^2	41	1.98	0.173
White Noise rms 3.00 m/s^2	** 19	1.95	0.150
Violet Noise rms 3.00 m/s^2	41	2.22	0.312
Violet Noise rms 6.00 m/s^2	41	2.04	0.200
Violet Noise rms 9.00 m/s^2	41	1.99	0.167
SWEV-B Configuration			
White Noise rms 1.00 m/s^2	41	2.00	0.158
White Noise rms 2.00 m/s^2	41	1.96	0.159
White Noise rms 3.00 m/s^2	** 20	1.93	0.161
Violet Noise rms 3.00 m/s^2	41	2.03	0.172
Violet Noise rms 6.00 m/s^2	41	1.99	0.143
Violet Noise rms 9.00 m/s^2	41	1.98	0.145

** Test was stopped prematurely due to issues with the random vibration controller.

The range of the sprung mass natural frequency estimates for the SWEV-A is 0.11 Hz for the white noise excitations and 0.23 Hz for the violet noise excitations. For the SWEV-B, the total range of the estimated natural frequencies is 0.10 Hz, with the range slightly greater for the white noise (0.07 Hz) than the violet noise excitation (0.05 Hz). For the SWEV-A, the estimated damping ratios were found to vary considerably more for the violet noise excitation than white noise, with ranges of 0.078 and 0.145, respectively. The variation in the estimated damping ratio of the SWEV-B from the white noise excitations is relatively insignificant (range of 0.003).

There is minor variation between the violet noise rms intensities of 6.00 m/s^2 and 9.00 m/s^2 (range of 0.002), however the lowest rms level of 3.00 m/s^2 is greater with a range of 0.027 and 0.029 between the 6.00 m/s^2 and 9.00 m/s^2 rms intensities, respectively. The results of these excitation-response experiments demonstrate the influence of the excitation type and intensity on the estimated dynamic characteristics of the SWEV-A (particularly the damping ratio). From the results, it is observed that the estimates of both the natural frequency and damping ratio of the sprung mass mode decrease as the rms acceleration level increases. The SWEV-B is also dependent on the type and level of excitation, however the variation in the dynamic characteristics is significantly reduced compared to the SWEV-A.

The statistical distributions of the excitation and response were also established. Only one set of PDFs for each excitation type (spectral shape) for the SWEV-A and SWEV-B are presented, as no significant difference was found between the differing rms levels. The excitation and response PDFs from the white noise 1.00 m/s^2 rms test are shown in *Figure 6-9* and *Figure 6-10* for the SWEV-A and SWEV-B, respectively. The established PDFs from the violet noise 6.00 m/s^2 rms test are presented in *Figure 6-11* and *Figure 6-12* for the SWEV-A and SWEV-B, respectively. The values of the kurtosis and skewness of the distributions are listed in *Table 6-E.*

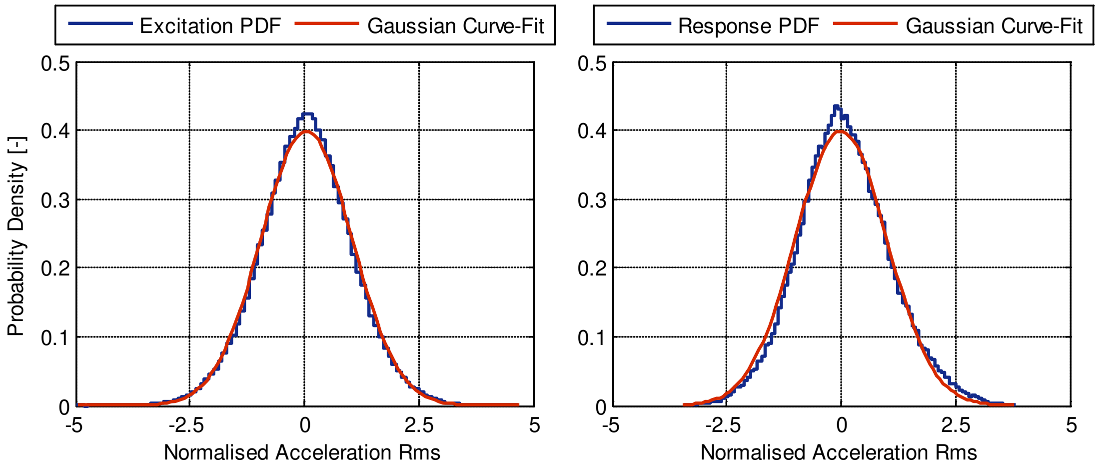

Figure 6-9: PDF of the excitation (left) and response (right), along with the best-fitting Gaussian distribution, for the SWEV-A subjected to white noise excitation at 1.00 m/s^2 rms.

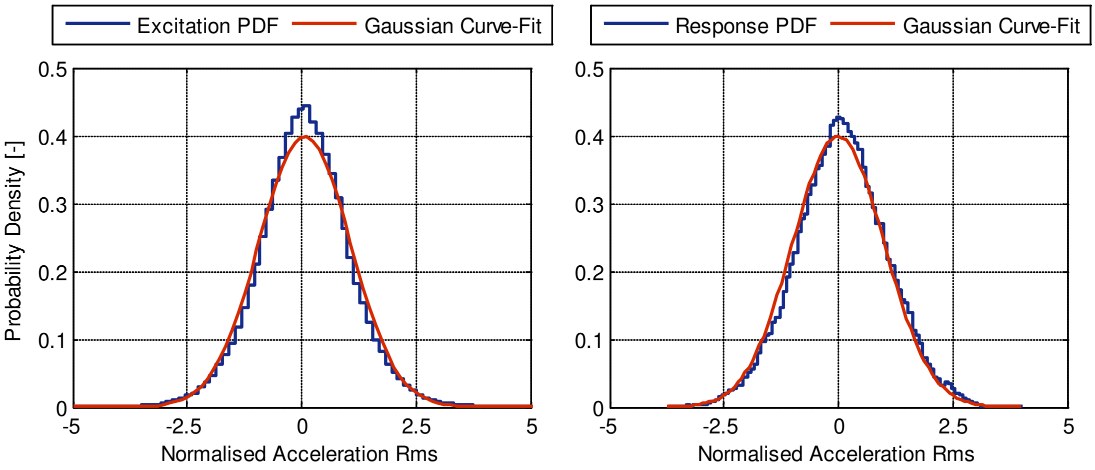

Figure 6-10: PDF of the excitation (left) and response (right), along with the best-fitting Gaussian distribution, for the SWEV-B subjected to white noise excitation at 1.00 m/s^2 rms.

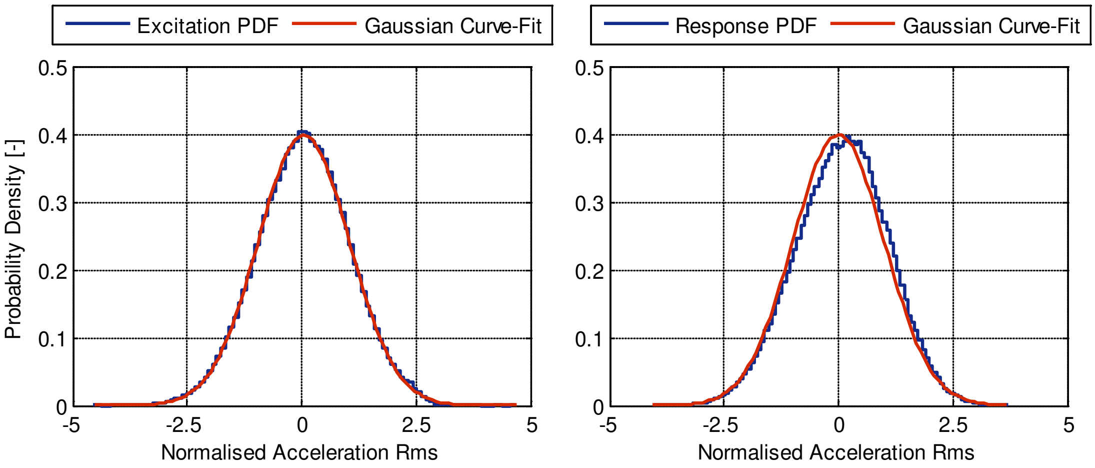

Figure 6-11: PDF of the excitation (left) and response (right), along with the best-fitting Gaussian distribution, for the SWEV-A subjected to violet noise excitation at 6.00 m/s^2 rms.

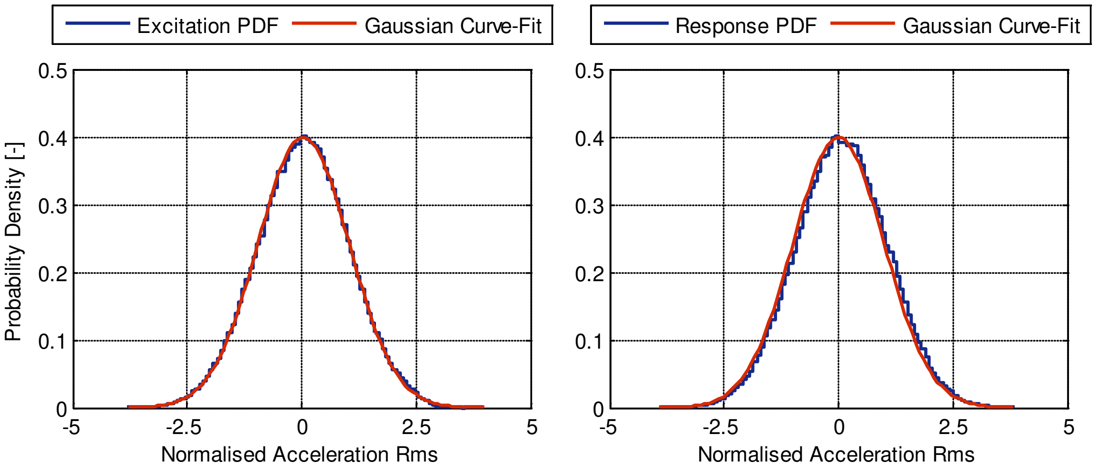

Figure 6-12: PDF of the excitation (left) and response (right), along with the best-fitting Gaussian distribution, for the SWEV-B subjected to violet noise excitation at 6.00 m/s^2 rms.

Table 6-E: The estimated values of the kurtosis and skewness of the excitation and response PDFs for the SWEV-A and SWEV-B from the excitation-response tests.

	Excitation PDF		**Response PDF**	
Excitation Type	**Kurtosis**	**Skewness**	**Kurtosis**	**Skewness**
SWEV-A Configuration				
White Noise rms 1.00 m/s^2	3.29	0.01	3.18	0.17
White Noise rms 2.00 m/s^2	3.48	0.01	3.16	0.04
White Noise rms 3.00 m/s^2	3.61	0.01	3.74	-0.30
Violet Noise rms 3.00 m/s^2	3.15	-0.01	2.76	-0.17
Violet Noise rms 6.00 m/s^2	2.93	-0.05	2.88	-0.10
Violet Noise rms 9.00 m/s^2	2.71	-0.10	2.85	-0.04
SWEV-B Configuration				
White Noise rms 1.00 m/s^2	3.93	0.02	3.10	0.00
White Noise rms 2.00 m/s^2	3.46	0.00	2.99	-0.01
White Noise rms 3.00 m/s^2	3.62	0.00	3.23	-0.13
Violet Noise rms 3.00 m/s^2	3.15	-0.02	2.93	0.02
Violet Noise rms 6.00 m/s^2	2.88	-0.05	2.93	0.00
Violet Noise rms 9.00 m/s^2	2.71	-0.10	2.91	-0.01

For both the SWEV-A and SWEV-B configurations, the excitation and response PDFs from the white noise excitation 1.00 m/s^2 rms test are quite close to following a Gaussian distribution, however both sets of distributions exhibit slight leptokurtic behavior with marginal skewness. The established PDFs from the violet noise 6.00 m/s^2 rms test for the SWEV-A and SWEV-B are all marginally platykurtic, with slight asymmetry (skew). From the PDFs there is no indication of nonlinearity or irregular behavior in either configuration of the SWEV.

6.3 DISCUSSION OF RESULTS

Table 6-E lists all the estimated values of the sprung mass dynamic characteristics (and the average estimates for the response-only (transient) methods) for the SWEV-A and SWEV-B. There is a slight inconsistency between the estimated dynamic characteristics of the SWEV-A from the various test methods, particularly the damping ratio. It is clear that the SWEV-A is nonlinear, as the estimated dynamic characteristics depend on the type and level of excitation. There is a significant decrease in the range of the estimated dynamic characteristics of the SWEV-B, with no significant difference between the estimated values between the excitation-response and response-only (transient) methods.

The reduction in the variation of the estimates is due to the introduction of the nominally linear shock absorber. The nonlinear nature of the SWEV-A configuration, manifested as variation in the estimated damping ratios, is due to the factory-fitted shock absorber. This prompted a thorough experimental study to characterise both shock absorbers using a variety of excitation types, presented in Appendix B. An investigation into the effect of conditioning the shock absorbers prior to the excitation-response experiments (by pumping the shock absorber) was also undertaken and is presented in Appendix B.

Despite the reduced variation in the estimated dynamic characteristics of the SWEV-B (due to the nominally linear shock absorber), it is not known which of the various approaches yield the true FRF (or dynamic characteristics) of both configurations of the SWEV or their relevance to the in-service operation of the vehicle. As these methods all require the vehicle to mobilised and removed from operation for testing, a method to establish the dynamic characteristics using only in-service response data would prove valuable to establish the actual dynamic characteristics of the vehicle as it travels over the road (in the actual operating conditions). Furthermore, the influence of vehicle operating speed will require careful investigation to ascertain the dynamic characteristics and may be a function of the operating speed and would result in a series of FRFs to characterise the vehicle, particularly for the SWEV-A configuration.

Table 6-E: The average estimated values of the sprung mass dynamic characteristics of both SWEV-A and SWEV-B from the response-only and excitation-response methods.

	SWEV-A		**SWEV-B**	
	Natural Frequency	**Damping Ratio**	**Natural Frequency**	**Damping Ratio**
Excitation Type	f_{sn} **[Hz]**	ζ_s **[-]**	f_{sn} **[Hz]**	ζ_s **[-]**
Response-Only (Transient)				
Ramp Test	2.04	0.158	1.97	0.144
Lift and Release Test	2.17	0.252	2.04	0.157
Push and Release (300 N) Test	2.10	0.209	2.05	0.151
Push and Release (600 N) Test	2.07	0.213	2.00	0.149
Excitation-Response				
White Noise rms 1.00 m/s^2	2.06	0.228	2.00	0.158
White Noise rms 2.00 m/s^2	1.98	0.173	1.96	0.159
White Noise rms 3.00 m/s^2	1.95	0.150	1.93	0.161
Violet Noise rms 3.00 m/s^2	2.22	0.312	2.03	0.172
Violet Noise rms 6.00 m/s^2	2.04	0.200	1.99	0.143
Violet Noise rms 9.00 m/s^2	1.99	0.167	1.98	0.145

6.4 CHAPTER SUMMARY

This Chapter critically evaluated a series of currently used experimental methods to establish the dynamic characteristics of road vehicles, using the idealised SWEV. Both configurations of the SWEV were subjected to the three CEU tests for road-friendliness, two of which were slightly modified to suit the vehicle, and various excitation-response random vibration spectra (acceleration white and violet noise) using a large-scale vibration table to estimate the sprung mass damped natural frequency and suspension damping ratio.

The estimated dynamic characteristics of the SWEV-A from the response-only (transient) methods were found to vary. There were minor variations in the estimated sprung mass damped natural frequency, however the damping ratio estimates significantly varied. The estimates of the sprung mass dynamic characteristics of the SWEV-B from the response-only (transient) methods exhibited noticeably less variation. Of the three response-only (transient) methods examined, the ramp test provided the most consistent estimates of the dynamic characteristics.

The excitation-response tests also yielded different estimates of the dynamic characteristics of SWEV-A depending on the type and intensity of the excitation applied. As noted for the response-only (transient) methods, the estimated dynamic characteristics of the SWEV-B were far more consistent than the SWEV-A. The statistical distributions of the measured excitation and response were found to slightly deviate from the Gaussian. The response PDFs were all fairly consistent compared to the excitation PDFs and does not indicate any nonlinear behavior.

While these approaches to estimate the dynamic characteristics appear to work fairly well (particularly with the nominally linear shock absorber in SWEV-B), there are various practical limitations associated with their implementation and use. The response-only (transient) methods depend on the mobility of the vehicle and specialised equipment to undertake the tests, while the excitation-response methods are limited by the need for a large-scale vibration table, which are expensive to install and maintain, and require the vehicle to be driven to the location of the table. Both types of approaches require the vehicle to be removed from normal operation (transportation of goods). Due to the variation in the dynamic characteristics, it is unclear which of the methods establishes the true FRF of the vehicle or their relevance to the vehicle's in-service operation.

An approach that uses the original vehicle configuration and does not require expensive or specialised equipment to induce excitation into the vehicle would provide a far cheaper and easier approach to estimate the dynamic characteristics of road vehicles and would be beneficial for numerous fields. As the SWEV-A configuration exhibits nonlinear behavior, it may be a case that a family of FRFs is required to adequately characterise the vehicle depending on operating speed. The SWEV-B, with the nominally linear shock absorber, exhibited far less variation in the dynamic characteristics obtained and it is expected that this configuration will perform better in terms of establishing a single FRF from the in-service experiments.

Chapter 7

DEVELOPMENT OF IN-SERVICE RESPONSE ANALYSIS TECHNIQUES

This Chapter describes the development of two techniques that will be used to analyse the vibration response data obtained from the in-service experiments to produce estimates of the dynamic characteristics of road vehicles. One of the main outcomes from the critical evaluation undertaken (Chapter 6) was that there are various issues and limitations with the currently used experimental approaches to estimate the dynamic characteristics of road vehicles. Furthermore, the relevance of these tests to a vehicle's normal operation (in-service) has not been established. There exists a great motivation for the development of an approach that can estimate the dynamic characteristics using only in-service response data. While the literature review (Chapter 3) investigated several attempts made to estimate the dynamic characteristics using in-service response data, the research was found to be underdeveloped.

It should also be noted that during the literature review stage, a broad investigation into the various techniques that may be implemented to estimate the dynamic characteristics (or modal parameters) of a system using only in-service response data was undertaken. Several techniques were investigated, such as the wavelet transform and the random decrement method. Another field of research that is gaining considerable interest is operational modal analysis, although the investigation found it is principally concerned with the estimation of the system's mode shapes from response data (requiring multiple measurement points) and not specifically the dynamic characteristics.

Of the various methods investigated, the spectral approach proposed by Rouillard and Sek (2010b) appears to be the most promising, however further work is required to develop and evaluate the approach. This technique aims to establish the FRF of a vehicle by assuming that the excitation PSD function follows the spectral model outlined by the ISO (1995). The second technique chosen for investigation is based on using the random decrement technique to estimate the dynamic characteristics of a vehicle. The random decrement-based technique is experimentally evaluated using response data obtained from a series of vibration table tests in order to determine the optimal parameters to establish the random decrement signature that provides the best estimates of the dynamic characteristics.

7.1 SPECTRAL APPROACH ANALYSIS TECHNIQUE

This section describes the development of a practical approach to establish the FRF of a vehicle using only in-service response data by assuming the excitation follows a predefined spectral shape. The experimental approach, discussed herein, is based on research originally developed by Rouillard and Sek (2010b) and also includes an initial overview of their work and findings.

7.1.1 Background

The principal issue with estimating the dynamic characteristics of vehicles during in-service operation is the difficulty in measuring the excitation applied through the wheels. As discussed in the literature review, Rouillard and Sek (2010b) proposed an alternative solution to the issue by assuming the shape of the pavement elevation profile follows the spectral model outlined under ISO standard 8608 (1995). One issue that has been raised by numerous authors is that the ISO (1995) recommended value of 2.0 for the spectral exponent, w, has been found to vary depending on the pavement. Assuming the excitation follows the ISO (1995) spectral model, Rouillard and Sek (2010b) proposed that the transmissibility FRF of a vehicle may be estimated, along with the spectral properties of the road, using only in-service response data. This forms the basis of an experimental approach to estimate the dynamic characteristics of road vehicles using only in-service response data.

7.1.2 Methodology

The basis of this technique relies on two principal assumptions; 1) the frequency distribution of the response of the vehicle does not vary with a change in operating speed and 2) the longitudinal pavement elevation PSD, G_d, may be adequately described by the ISO 8608 (1995) spectral model in Equation 7-1 (Rouillard & Sek 2010b).

$$G_d = G(n_0)\left(\frac{n}{n_0}\right)^{-w} \tag{7-1}$$

The spectral model of the pavement elevation profile is in spatial frequency, however when analysing vehicle vibration response data it is useful to describe the spectrum in the temporal frequency domain. The spectrum may be converted from the spatial to the temporal frequency domain via Equation 7-2.

$$f = nv \tag{7-2}$$

The conversion of Equation 7-1 from the spatial to the temporal frequency domain is made using Equation 7-2 to obtain the spectral model in the temporal domain and is given in Equation 7-3.

$$G_x = G(n_0)\frac{1}{v}\left(\frac{f}{v\,n_0}\right)^{-w} \tag{7-3}$$

As vehicle vibration response is often measured in acceleration, it is also beneficial to convert the pavement elevation spectrum to acceleration. Taking the double-derivative of the displacement spectrum from Equation 7-3 yields the temporal acceleration spectrum of the pavement, $G_{\ddot{x}}$, shown in Equation 7-4.

$$G_{\ddot{x}} = (2\pi f)^4\, G(n_0)\frac{1}{v}\left(\frac{f}{v\,n_0}\right)^{-w} \tag{7-4}$$

Rouillard and Sek (2010b) stated that the transmissibility FRF of a quarter car travelling at a constant speed, v, can be established from the measured acceleration response PSD function, $R_{\ddot{x}}(f)$, and the predicted acceleration PSD of the pavement profile from Equation 7-4, presented in Equation 7-5.

$$T(f)=\sqrt{\frac{R_{\ddot{x}}(f)}{G_{\ddot{x}}(f)}}=\sqrt{\frac{R_{\ddot{x}}(f)}{G(n_0)}\frac{f^{\left(\frac{w}{2}-2\right)}}{(2\pi)^2\,{n_0}^{w/2}\,v^{(w-1)/2}}} \tag{7-5}$$

Provided that the quarter car is linear, such that the frequency response does not vary with a change in operating speed, the transmissibility FRF of the quarter car at two different constant operating speeds, v_1 and v_2, will be equal, as shown in Equation 7-6.

$$T(f)_{v_1}=T(f)_{v_2} \tag{7-6}$$

where $T(f)_{v_1}$ and $T(f)_{v_2}$ are the transmissibility FRFs of a vehicle travelling at two different constant operating speeds v_1 and v_2.

Equations 7-5 and 7-6 reveal the motivation to convert the pavement spectral model to the spatial frequency domain, since a vehicle travelling over the same pavement at two different nominally constant operating speeds will be subjected to a different spatial frequency bandwidth, but the same temporal frequency bandwidth. Substituting the relationship of the transmissibility FRF of a quarter car (Equation 7-5) at two different operating speeds into Equation 7-6 yields Equation 7-7.

$$\sqrt{\frac{R_{\ddot{x}_1}(f)}{G(n_0)}\frac{f^{\left(\frac{w}{2}-2\right)}}{(2\pi)^2\,{n_0}^{w/2}\,{v_1}^{(w-1)/2}}}=\sqrt{\frac{R_{\ddot{x}_2}(f)}{G(n_0)}\frac{f^{\left(\frac{w}{2}-2\right)}}{(2\pi)^2\,{n_0}^{w/2}\,{v_2}^{(w-1)/2}}} \tag{7-7}$$

Equation 7-7 is then simplified:

$$\sqrt{R_{\ddot{x}_1}(f)\frac{1}{{v_1}^{(w-1)/2}}}=\sqrt{R_{\ddot{x}_2}(f)\frac{1}{{v_2}^{(w-1)/2}}} \tag{7-8}$$

A further simplification of Equation 7-8 can be achieved by combining the related terms together, shown in Equation 7-9.

$$\sqrt{\frac{R_{\ddot{x}_1}(f)}{R_{\ddot{x}_2}(f)}}=\left(\frac{v_1}{v_2}\right)^{(w-1)/2} \tag{7-9}$$

The only unknown term is the spectral exponent, w. By squaring and then taking the natural logarithm of both sides of Equation 7-9, the relationship described in Equation 7-10 is obtained.

$$\ln\left(\frac{R_{\ddot{x}_1}(f)}{R_{\ddot{x}_2}(f)}\right)=(w-1)\ln\left(\frac{v_1}{v_2}\right) \tag{7-10}$$

Finally, transposing Equation 7-10 yields a relationship to establish the spectral exponent, w, given in Equation 7-11.

$$w=\frac{\ln\left(\frac{R_{\ddot{x}_1}(f)}{R_{\ddot{x}_2}(f)}\right)}{\ln\left(\frac{v_1}{v_2}\right)}+1 \tag{7-11}$$

The relationship described in Equation 7-11 was originally derived by Rouillard and Sek (2010b) to estimate the value of the spectral exponent of the pavement (assuming it converges to the standard ISO spectral model). This approach establishes an estimate of the spectral exponent as a function of temporal frequency. It is to be expected that the frequency response of real vehicles will be contaminated with noise and other effects associated with real vehicles (such as drive-train noise and MISO effects), care should be exercised when selecting the relevant frequency range to estimate the spectral exponent. It is expected that the region of the sprung mass mode, where the response is most significant and least likely to be contaminated with noise or other components, will provide the best estimate of the spectral exponent of the pavement.

As a further development to this approach, an alternative method to establish the spectral exponent can be deduced using only the root-mean-square of the acceleration response. The square-root of the integral of the response PSD function is equal to the rms of the acceleration response, shown in Equation 7-12.

$$\sqrt{\int_{f_{\min}}^{f_{\max}} R_{\ddot{x}_1}(f)\,df} = \sqrt{\frac{1}{N}\sum \ddot{x}_1^{\,2}} = rms_{\ddot{x}_1} \tag{7-12}$$

where $f_{\min}$ and $f_{\max}$ are the lower and upper limits of the frequency response.

Still assuming that the frequency distribution of the response PSD functions do not vary for different constant operating speeds, the square-root of the ratio of the two PSD functions is equal to the ratio of the rms acceleration response, given in Equation 7-13.

$$\sqrt{\frac{R_{\ddot{x}_1}(f)}{R_{\ddot{x}_2}(f)}} = \frac{rms_{\ddot{x}_1}}{rms_{\ddot{x}_2}} \tag{7-13}$$

Finally, substituting Equation 7-13 into Equation 7-11 yields another relationship to establish the spectral exponent, this time as a function of the ratio of the rms acceleration response values, shown in Equation 7-14.

$$w = \frac{2\ln\left(\dfrac{rms_{\ddot{x}_1}}{rms_{\ddot{x}_2}}\right)}{\ln\left(\dfrac{v_1}{v_2}\right)} + 1 \tag{7-14}$$

An estimate of the spectral exponent can be obtained using either Equations 7-11 or 7-14. Once the spectral exponent has been estimated, the remaining unknown parameter of the spectral model of the pavement is the roughness constant, $G(n_0)$. To estimate the roughness constant of the pavement spectrum, and therefore obtain the transmissibility FRF of the vehicle, Equation 7-5 is used to adjust the value of the roughness constant (shifting the spectrum up or down) until it approaches one (unity) at low frequency. The advantage of this approach is that not only is the transmissibility FRF of the vehicle estimated, but also the pavement spectral model.

7.1.3 Evaluation of the Spectral Approach

As discussed in the literature review, Rouillard and Sek (2010b) undertook a series of in-service experiments using a light transport vehicle over a rural country road in Victoria, Australia. A comparison between the measured FRF using broad-band excitation on a vibration table and the predicted vehicle FRF (using measured response data and an assumed spectral model for the excitation) did not yield the best agreement when the standard value of the spectral exponent of 2.0 was used. Furthermore, difficulties were encountered with the frequency response contaminated by the presence of an "unidentified response spectral peak" within the region of 25 – 30 Hz. These harmonics were believed to be due to wheel imbalance and drive-train noise. The authors concluded that while the approach is promising, further work is required to establish the technique for a variety of experimental vehicles and roads and to quantify the effects of vehicle speed and suspension type. The influence of the record length (road length) on the response PSD must also be investigated and whether the spectral exponent actually tends towards 2.0 as the length of the road increases.

The authors did not discuss how to extract an estimate of the spectral exponent. The estimate was originally presented as a function of frequency, but due to fluctuations in the measured response spectra it was difficult to select a single value. Three possible approaches could be used to establish a single estimate of the spectral exponent:

1) Use the original approach (as a function of frequency) and take an average value.
2) Select an appropriate frequency bandwidth (ideally around the region of the sprung mass mode) and take an average value (or statistical distribution).
3) Use the ratio of the rms of the response.

A simple numerical model was developed to provide an initial evaluation of the feasibility and sensitivity of the approach to identify any potential pitfalls or issues that may arise. A numerical quarter car FRF model developed by Prem (1987) was used with a generated ISO 8608 (1995) road spectral model (violet noise) in the spatial domain with a spectral exponent of 2.0. *Figure 7-1* shows the pavement elevation PSD functions converted into the temporal domain for three vehicle operating speeds, along with the FRF of the vehicle for these simulations. In *Figure 7-2*, the obtained response spectra are computed by combining the FRF with each of the pavement elevation spectra and the estimated value of the spectral exponent using the ratio of the response spectra only are presented. The estimated spectral exponents using the ratio of the rms of the acceleration response for all speed ratios was 2.00. As expected, for a completely idealised system, the approach is able to correctly estimate the value of the spectral exponent of the excitation for all vehicle speed ratios. The results from the model show that if Rouillard and Sek's (2010b) assumption that the excitation applied to the vehicle is the same, then the spectral exponent of the pavement is able to be estimated using only in-service response data.

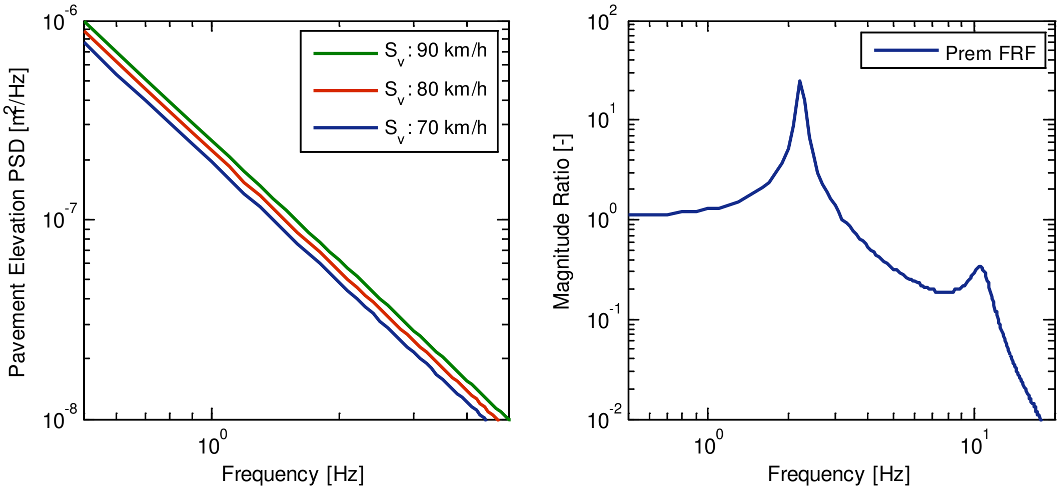

Figure 7-1: The pavement spectra for each vehicle speed (left) and the transmissibility FRF by Prem (1987) (right) from the numerical model.

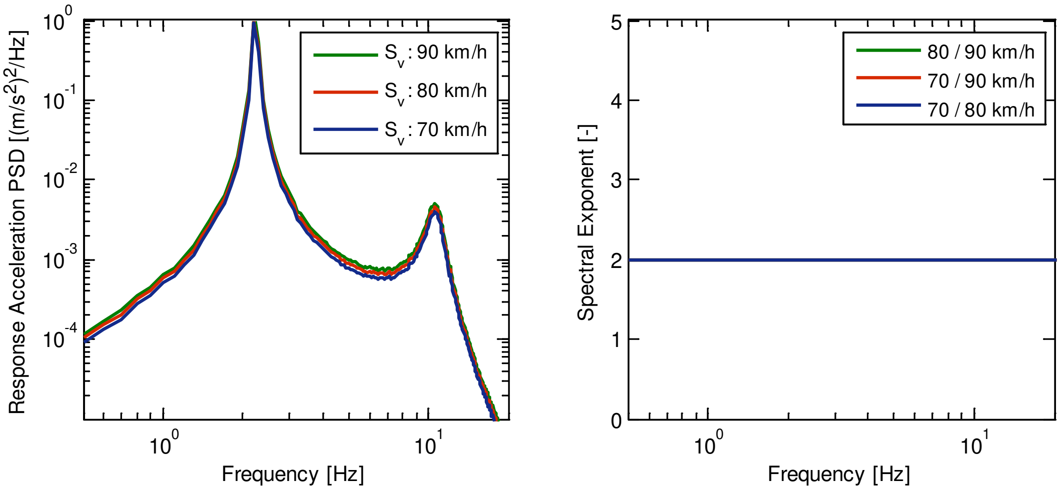

Figure 7-2: The computed response spectra for each idealised vehicle speed (left) and the estimated spectral exponents for each speed ratio (right) from the numerical model.

While it is obvious that the approach correctly estimates the spectral exponent for an idealised case, it can be used to provide an insight into issues that may be encountered. One possible issue that may arise is if the pavement spectral shape changes slightly between two experimental runs. Equation 7-5 assumes the vehicle travels over exactly the same pavement, however in practice it is unlikely that a vehicle will travel along exactly the same wheel paths twice. If the ISO spectral model is able to adequately characterise the pavement, then only two parameters may vary; the roughness constant, $G(n_0)$, and the spectral exponent, w.

7.1.3.1 Influence of Variation of the Spectral Exponent

The first parameter to investigate the effect of slight variation between experimental runs is the spectral exponent. Recall from *Table 3-A* in the literature review, Kropac and Mucka (2008) established the spectral exponent for a variety of pavements and found that the standard deviation of the exponent can be a significant. Using the same quarter car FRF model, the pavement spectra were slightly varied for the two different speeds; the 70 km/h excitation spectrum had an exponent of 2.0, while the 80 km/h excitation spectrum had an exponent of 1.9. The two pavements are shown in *Figure 7-3*, along with the vehicle FRF used, while the computed response spectra and the estimated spectral exponent are shown in *Figure 7-4*.

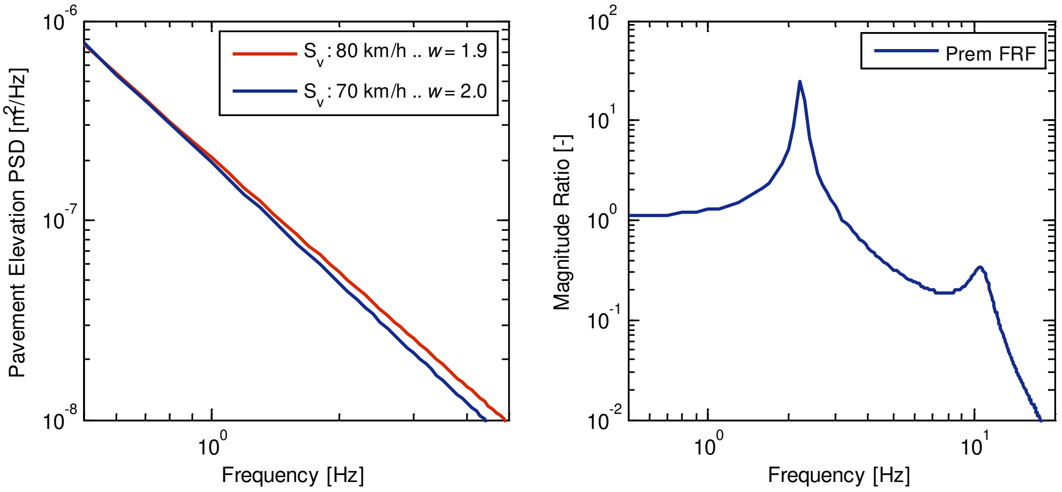

Figure 7-3: The pavement spectra for the two vehicle speeds with a slightly different spectral exponent (left) and the transmissibility FRF by Prem (1987) (right) from the numerical model.

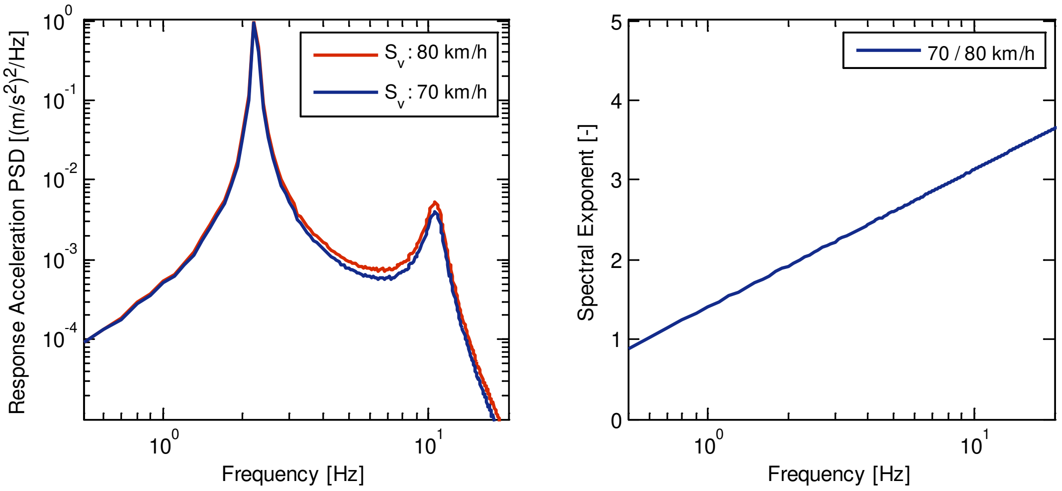

Figure 7-4: The response spectra for each vehicle speed (left) and the estimated spectral exponent (right) from the numerical model.

Interestingly, the spectral exponent (as a function of frequency) estimated using the spectral approach takes the form of a linear function in semi-logarithmic scales. The estimated spectral exponent using the ratio of the response rms for the speed ratio of 70 / 80 km/h was 2.08. The results indicate that if the excitation spectrum between two experiments are not the same, such that the slope of the spectrum varies (even if only slightly), then neither the spectral or rms approaches will be able to accurately estimate the spectral exponent.

7.1.3.2 Influence of Variation of the Roughness Constant

The roughness constant, $G(n_0)$, was varied between two vehicle speeds. Using the same quarter car transmissibility FRF model, the pavement spectra were varied for the two different runs; the 70 km/h excitation spectrum had a roughness constant of 1×10^{-6} m^3, while for the 80 km/h excitation spectrum a roughness constant of 2×10^{-6} m^3 was used, corresponding to a class A and B road under the ISO standard 8608 (1995), respectively.

From *Figure 7-5*, the two excitation spectra may be seen along with the FRF used. The established response spectra are shown in *Figure 7-6*, along with the estimated spectral exponent using the spectral approach. The estimated spectral exponent using the ratio of the rms of the response data for 70 / 80 km/h was 7.19. If the roughness constant is varied between two experimental runs, the spectral exponent is unable to be accurately estimated. It is clear that the technique is sensitive to minor variations in the excitation spectrum. In practice, a measurement of the pavement elevation profile may be required to identify any unusual characteristics or features of the pavement surface.

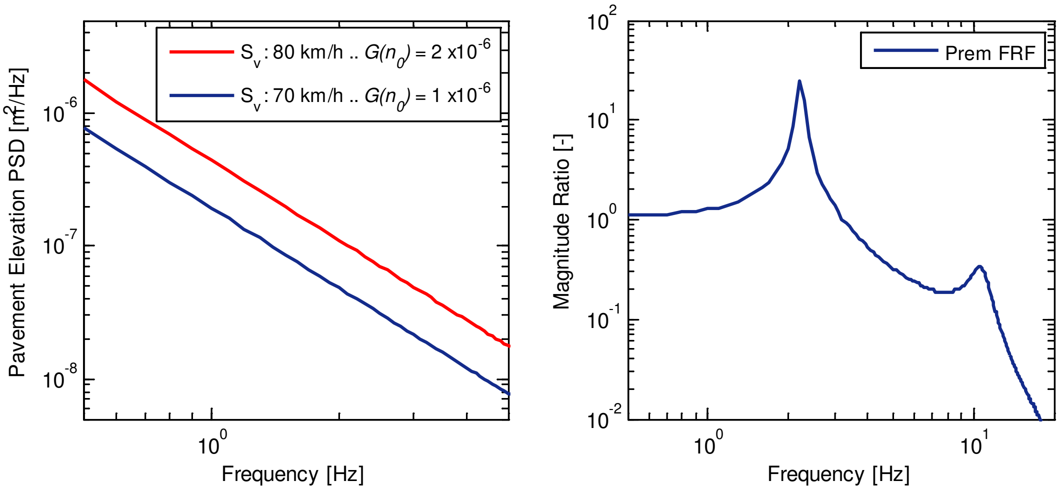

Figure 7-5: The pavement spectra with two different roughness constants (left) and the transmissibility FRF by Prem (1987) (right) for the numerical model.

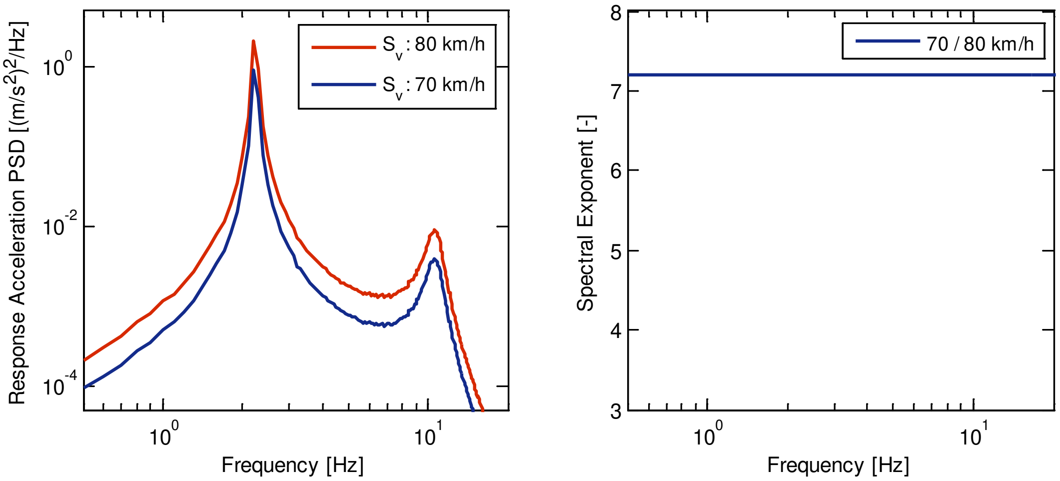

Figure 7-6: The response spectra for each vehicle speed (left) and the estimated spectral exponent (right) from the numerical model.

7.2 RANDOM DECREMENT BASED ANALYSIS TECHNIQUE

This section describes the development of an analytical technique based on the random decrement method to estimate the dynamic characteristics of road vehicles using only in-service response data. While the random decrement has been used for many years, it is not a straightforward technique to implement and has not, up until this point at least, been used to analyse vehicle response data. A review of the random decrement technique was presented in the literature review (Chapter 3). This section is focused on describing the methodology to analyse in-service response data from road vehicles to establish the random decrement signature to estimate the dynamic characteristics, along with an experimental evaluation to identify the optimum parameters for the technique. For the experimental evaluation, the SWEV-B (100 kg) configuration was placed on a vibration table and subjected to various excitations while the excitation and response were simultaneously measured to establish the FRF as a reference. The various parameters that may be implemented to establish the random decrement signature vary depending on the system under analysis. As no literature examined has discussed the use of the random decrement technique for estimating the dynamic characteristics of road vehicles, an experimental evaluation was undertaken to assist in the identification of the optimal parameters.

7.2.1 Methodology

This section outlines the methodology and the various considerations that must be made in order to obtain the best possible random decrement signature from the in-service response data once it has been measured. The general methodology for the random decrement analysis of in-service response data is presented in the form of a flow chart in *Figure 7-7* below.

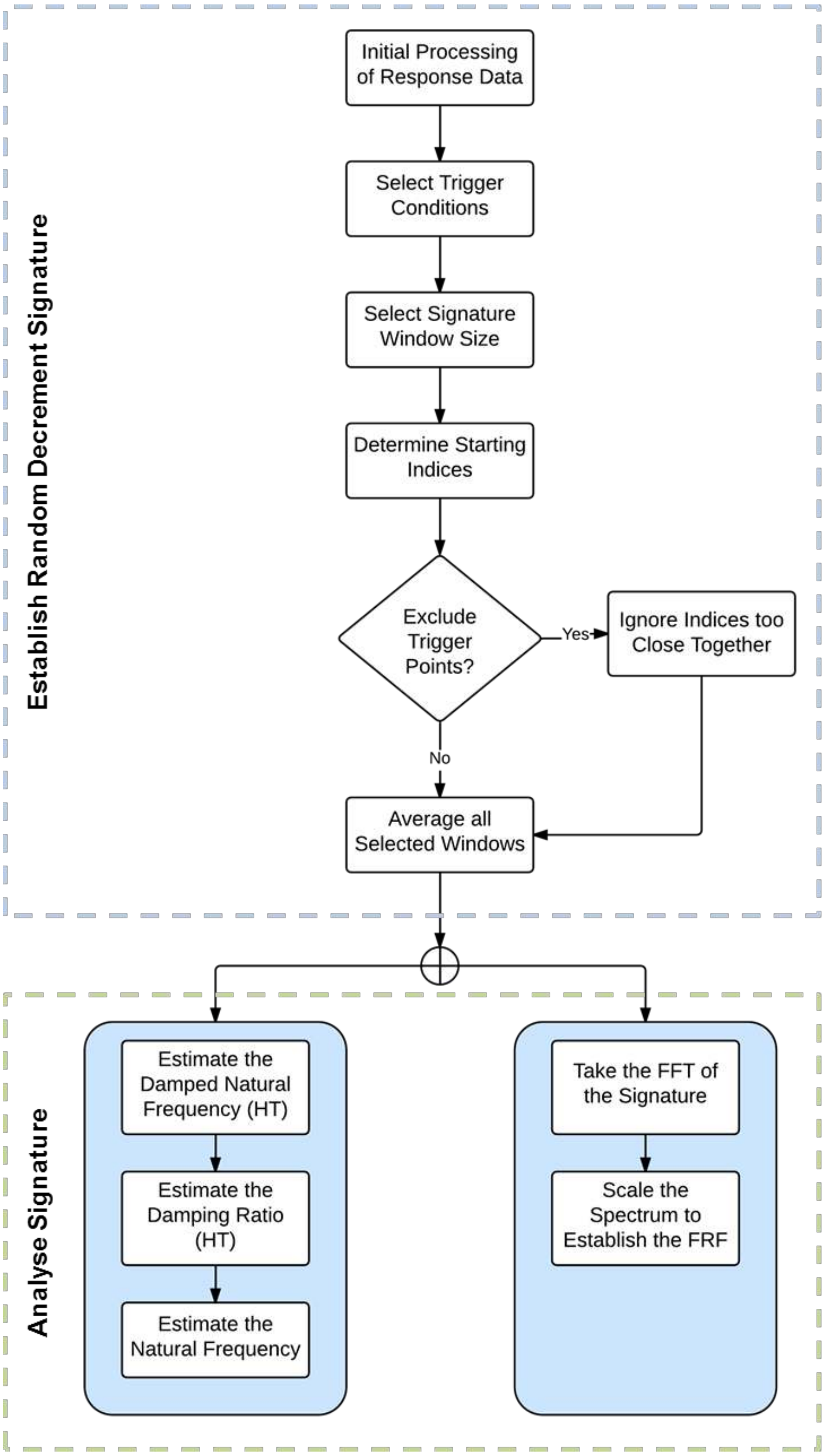

Figure 7-7: A flow chart of the general methodology of the random decrement technique.

The various steps outlined in the above flow chart above are described in detail in this section.

1) Initial processing of the response data.

Standard signal processing of the vibration response data is often required prior to the analysis. This may include removing the mean offset of the signal or visually inspecting the data to determine whether the measured signal appears ‘as expected’ or is corrupted due to faults with the instrumentation or measurement procedures and set-up. The vibration response data may require filtering in order to separate the response of the sprung and unsprung mass modes and may require a random decrement signature to be obtained for each mode. It is sufficient to isolate the response of the sprung mass using a low-pass filter, while isolating the unsprung mass will require the use of both a low-pass and high-pass filter or a band-pass filter.

2) Selection of the trigger conditions and random decrement signature type.

The trigger level condition determines when each section, or window, begins and affects the number of averages obtained. Generally, the higher the trigger level is set, the fewer number of averages will be obtained for the random decrement signature, and vice-versa. While some triggers are able to obtain a significantly greater number of averages than others; they are often more relaxed with their conditions. The shape of random decrement signature obtained will depend on the selected trigger type. This emphasises the importance of selecting a suitable triggering type and level that not only acquires a sufficient number of averages, but is able to establish the most accurate estimates of the dynamic characteristics of the vehicle. A wide variety of trigger types and levels exist that can be implemented to establish the random decrement signature, such as crossing up or down through a selected trigger level or selecting all positive points within the signal.

3) Selection of the random decrement signature window size.

The window size, often expressed in terms of duration, is the length of the obtained random decrement signature. Depending on the approach used to analyse the random decrement signature, the window size may need to be sufficiently long to provide a reasonable frequency resolution when analysing the signature using the FFT, or at least is long enough to capture the full decay of the response. A system with light damping often requires a longer window size, while increased levels of damping will not always necessitate (or allow) a longer duration. The window size will also have a small influence on the number of averages obtained.

4) Determine the indices of all points in the signal that occur just before the threshold.

Once the trigger conditions have been set, the indices of the beginning of each section must be established. It is important to consider whether every window that is selected by the trigger conditions can be used. While Asmussen (1997) stated that it was “very difficult to exclude some of the triggering points without introducing bias” it still is a factor that requires consideration. Similar to the effect of double-tapping with a modal hammer, obtaining and averaging windows that begin too close together may distort the obtained random decrement signature.

5) Average all selected sections to establish the random decrement signature.

A sufficient number of averages are required to remove the influence of noise and other artifacts present in the vibration response. The factors that affect the number of averages obtained are the trigger type and level, the window size, whether any sections are skipped and the total duration of the experimental measurement. The minimum number of averages required varies significantly between different authors and applications, ranging from 200 to 2,000 averages.

6) Estimate the dynamic characteristics from the random decrement signature.

Once the random decrement signature has been established, the dynamic characteristics of the system may be estimated using two different approaches. The first approach estimates the dynamic characteristics in the Hilbert domain. While the FFT was initially used to estimate the sprung mass mode damped natural frequency, the magnitude spectrum (in some cases) contained split peaks, known as the “picket fence effect” (Randall 1987, p. 161). To circumvent this issue, the damped natural frequency is estimated from the slope of the unwrapped instantaneous phase (Equation 3-35). The damping ratio is estimated using the instantaneous envelope of the signature via the Hilbert Transform.

The second approach estimates the FRF of the vehicle directly from the random decrement signature. In the literature review, Equation 3-42 demonstrated that the FRF of a system can be established by taking the FT of its impulse response function. The obtained random decrement signature is an estimate of the impulse response function and taking the FFT of the signature establishes the unscaled FRF. The unscaled FRF is then scaled so the low frequency tends to unity to estimate the vehicle’s transmissibility FRF.

7.2.2 Dynamic Characteristics Estimation (Hilbert Domain)

As outlined in the previous section, establishing the random decrement signature alone is insufficient; further analysis is required to establish the dynamic characteristics of the vehicle. The first approach investigated aims to estimate the dynamic characteristics of the vehicle (in the form of the natural frequency and damping ratio) using the response-only (transient) analysis techniques (in the Hilbert domain). This section describes the experimental development and optimisation of parameters to establish the best random decrement signature for analysis.

7.2.2.1 Initial Experimental Parameter Selection and Processing

From the general methodology and the literature review, some of the parameters of the random decrement technique may be initially selected to form a basis for the forthcoming experimental evaluation section. Prior to the initial processing of the data, it is recommended to inspect the response data in the frequency domain (by computing the autospectrum) to identify the approximate frequency location of the sprung and unsprung mass modes. This enables the most appropriate filtering to be used depending on which mode is isolated. The sprung mass mode is easily isolated using a low-pass filter, however the unsprung mass mode may be more difficult to identify, particularly if its contribution to the response is significantly less in comparison to the sprung mass mode. If this is the case, then it will prove relatively difficult to establish the dynamic characteristics of the unsprung mass mode.

From the literature review, Asmussen (1997) stated that the random decrement signatures obtained for highly-damped systems will be subject to bias and in order to avoid this, the response of the system must be measured with a high sampling frequency. Using a high sampling frequency is no longer a significant issue due to the vast improvements made in computational power and storage. As with the critical evaluation experiments (Chapter 6), a sampling frequency of 1000 Hz is used. This sampling frequency is significantly higher than either the sprung or unsprung natural frequencies expected for vehicles, recalling that Gillespie (1992b, p. 125) stated that the vibration associated with vehicle ride is within the region of 0 – 25 Hz.

Given that the damped natural frequency of the system is estimated by finding the slope of the unwrapped instantaneous phase of the random decrement signature, the length of the phase is dependent on the window size. Also, as the level of damping in vehicle suspension systems is relatively high in comparison with many of the structures often analysed using the random decrement technique, a window size of 5 s can be considered a sufficient starting point. The effect of the window size on the random decrement signature and the estimated dynamic characteristics will be experimentally evaluated in the following section to ensure the most appropriate window size is selected.

7.2.2.2 Experimental Optimisation of Parameters

No publications have been encountered describing the use of the random decrement technique to analyse the vibration response of road vehicles. In order to evaluate and identify the optimum approach and parameters, this section describes an experimental evaluation of the random decrement technique to establish the dynamic characteristics of the SWEV (Hilbert Domain). In order to experimentally evaluate the parameters used to establish the dynamic characteristics using the random decrement signature obtained from in-service response data, the SWEV-B (100 kg loading) configuration was placed on a vibration table and subjected to band-limited white noise acceleration excitation at three different rms intensities of 0.25, 0.50 and 0.75 g (1 – 100 Hz frequency bandwidth). The excitation and response were simultaneously measured for a total duration of 300 s. While it was considered to use a spectral shape similar to that of longitudinal pavement profiles, from the literature review it was found that the random decrement technique is unaffected by a variety of excitation spectral shapes (Ibrahim 1980).

The excitation-response data obtained for the two configurations of the SWEV presented in the critical evaluation Chapter were unable to be used as the dynamic motion of the seismic mass was found to influence the data (around the sprung mass resonant frequency). While this did not affect the measurement of the FRFs, the random decrement technique will be unable to distinguish the response of the vehicle from the motion of the seismic mass. To prevent the seismic mass from moving, it was chocked for the duration of the tests. The FRFs for each of the three excitation intensities were established and are shown in *Figure 7-8*. The estimated natural frequencies and damping ratios of the sprung mass mode were established by curve-fitting each of the FRFs and are presented in *Table 7-A*.

Table 7-A: Natural frequency and damping ratio estimates (via curve-fitting) of the sprung mass mode of the SWEV-B configuration loaded with 100 kg dead weight subjected to various band-limited white noise excitation intensities.

Excitation Type	**Damped Natural Frequency f_{sd} [Hz]**	**Natural Frequency f_{sn} [Hz]**	**Damping Ratio ζ_s [-]**
White Noise rms 0.25 g	1.92	1.94	0.150
White Noise rms 0.50 g	1.87	1.90	0.156
Violet Noise rms 0.75 g	1.89	1.91	0.142

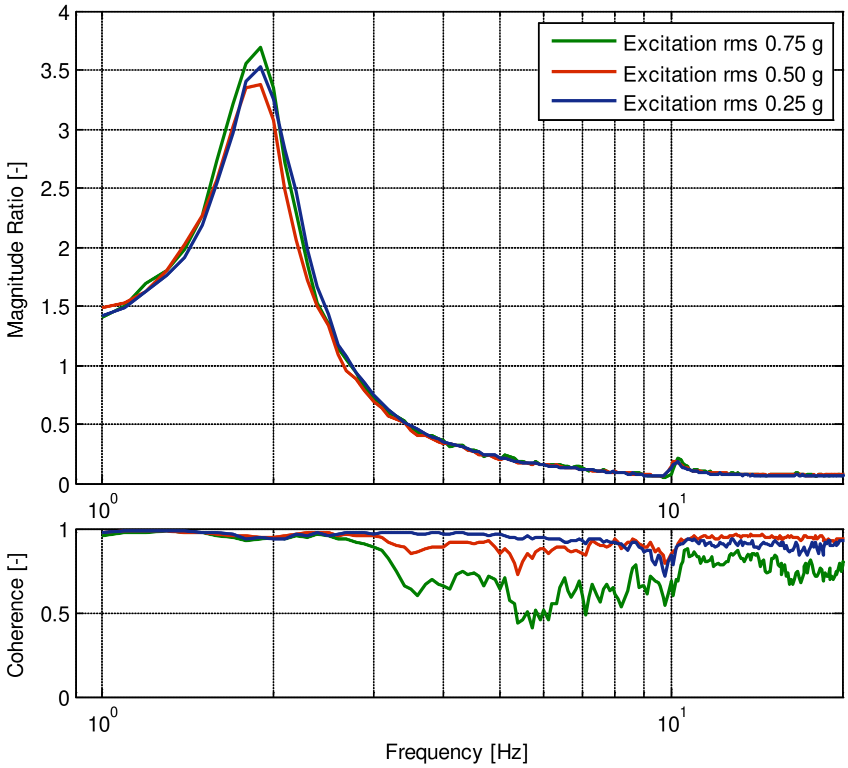

Figure 7-8: The established FRFs of the SWEV-B (100 kg) subjected to various band-limited white noise excitations at various rms intensities (Δf = 0.10 Hz).

Inspection of the FRFs and the estimated dynamic characteristics show that there is no significant difference between the various excitation intensities, and so only the response data from the band-limited white noise 0.25 g rms test will be used for the experimental evaluation. The established FRFs of the SWEV-B (100 kg) in *Figure 7-8* also show the significantly smaller contribution of the unsprung mass mode in comparison to the sprung mass mode. This indicates that it may be difficult to identify the natural frequency and damping ratio of the unsprung mass using in-service response data.

The parameters that have been set to establish the random decrement and the dynamic characteristics, unless stated otherwise, are:

- Sampling frequency of 1,000 Hz for the measurement of the response data.
- A 5th order Butterworth low-pass filter with a cut-off frequency of 8 Hz to isolate the response of the sprung mass.
- Window size of 5 s for the random decrement signature.

The various cases examined all use the measured vibration response from the band-limited white noise 0.25 g rms excitation. The first case evaluates the various trigger types and levels. While a wide variety of triggering conditions exist, this experimental evaluation is focused on four different trigger types: 1) trigger crossing up, 2) trigger crossing down, 3) the local positive extremum trigger and 4) the positive point triggering condition. Both the trigger crossing up and down conditions begin when the signal crosses up or down through a selected level. The trigger level is often described in terms of the standard deviation of the response, with values of 0 (zero-crossing), 0.5, 1.0, 1.5, 2.0 and 2.5-times the standard deviation (σ) evaluated.

The local positive extremum triggering condition finds the maximum value within a predefined tracking window and then takes an equal amount of data either side of this maximum value. The tracking window is independent of the random decrement signature window size. If, for example, a tracking window of 1 s and a random decrement signature window of 5 s are selected then the positive maximum is detected within this 1 s tracking window, while the random decrement section selected is 2.5 s either side of the detected maximum. The positive points triggering condition begins when a positive value is encountered (within a predefined bandwidth) and is expected to acquire the most number of averages compared to any of the other triggers.

A comparison of the four different random decrement signatures (different trigger types) is presented in *Figure 7-9*. From the figure, the trigger up, trigger down and positive points trigger conditions obtain a similarly shaped signature. The local extremum trigger condition obtains a random decrement signature that is different to the other three triggering conditions and resembles an autocorrelation function. The estimated values of the damped natural frequency and damping ratio of the sprung mass mode for each trigger are given in *Table 7-B*.

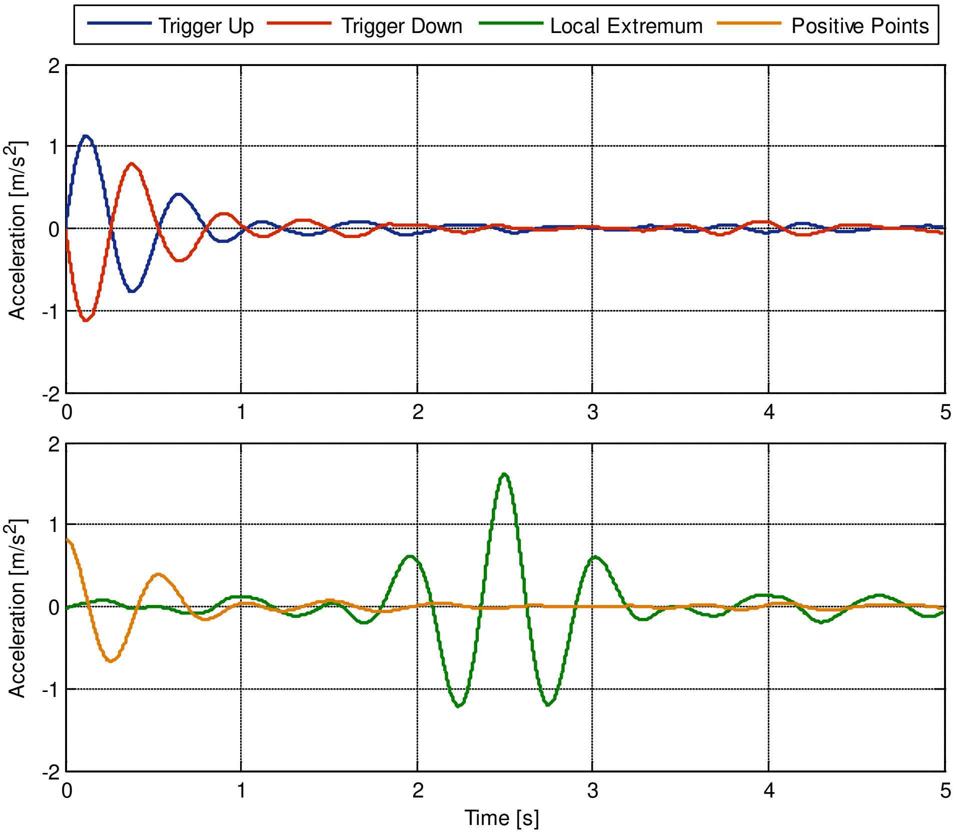

Figure 7-9: Typical examples of the various random decrement signatures from the band-limited white noise 0.25 g rms response data using various triggering conditions.

Table 7-B: The estimates of the sprung mass mode dynamic characteristics and number of averages obtained for each random decrement signature subjected to band-limited white noise 0.25 g rms.

Trigger Type	**Signature Averages N_{RD}**	**Natural Frequency f_{sn} [Hz]**	**Damping Ratio ζ_s [-]**
Trigger Up			
0	592	1.94	0.151
0.5 × σ	523	1.95	0.159
1.0 × σ	366	1.95	0.153
1.5 × σ	198	1.96	0.151
2.0 × σ	69	2.17	0.153
2.5 × σ	16	2.15	0.149
Trigger Down			
0	593	1.96	0.152
0.5 × σ	524	1.94	0.146
1.0 × σ	366	1.97	0.153
1.5 × σ	198	1.97	0.154
2.0 × σ	69	2.12	0.163
2.5 × σ	16	2.16	0.152
Local Positive Extremum			
1 s	297	1.88	0.156
2 s	148	1.92	0.169
5 s	59	2.05	0.161
Positive Points			
(0 ∞]	148,460	1.95	0.149
(0.5 × σ ∞]	94,989	1.96	0.148
(1.0 × σ ∞]	48,584	1.95	0.152
(1.5 × σ ∞]	19,639	1.92	0.151
(2.0 × σ ∞]	5,614	2.15	0.161
(2.5 × σ ∞]	1,107	2.01	0.113

The closest agreement with the estimates of the dynamic characteristics obtained from the measured FRF occurs when the triggering conditions are either: 1) trigger up with a zero-crossing trigger level or 2) trigger down with a trigger level of 0.5 × σ. As mentioned, the triggering conditions directly influence the number of averages obtained and from the results it appears that at least 500 averages is required to provide the best estimates of the dynamic characteristics. Despite the positive points triggering condition obtaining a substantially greater number of averages than the other triggering conditions, the estimates of the dynamic characteristics are not in close agreement with the established FRF.

One further consideration that may be made is to use the same number of averages for each triggering condition by ignoring any extra averages that may be obtained, however recall that in the literature review Asmussen (1997) stated that it was "very difficult to exclude some of the triggering points without introducing bias" and so it is not recommended to evaluate the triggering conditions while limiting the number of averages. For simplicity, the trigger up with a zero-crossing level will be used for the in-service experiments as the trigger level remains the same, not as a function of the standard deviation.

The second case investigated the effect of the window size on the random decrement signature (and therefore on the estimated dynamic characteristics of the sprung mass). Four different window sizes are to be investigated: 1, 2, 5 and 10 s. The random decrement signatures for each of the four window sizes are presented in *Figure 7-10*, while the estimated natural frequencies and damping ratios are listed in *Table 7-C*. From *Figure 7-10*, the various random decrement signatures do not vary significantly, particularly at the beginning of the signature up to approximately 3 s. This is due to the marginal difference between the number of acquired averages for each signature.

From *Table 7-C*, a window size of 5 s provides the best agreement to the established dynamic characteristics of the SWEV-B sprung mass mode, particularly the natural frequency estimates. For the estimation of the damping ratio, the best fit was obtained between approximately 0.2 – 0.8 s, so the additional length of the window size is only useful for estimating the damped natural frequency, however a 10 s window does not provide an estimate as close as the established sprung mass dynamic characteristics. This is likely a result of the additional 5 s of the signature containing no significant component of the decayed response (as the SWEV-B's damping level is quite high and decays in a shorter duration).

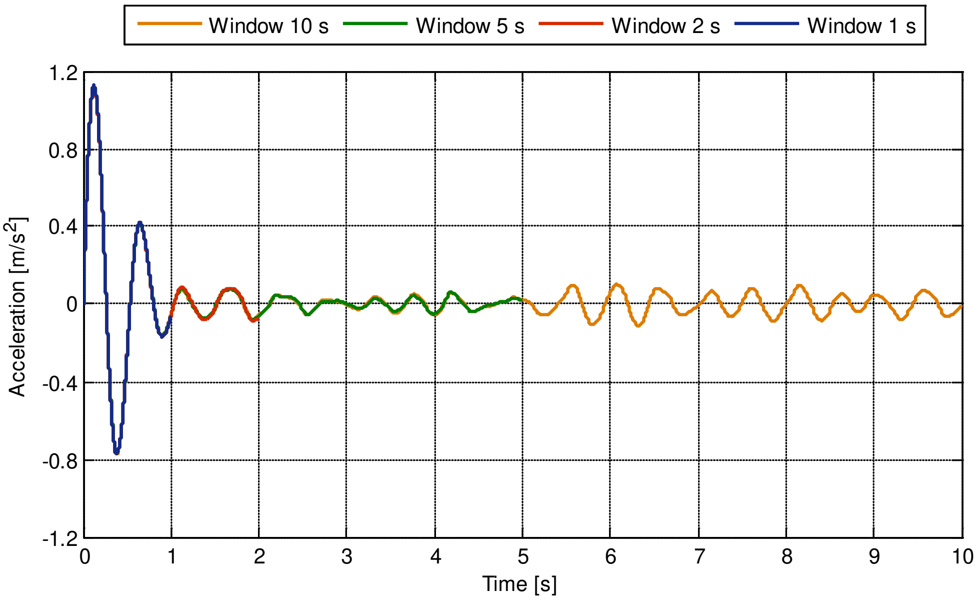

Figure 7-10: Obtained random decrement signatures with window sizes of 1 s (blue), 2 s (red), 5 s (green) and 10 s (orange) subjected to band-limited white noise 0.25 g rms.

Table 7-C: The estimates of the sprung mass mode dynamic characteristics and number of averages obtained for each random decrement signature obtained for different window sizes subjected to band-limited white noise 0.25 g rms.

Window Size [s]	Signature Averages N_{RD}	Natural Frequency f_{sn} [Hz]	Damping Ratio ζ_s [-]
1	600	1.85	0.164
2	599	1.95	0.157
5	592	1.94	0.151
10	583	1.87	0.146

Finally, the influence of implementing a time delay (spacing) between each trigger point on the random decrement signature and the estimated dynamic characteristics estimates was examined. Four different conditions were set for the spacing between triggers; 0 s (no spacing), 1 s, 2 s and 5 s (same as window size). The established random decrement signatures for different trigger spacings are shown in *Figure 7-11*, while *Table 7-D* lists the number of averages for each random decrement signature and the estimated dynamic characteristics.

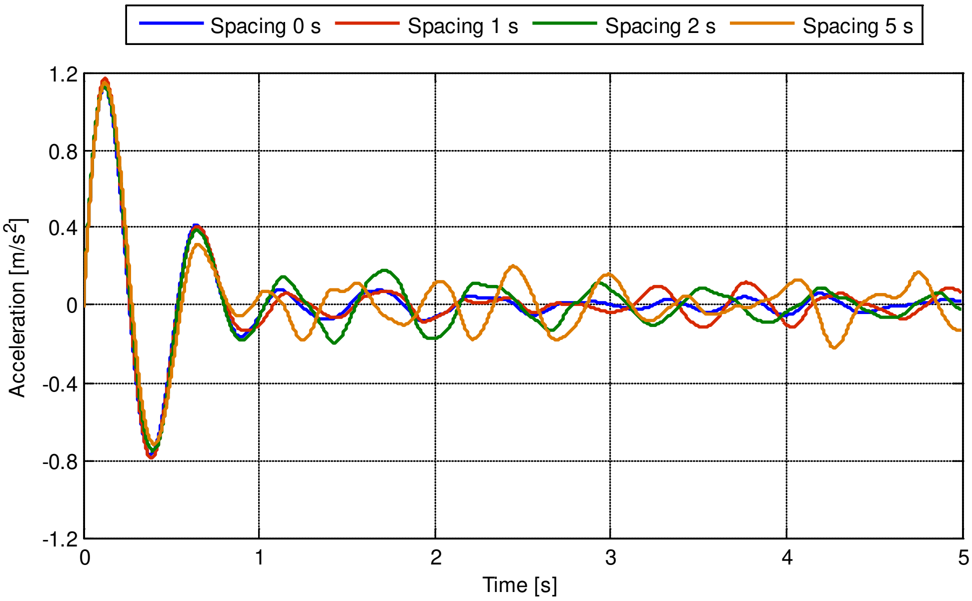

Figure 7-11: Obtained random decrement signatures with different trigger spacings from the band-limited white noise 0.25 g rms excitation.

Table 7-D: The estimates of the sprung mass mode dynamic characteristics and number of averages obtained for each random decrement signature obtained for different trigger spacing subjected to band-limited white noise 0.25 g rms.

Trigger Spacing [s]	**Signature Averages** N_{RD}	**Natural Frequency** f_{sn} **[Hz]**	**Damping Ratio** ζ_s **[-]**
0	592	1.94	0.151
1	238	1.94	0.154
2	131	1.79	0.162
5	57	2.20	0.168

From the results presented in *Table 7-D*, it is clear that the implementation of trigger spacing provides no benefit to the random decrement signature, instead reducing the number of averages available and obtaining inaccurate estimates of both the natural frequency and the damping ratio. It is recommended that trigger spacing is not implemented.

7.2.2.3 Evaluation of the Optimum Parameters

The various parameters and conditions used to establish the random decrement signature have been experimentally evaluated to determine their influence on estimating the dynamic characteristics of the sprung mass mode of the SWEV-B (100 kg). The experimentally established optimum parameters and conditions used to establish the random decrement signature using in-service response data are given in *Table 7-E.*

Table 7-E: The final optimum parameters selected to establish the dynamic characteristics of the sprung mass using the random decrement technique (Hilbert Domain).

Parameter	**Value / Condition**
Sampling Frequency	1,000 Hz
Window Size	5 s
Low-Pass Filter:	
Order	5th
Cut-Off Frequency	8 Hz
Trigger Type	Trigger Up
Trigger Level	Zero-Crossing
Trigger Spacing	None
Minimum Number of Averages	500

The three sets of measured response data from the SWEV-B excited on a vibration table were analysed using the optimised parameters to establish the dynamic characteristics for comparison with the dynamic characteristics obtained from the FRFs. The estimated dynamic characteristics of the sprung mass mode of the SWEV-B are presented in *Table 7-F* and show good agreement with those measured. Once the dynamic characteristics of the sprung mass mode have been estimated, they are input into a numerical transmissibility FRF model (Equation 3-53) and compared with the measured FRFs, shown in *Figure 7-12*. From the figure, it is quite clear that there is good agreement between the measured and estimated FRFs of the sprung mass mode.

Table 7-F: The measured and estimated dynamic characteristics of the SWEV-B (100 kg) from the vibration table experiments.

	FRF Curve-Fit		**Random Decrement**	
	Natural Frequency	**Damping Ratio**	**Natural Frequency**	**Damping Ratio**
Excitation Type	f_{sn} **[Hz]**	ζ_s **[-]**	f_{sn} **[Hz]**	ζ_s **[-]**
White Noise rms 0.25 g	1.92	0.150	1.91	0.152
White Noise rms 0.50 g	1.87	0.156	1.91	0.156
White Noise rms 0.75 g	1.89	0.142	1.88	0.144

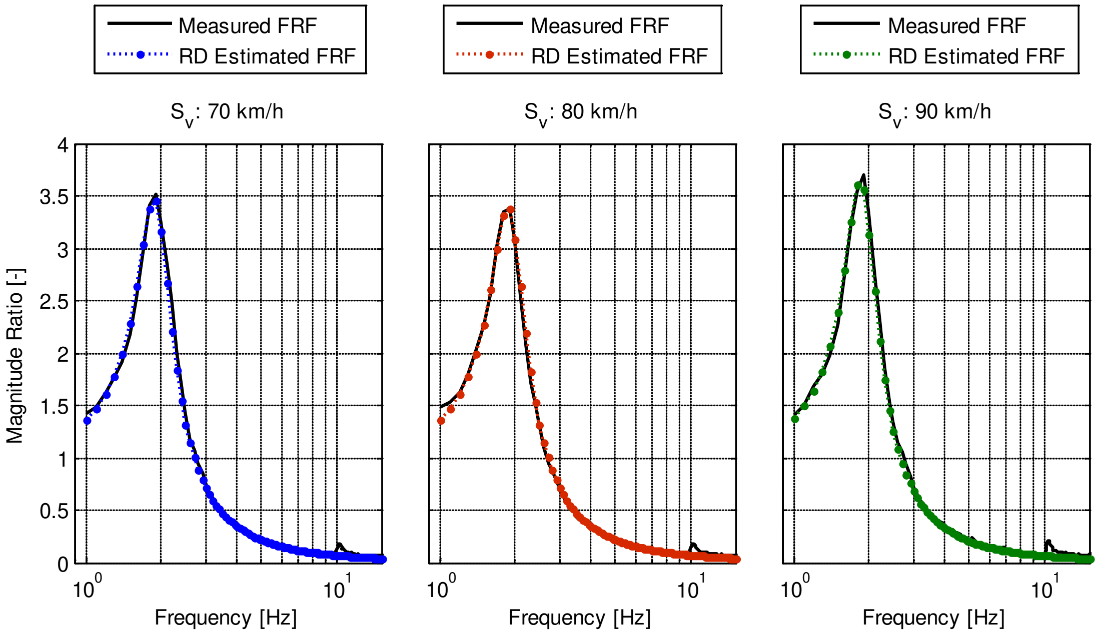

Figure 7-12: A comparison of the measured and random decrement estimated FRFs (Hilbert Domain) subjected to band-limited white noise at various rms intensities.

7.2.3 Frequency Response Function Estimation (Frequency Domain)

This section discusses the development of the analytical approach to estimate the FRF of the vehicle directly from the random decrement signature. As with the first approach (Hilbert Domain), a preliminary experimental evaluation of the parameters to establish the random decrement signature was undertaken. In the previous section describing the first approach using the random decrement technique, it was mentioned that the seismic mass was found to influence the measured excitation and response data and was chocked for the duration of the tests.

Despite the chocks, the motion of the seismic base was still found to contaminate the excitation and response data, shown for the 0.25 g rms excitation in *Figure 7-13*. While this did not have a considerable influence on the first approach, it poses an issue with the estimation of the FRF. It would be expected that the estimated FRF of the SWEV from the random decrement signature would possess a slightly wider band around the sprung mass mode than would be established from the measured FRF due to this added influence of the seismic base.

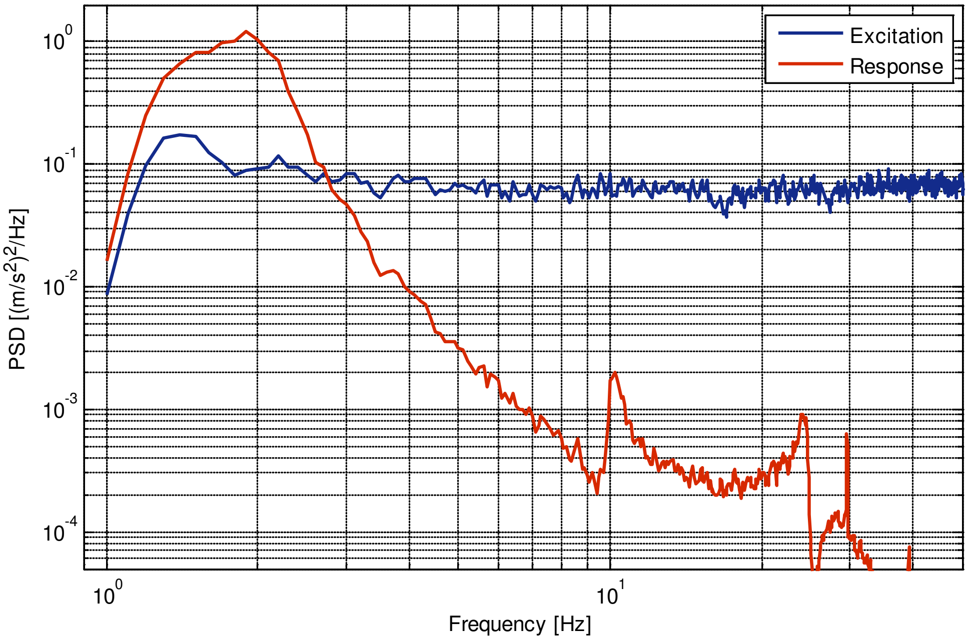

Figure 7-13: The measured excitation and response PSD functions of the SWEV-B (100 kg) subjected to band-limited white noise 0.25 g rms.

7.2.3.1 Initial Experimental Parameter Selection and Processing

The initial parameters for the experimental evaluation, unless stated otherwise, are:

- Sampling frequency of 1,000 Hz for the measured vibration response.
- 5th order Butterworth low-pass filter with a cut-off frequency of 20 Hz and a 5th order Butterworth high-pass filter with a cut-off frequency of 1 Hz.
- Window size of 10 s for the random decrement signature.

Preliminary analysis revealed that the established FRF requires smoothing. A number of different approaches to smooth the estimated FRF were investigated, such as cepstral analysis, moving average and data smoothing splines. The selected smoothing approach was developed by Garcia (2010) to smooth noisy data using a penalised least-squares method and is based on the Discrete Cosine Transform for one and higher dimensional data. A full description of the smoothing process is presented by Garcia (2010). As with the development of the first approach using the random decrement method, the same cases were examined to experimentally optimise the parameters.. The response data from the band-limited white noise 0.25 g rms excitation is again used for the evaluation of the FRF estimation.

7.2.3.2 Experimental Optimisation of Parameters

The various cases examined for the optimisation of the parameters to establish the best random decrement signature for the estimation of the vehicle FRF are discussed herein. The first case to experimentally evaluate is the effect of various trigger types and conditions. The evaluation for the first approach proved to be a reasonable guide for evaluating and excluding certain conditions, resulting in fewer conditions investigated. The trigger types evaluated were the trigger up, trigger down, the local extremum trigger and the positive points trigger. A sample of the random decrement signatures obtained from the various trigger types is presented in *Figure 7-15*, while *Table 7-G* lists the number of averages obtained for each trigger type and condition (all that were evaluated).

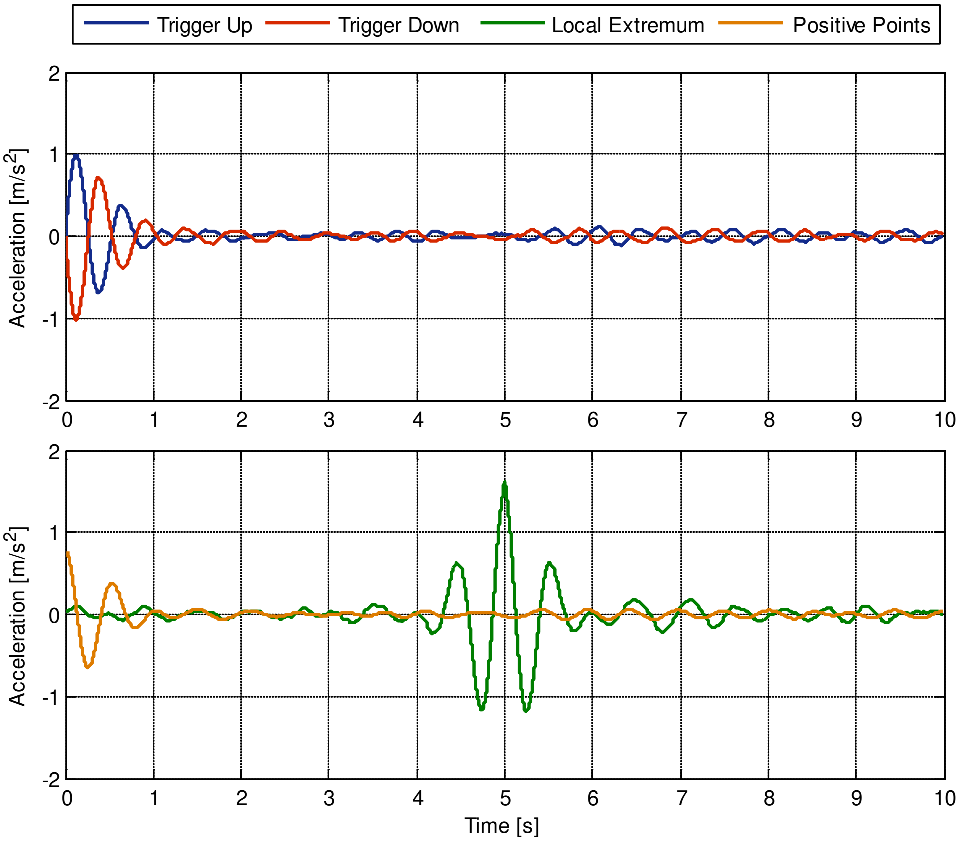

Figure 7-14: Sample of the various obtained random decrement signatures established from the response data during the band-limited white noise 0.25 g rms test using various trigger conditions.

Table 7-G: The obtained number of averages of the random decrement signature for various triggering type and subjected to band-limited white noise 0.25 g rms.

Trigger Type	**Signature Averages** N_{RD}
Trigger Up	
0	651
0.5 × σ	579
1.5 × σ	219
Trigger Down	
0	652
0.5 × σ	579
1.5 × σ	219
Local Positive Extremum	
1 s	292
2 s	146
5 s	59
Positive Points	
(0 ∞]	150,089,460
(0.5 × σ ∞]	96,271
(1.0 × σ ∞]	18,965

From the evaluation it was found that, of the various cases investigated, the FRF estimated from the random decrement signature using the trigger up (zero-crossing) condition provides the best agreement with the measured FRF and are shown in *Figure 7-15*. While the unsmoothed FRF fluctuates significantly, the smoothing process reduces these deviations and an FRF with close agreement to the measured FRF is established, only slightly underestimated in the magnitude ratio (overestimated level of damping). For all the estimated FRFs, the magnitude ratio at the unsprung mass is significantly underestimated. The other established FRFs (different trigger types and levels) were found to over or underestimate the measured FRF depending on the trigger used. Interestingly, the positive points triggering condition, while obtaining an exceedingly large number of averages for the random decrement signature (compared to the other triggers), did not yield an estimate of the FRF close to the measured FRF. From these results, it appears that at least 500 averages are required for the random decrement signature to provide a reasonably well-matched FRF.

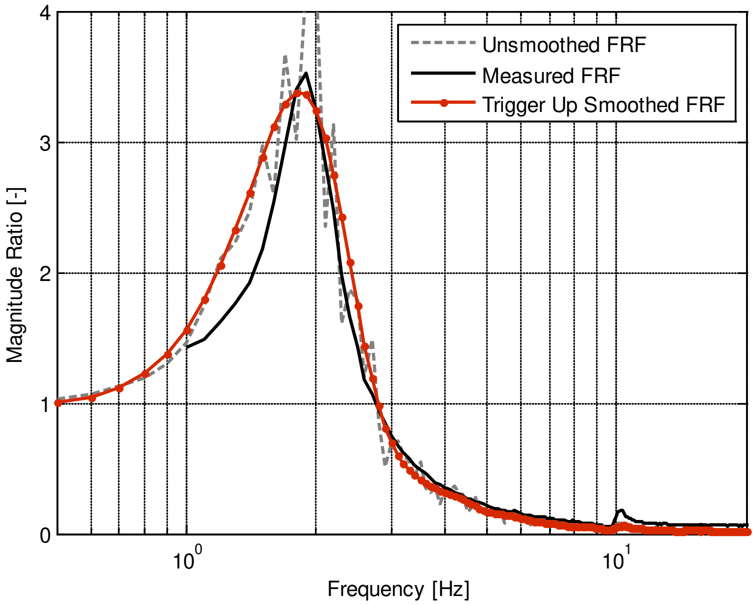

Figure 7-15: A comparison of the unsmoothed (grey) and smoothed (red) FRFs from the random decrement signature using a trigger up (zero-crossing level) and the measured FRF (black) for the band-limited white noise 0.25 g rms excitation.

The second case investigated the effect of the random decrement signature window size on the estimated FRF. The window size (length of the signature) is inversely related to the frequency resolution of the estimated FRF. This compromise is the most significant consideration for the estimation of the FRF using the random decrement approach. Four window sizes were investigated; 5, 10, 15 and 20 s (Δf of 0.20, 0.10, 0.07 and 0.05 Hz, respectively). The established random decrement signatures using the various window sizes are presented in *Figure 7-16*. It is important to reiterate that the filtering used for this approach results in a random decrement signature with higher frequency content than in the first approach (which isolated the response of the sprung mass mode). The number of averages obtained for each random decrement signature are listed in *Table 7-H*.

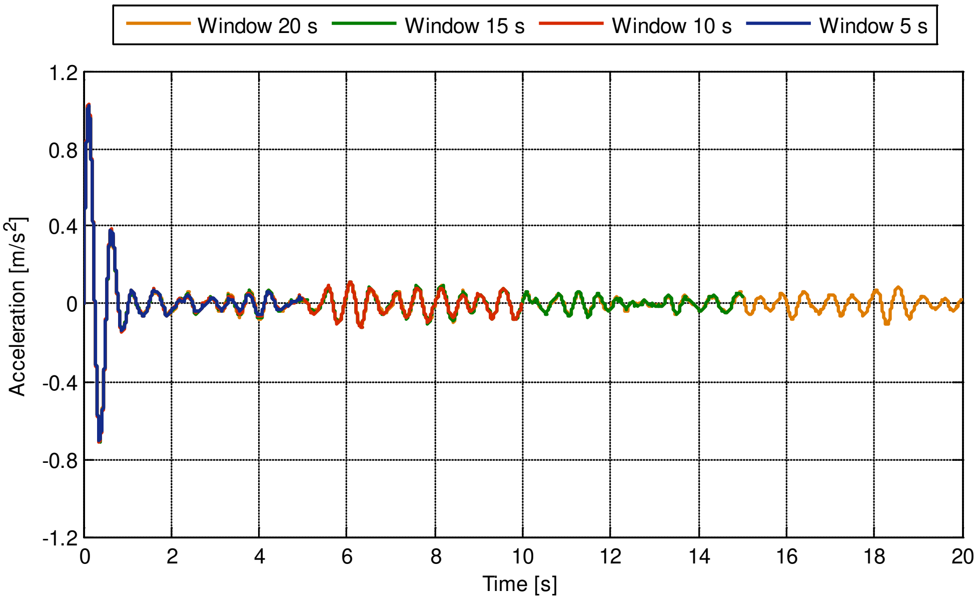

Figure 7-16: Sample of the various random decrement signatures established from the response data from the band-limited white noise 0.25 g rms for different window sizes.

Table 7-H: The number of averages of the random decrement signature established for various window sizes subjected to band-limited white noise 0.25 g rms.

Window Size [s]	**Signature Averages** N_{RD}
5	641
10	631
15	621
20	611

The estimated FRFs (with smoothing) for a random decrement window size of 5, 10 and 20 s and the measured FRF are presented in *Figure 7-17*. The window sizes of 5 s and 20 s both significantly underestimate the magnitude ratio around the sprung mass resonance frequency, while the 10 s window provides a reasonably good agreement with the measured FRF. Increasing the window size (and therefore the frequency resolution) at the expense of a small number of averages does not improve the estimated FRF.

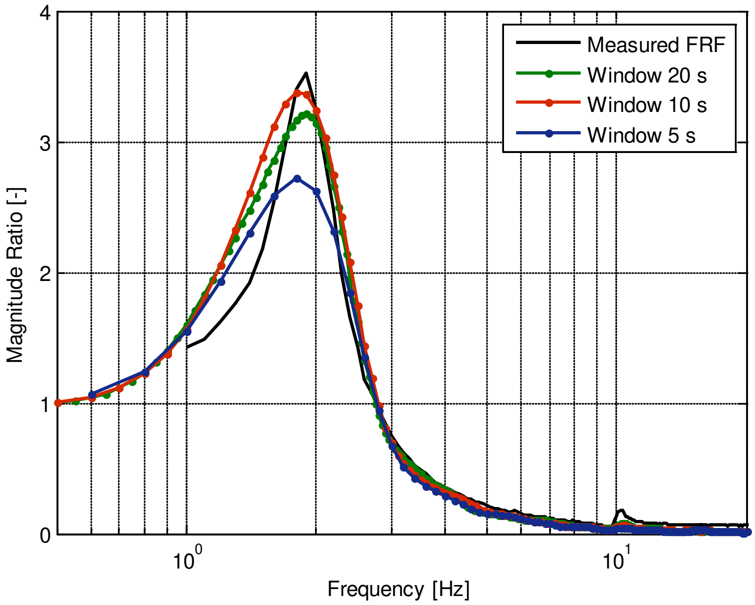

Figure 7-17: A comparison of the estimated smoothed FRFs estimated from the random decrement signatures with a window size of 5 s (blue), 10 s (red) and 20 s (green) and the measured FRF (black) from the band-limited white noise 0.25 g rms test.

Finally, the last case investigated was the influence of spacing between the selected trigger points. Three trigger spacing sizes were selected for investigation, 0 s (none), 5 s and 10 s (same as window size). The random decrement signatures obtained using the various trigger spacing sizes are shown in *Figure 7-18* and the obtained number of averages are presented in *Table 7-I*. It is evident that using a trigger spacing of 5 s and 10 s (window size) significantly reduces the number of averages such that the random decrement signature obtained does not average out the noisy components, particularly once the signature has decayed.

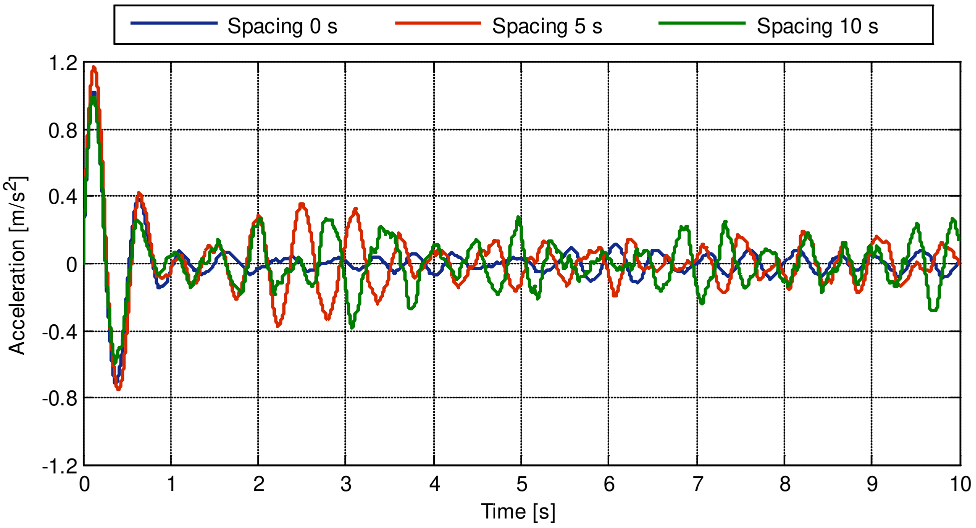

Figure 7-18: The obtained random decrement signatures from the response data during the band-limited white noise 0.25 g rms test for various trigger spacings.

Table 7-I: The obtained number of averages of the random decrement signature established for various trigger spacings subjected to band-limited white noise 0.25 g rms.

Trigger Spacing [s]	**Signature Averages** N_{RD}
0	631
5	56
10	29

The estimated smoothed FRFs for trigger spacing sizes of 0, 5 and 10 s are presented along with the measured FRF in *Figure 7-19*. The significant reduction in the number of averages results in an estimated FRF that is considerably distorted and significantly underestimates the magnitude ratio. From the experimental results, it is strongly recommended that trigger spacing is avoided.

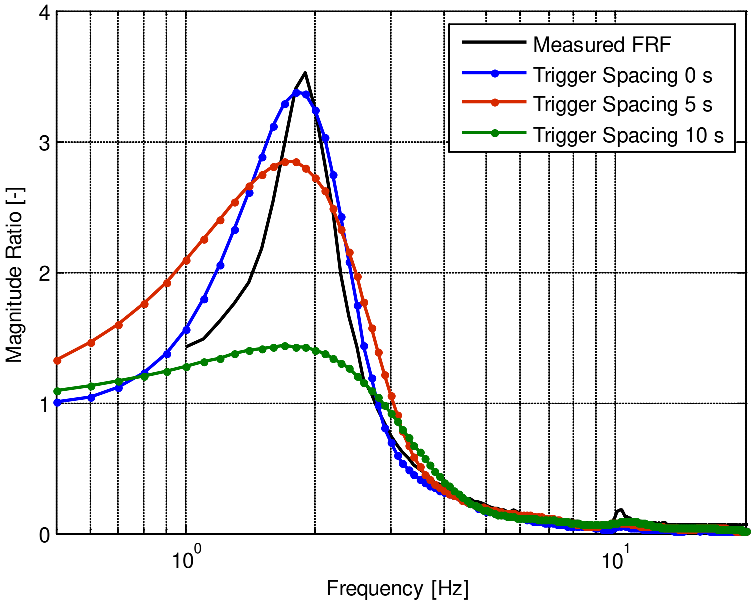

Figure 7-19: A comparison of the estimated smoothed FRF established from the random decrement signatures with a trigger spacing size of 0 s (blue), 5 s (red) and 10 s (green) and the measured FRF (black) from the band-limited white noise 0.25 g rms test.

7.2.3.3 Evaluation of the Optimum Parameters

The experimental evaluation of the various parameters and conditions that affect the established random decrement signature, and hence the estimated FRF, was undertaken using the vibration response of the SWEV-B (100 kg). The optimum parameters for establishing the FRF of the vehicle using the random decrement technique from response data are presented in *Table 7-J*. The parameters are the same as those identified using the first approach, however the window size is doubled and the filtering now includes a low-pass and a high-pass filter. It should be reiterated again that the unsprung mass is underestimated significantly is not accurately estimated using the random decrement method.

Table 7-J: The final optimum parameters selected to establish the dynamic characteristics of the sprung mass using the random decrement technique (Frequency Domain).

Parameter	**Value / Condition**
Sampling Frequency	1,000 Hz
Window Size	10 s
Low-Pass Filter:	
Order	5th
Cut-Off Frequency	8 Hz
High-Pass Filter:	
Order	5th
Cut-Off Frequency	20 Hz
Trigger Type	Trigger Up
Trigger Level	Zero-Crossing
Trigger Spacing	None
Minimum Number of Averages	500

A comparison between the measured and estimated FRFs for the three excitation rms intensities is presented in *Figure 7-20*. From the figure, the FRFs appear to agree well with the measured FRFs established using the excitation and response data. As expected, the estimated FRFs have a wider band around the sprung mass resonant frequency due to the contamination of the response by the seismic mass of the vibration table. Overall, this approach appears to be promising, however, if only the sprung mass mode can be estimated, the first approach may yield better estimates.

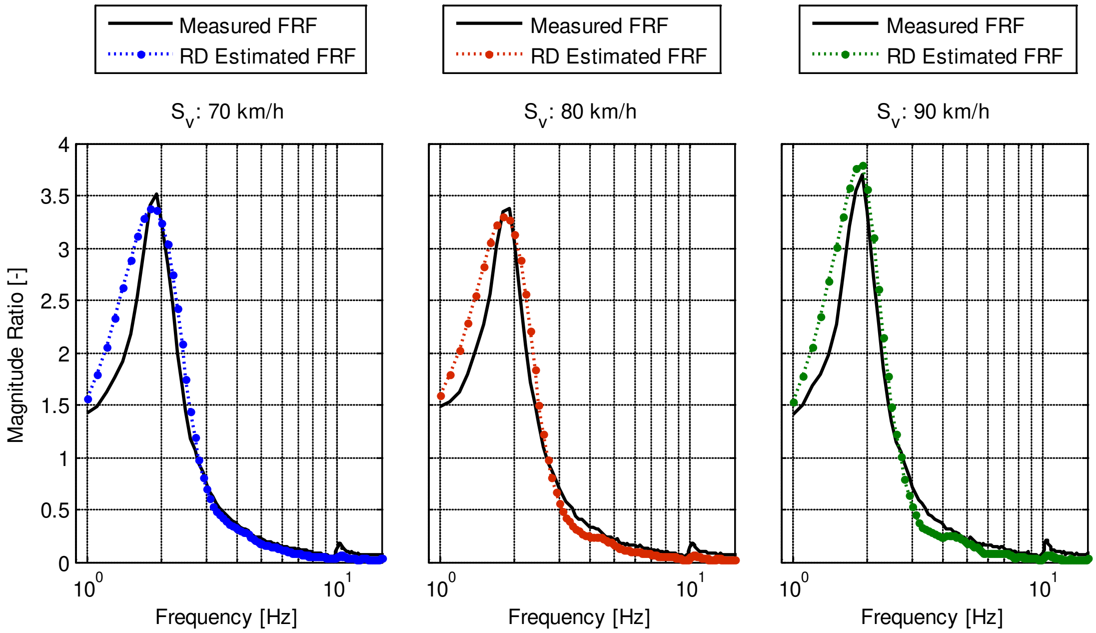

Figure 7-20: A comparison of the measured and random decrement estimated FRFs subjected to band-limited white noise excitation at various rms intensities.

7.3 CHAPTER SUMMARY

This Chapter described the development of two analysis techniques to estimate the dynamic characteristics of road vehicles using only in-service response data. The first technique, originally proposed by Rouillard and Sek (2010b), is based on the assumption that the pavement profile follows the spectral model outlined by the ISO (1995) under standard 8608. This analysis technique, known as the spectral approach, also depends on the vehicle response to be linear within the range of two nominally constant operating speeds. The major advantage of this approach is that an estimate of the vehicle's transmissibility FRF is obtained along with the spectral properties of the pavement. A simple numerical model was developed to investigate the approach and found that if the spectral model of the pavement differs between two experimental runs, the approach will not be able to accurately estimate the spectral exponent of the excitation (pavement) and hence, the vehicle's FRF.

The second technique uses the random decrement method to analyse vehicle vibration response to estimate the dynamic characteristics. Once the random decrement signature has been established, there are two possible approaches that may be undertaken; 1) estimate the dynamic characteristics of the sprung mass mode in the Hilbert Domain, or 2) estimate the FRF of the vehicle by taking the FFT of the established signature (and scale). While the random decrement technique has been used to establish the dynamic characteristics of large structures (with relatively low damping), it has never been used to analyse vehicle vibration response data.

An experimental evaluation was required to identify the most suitable parameters for establishing the random decrement signature to obtain the best estimates of the dynamic characteristics. As a means of validation, the estimated dynamic characteristics of the sprung mass mode were compared with the FRF established by subjecting the SWEV-B configuration to band-limited white noise at various intensities. The experimental evaluation of the random decrement analysis technique indicates that both approaches are able to establish accurate estimates of the sprung mass dynamic characteristics using in-service response data.

The estimated FRFs using the first approach (Hilbert Domain) agreed well with the measured FRFs; however the dynamic characteristics of the unsprung mass were unable to be obtained due to small energy content. The estimated FRFs using the second approach (Frequency Domain) were able to identify the unsprung mass mode, but were significantly underestimated. For both approaches, it remains to be seen if the response of the unsprung mass is significantly greater during the in-service experiments. A series of in-service (on-the-road) experiments using both the SWEV-A and SWEV-B are the focus of the next Chapter.

Chapter 8

VALIDATION OF IN-SERVICE EXPERIMENTS

The main focus of this Chapter is the results of two series of in-service (on-the-road) experiments for the two configurations of the SWEV and the corresponding analysis of the in-service response data using the two techniques developed in Chapter 7. This Chapter is organised as follows:

- A series of in-service experiments using the SWEV (loaded with 100 kg) over one road.
- A second series of experiments using the SWEV (loaded with 50 kg) instrumented as a profilometer to measure the road profile along the SWEV wheel track (two roads).
- The two analysis techniques described in the previous Chapter are used to analyse the measured response data. Also, the FRFs established from the excitation-response experiments are used for comparison.
- An investigation using a Monte Carlo simulation into the minimum length of road required to obtain a sufficient estimate of the response spectrum and random decrement signature is also presented.
- The final section contains a series of in-service experiments using two unmodified trucks to estimate the dynamic characteristics using the random decrement technique.

8.1 EXPERIMENTAL PROCEDURE

This section describes the experimental procedure for the in-service (on-the-road) experiments undertaken using the SWEV. The experimental set-up of the SWEV is also discussed, along with the selection of appropriate routes and the procedure for the in-service experiments.

8.1.1 SWEV Configuration

For the first series of in-service experiments (part 1), the SWEV was loaded with 100 kg of dead weight at the body and instrumented with an accelerometer at the sprung mass and towed using a light transport vehicle. Additional sensors were required for the second series of in-service experiments (part 2), where the SWEV was loaded with 50 kg of dead weight and modified to operate as an inertial profilometer and instrumented with a laser displacement sensor, an accelerometer on the laser and a wheel encoder (for further details see Appendix C). All the instrumentation was powered by a custom-made power unit that uses the 12 V DC auxiliary power outlet in the vehicle and the data acquisition system was located within the light transport vehicle.

8.1.2 Route Selection

As discussed in the methodology, it is important to carefully select an appropriate route for the in-service experiments. To undertake a series of in-service experiments using the SWEV required numerous resources and time, and so it was decided that, for a concept validation exercise, two different routes would be sufficient. The most important considerations were to use a route with as long a length as possible that is devoid of stops or sharp turns (roundabouts, traffic lights, etc.), has only light traffic at worst and is relatively rough so as to induce reasonable excitation into the vehicle. The speed limits along the routes were checked to determine the operating speeds that may be used. For the initial series of in-service experiments, a rural country road, designated C704, between Bacchus Marsh and Geelong was used. The road is located west of Melbourne, Victoria, Australia and is approximately 40 km in length. The map of the route is presented in *Figure 8-1*. The route starting at Bacchus Marsh is denoted as BG and the return route is denoted as GB.

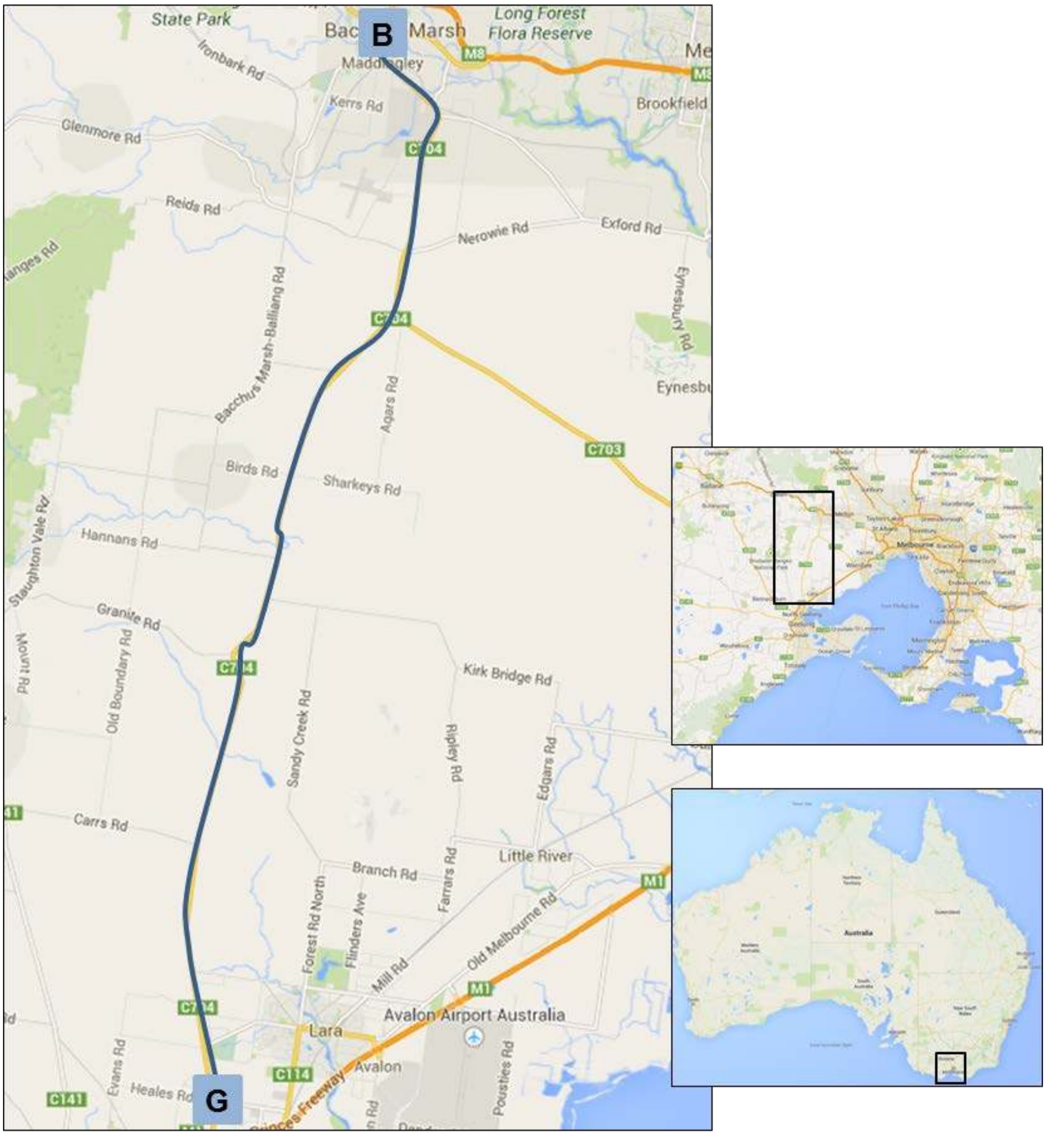

Figure 8-1: Route C704 (between Bacchus Marsh and Geelong) highlighted on the map of Victoria, Australia.

The second road selected as part of the second series of in-service experiments is located north-west of Melbourne, between the rural Victorian towns of Sunbury and Romsey. The road, known as C325, shown in *Figure 8-2*, is approximately 26 km in length. The route from Sunbury to Romsey is designated as SR, with the return route RS.

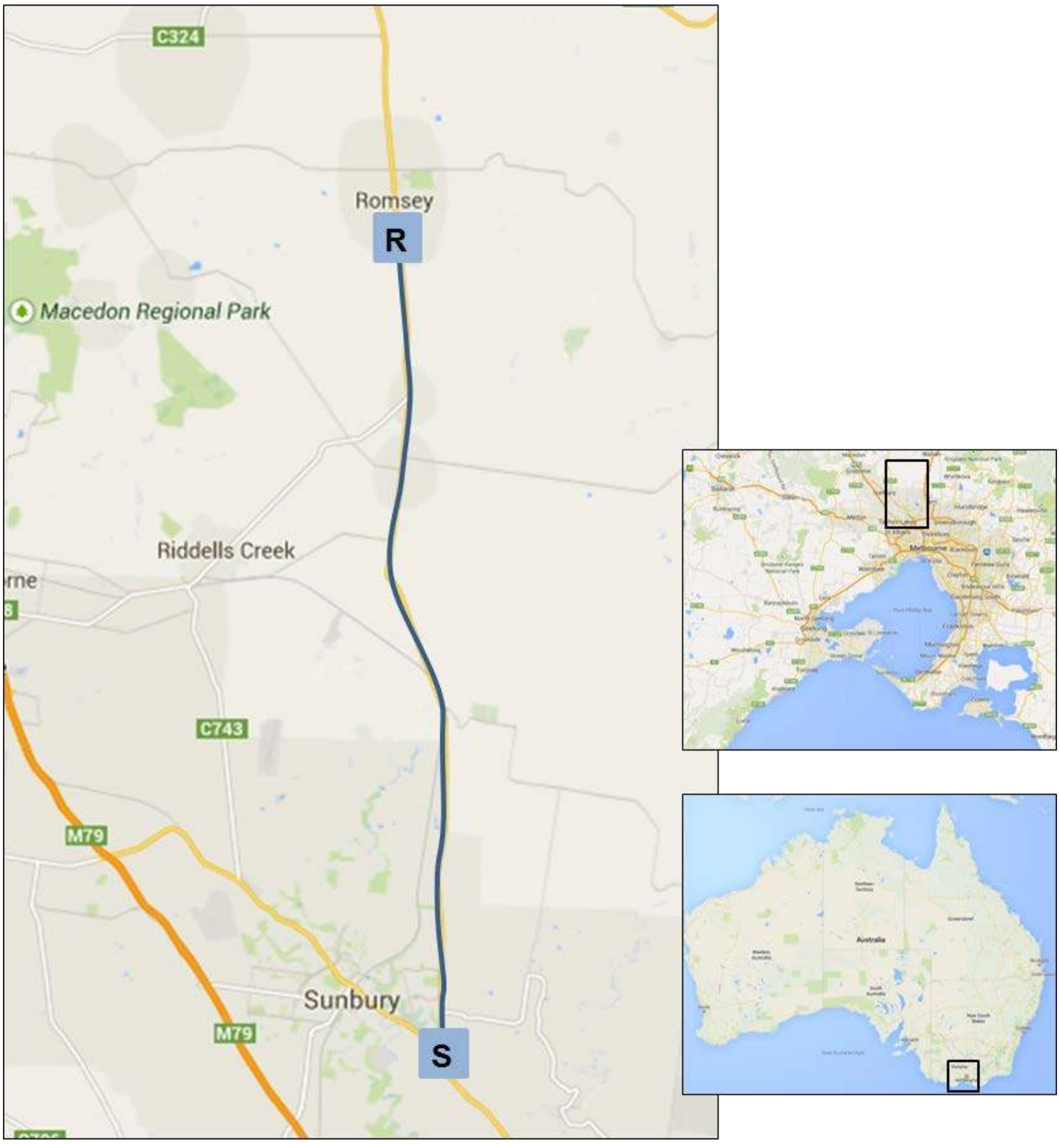

Figure 8-2: Route C325 (between Sunbury and Romsey) highlighted on the map of Victoria, Australia.

8.1.3 In-Service Experimental Procedure

For the initial series of in-service experiments (part 1), only routes BG and GB were used. Both configurations of the SWEV were loaded with 100 kg of dead weight and instrumented with an accelerometer to measure the vertical vibration acceleration at the body (sprung mass). Both the SWEV-A and SWEV-B were towed along both routes using a light transport vehicle at nominally constant operating speeds of 70, 80 and 90 km/h (± 5 km/h). These operating speeds were considered reasonable as the speed limit is 100 km/h along the entire route.

For the second series of in-service experiments (part 2), the SWEV was instrumented with a laser displacement sensor, a second accelerometer (mounted on the laser) and a wheel encoder to operate as inertial profilometer to measure the exact wheel path travelled for each run. Both configurations of the SWEV were loaded with only 50 kg of dead weight to prevent the dynamic motion of the SWEV exceeding the operational limits of the displacement sensor. The SWEV-A and SWEV-B were both towed using a light transport vehicle along all four routes outlined in the previous section; BG, GB, SR and RS, at nominally constant operating speeds of 70, 80 and 90 km/h. For both roads, the speed limit is 100 km/h throughout the entire length and the operating speeds selected were considered reasonable so as to not disrupt any other vehicles significantly (or be caught behind one travelling slightly under the limit).

A sampling frequency of 1,000 Hz was set to measure the data for both series of in-service experiments and the data acquisition system was located inside the light transport vehicle and operated by a passenger. The passenger operated the system to start and stop the measurements and monitored the data throughout the experiments in the event of any disturbance or error occurring (e.g. data clipping).

8.2 SWEV IN-SERVICE EXPERIMENTS PART 1

The preliminary series of in-service experiments are focused on the SWEV-A and SWEV-B configurations loaded with 100 kg of dead weight. The SWEV was towed along routes BG and GB at three nominally constant operating speeds (70, 80 and 90 km/h) and the vibration response data was measured. The measured response PSD functions from routes BG and GB are presented in *Figure 8-3* for the SWEV-A and *Figure 8-4* for the SWEV-B travelling at various nominally constant operating speeds, S_v.

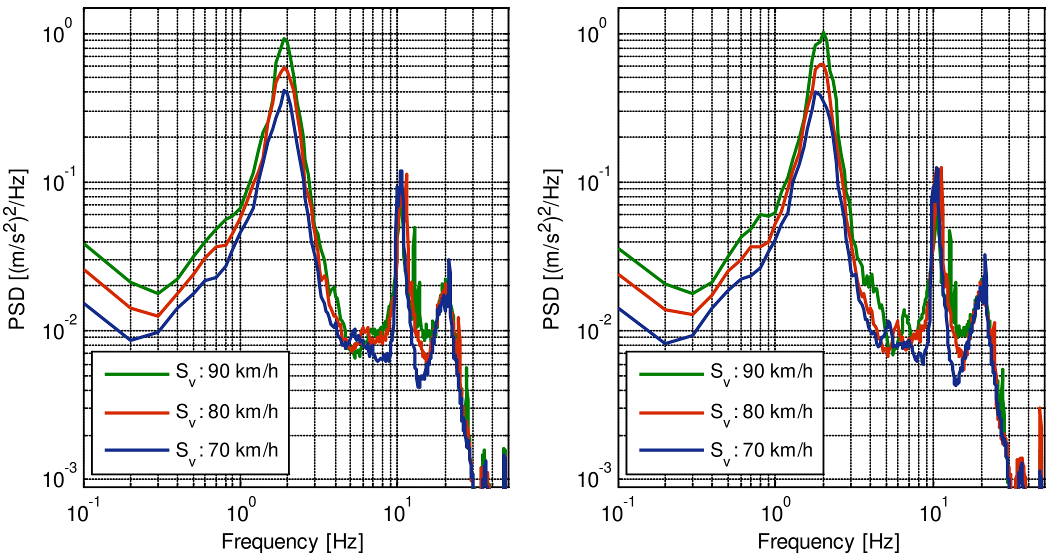

Figure 8-3: Measured response PSD functions of the SWEV-A (100 kg) sprung mass travelling over routes BG (left) and GB (right) (Δf = 0.1 Hz).

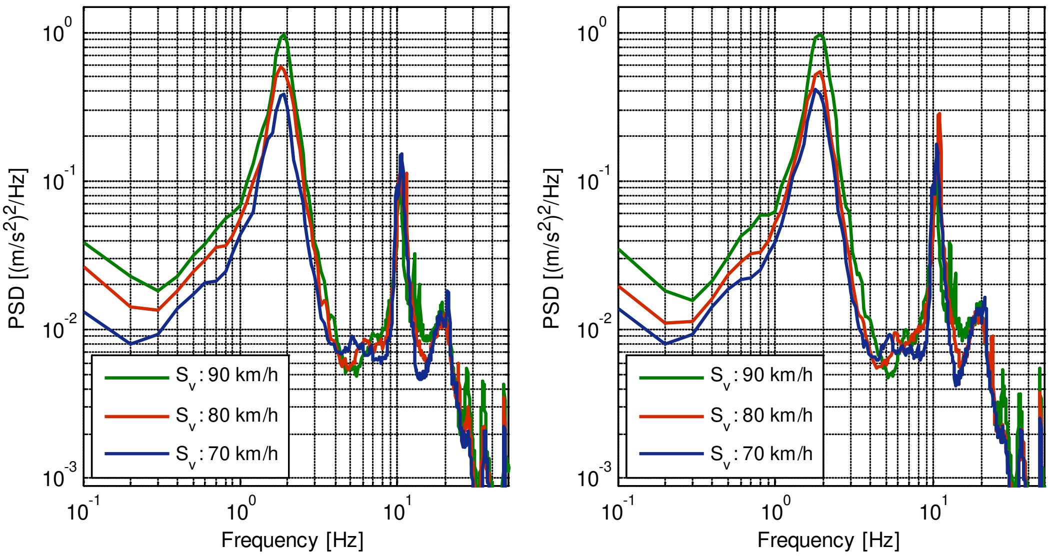

Figure 8-4: Measured response PSD functions of the SWEV-B (100 kg) sprung mass travelling over routes BG (left) and GB (right) (Δf = 0.1 Hz).

From the measured response spectra, a harmonic component is clearly present around the unsprung mass mode. An investigation to identify the cause revealed it to be a result of the unavoidable residual wheel imbalance of the wheel, superimposed onto the response spectra. As expected, this harmonic is a function of vehicle speed, calculated in *Table 8-A*, and is not present in the vibration table FRFs (from Chapter 6).

Table 8-A: Calculated wheel imbalance frequencies for the SWEV for the various nominally constant operating speeds.

Vehicle Speed [km/h]	**Imbalance Frequency [Hz]**
70	9.9
80	11.3
90	12.7

8.2.1 FRF Comparison with Laboratory Measurements

According to the methodology developed in Chapter 7 for the spectral approach, an estimate of the transmissibility FRF may be obtained using only the measured response PSD function, shown in Equation 8-1 (reproduced from Equation 7-5).

$$T(f)=\sqrt{\frac{R_{\ddot{x}}(f)}{G_{\ddot{x}}(f)}}=\sqrt{\frac{R_{\ddot{x}}(f)}{G(n_0)}}\,\frac{f^{\left(\frac{w}{2}-2\right)}}{(2\pi)^2\,n_0^{\,w/2}\,v^{(w-1)/2}} \tag{8-1}$$

The relationship described in Equation 8-1 assumes that the pavement excitation can be approximated by the ISO standard 8608 spectral model. Since the response of the vehicle has been measured, the only unknown values are for the assumed excitation spectrum; the spectral exponent, w, and the roughness constant, $G(n_0)$. Three values of the spectral exponent were set; 2.0, 2.5 and 3.0 and the roughness constant was iteratively adjusted to obtain an estimate of the FRF (using in-service response data). The approach is validated by comparing the in-service estimated FRF with those measured in the laboratory (using a vibration table). For comparison, both the SWEV-A and SWEV-B were placed on a large servo-hydraulic vibration table and subjected to violet noise acceleration excitation (corresponding to the ISO 8608 spectral model) at three rms intensities; 3.00, 6.00 and 9.00 m/s².

A comparison between the in-service estimated FRFs and the laboratory measured FRFs (using a vibration table) are shown in *Figure 8-5* and *Figure 8-6* for the SWEV-A and SWEV-B (100 kg), respectively, travelling at a nominally constant operating speed of 80 km/h along route BG. Only the in-service response data from route BG at 80 km/h for the SWEV-A and SWEV-B are presented with the laboratory measured FRFs as the results typify all the measurements.

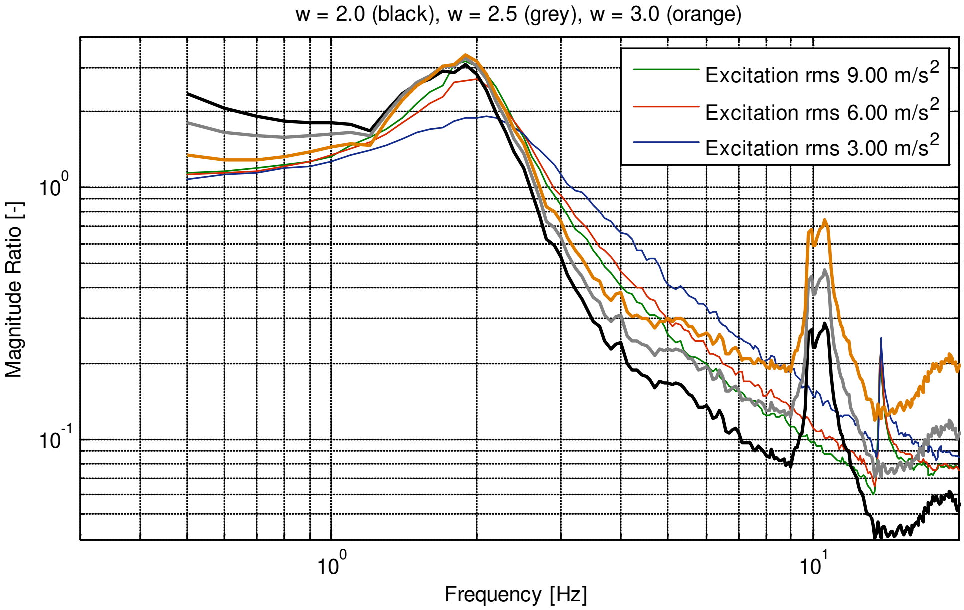

Figure 8-5: A comparison of the SWEV-A (100 kg) measured transmissibility FRFs and the estimated FRFs using in-service response data travelling over route BG (80 km/h) with an assumed excitation spectral exponent set to 2.0, 2.5 and 3.0 (Δf = 0.1 Hz).

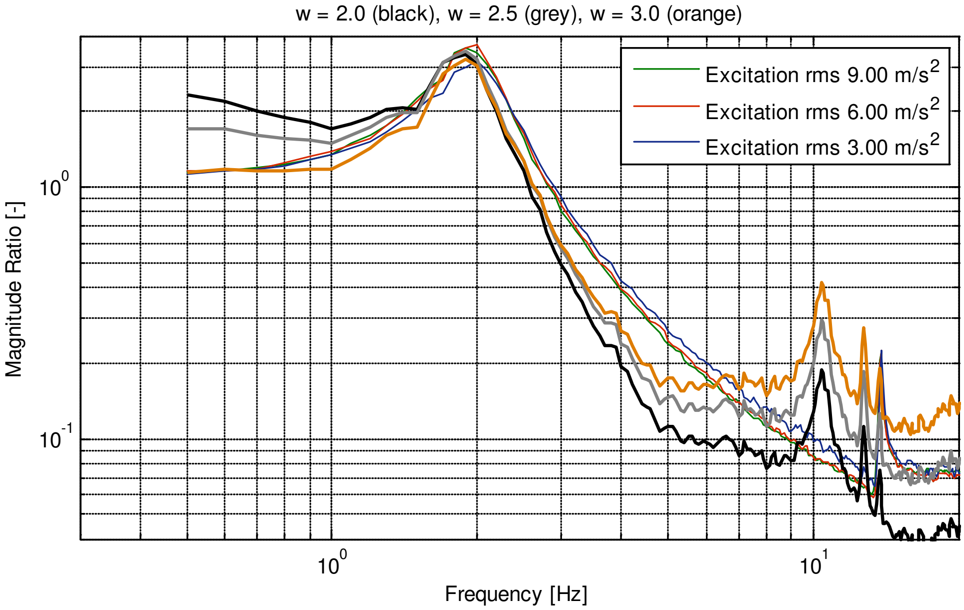

Figure 8-6: A comparison of the SWEV-B (100 kg) measured transmissibility FRFs and the estimated FRFs using in-service response data travelling over route BG (80 km/h) with an assumed excitation spectral exponent set to 2.0, 2.5 and 3.0 (Δf = 0.1 Hz).

The SWEV-A FRFs are more difficult to compare as the nonlinear suspension produces variations in the FRF measured in the laboratory at various excitation (rms intensity) levels. The laboratory FRFs of the SWEV-B configuration do not vary significantly, and better agreement is obtained with the estimates using response data. However, for both vehicles the comparisons show that there is a reasonable agreement only around the main resonant frequency (between 1 – 3 Hz) and the estimated FRFs deviate at higher frequencies (notably the location of the unsprung mass mode). Around the sprung mass mode, a spectral exponent of 3.0 appears to provide the best agreement, although beyond the resonant frequency all three in-service FRFs are not well-matched with the laboratory measurements. There is a clear discrepancy between the laboratory measurements and the in-service FRFs using an assumed excitation spectral model. Furthermore, it does not appear that a spectral exponent of 2.0 provides the best agreement, as recommended by the ISO (1995), particularly around the sprung mass mode which is of significant interest. The next section is concerned with the estimation of the spectral exponent of the pavement elevation spectrum using only measured in-service response data.

8.2.2 Spectral Exponent Estimation

The approach described above to estimate the FRF of a vehicle requires an estimate of the spectral properties of the pavement based on the ISO spectral model and uses only in-service response data. Two relationships to estimate the spectral exponent, w, of the longitudinal pavement elevation spectrum using in-service response data were also shown in Chapter 7. The approaches rely on using either the ratio of the spectral response (PSD) or the ratio of the response rms measured from the sprung mass of the vehicle travelling at two distinct nominally constant operating speeds. Using the rms ratio of the response, the estimated spectral exponents from route BG and GB are presented in *Table 8-B*.

From the results presented in *Table 8-B*, there is no consistency in the estimates of the spectral exponent regardless of the vehicle configuration or operating speed ratio. One possible explanation for the inconsistent results is the influence of the imbalance (and other) harmonics contaminating the response data. The estimates of the spectral exponent were recalculated with a low-pass filter to isolate only the response of the sprung mass, but yielded no improvement in the consistency of the results. It is suggested that the lack of consistency may be due to a variety of reasons, including (but not limited to) the nonlinear nature of the system or that the SWEV travels over a slightly different wheel track for each run.

Table 8-B: The average nominal operating speed ratios and the estimated spectral exponents using the rms response ratios from the SWEV-A and SWEV-B (100 kg) for both routes BG and GB.

Nominal Operating Speed Ratio [-]	**Estimated Spectral Exponent, *w* [-]**	
	Route BG	**Route GB**
SWEV-A (100 kg) Configuration		
70 / 80	4.08	3.15
70 / 90	3.40	3.65
80 / 90	2.63	4.21
SWEV-B (100 kg) Configuration		
70 / 80	4.43	2.58
70 / 90	3.86	3.81
80 / 90	3.21	5.20

Estimating the spectral exponent using the ratio of the response PSD functions was also undertaken. The estimated spectral exponents (as a function of frequency) for the various operating speed ratios travelled by the SWEV-A (100 kg) over routes BG and GB are presented in *Figure 8-7* and *Figure 8-9*, respectively. For the SWEV-B (100 kg) configuration, the estimated spectral exponents (as a function of frequency) from the various operating speed ratios over routes BG and GB are presented in *Figure 8-8* and *Figure 8-10*, respectively. From the figures, there is a clear inconsistency in the estimates for all route-vehicle combinations and nominally constant operating speed ratios. The spectral exponent significantly varies around the region of the unsprung mass (10 – 15 Hz) due to the wheel imbalance harmonics.

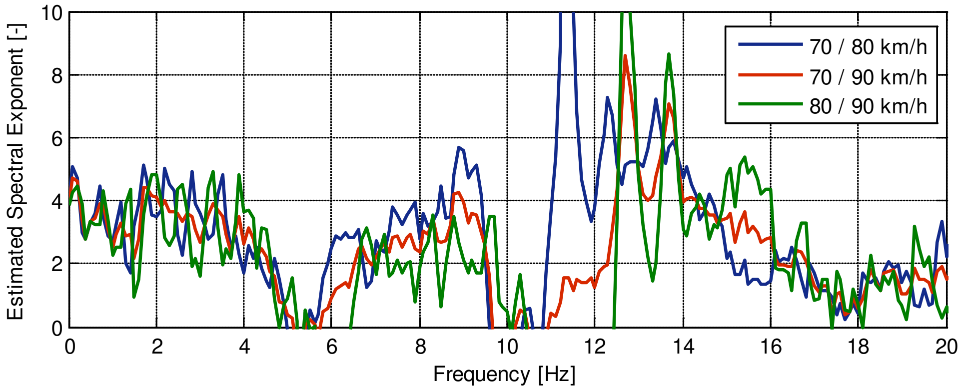

Figure 8-7: Estimated spectral exponent (as a function frequency) from various nominally constant speed ratios from the SWEV-A (100 kg) travelling over route BG.

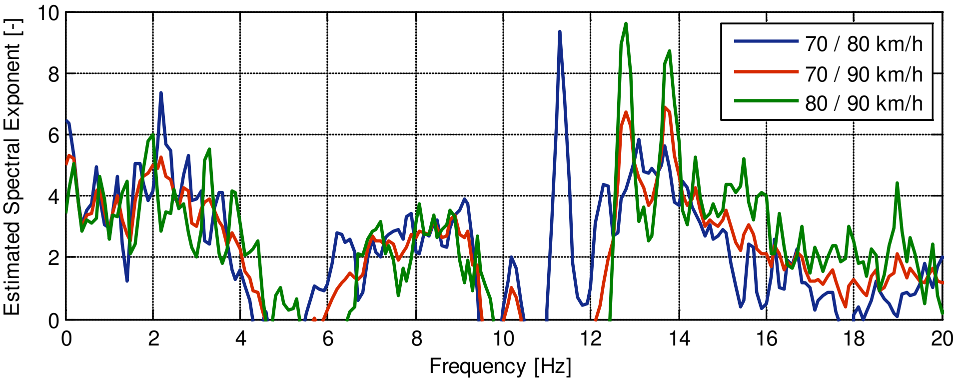

Figure 8-8: Estimated spectral exponent (as a function frequency) from various nominally constant speed ratios from the SWEV-B (100 kg) travelling over route BG.

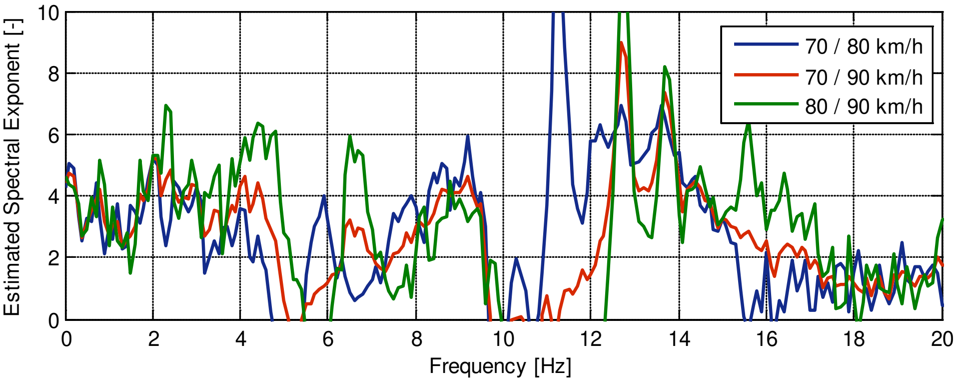

Figure 8-9: Estimated spectral exponent (as a function frequency) from various nominally constant speed ratios from the SWEV-A (100 kg) travelling over route GB.

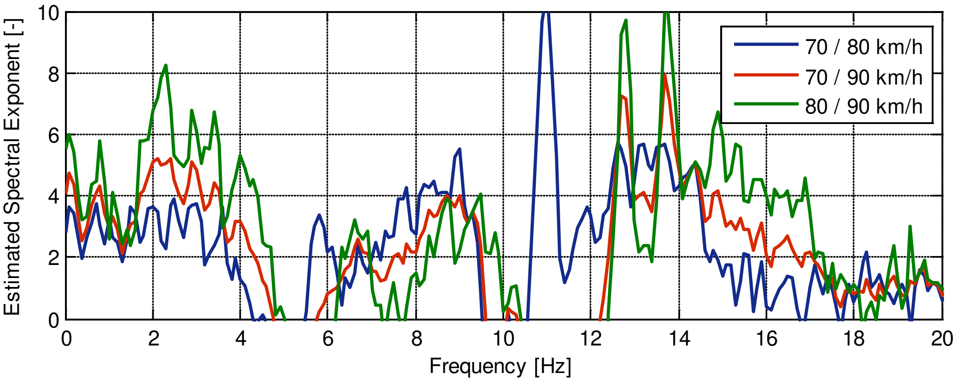

Figure 8-10: Estimated spectral exponent as a function frequency from various nominally constant speed ratios from the SWEV-B (100 kg) travelling over route GB.

In an attempt to isolate the response of only the sprung mass, the mean value of the spectral exponent estimates were obtained for each of the operating speed ratios between 0.5 – 2.0 Hz and are presented in *Table 8-C*.

Table 8-C: The estimated spectral exponents from the SWEV-A and SWEV-B (100 kg) travelling over routes BG and GB for various nominally constant operating speed ratios, using the spectral approach by taking the mean value around the sprung mass resonant frequency (0.5 – 2.0 Hz).

Nominal Operating Speed Ratio [-]	Estimated Spectral Exponent, *w* [-]	
	Route BG	**Route GB**
SWEV-A (100 kg) Configuration		
70 / 80	3.41	3.21
70 / 90	3.30	3.27
80 / 90	3.18	3.33
SWEV-B (100 kg) Configuration		
70 / 80	3.64	2.86
70 / 90	3.63	3.39
80 / 90	3.62	3.99

Some consistent estimates are obtained, however the value of the spectral exponent does not correspond to the value established from the comparison FRFs. Another possible approach that may yield beneficial results is to select stationary sections of road. It is possible to analyse the road in terms of lengths (i.e. half of the road length), but for smaller sections it is difficult to justify a selected section for analysis. The estimated spectral exponents using only the measured in-service response data do not establish consistent estimates. This may be due to two reasons; 1) the response spectra are contaminated by noise, or 2) the pavement elevation profile is different between each experiment or does not follow the ISO spectral model.

The actual longitudinal pavement elevation profile traversed by the SWEV during these experiments is not known. The two approaches used to estimate the spectral exponent of the assumed excitation spectral model are not able to obtain consistent estimates. Furthermore, the actual value of the spectral exponent is not known, nor if the pavement elevation profile follows the assumed model. The longitudinal pavement elevation profile must be obtained for further investigation.

8.2.3 Longitudinal Pavement Elevation Profile Analysis

In order to understand why the estimates of the spectral exponent were inconsistent and inaccurate (and to validate the spectral exponent predicted from the comparison FRFs), the longitudinal pavement elevation profile data of the left and right wheel tracks of route C704 was obtained from the Australian Road Research Board (ARRB). The ARRB is, among other things, responsible for measuring and monitoring the road elevation profiles of the Victorian road network. The data obtained was measured using a high-speed inertial profilometer and samples were taken at an interval of 25 mm. The pavement elevation profiles were analysed and are presented in this section.

The pavement elevation PSD functions of the left and right wheel tracks for routes BG and GB were established and the difference between the two routes was found to be negligible. The pavement elevation PSD functions of the left and right wheel tracks of route BG, along with the best-fitting ISO spectral model based on Equation 3-19 of the left wheel track, and the coherence between the left and right wheel tracks are presented in *Figure 8-11*. The single-band curve-fit was applied between a band-width of 0.01 – 2.83 c/m, as outlined under ISO standard 8608 (1995).

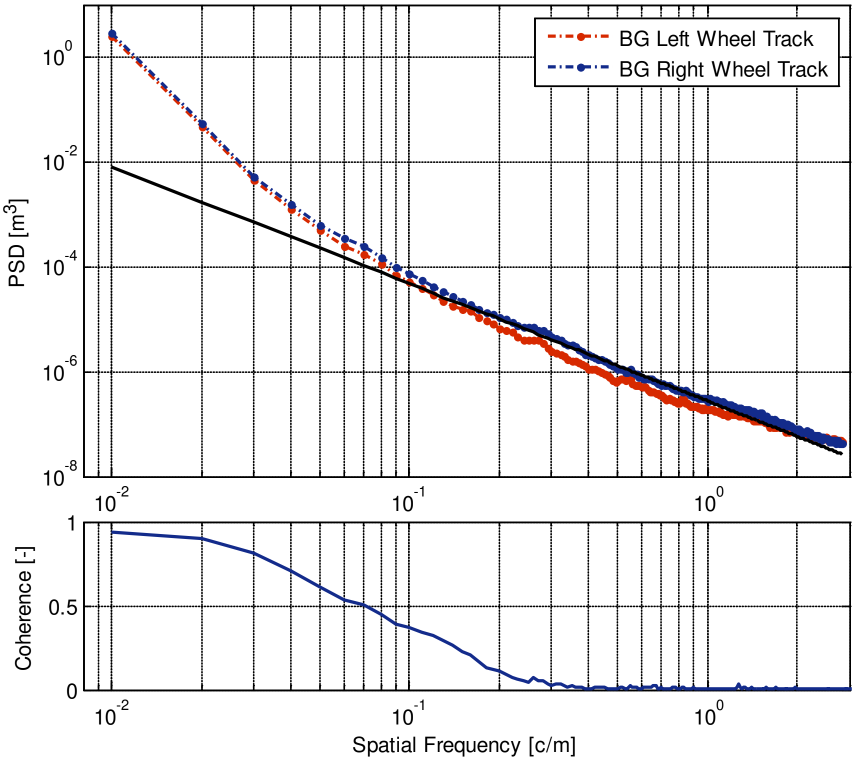

Figure 8-11: Pavement elevation PSD functions of the left (red) and right (blue) wheel tracks of route BG, with the best-fitting ISO model (black) for the left wheel track, and the magnitude-squared coherence between the left and right wheel tracks (bottom).

From *Figure 8-11*, the left and right wheel path elevation PSD functions have a similar same shape, with the right wheel track having slightly greater energy content (higher overall roughness) than the left. The coherence function indicates that the left and right wheel tracks are uncorrelated, particularly at spatial frequencies greater than 0.06 c/m. It also appears that the left wheel track elevation PSD function is not in very good agreement with the ISO model. The clear deviation from the standard spectral model may explain the inability to accurately estimate the spectral exponent using the ISO spectral model.

A more complex model may be able to provide a better description of the spectral characteristics of the pavement. While the ISO standard 8608 (1995) mentions that two or more straight-lines may be fitted to the profile, it is impossible to standardise the approach in order to guarantee a unique solution. Several authors have investigated the use of more complex spectral models to provide a better fit to various pavement elevation PSD functions, such as separating the profile into two separate bands (Dodds & Robson 1973), described in Equation 3-10. This spectral model is separated into two bands by the discontinuity frequency at a wavelength of approximately 6.3 m. As shown in *Figure 8*-12, fitting the two-band model to the measured pavement elevation PSD function of the left wheel track of route BG provides a significant improvement over the single-band fit.

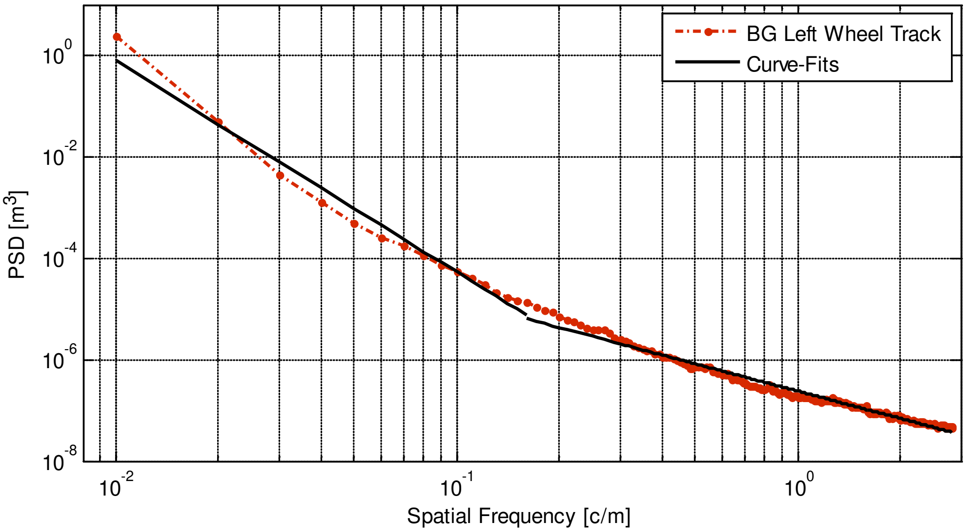

Figure 8-12: Pavement Elevation PSD function of the left wheel track of route BG (red) and the best-fitting two-band model (black) based on Equation 3-10.

A further improvement to the two-band model is to include a third band to separate the elevation PSD function into short, medium and long wavelengths. The three-band, or two-split, spectral model was outlined by Andren (2006) and Kropac and Mucka (2007) and is presented in Equation 3-20. Defining appropriate discontinuity frequencies for the three-band model was discussed briefly by Andren (2006); however the author's final selection was determined by which discontinuity frequencies produce the lowest total least-square error based on the PSD elevation functions of the entire Swedish road network. These discontinuity frequencies selected by Andren (2006) were used to separate the pavement elevation PSD into three individual bands. The pavement elevation PSD function for the left wheel track of route BG, along with the best-fitting three-band spectral model, is presented in *Figure 8-13*.

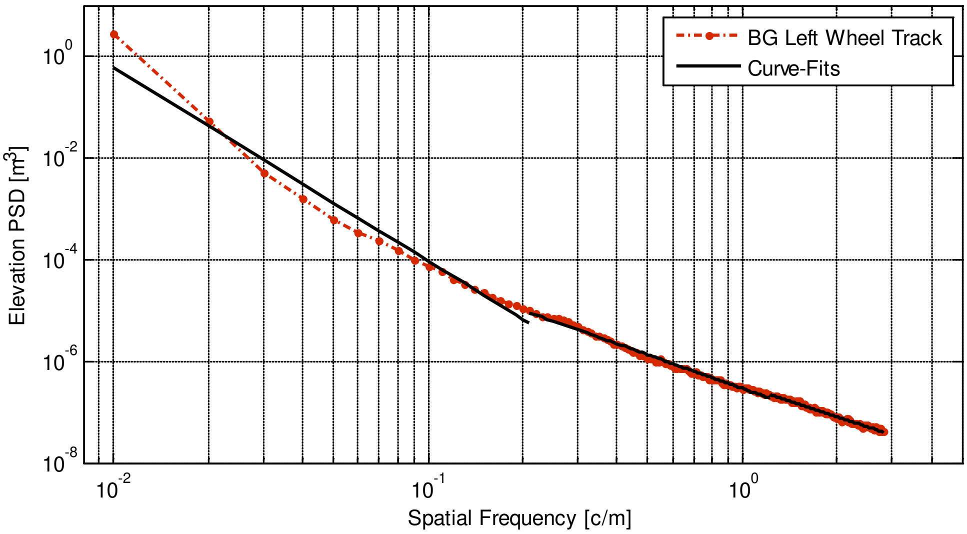

Figure 8-13: Pavement Elevation PSD functions of the left wheel track of route BG (red) and the best-fitting three-band model (black) using Equation 3-20.

The model, as expected, provides an improved fit over the one and two-band models. A comparison of the spectral models, with their estimated values and goodness of fit, is presented in *Table 8-D*. If the two configurations of the SWEV travelled over the same wheel track each time (and the pavement is the same across the entire surface as may be expected due to the similar shape of the left and right wheel tracks), then the spectral exponent would have been estimated to be around 2.23, not closer to 3.00.

Table 8-D: The estimated spectral properties (established via curve-fitting) for the one, two and three-band models of the left wheel track pavement elevation PSD function of route BG.

	ISO Model	**Two-Band Model**		**Three-Band Model**		
Band	*First*	*First*	*Second*	*First*	*Second*	*Third*
Frequency Range [c/m]	0.01 – 2.83	0.01 – 0.16	0.16 – 2.83	0.01 – 0.21	0.21 – 1.22	1.22 – 2.83
***w* [-]**	2.23	4.05	2.05	3.81	2.20	2.03
$G(n_0)$ [m^3]	4.732×10^{-5}	7.417×10^{-5}	3.702×10^{-5}	9.296×10^{-5}	4.645×10^{-5}	3.561×10^{-5}
r^2	0.9385	0.9748	0.9951	0.9711	0.9910	0.9899

Assuming that the pavement is isotropic, the transmissibility FRFs of both configurations of the SWEV can be established by combining the measured response and obtained excitation spectra of route BG. The in-service transmissibility FRFs of the SWEV-A and SWEV-B are presented in *Figure 8-14* and *Figure 8-15*, respectively, travelling over route BG at various nominally constant speeds in comparison with the FRFs established in the laboratory.

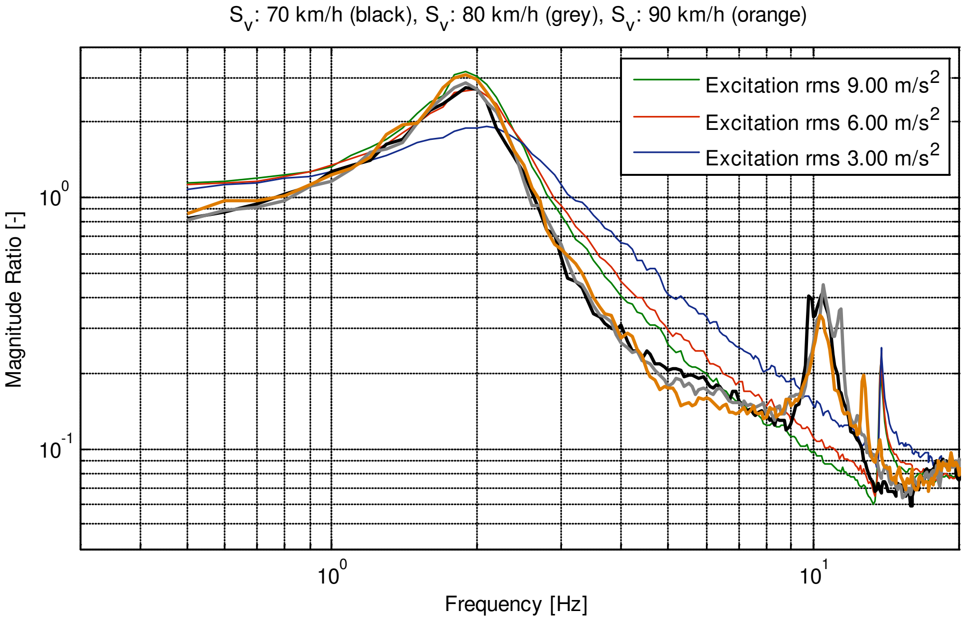

Figure 8-14: The transmissibility FRFs established using the obtained pavement elevation profile of the left wheel track of route BG combined with the measured acceleration response of the SWEV-A (100 kg) in comparison with the laboratory measured FRFs (Δf = 0.1 Hz).

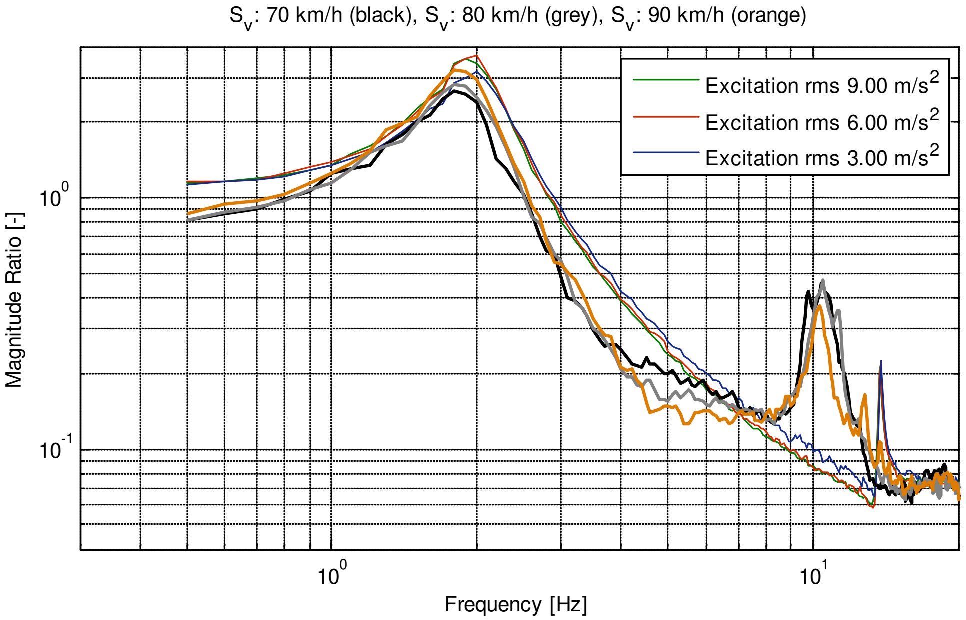

Figure 8-15: The transmissibility FRFs established using the obtained pavement elevation profile of the left wheel track of route BG combined with the measured acceleration response of the SWEV-B (100 kg) in comparison with the laboratory measured FRFs (Δf = 0.1 Hz).

There still remains a significant difference between the calculated transmissibility FRFs using the in-service response and excitation with those measured in the laboratory. As with the comparison figures established using the assumed ISO spectral model from Equation 3-19 as the excitation, the main resonance is in reasonable agreement (around 1 – 3 Hz) but beyond there is still a difference between the laboratory and field data. Ultimately, it appears as though the approach is limited as there is no improvement over using an assumed spectral model compared to the actual pavement elevation profile.

8.2.4 Discussion of Results

The investigation to determine the difference and improve the accuracy between the estimated FRFs using only in-service response data with those measured in the laboratory led to the acquisition of the longitudinal pavement elevation profiles of routes BG and GB from a local authority (ARRB). There was no significant improvement through the introduction of the measured pavement elevation profile to establish the transmissibility FRF of the vehicle. If the FRF comparison figures are presented with linear scales, a different perspective of the results is afforded. The comparison FRFs from *Figure 8-5* and *Figure 8-6* are re-presented in linear scales in *Figure 8-16* and *Figure 8-17*, respectively.

From these figures it can be seen that, with linear scales, varying the spectral exponent of the road has little effect on the estimated FRF, particularly around the main resonant frequency, while the resonance of the unsprung mass (axle hop) for both configurations of the SWEV appear to vary between the estimated and measured FRFs. This difference may be attributed to a number of factors one of which being the influence of the rotating wheel on the dynamic behaviour of the vehicle. Another is the transmission of vibration from the towing vehicle to the SWEV. In summary, given that the purpose of the approach was to obtain reasonable estimates of the FRF of a vehicle using response vibration data, the method appears, when viewed in linear scales, to yield reasonable estimates of the vehicle FRF especially in the region of the main resonant frequency. Some of the issues associated with presenting and analysing dynamic data using logarithmic scales is discussed in detail by Hickling (2006).

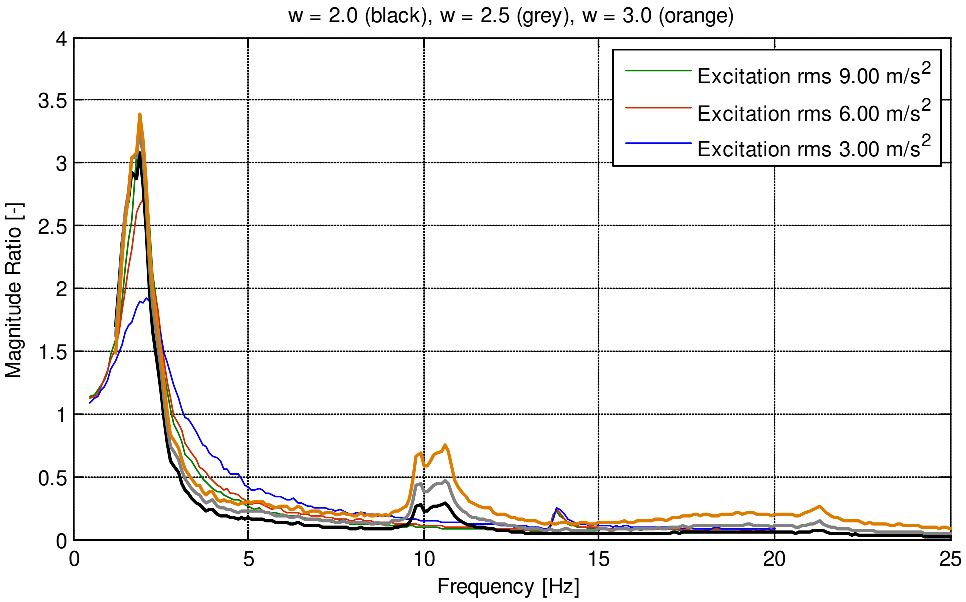

Figure 8-16: The comparison FRFs of the SWEV-A (100 kg) from *Figure 8-5*, re-presented on linear scales (Δf = 0.1 Hz).

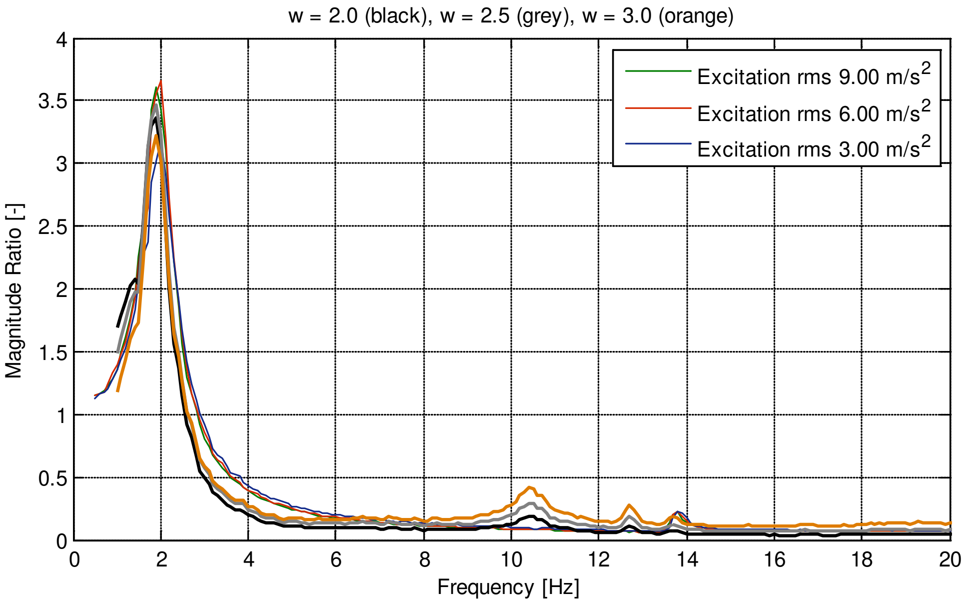

Figure 8-17: The comparison FRFs of the SWEV-B (100 kg) from *Figure 8-6*, re-presented on linear scales (Δf = 0.1 Hz).

While the approach using the ratio of the vehicle response data to estimate the spectral exponent appears limited, it is interesting to note that the sprung mass mode fits reasonably well regardless of the excitation spectral model (spectral exponent) used. Also, the FRFs established using the longitudinal pavement elevation data provided are not without issues. The most notable drawback is that the SWEV travels down the middle of the pavement between the left and right wheel tracks and it could quite possibly have a different spectral shape.

Furthermore, the pavement elevation data provided was measured months prior to the experiments and so the pavement may have changed due to damage and deterioration. It is clear that the pavement elevation profile along the middle wheel track requires measurement, but it is also equally important that the measured excitation and response data are synchronised. While it is possible to utilise existing profilometers, they would require modification to measure the middle wheel track. It is also practically impossible to measure the same wheel track as the SWEV travels over during each experimental run using a separate profilometer system. For these reasons, it was deemed necessary to instrument the SWEV to operate as an inertial profilometer in order to measure the true excitation applied to SWEV along the actual wheel path traversed for each run. The next section is focused on a second series of in-service experiments using the SWEV to simultaneously measure the excitation and response along the actual wheel track travelled.

8.3 SWEV IN-SERVICE EXPERIMENTS PART 2

The results obtained from the first series of in-service experiments revealed that assuming the spectral function (including the exponent, w) for the longitudinal profile of a road does not appear to yield consistent results. It appears that, in effect, individual roads of finite length will nearly always have spectral characteristics that deviate, to varying extents, from the standard model. In order to establish the true excitation signal (road elevation profile) a second series of experiments were undertaken to measure the longitudinal pavement elevation profile along the SWEV wheel track. A full description of the process to configure, calibrate and test the profilometer system on the SWEV is given in Appendix C. Due to the limited range of the laser displacement sensor used in the profilometer, both configurations of the SWEV were loaded with 50 kg of mass at the body to limit the dynamic motion.

As part of the profilometer, frequency limits were identified and the data required both high-pass and low-pass filtering (required to remove the presence of trends caused by signal integration). Both the measured excitation and response data were filtered using a 5th order Butterworth low-pass filter with a cut-off frequency of 50 Hz and a 4th order Butterworth high-pass filter with a cut-off frequency of 1 Hz. The SWEV-A and SWEV-B were towed along two selected roads for in-service experiments; the original routes BG and GB, along with a second road with the routes SR and RS. Measuring the excitation of the pavement at the exact wheel track travelled by the SWEV enables the actual excitation to be measured and determine if they vary between experimental runs (for different operating speeds).

8.3.1 Routes BG and GB

The newly-modified SWEV was taken back to the rural routes BG and GB and towed along the entire length at three nominally constant operating speeds of 70, 80 and 90 km/h. The SWEV-A and SWEV-B were both used to undertake the in-service experiments. The measured (and filtered) response spectra for both configurations of the SWEV are presented below. The measured response spectra from the SWEV-A and SWEV-B (50 kg) travelling along routes BG and GB are presented in *Figure 8-18* and *Figure 8-19*, respectively.

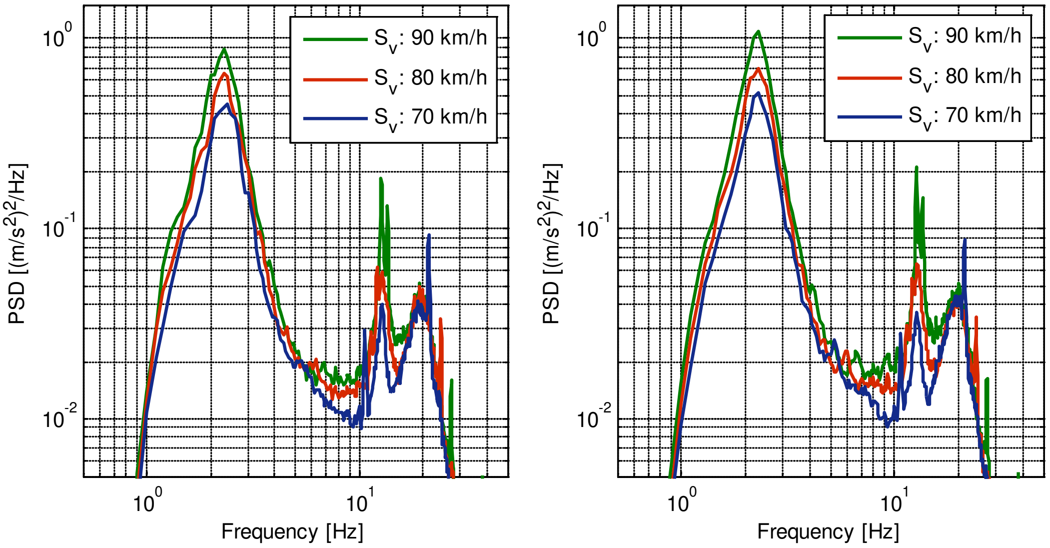

Figure 8-18: The filtered response PSD functions from the SWEV-A (50 kg) travelling over routes BG (left) and GB (right) (Δf = 0.1 Hz).

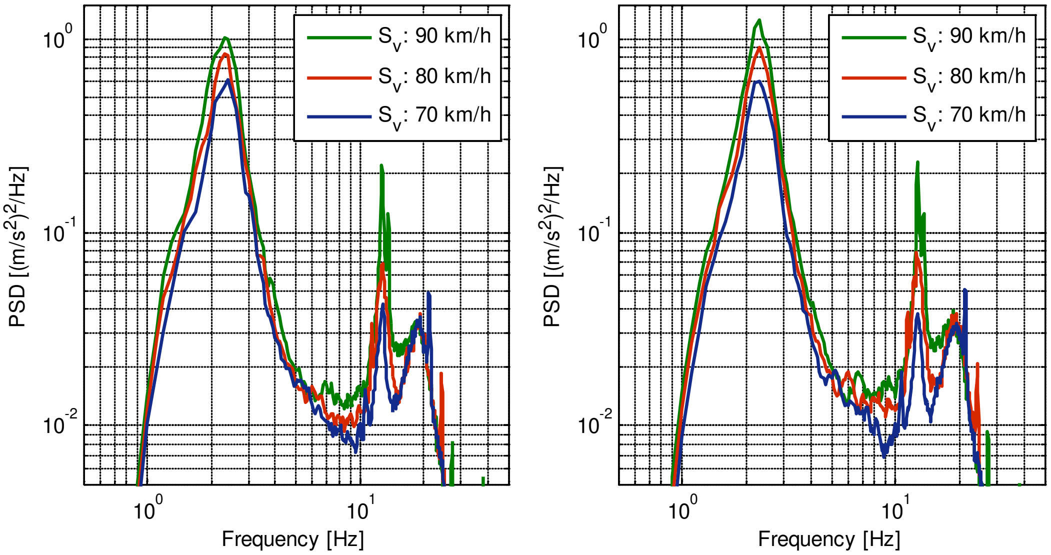

Figure 8-19: The filtered response PSD functions from the SWEV-B (50 kg) travelling over routes BG (left) and GB (right) (Δf = 0.1 Hz).

The longitudinal pavement elevation profiles were also measured using the profilometer capabilities of the SWEV and the excitation spectra were established. The rms values of the displacement, velocity and acceleration of each of the measured pavement elevation profiles are presented in *Table 8-E*. The measured excitation PSD functions from the SWEV-A travelling over routes BG and GB are presented in *Figure 8-20*, while the measured spectra from the SWEV-B over both routes are given in *Figure 8-21*.

Table 8-E: The average nominal operating speeds and rms values of the measured longitudinal pavement elevation profiles of routes BG and GB obtained using the SWEV-A and SWEV-B (50 kg) configurations.

		Measured Pavement Elevation rms		
Nominal Operating Speed [km/h]	**Vehicle (50 kg)**	**Acceleration [m/s^2]**	**Velocity [m/s]**	**Displacement [mm]**
Route BG				
70	SWEV-A	17.45	0.09	1.91
80	SWEV-A	17.83	0.10	2.15
90	SWEV-A	18.26	0.10	2.38
70	SWEV-B	17.58	0.09	1.92
80	SWEV-B	17.39	0.10	2.12
90	SWEV-B	18.62	0.10	2.37
Route GB				
70	SWEV-A	17.95	0.10	1.98
80	SWEV-A	18.31	0.10	2.20
90	SWEV-A	18.62	0.10	2.49
70	SWEV-B	17.88	0.10	1.95
80	SWEV-B	18.16	0.10	2.22
90	SWEV-B	18.86	0.10	2.43

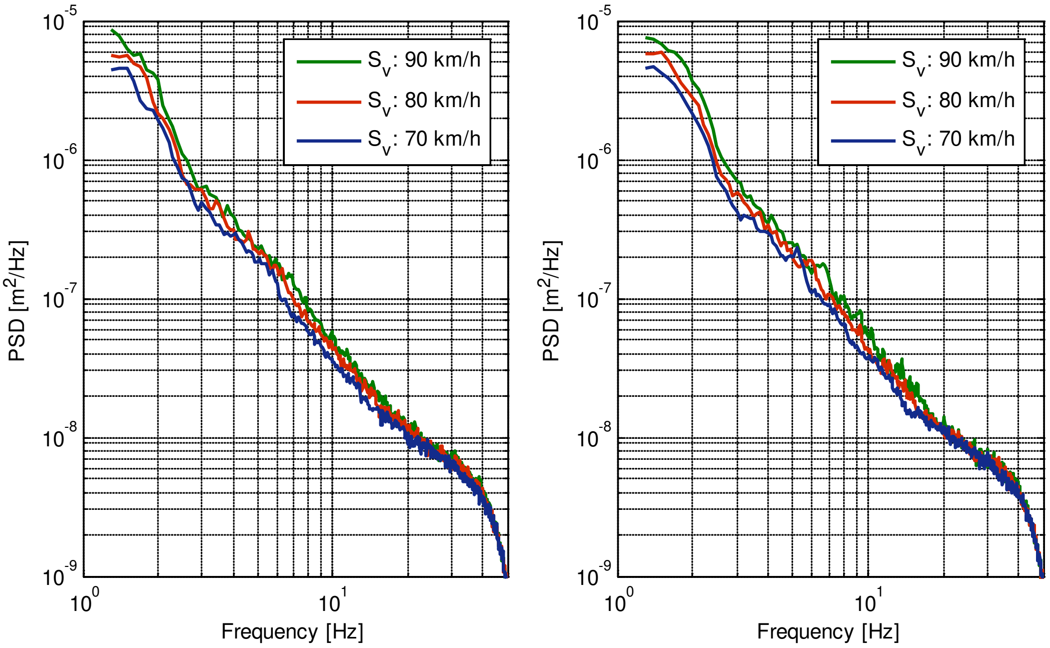

Figure 8-20: Measured excitation PSD functions from the SWEV-A (50 kg) travelling over routes BG (left) and GB (right).

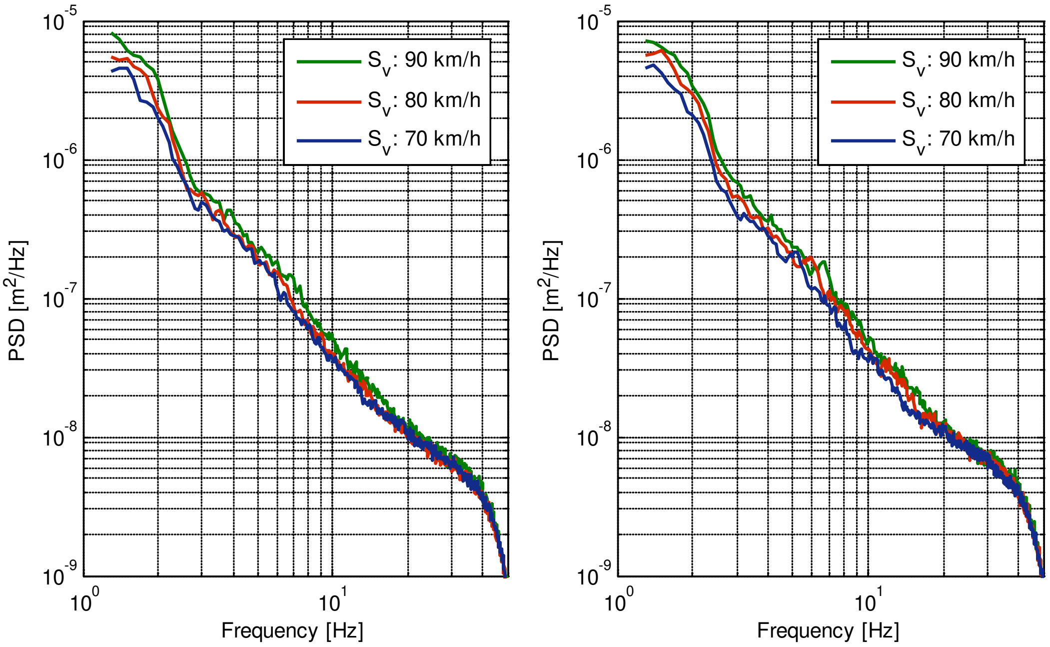

Figure 8-21: Measured excitation PSD functions from the SWEV-B (50 kg) travelling over routes BG (left) and GB (right).

There is variation between each of the measured elevation spectra for the various operating speeds. It was theorised that this may be the case and the source of the inconsistent estimates of the spectral exponent. The information revealed justifies the motivations for instrumenting the SWEV to operate as an inertial profilometer. The measured response spectra all are significantly different from the left and right wheel tracks obtained from the ARRB that were analysed in the previous section. It is evident that the middle of the pavement possesses different spectral characteristics compared to the left and right wheel tracks, likely due to the propensity of traffic to travel along the left and right wheel tracks instead of in the centre.

The measured excitation spectra were curve-fitted using the ISO (1995) spectral model and the values of the roughness constant, $G(n_0)$, and the spectral exponent, w, were obtained for a spatial frequency bandwidth of 0.06 – 2.00 c/m. Two examples of the measured pavement elevation PSD functions and the single-band curve-fits are provided in *Figure 8-22*, shown for the SWEV-A (50 kg) travelling over route BG at nominally constant operating speeds of 70 and 90 km/h. The established values of the single-band spectral model obtained via curve-fitting are presented in *Table 8-F* and *Table 8-G* for the SWEV-A and SWEV-B, respectively.

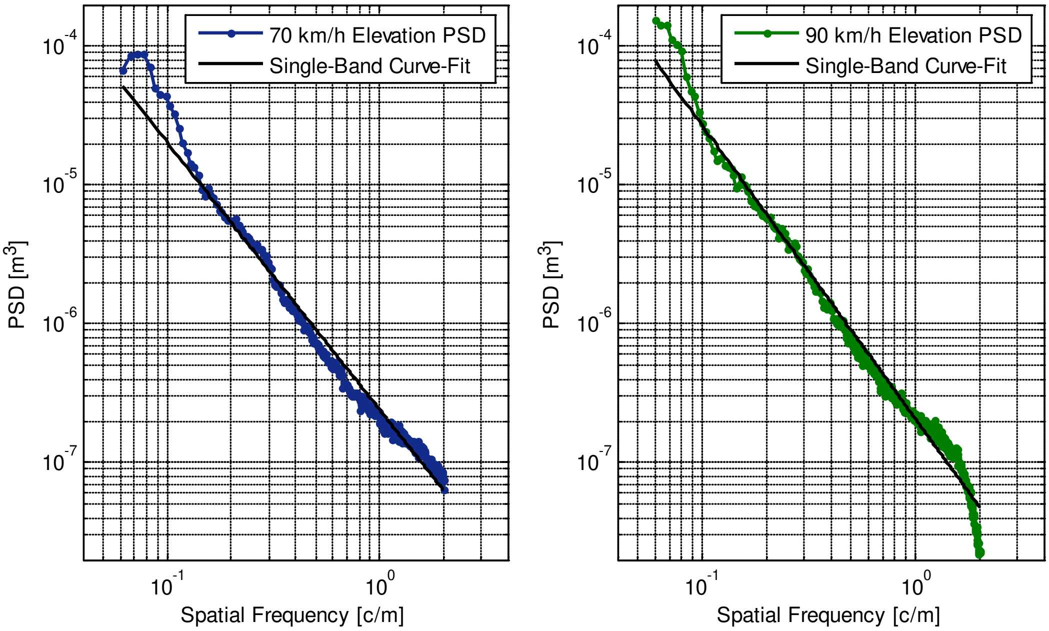

Figure 8-22: Typical examples of the measured excitation PSD functions, shown for the SWEV-A (50 kg) travelling over route BG at 70 km/h (left) and 90 km/h (right), along with the best single-band curve-fits.

Table 8-F: The average nominal operating speeds and the spectral properties from the single-band curve-fits of the measured excitation data from the SWEV-A (50 kg) for routes BG and GB.

Pavement Elevation Single-Band Curve-Fit (SWEV-A 50 kg)		
Nominal Operating Speed [km/h]	**Roughness Constant, $G(n_0)$ [m^3]**	**Spectral Exponent, w [-]**
Route BG		
70	2.026×10^{-5}	1.93
80	2.262×10^{-5}	1.99
90	2.685×10^{-5}	2.11
Route GB		
70	2.112×10^{-5}	1.92
80	2.289×10^{-5}	1.97
90	2.926×10^{-5}	2.13

Table 8-G: The average nominal operating speeds and the spectral properties from the single-band curve-fits of the measured excitation data from the SWEV-B (50 kg) for routes BG and GB.

Pavement Elevation Single-Band Curve-Fit (SWEV-B 50 kg)		
Nominal Operating Speed [km/h]	**Roughness Constant, $G(n_0)$ [m^3]**	**Spectral Exponent, w [-]**
Route BG		
70	2.035×10^{-5}	1.92
80	2.081×10^{-5}	1.98
90	2.605×10^{-5}	2.10
Route GB		
70	2.041×10^{-5}	1.91
80	2.287×10^{-5}	1.98
90	2.711×10^{-5}	2.10

There is a difference between the measured longitudinal pavement elevation PSD functions for each vehicle configuration, although it appears to obtain the same, or very close, estimates of the spectral exponent for each nominally constant operating speed over the two routes. From the previous Chapter outlining the development of the two in-service response analysis techniques, a rudimentary numerical model was developed to investigate the spectral approach (estimating the spectral properties of the excitation assuming it follows the ISO 8608 model) and found that if the vehicle travels over two different roads (with a different roughness constant or spectral exponent) then the technique would not be able to establish accurate estimates of the spectral exponent. It is expected that the estimated spectral exponents using only response data will not be accurate for either the SWEV-A or SWEV-B configurations. An examination of the FRFs measured from the laboratory and in-service experiments was undertaken next.

8.3.1.1 FRF Comparison with Laboratory Measurements

In the first series of in-service experiments, FRF estimates were made by combining the measured response data combined with an assumed ISO spectral model with varying parameters and compared to the FRFs measured in the laboratory (excited with violet noise acceleration at various intensities). Since the excitation was measured for each run using the profilometer capabilities of the SWEV, the actual transmissibility FRF of the SWEV for each experimental run undertaken can be used (instead of using an assumed excitation spectrum).

Having established the in-service FRFs for the various vehicle-speed-route combinations, they can be compared with the laboratory measured FRFs. The laboratory measured FRFs were excited using violet noise acceleration at various rms intensities. The comparison between the in-service (route BG) and laboratory measured FRFs are shown in *Figure 8-23* for the SWEV-A and *Figure 8-24* for the SWEV-B. The comparison FRFs established from route GB are presented in *Figure 8-25* for the SWEV-A and *Figure 8-26* for the SWEV-B.

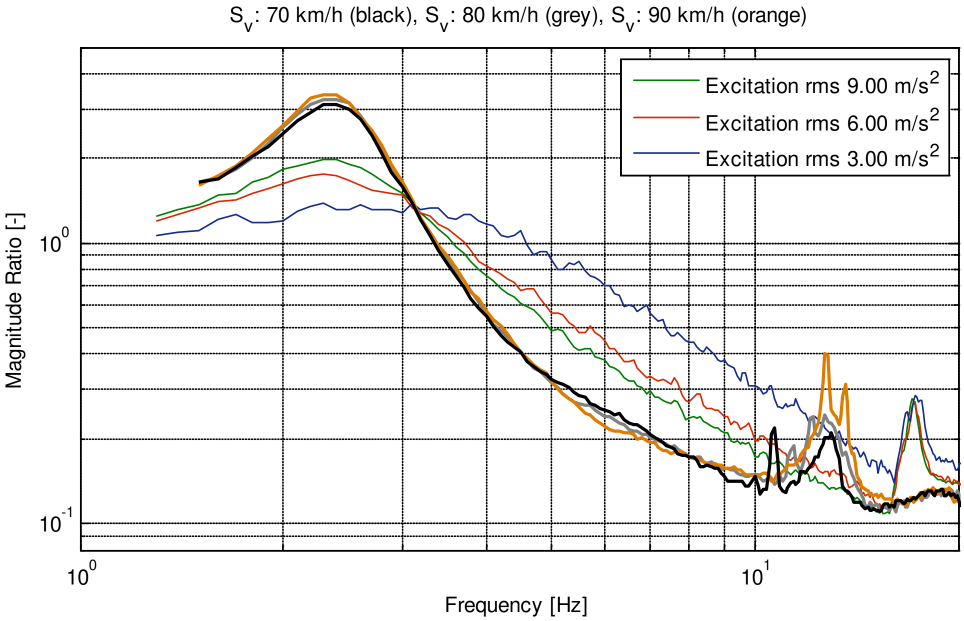

Figure 8-23: Comparison of the SWEV-A (50 kg) measured transmissibility FRFs from the laboratory (subjected to violet noise acceleration excitation at various rms intensities) and the transmissibility FRFs established in-service from route BG ($\Delta f = 0.1$ Hz).

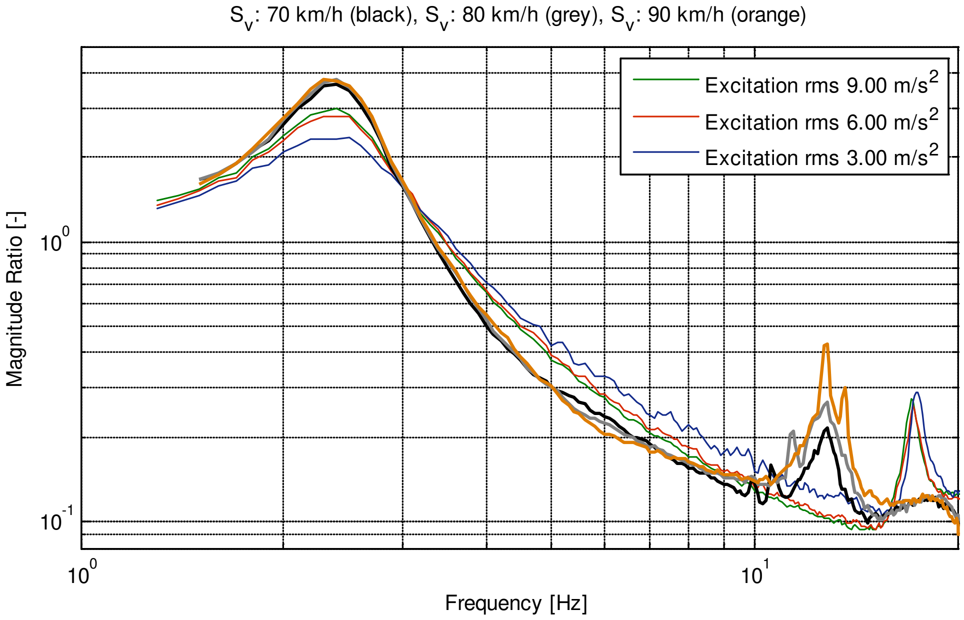

Figure 8-24: Comparison of the SWEV-B (50 kg) measured transmissibility FRFs from the laboratory (subjected to violet noise acceleration excitation at various rms intensities) and the transmissibility FRFs established in-service from route BG ($\Delta f = 0.1$ Hz).

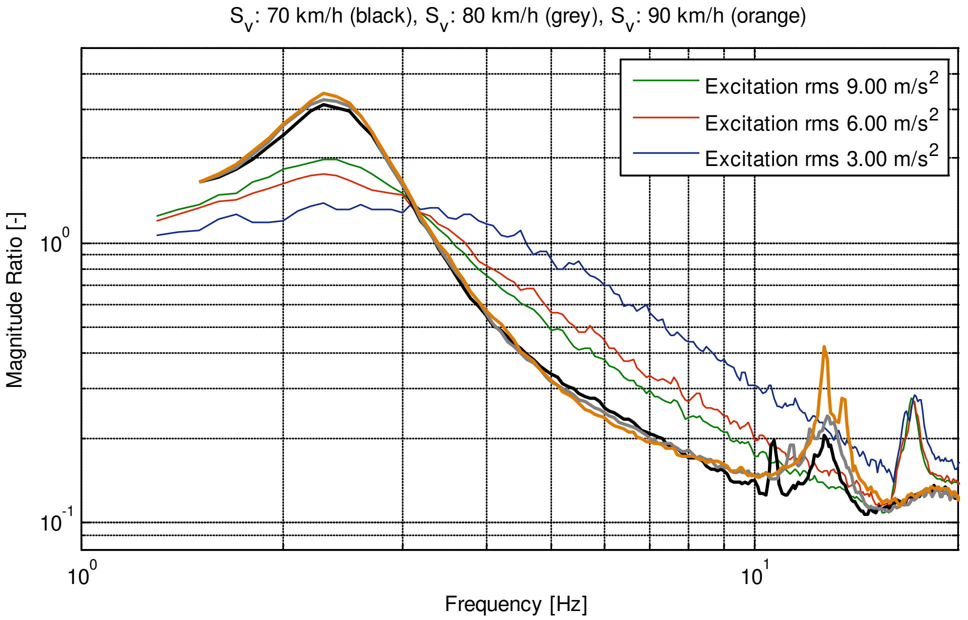

Figure 8-25: Comparison of the SWEV-A (50 kg) measured transmissibility FRFs from the laboratory (subjected to violet noise acceleration excitation at various rms intensities) and the transmissibility FRFs established in-service from the return route GB (Δf = 0.1 Hz).

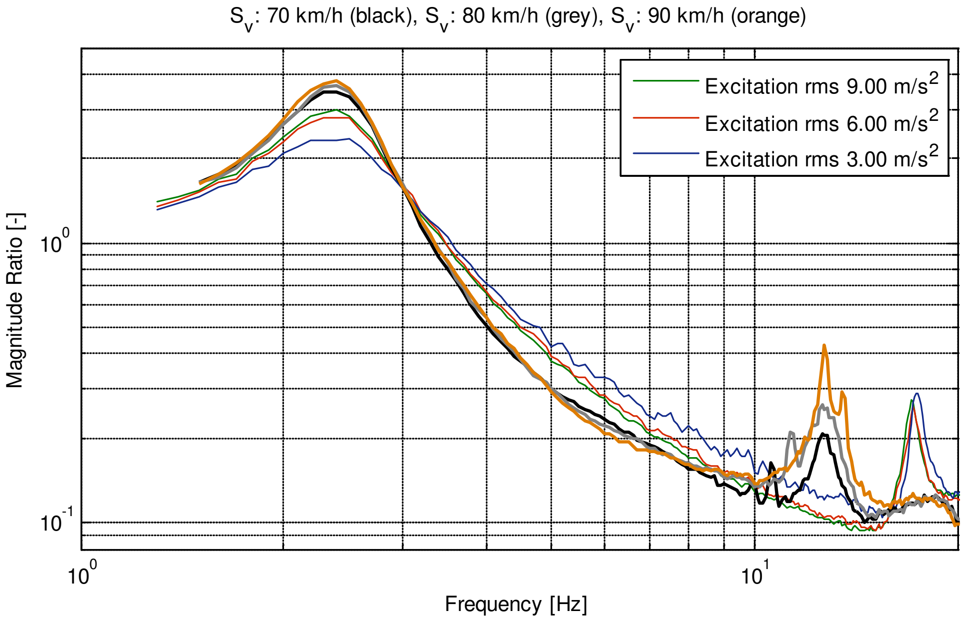

Figure 8-26: Comparison of the SWEV-B (50 kg) measured transmissibility FRFs from the laboratory (subjected to violet noise acceleration excitation at various rms intensities) and the transmissibility FRFs established in-service from the return route GB (Δf = 0.1 Hz).

For both configurations of the SWEV, the in-service FRFs are significantly different to the laboratory FRFs. While the sprung mass resonant frequency does not significantly vary between the laboratory and in-service FRFs, the level of damping is considerably different. It appears that the damping ratio, generally, is decreased during the vehicle's normal operation.

Interestingly, as was found in the previous comparison FRFs established the unsprung mass natural frequency is consistently lower than measured in the laboratory. There is also contamination around the unsprung mass resonant frequency due to wheel imbalance, only present in the in-service FRFs. This provides further impetus that establishing the dynamic characteristics of road vehicles using in-service response data is important to obtain an accurate representation of the vehicle as the laboratory measurements are significantly different from those measured in-service.

8.3.1.2 Spectral Exponent Estimation

The analysis of the measured longitudinal pavement elevation data indicates that the spectral exponent will not be able to accurately estimated using either the ratio of the response spectra or acceleration rms approaches as the pavement elevation PSD functions differ between experimental runs (different operating speeds). The estimated spectral exponents using the ratio of the response acceleration rms for the various nominally constant operating speed ratios of the SWEV-A and SWEV-B configurations travelling over routes BG and GB are presented in *Table 8-H.* As expected, there is no consistency in the estimates due to the varying excitation spectra measured between each run.

Table 8-H: The average nominal operating speed ratios and the estimated spectral exponents using the rms response ratios of the SWEV-A and SWEV-B (50 kg) for both routes BG and GB.

Nominal Operating Speed Ratio [-]	**Estimated Spectral Exponent, *w* [-]**	
	Route BG	**Route GB**
SWEV-A (50 kg) Configuration		
70 / 80	1.96	2.14
70 / 90	2.53	2.69
80 / 90	3.17	3.31
SWEV-B (50 kg) Configuration		
70 / 80	0.78	0.92
70 / 90	2.00	2.07
80 / 90	3.39	3.37

The approach to estimate the spectral exponent using the ratio of the response PSD functions was also investigated. Due to filtering and the fact that the sprung mass resonant frequency has shifted from the previous configuration of the SWEV due to the decreased mass loading, the mean value of the spectral exponent was estimated between 1.0 – 4.0 Hz (± 1.5 Hz from the resonant frequency). For the SWEV-A (50 kg) configuration, the estimated spectral exponents as a function of frequency for the different operating speed ratios over both routes BG and GB are shown in *Figure 8-27* and *Figure 8-29*, respectively. For the SWEV-B (100 kg) configuration, the estimated spectral exponents (as a function of frequency) from the various operating speed ratios over routes BG and GB are presented in *Figure 8-28* and *Figure 8-30*, respectively. The average value of estimated spectral exponents (between 1 – 4 Hz) from the various vehicle-route-speed combinations are given in *Table 8-I*.

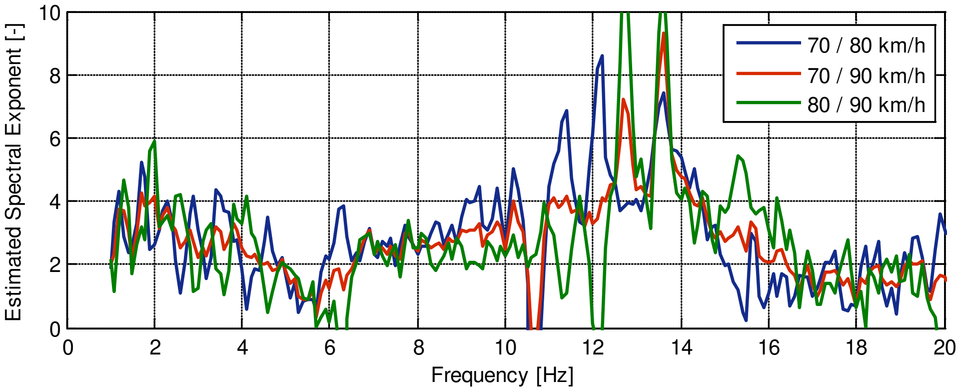

Figure 8-27: Estimated spectral exponent (as a function of frequency) from various nominally constant speed ratios from the SWEV-A (50 kg) travelling over route BG.

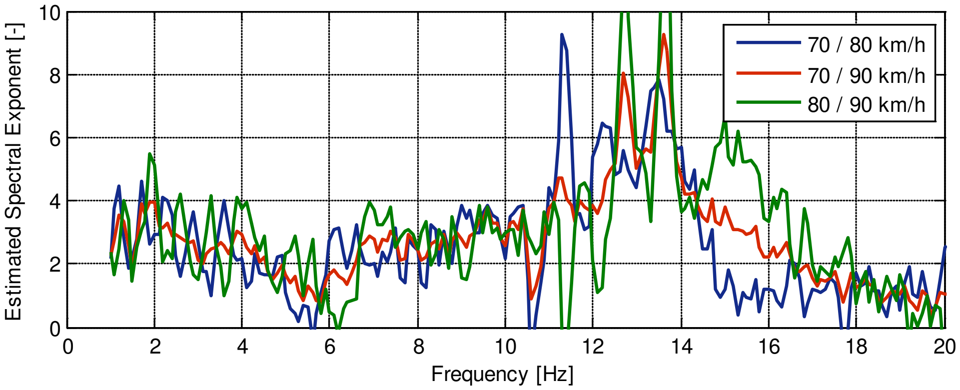

Figure 8-28: Estimated spectral exponent (as a function of frequency) from various nominally constant speed ratios from the SWEV-B (50 kg) travelling over route BG.

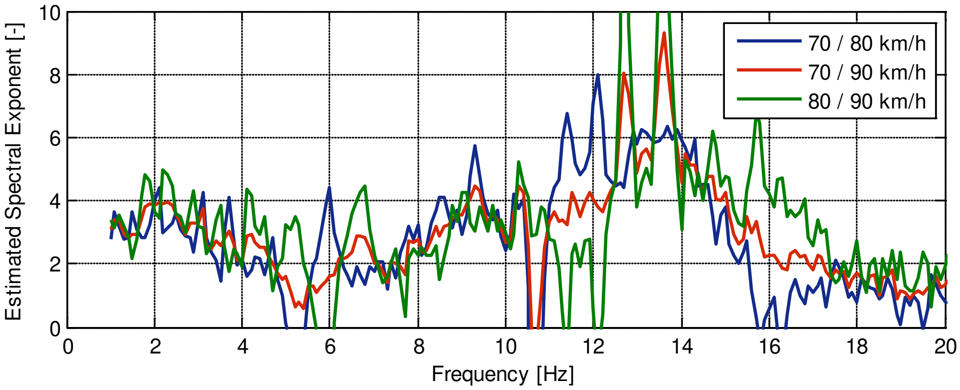

Figure 8-29: Estimated spectral exponent (as a function of frequency) from various nominally constant speed ratios from the SWEV-A (50 kg) travelling over route GB.

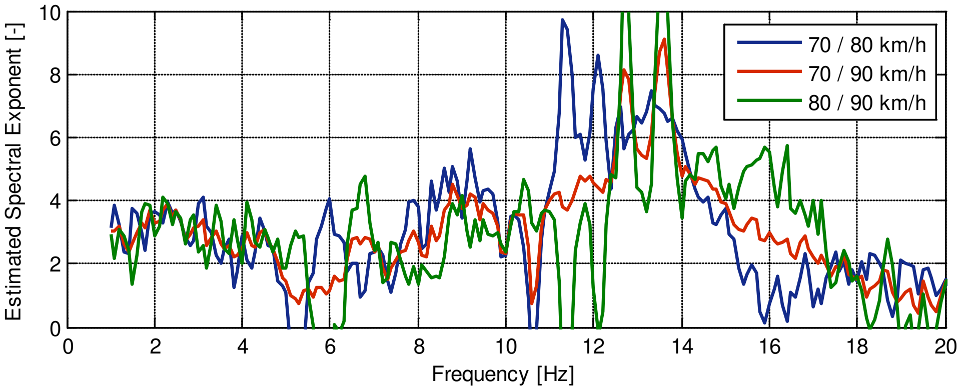

Figure 8-30: Estimated spectral exponent (as a function of frequency) from various nominally constant speed ratios from the SWEV-B (50 kg) travelling over route GB.

Table 8-I: The estimated spectral exponents from the SWEV-A and SWEV-B (50 kg) travelling over routes BG and GB for various nominally constant operating speed ratios, using the spectral approach by taking the mean value around the sprung mass resonant frequency (1.0 – 4.0 Hz).

Nominal Operating Speed Ratio [-]	Estimated Spectral Exponent, w [-]	
	Route BG	**Route GB**
SWEV-A (50 kg) Configuration		
70 / 80	3.08	3.03
70 / 90	3.04	3.18
80 / 90	2.99	3.34
SWEV-B (50 kg) Configuration		
70 / 80	2.85	3.04
70 / 90	2.86	3.01
80 / 90	2.87	2.98

The average estimated values of the spectral exponent are consistent but not accurate, due to the variation in the pavement elevation spectra between experimental runs. While it is not expected that the approach would yield accurate results for another route, as part of this research, further in-service experiments were undertaken using a different road to confirm the issues encountered are not related to the original road.

8.3.2 Routes SR and RS

The measured response spectra from routes SR and RS of the SWEV-A and the SWEV-B (50 kg) at various constant speeds are presented in *Figure 8-31* and *Figure 8-32*, respectively.

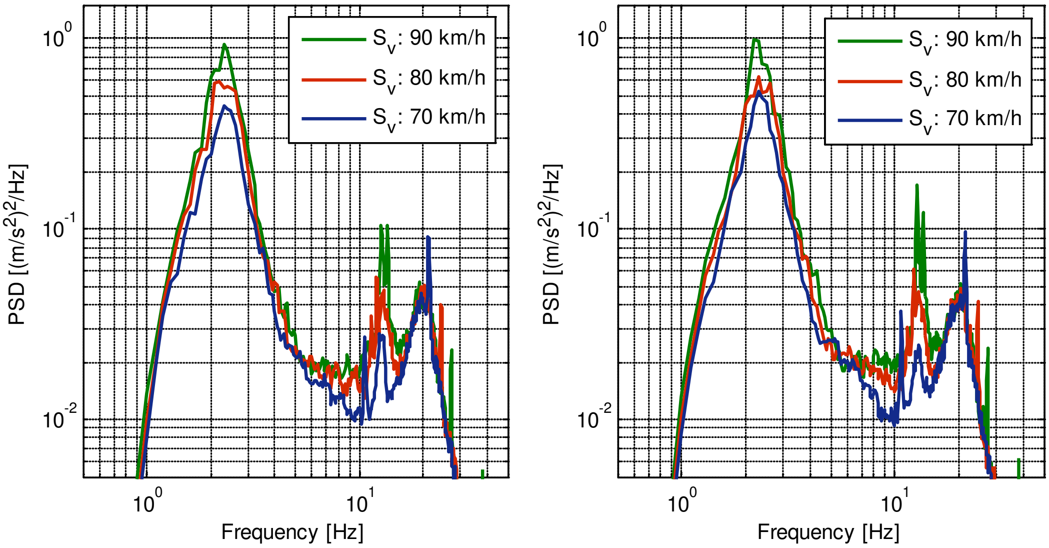

Figure 8-31: The filtered response PSD functions from the SWEV-A (50 kg) travelling over routes SR (left) and RS (right) (Δf = 0.1 Hz).

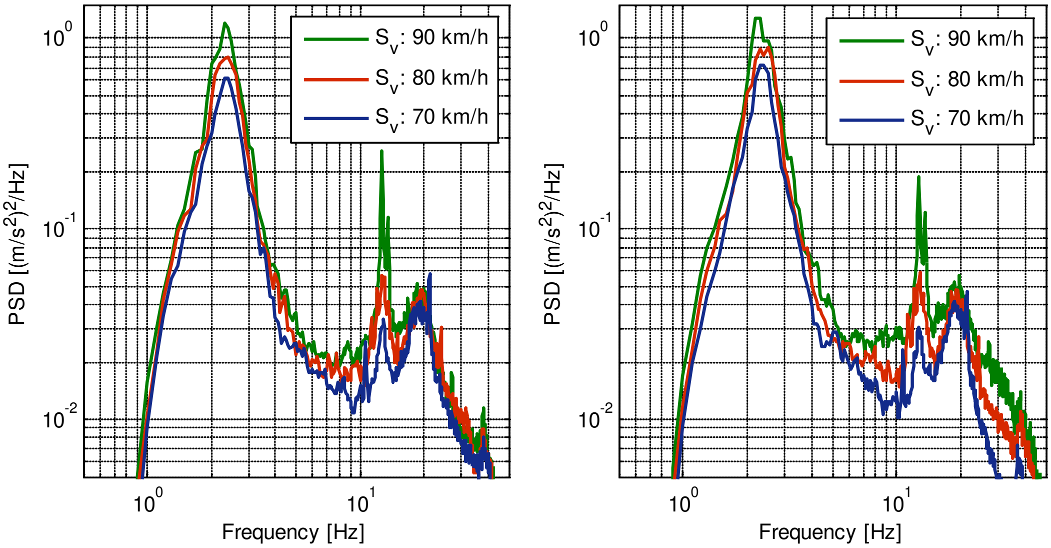

Figure 8-32: The filtered response PSD functions from the SWEV-B (50 kg) travelling over routes SR (left) and RS (right) (Δf = 0.1 Hz).

The measured longitudinal pavement elevation spectra were computed for each experimental run and the rms values of the displacement, velocity and acceleration are presented in *Table 8-J*. The measured excitation spectra of routes SR and RS are presented in *Figure 8-33* from the SWEV-A and *Figure 8-34* from the SWEV-B.

Table 8-J: The average nominal operating speed and the rms values of the measured longitudinal pavement elevation profiles of routes SR and RS obtained using the SWEV-A and SWEV-B (50 kg) configurations.

		Measured Pavement Elevation rms		
Nominal Operating Speed [km/h]	**Vehicle (50 kg)**	**Acceleration [m/s^2]**	**Velocity [m/s]**	**Displacement [mm]**
Route SR				
70	SWEV-A	17.95	0.10	2.02
80	SWEV-A	18.05	0.10	2.28
90	SWEV-A	18.04	0.10	2.46
70	SWEV-B	23.33	0.12	2.09
80	SWEV-B	23.84	0.12	2.29
90	SWEV-B	24.08	0.12	2.53
Route RS				
70	SWEV-A	18.37	0.10	2.02
80	SWEV-A	18.38	0.10	2.20
90	SWEV-A	18.52	0.10	2.40
70	SWEV-B	24.24	0.12	2.09
80	SWEV-B	24.86	0.12	2.28
90	SWEV-B	24.86	0.13	2.48

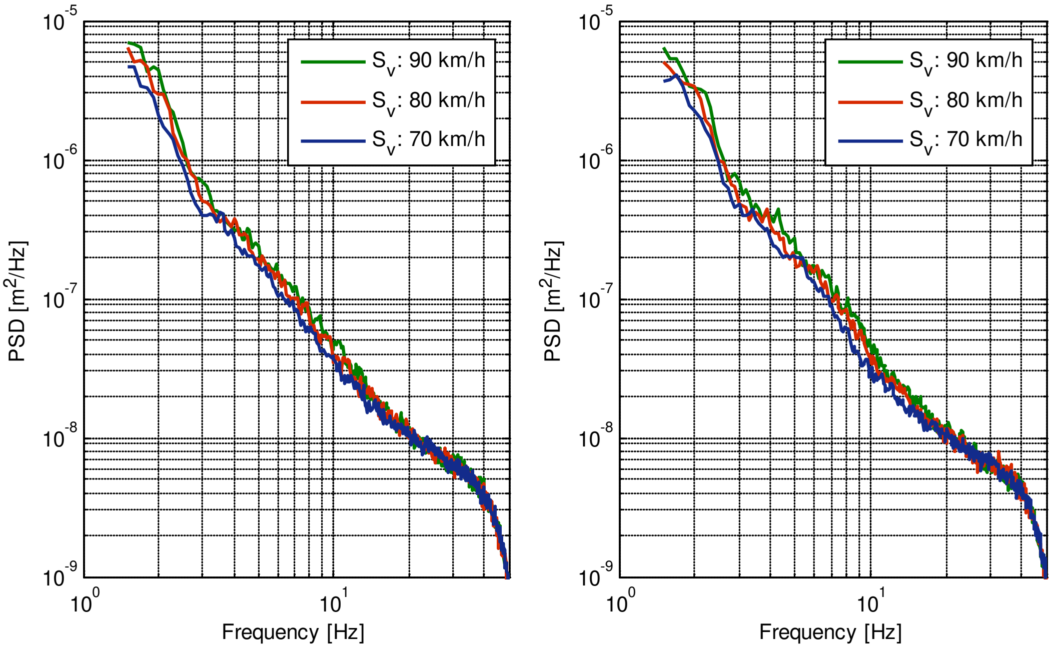

Figure 8-33: Measured excitation PSD functions from the SWEV-A (50 kg) travelling over routes SR (left) and RS (right).

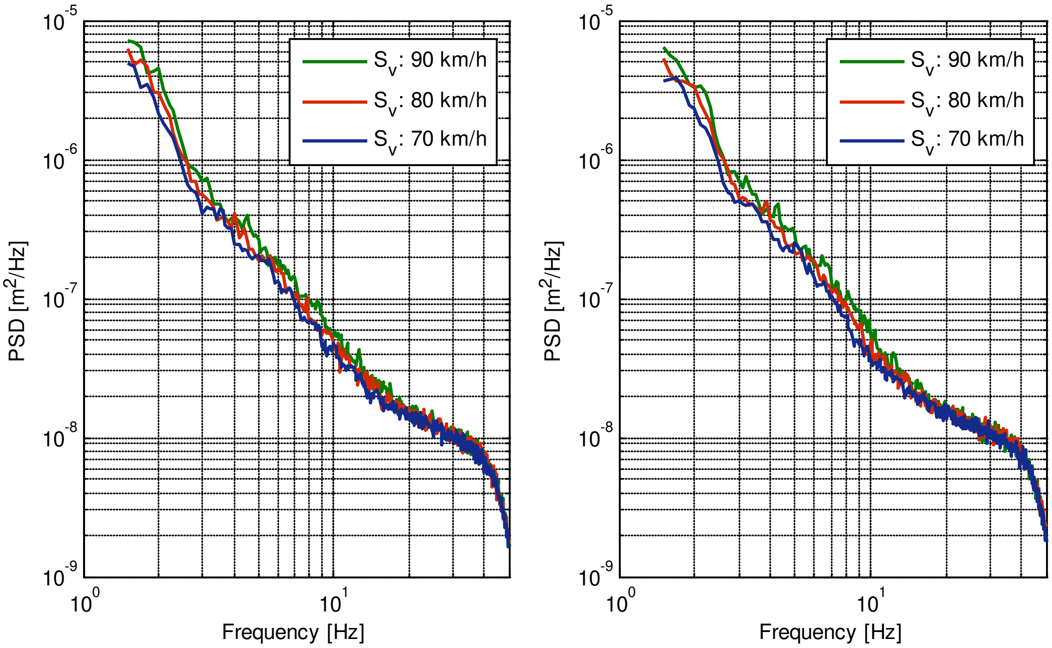

Figure 8-34: Measured excitation PSD functions from the SWEV-B (50 kg) travelling over routes SR (left) and RS (right).

The measured spectra vary between each experimental run at different operating speeds. The pavement elevation PSD functions were then curve-fitted using the ISO 8608 (1995) spectral model to establish the roughness constant, $G(n_0)$, and the spectral exponent, w, between a spatial frequency bandwidth of 0.06 – 2.00 c/m. Two typical examples of the established curve-fits are shown in *Figure 8-35* for the SWEV-A (50 kg) travelling at a nominally constant operating speed of 70 and 90 km/h over route SR. The established values of the spectra from the curve-fits are presented in *Table 8-K* and *Table 8-L* for the SWEV-A and SWEV-B, respectively. The estimates of both the roughness constant and spectral exponent vary between each experimental run, which again would result in difficulties estimating the spectral properties of the pavement using the spectral approach. A comparison between the in-service and laboratory FRFs is presented in the following section.

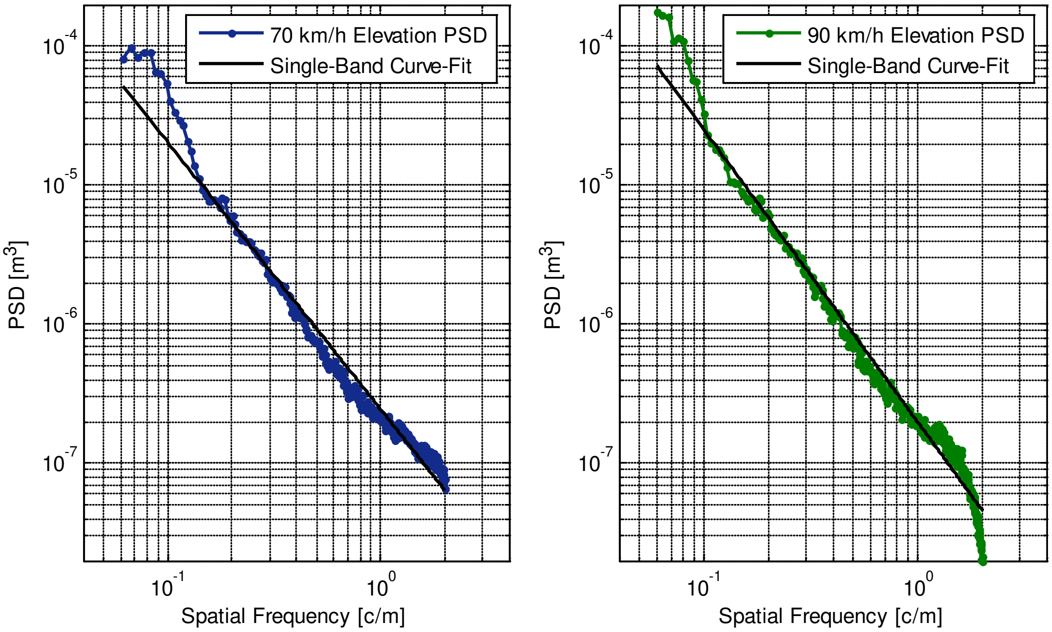

Figure 8-35: Measured excitation PSD functions from the SWEV-A (50 kg) travelling over route SR at operating speeds of 70 km/h (left) and 90 km/h (right), along with the best fitting single-band curve-fit.

Table 8-K: The average nominal operating speeds and the spectral properties from the single-band curve-fits of the measured excitation data from the SWEV-A (50 kg) for routes SR and RS.

Pavement Elevation Single-Band Curve-Fit (SWEV-A 50 kg)		
Nominal Operating Speed [km/h]	**Roughness Constant, $G(n_0)$ [m^3]**	**Spectral Exponent, w [-]**
Route SR		
70	2.047×10^{-5}	1.92
80	2.250×10^{-5}	1.99
90	2.519×10^{-5}	2.10
Route RS		
70	1.989×10^{-5}	1.91
80	2.125×10^{-5}	1.96
90	2.514×10^{-5}	2.09

Table 8-L: The average nominal operating speeds and the spectral properties from the single-band curve-fits of the measured excitation data from the SWEV-B (50 kg) for routes SR and RS.

Pavement Elevation Single-Band Curve-Fit (SWEV-B 50 kg)		
Nominal Operating Speed [km/h]	**Roughness Constant, $G(n_0)$ [m^3]**	**Spectral Exponent, w [-]**
Route SR		
70	1.885×10^{-5}	1.74
80	1.872×10^{-5}	1.73
90	2.284×10^{-5}	1.86
Route RS		
70	1.866×10^{-5}	1.72
80	1.896×10^{-5}	1.72
90	2.289×10^{-5}	1.84

8.3.2.1 FRF Comparison with Laboratory Measurements

The FRFs established from the in-service experiments are compared with the FRFs measured in the laboratory (violet noise acceleration excitation at various rms intensities). The comparison FRFs of the SWEV-A (50 kg) from routes SR and RS are presented in *Figure 8-36* and *Figure 8-38*, respectively. The comparison FRFs of the SWEV-B (50 kg) are presented in *Figure 8-37* for route SR and *Figure 8-39* for the return route RS.

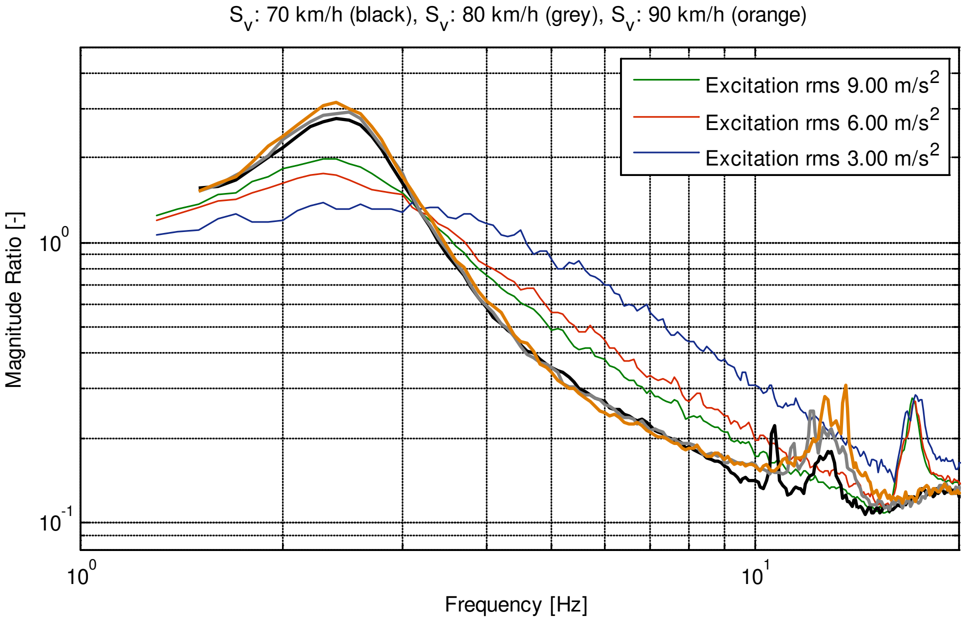

Figure 8-36: Comparison of the SWEV-A (50 kg) measured transmissibility FRFs from the laboratory (subjected to violet noise acceleration excitation at various rms intensities) and the transmissibility FRFs established in-service from route SR (Δf = 0.1 Hz).

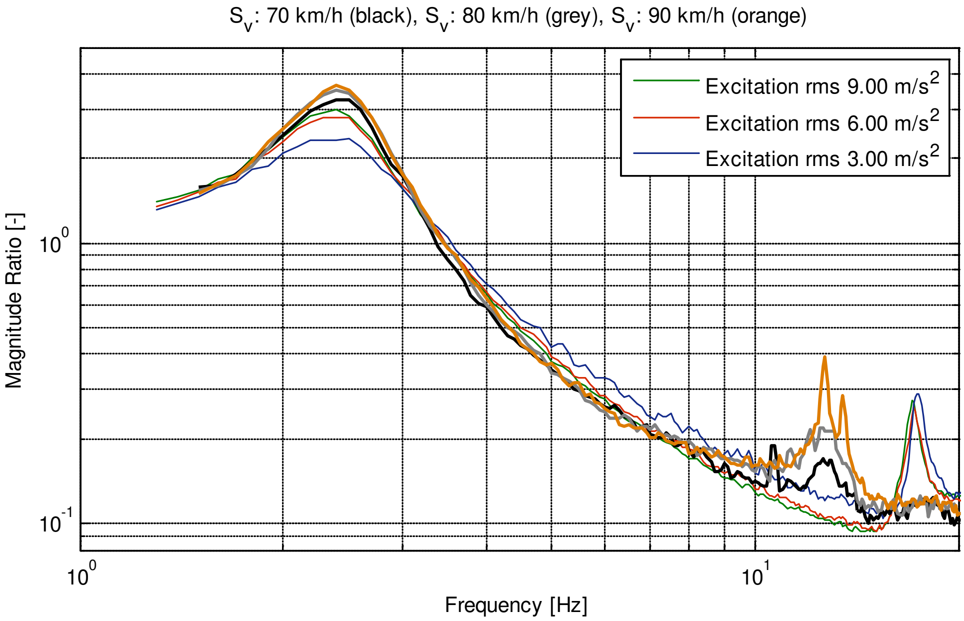

Figure 8-37: Comparison of the SWEV-B (50 kg) measured transmissibility FRFs from the laboratory (subjected to violet noise acceleration excitation at various rms intensities) and the transmissibility FRFs established in-service from route SR (Δf = 0.1 Hz).

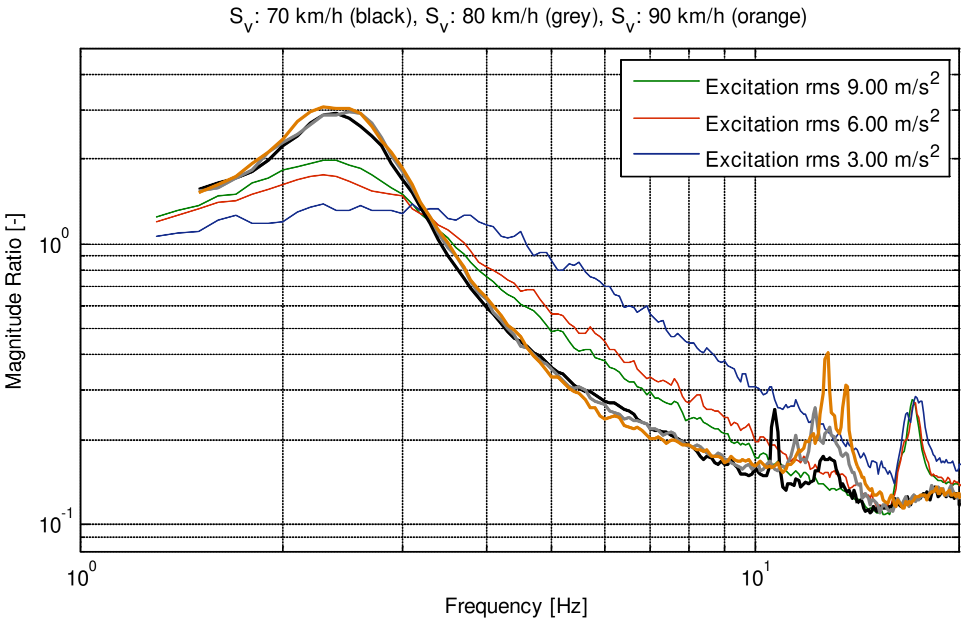

Figure 8-38: Comparison of the SWEV-A (50 kg) measured transmissibility FRFs from the laboratory (subjected to violet noise acceleration excitation at various rms intensities) and the transmissibility FRFs established in-service from the return route RS (Δf = 0.1 Hz).

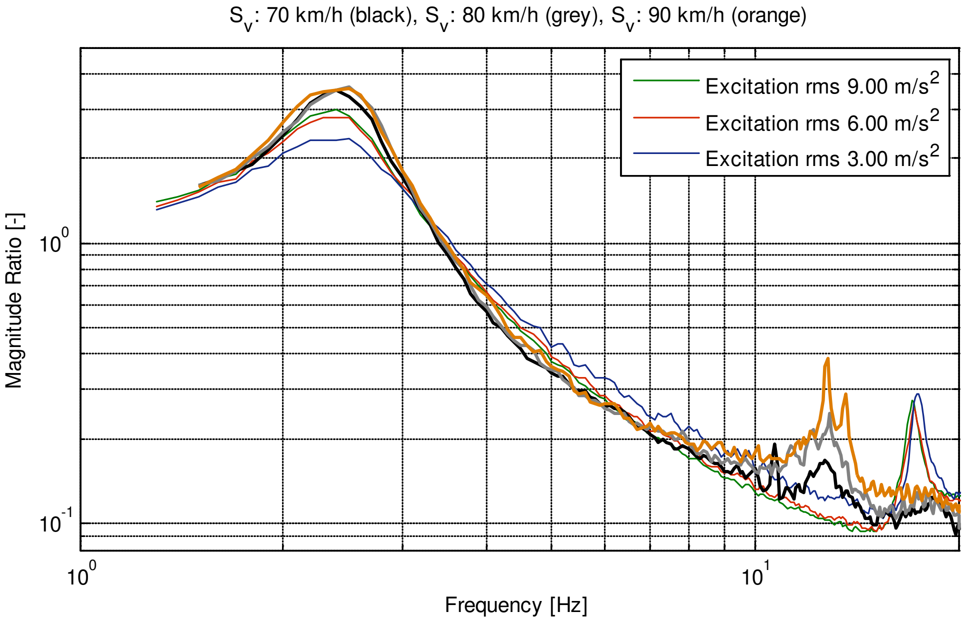

Figure 8-39: Comparison of the SWEV-B (50 kg) measured transmissibility FRFs from the laboratory (subjected to violet noise acceleration excitation at various rms intensities) and the transmissibility FRFs established in-service from the return route RS (Δf = 0.1 Hz).

As encountered for the results from routes BG and GB, there is a significant difference between the established FRFs for both configurations of the SWEV, particularly in the level of damping of the sprung mass mode. The level of the sprung mass mode damping of both the SWEV-A and SWEV-B appears to be considerably reduced during normal operation (in-service). Further to this, the unsprung mass mode is again observed to shift to a lower frequency during operation compared to what is measured in the laboratory.

8.3.2.2 Spectral Exponent Estimation

The previous spectral exponent estimation attempts made for routes BG and GB revealed that the spectral approach will not be able to accurately estimate the spectral exponent, w, using either the ratio of the response spectra or acceleration rms. For completeness, the spectral exponent was estimated using the ratio of the rms acceleration response for each vehicle and speed ratio combination, presented in *Table 8-M*. The estimated spectral exponents are neither consistent nor accurate for either the SWEV-A or SWEV-B configurations.

Table 8-M: The average nominal operating speed ratios and the estimated spectral exponents using the rms response ratios of the SWEV-A and SWEV-B (50 kg) for both routes SR and RS.

Nominal Operating Speed Ratio [-]	**Estimated Spectral Exponent, *w* [-]**	
	Route SR	**Route RS**
SWEV-A (50 kg) Configuration		
70 / 80	2.56	2.28
70 / 90	2.67	2.47
80 / 90	2.80	2.69
SWEV-B (50 kg) Configuration		
70 / 80	3.55	4.00
70 / 90	3.35	4.32
80 / 90	3.12	4.68

Next, the spectral exponent was estimated using the ratio of the response PSD functions. The exponent was estimated between a frequency bandwidth of 1.0 – 4.0 Hz, corresponding to ± 1.5 Hz around the sprung mass resonant frequency. The estimated spectral exponent (as a function of frequency) is presented for both the SWEV-A and SWEV-B for the three operating speed ratios over route SR in *Figure 8-40* and *Figure 8-41*, respectively. The estimated spectral exponents for the return route RS are presented in *Figure 8-42* for the SWEV-A and in *Figure 8-43* for the SWEV-B. The estimates of the spectral exponents obtained using the mean value around the sprung mass mode are listed in *Table 8-N* for both routes SR and RS.

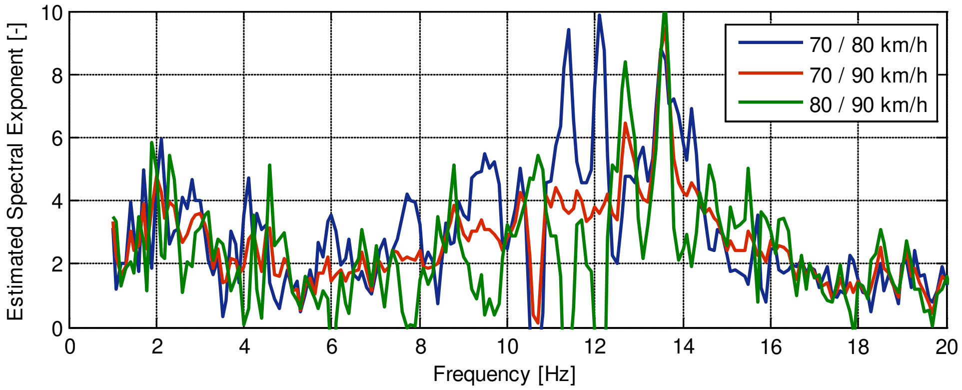

Figure 8-40: Estimated spectral exponent (as a function of frequency) from various nominally constant speed ratios from the SWEV-A (50 kg) travelling over route SR.

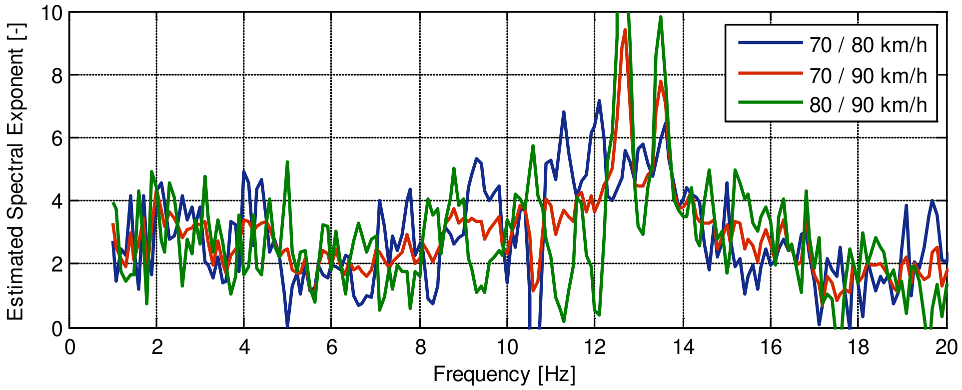

Figure 8-41: Estimated spectral exponent (as a function of frequency) from various nominally constant speed ratios from the SWEV-B (50 kg) travelling over route SR.

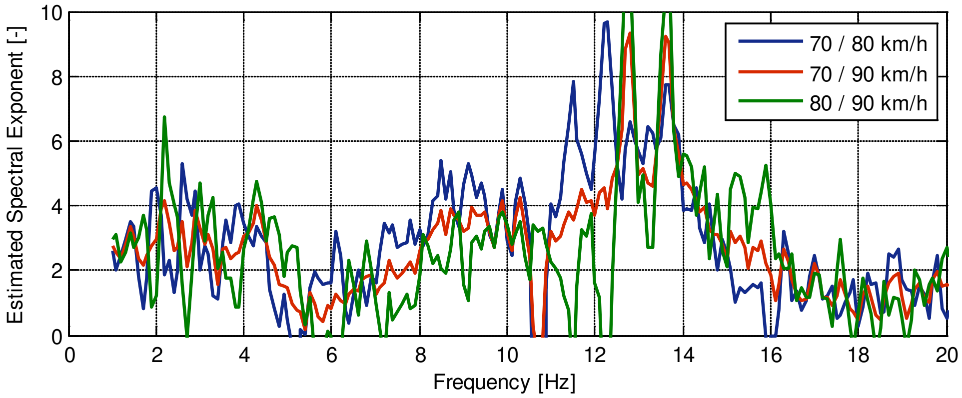

Figure 8-42: Estimated spectral exponent (as a function of frequency) from various nominally constant speed ratios from the SWEV-A (50 kg) travelling over route RS.

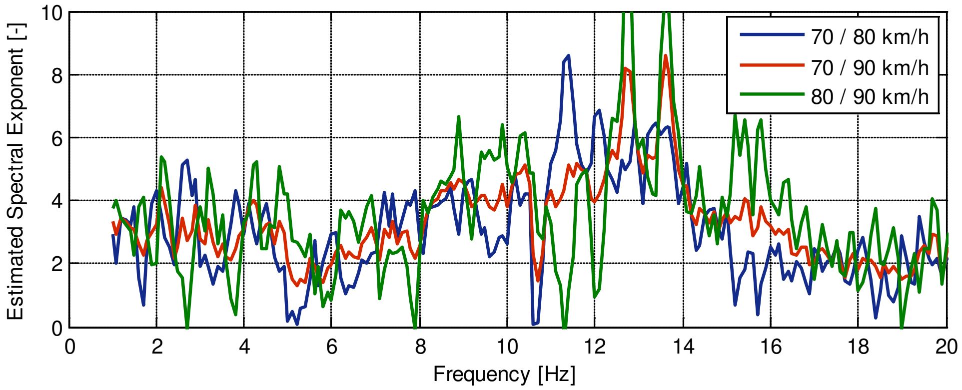

Figure 8-43: Estimated spectral exponent (as a function of frequency) from various nominally constant speed ratios from the SWEV-B (50 kg) travelling over route RS.

Table 8-N: The estimated spectral exponents from the SWEV-A and SWEV-B (50 kg) travelling over routes SR and RS at various nominally constant operating speed ratios, using the spectral approach by taking the mean value around the sprung mass resonant frequency (1.0 – 4.0 Hz).

Nominal Operating Speed Ratio [-]	**Estimated Spectral Exponent, *w* [-]**	
	Route SR	**Route RS**
SWEV-A (50 kg) Configuration		
70 / 80	2.99	2.89
70 / 90	2.84	2.85
80 / 90	2.66	2.80
SWEV-B (50 kg) Configuration		
70 / 80	2.88	3.00
70 / 90	2.85	2.96
80 / 90	2.82	2.91

As found for the routes BG and GB, there is an increased consistency in the estimates using the ratio of the response PSD functions, however they are not accurate. The results presented confirm that, even for a completely different route, the approach is unable to accurately estimate the spectral exponent of the pavement using only in-service response data. The use of a profilometer to measure the actual pavement elevation profiles revealed that the use of an assumed excitation spectrum is not correct and does not represent the actual pavement spectrum the vehicle travels over.

8.4 RANDOM DECREMENT EXPERIMENTAL ANALYSIS

This section describes the implementation of the random decrement technique to estimate the dynamic characteristics of the SWEV. The two approaches, described in detail in Chapter 7, establish the random decrement signature from the measured response data and analyse them differently. The first approach employs the Hilbert Transform to obtain the instantaneous phase to estimate the sprung mass damped natural frequency and the Hilbert envelope to estimate the damping ratio. The second approach uses the FFT to obtain the magnitude spectrum, which is considered to be the unscaled FRF. The excitation and response data measured from the second series of in-service experiments are used to validate the random decrement analysis technique to establish the dynamic characteristics of the SWEV-A and SWEV-B configurations loaded with 50 kg dead weight over the four routes BG, GB, SR and RS.

8.4.1 Routes BG and GB

The measured sprung mass acceleration response data from each experimental run over routes BG and GB were analysed to establish the random decrement signature for both approaches to estimate the dynamic characteristics of both the SWEV-A and SWEV-B (50 kg) configurations.

8.4.1.1 Estimation of the Sprung Mass Dynamic Characteristics (Hilbert Domain)

The first approach estimates the dynamic characteristics of the SWEV sprung mass mode (in the Hilbert Domain) from the random decrement signature. The obtained random decrement signatures from routes BG and GB are presented in *Figure 8-44* for the SWEV-A and in *Figure 8-45* for the SWEV-B. The lack of high frequency components within the random decrement signatures is due to the low-pass filter (cut-off frequency of 8 Hz) that was applied to the response data.

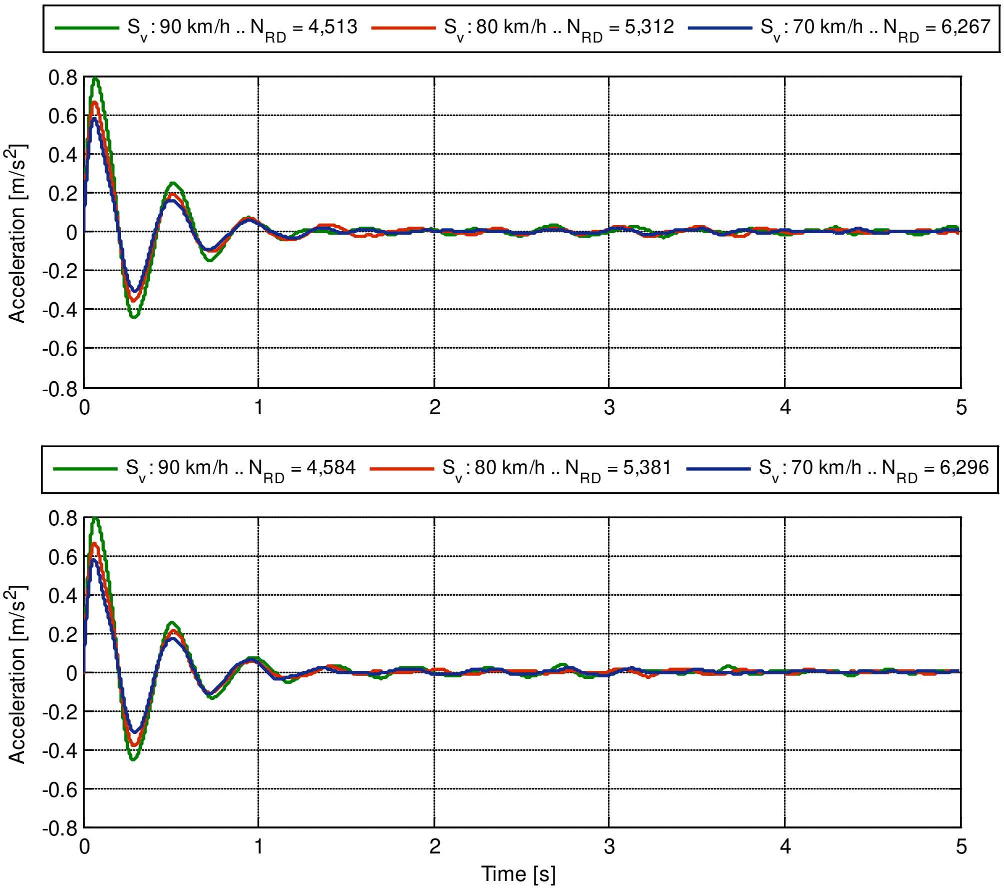

Figure 8-44: Established random decrement signatures from the sprung mass acceleration of the SWEV-A (50 kg) travelling over routes BG (top) and GB (bottom) for various nominally constant operating speeds.

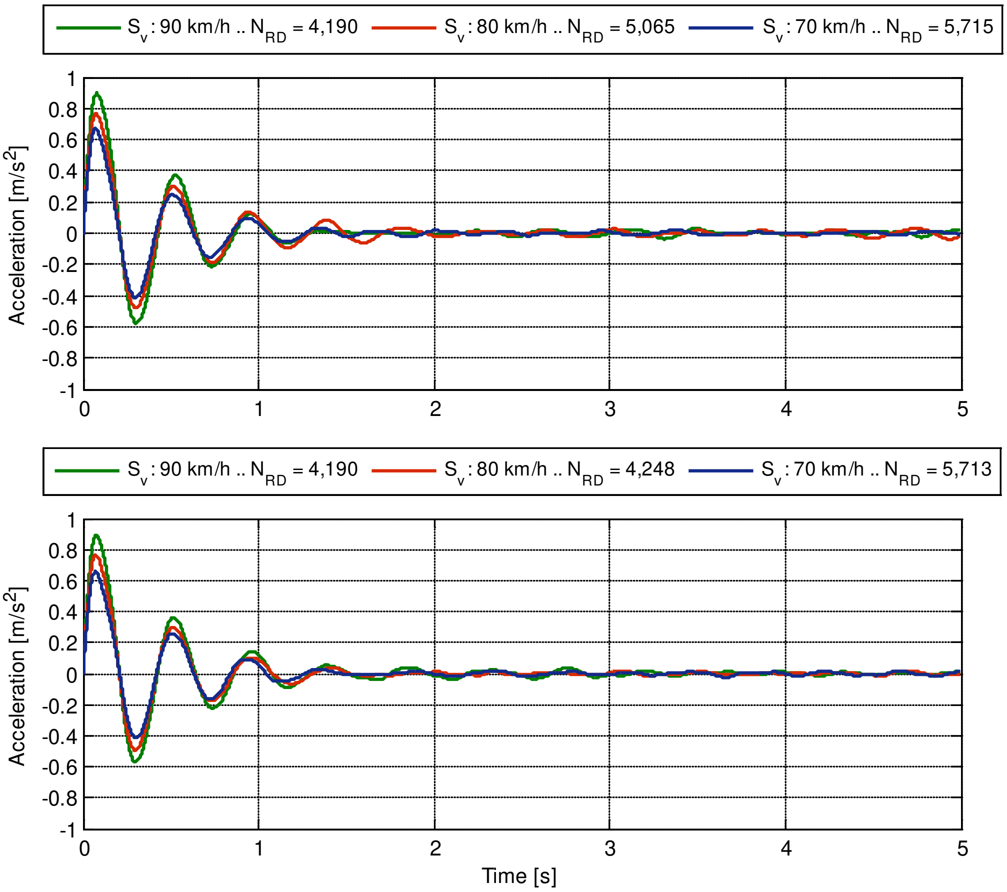

Figure 8-45: Established random decrement signatures from the sprung mass acceleration of the SWEV-B (50 kg) travelling over routes BG (top) and GB (bottom) for various nominally constant operating speeds.

Each of the random decrement signatures were analysed using the unwrapped instantaneous phase to estimate the damped natural frequency and the Hilbert envelope to estimate the damping ratio. A typical example of the established unwrapped instantaneous phase and Hilbert envelope are presented in *Figure 8-46*. The estimated dynamic characteristics of the sprung mass mode of the SWEV-A and SWEV-B travelling along routes BG and GB are presented in *Table 8-O* and *Table 8-P*, respectively, along with the measured dynamic characteristics obtained by curve-fitting the measured transmissibility FRFs.

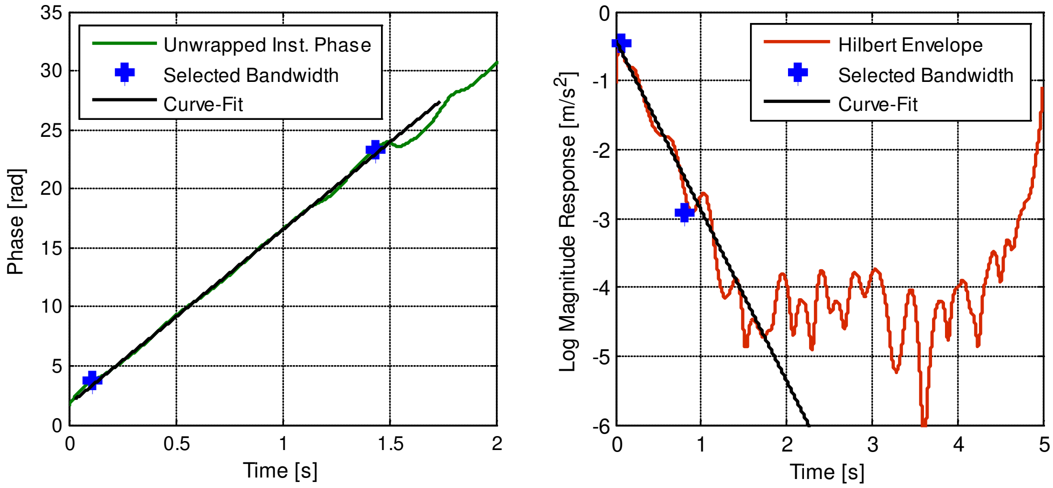

Figure 8-46: Typical example of the obtained unwrapped instantaneous phase (left) and the Hilbert envelope (right), shown for the SWEV-A (50 kg) travelling over route GB at a nominally constant operating speed of 70 km/h.

Table 8-O: The average nominal operating speed and the estimated and measured dynamic characteristics of the SWEV-A (50 kg) sprung mass mode travelling over routes BG and GB.

	FRF Curve-Fit		**Random Decrement**	
Nominal Operating Speed [km/h]	**Natural Frequency f_{sn} [Hz]**	**Damping Ratio ζ_s [-]**	**Natural Frequency f_{sn} [Hz]**	**Damping Ratio ζ_s [-]**
Route BG				
70	2.42	0.169	2.41	0.172
80	2.42	0.158	2.39	0.163
90	2.42	0.152	2.39	0.165
Route GB				
70	2.43	0.171	2.41	0.171
80	2.41	0.159	2.40	0.174
90	2.41	0.153	2.41	0.160

Table 8-P: The average nominal operating speed and the estimated and measured dynamic characteristics of the SWEV-B (50 kg) sprung mass mode travelling over routes BG and GB.

	FRF Curve-Fit		**Random Decrement**	
Nominal Operating Speed [km/h]	**Natural Frequency f_{sn} [Hz]**	**Damping Ratio ζ_s [-]**	**Natural Frequency f_{sn} [Hz]**	**Damping Ratio ζ_s [-]**
Route BG				
70	2.42	0.142	2.43	0.150
80	2.42	0.137	2.41	0.136
90	2.42	0.133	2.40	0.143
Route GB				
70	2.42	0.148	2.42	0.152
80	2.42	0.141	2.41	0.148
90	2.41	0.134	2.33	0.138

From the results, the estimates of the SWEV-A sprung mass dynamic characteristics using the random decrement approach are in good agreement with the measured transmissibility FRFs. For the SWEV-B configuration the estimated dynamic characteristics also agree well to the actual dynamic characteristics, with the exception of the GB 90 km/h experimental run. In some cases, the damping ratio is accurately estimated using the Hilbert envelope of the random decrement signature; however for both configurations there is a tendency for the damping to be slightly overestimated.

Overall, the estimates are quite close to those measured from the actual transmissibility FRFs established. The estimated dynamic characteristics are then combined with the SDoF transmissibility FRF model (Equation 3-53), limited to the sprung mass mode. The measured and estimated FRFs for the SWEV-A and SWEV-B travelling along route BG are presented in *Figure 8-47* and *Figure 8-48*, respectively. The SWEV-A and SWEV-B measured and estimated FRFs for the return route, GB, are shown in *Figure 8-49* and *Figure 8-50*, respectively.

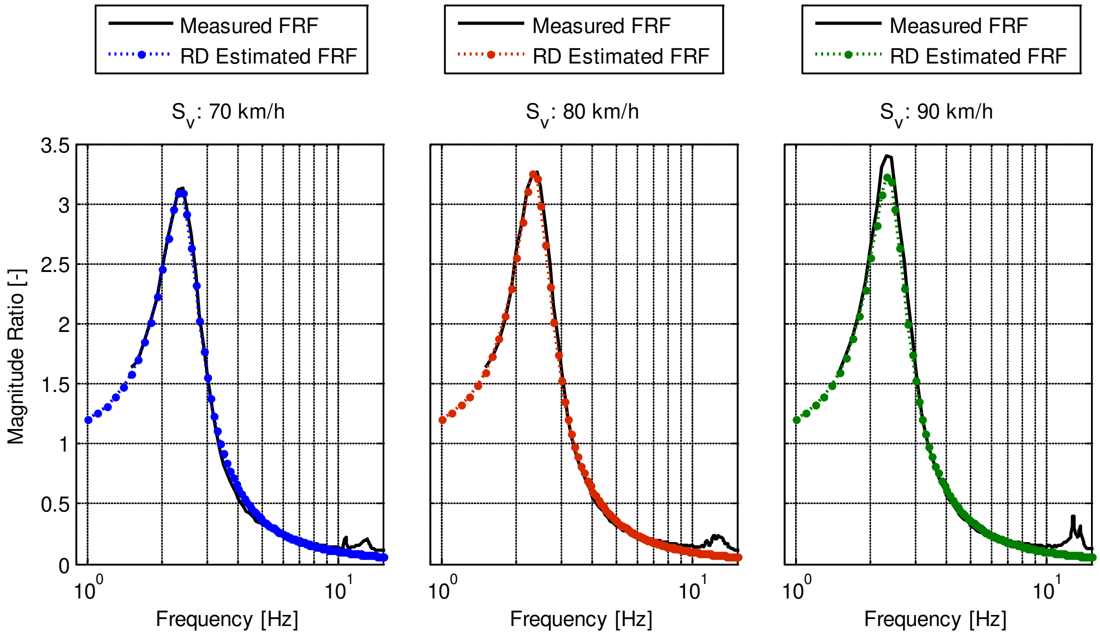

Figure 8-47: Measured and estimated (random decrement – Hilbert Domain) transmissibility FRFs of the SWEV-A (50 kg) travelling over route BG at nominally constant operating speeds of 70, 80 and 90 km/h.

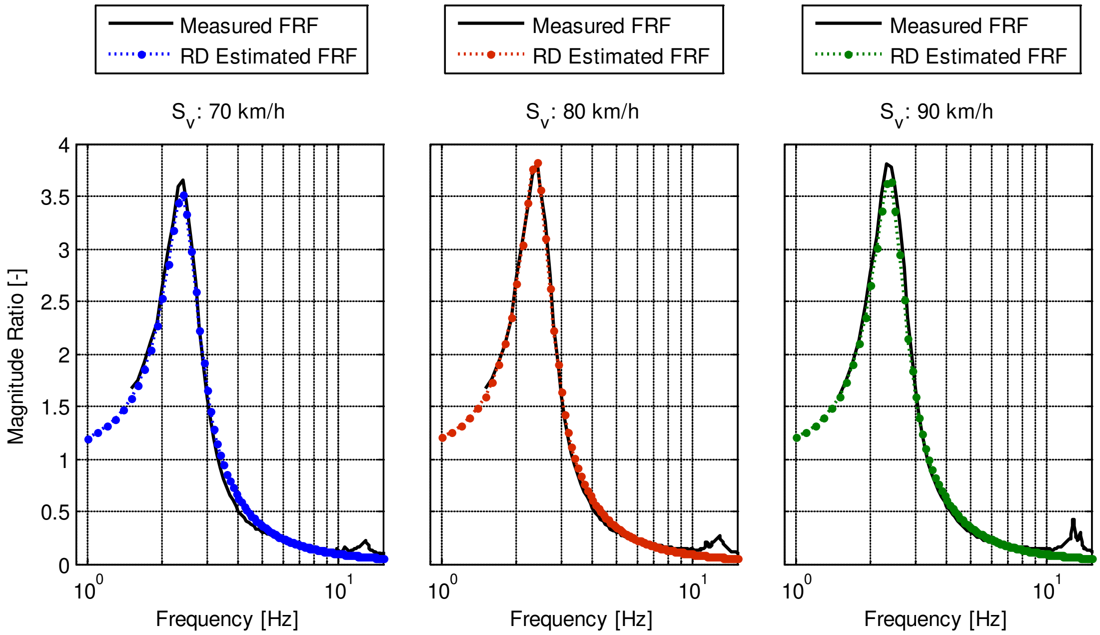

Figure 8-48: Measured and estimated (random decrement – Hilbert Domain) transmissibility FRFs of the SWEV-B (50 kg) travelling over route BG at nominally constant operating speeds of 70, 80 and 90 km/h.

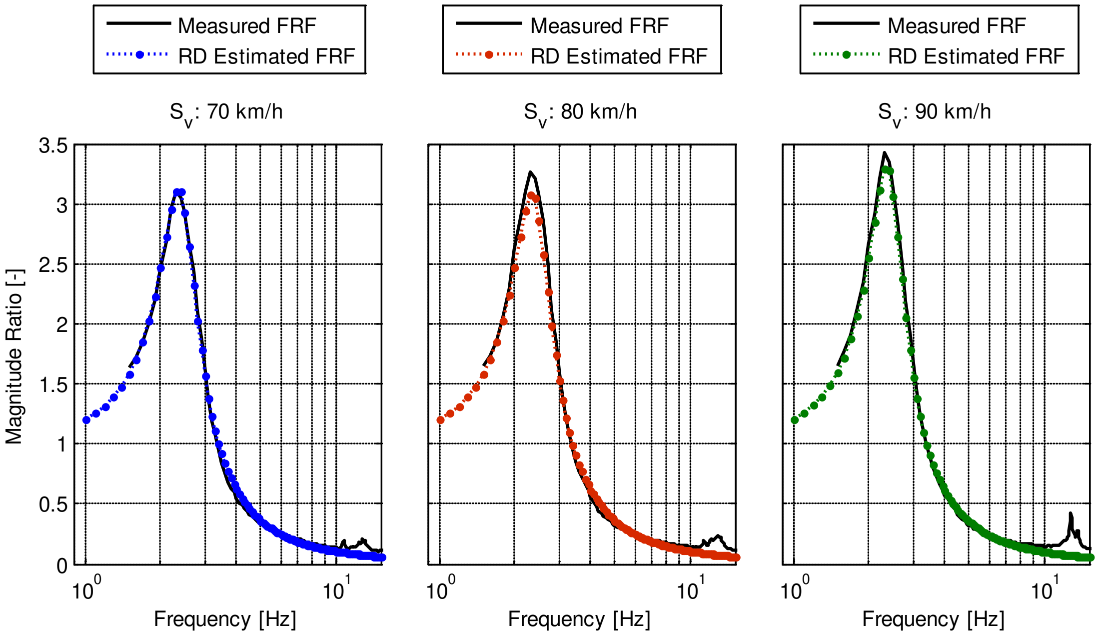

Figure 8-49: Measured and estimated (random decrement – Hilbert Domain) transmissibility FRFs of the SWEV-A (50 kg) travelling over route GB at nominally constant speeds of 70, 80 and 90 km/h.

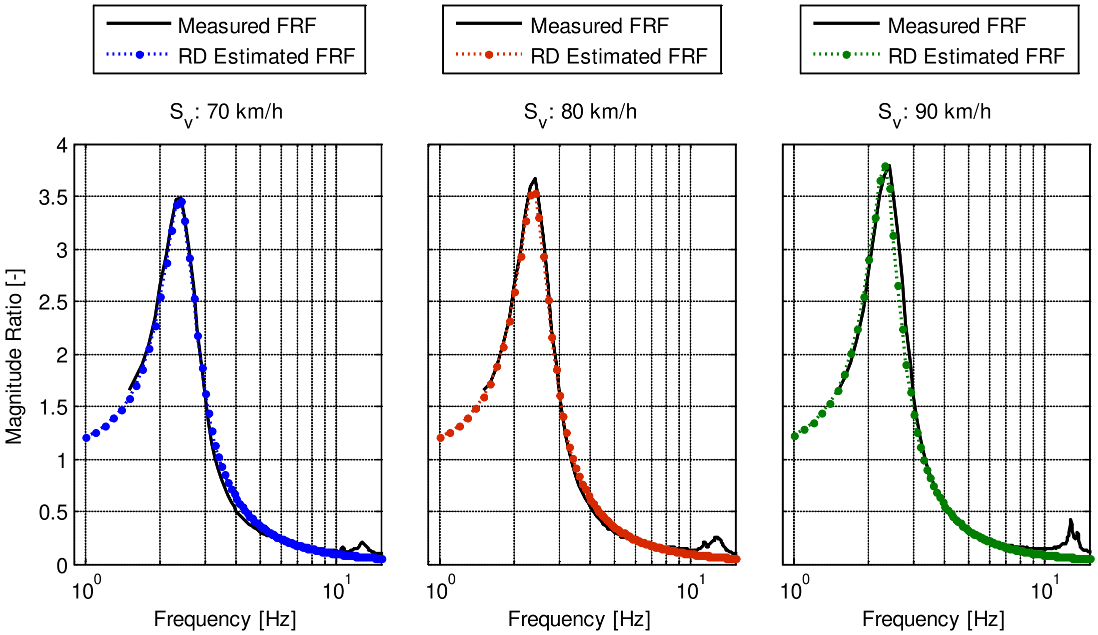

Figure 8-50: Measured and estimated (random decrement – Hilbert Domain) transmissibility FRFs of the SWEV-B (50 kg) travelling over route GB at nominally constant speeds of 70, 80 and 90 km/h.

From the figures, the random decrement estimated FRFs provide a good agreement with the in-service FRFs measured. The main drawback of the approach is that, in some cases, there is a slight overestimation in the damping ratio of the sprung mass mode. The technique is still limited to the estimation of only the sprung mass (body) of the vehicle's FRF, however given that the response of the following modes are relatively insignificant, it may be considered that the approach provides a good estimate of the idealised vehicle's FRF.

8.4.1.2 Estimation of the Frequency Response Function (Frequency Domain)

The second random decrement approach attempts to estimate the FRF directly from the FFT of the random decrement signature (and then scaling the obtained spectrum). From the development of the approach in Chapter 7, it was anticipated that the estimated FRF would be able to detect both the sprung and unsprung masses. While the unsprung mass was able to be detected using the measured in-service response data, it was always significantly overestimated in the magnitude ratio. A typical example of the overestimation of the unsprung mass is shown in *Figure 8-51* for the measured and estimated transmissibility FRFs of the SWEV-B (50 kg) travelling over route BG at operating speed of 70 km/h.

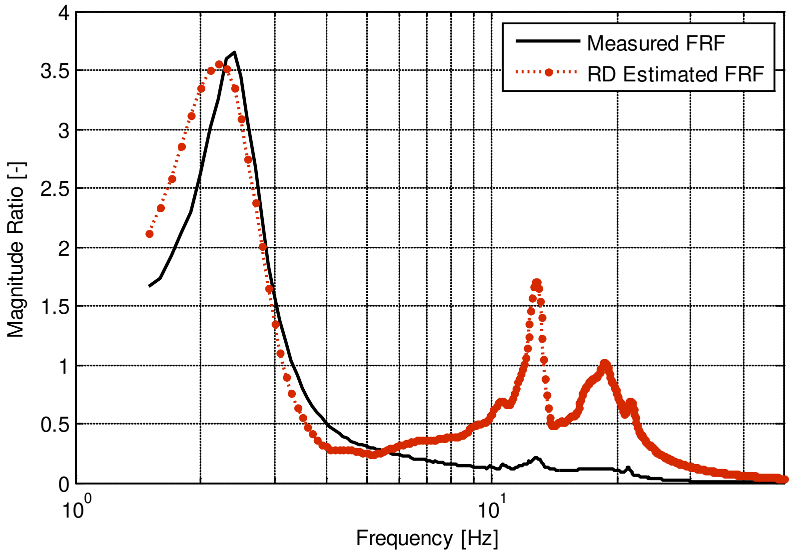

Figure 8-51: Measured and estimated transmissibility FRFs of the SWEV-B (50 kg) configuration travelling over route BG at a nominally constant operating speed of 70 km/h.

While the location of the unsprung mass resonant frequency is identified by the estimated FRF, the overestimation in the magnitude ratio is due to the non-white excitation applied to the vehicle (via the pavement elevation). Despite Ibrahim's (1980) conclusions that establishing the dynamic characteristics from the random decrement is unaffected by the shape of the PSD function used, the preliminary results suggested otherwise. Considering that the measured acceleration spectra of the pavement approaches violet noise, it is expected that the velocity spectra would approach white noise. The analysis could then be undertaken in the velocity domain, however measuring the velocity is difficult as it is a relative quantity. Whether measuring the velocity of the sprung mass (or integrating the acceleration response) to establish the random decrement signature is a sensible approach is considered to be beyond the scope of this research but may be addressed in the future.

Further work should be undertaken to investigate and characterise the effect of various types of PSD functions on the influence of multi-degree-of-freedom systems. The spectral shape of a longitudinal pavement elevation profile is such that the acceleration PSD function exhibits low energy at low frequency, increasing in power as the frequency increases (by a factor of approximately two). The overestimation is due to the increased excitation energy at high frequencies. Instead of using the two filters to allow for a band between 1 – 20 Hz, the focus for this second approach will now be solely on the estimation of the sprung mass mode and will use the same low-pass filter (5th order Butterworth with a cut-off of 8 Hz) that was used for the first approach.

In order to estimate the FRF of the SWEV, the random decrement signatures must first be established from the sprung mass acceleration vibration response data. Since only the sprung mass mode will be estimated, the only remaining difference between the random decrement signatures established for the first (Hilbert Domain) and second (Frequency Domain) approaches is the window size (5 s and 10 s, respectively). The established random decrement signatures from the SWEV-A for routes BG and GB are presented in *Figure 8-52*. The SWEV-B (50 kg) random decrement signatures obtained from routes BG and GB at various operating speeds are given in *Figure 8-53*.

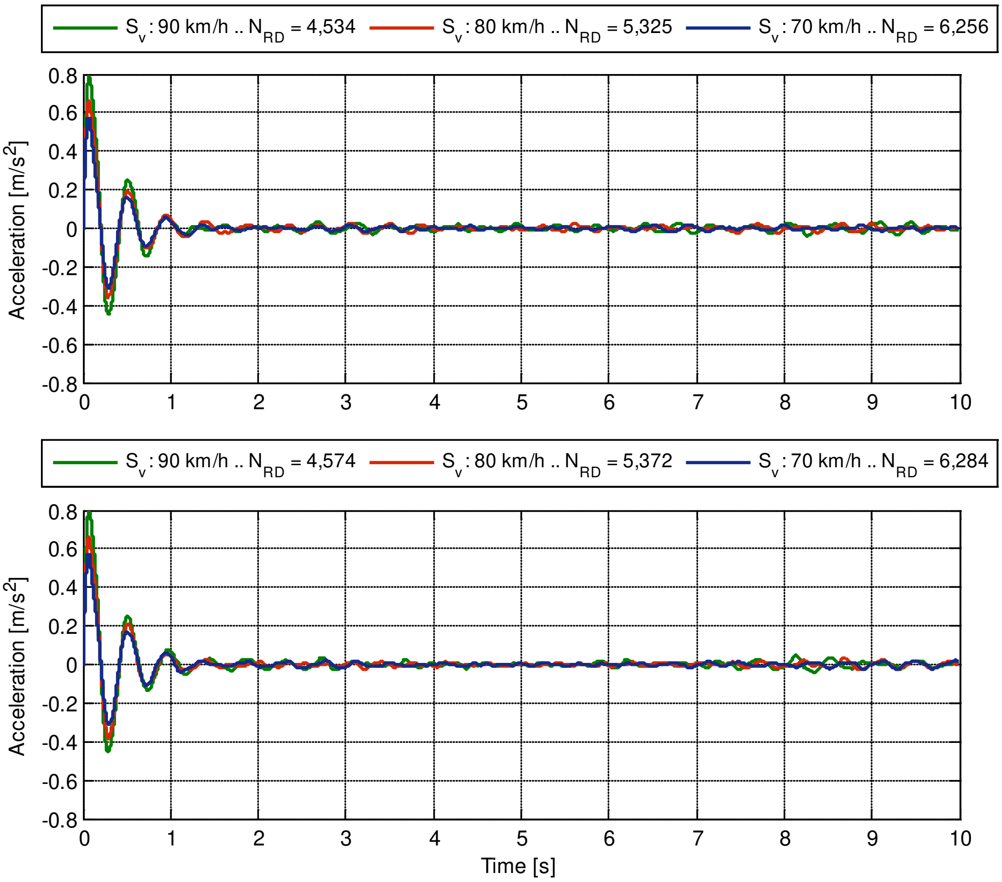

Figure 8-52: Established random decrement signatures from the sprung mass acceleration of the SWEV-A (50 kg) travelling over routes BG (top) and GB (bottom) for various nominally constant operating speeds.

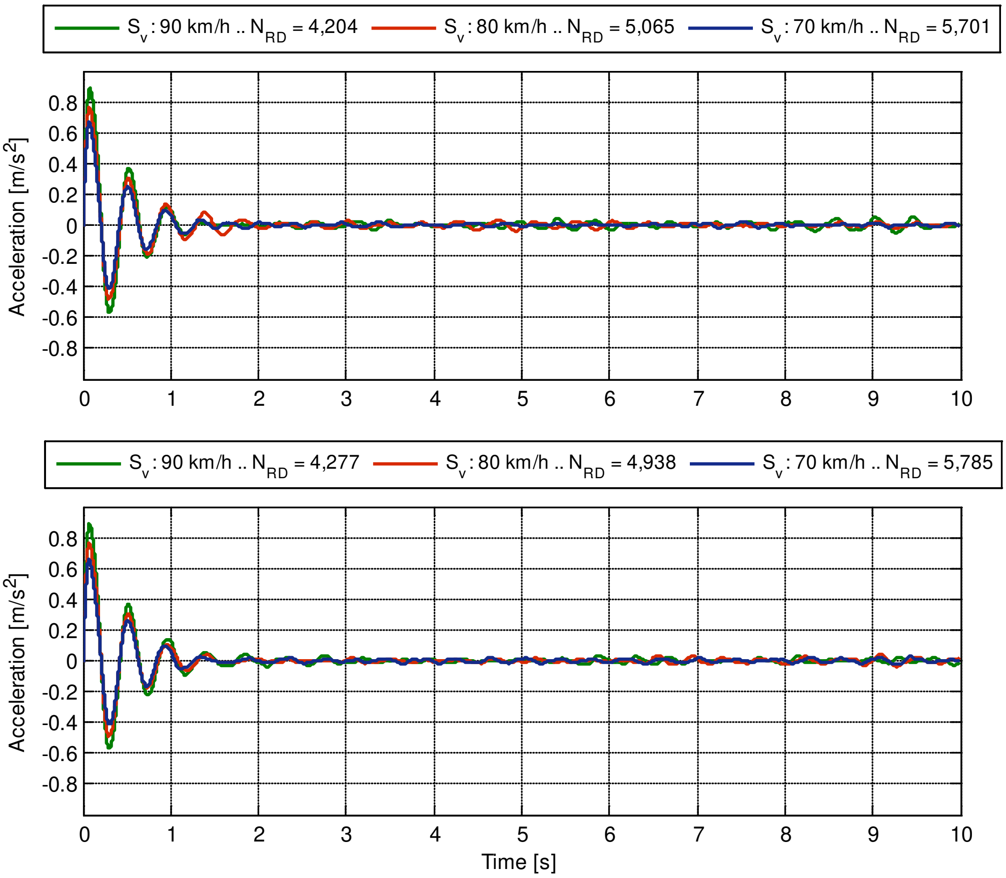

Figure 8-53: Established random decrement signatures from the sprung mass acceleration of the SWEV-B (50 kg) travelling over routes BG (top) and GB (bottom) for various nominally constant operating speeds.

The FFT was used to establish the magnitude spectrum from the obtained signatures, which is considered to be the unscaled FRF, which is then scaled to approach one at low frequency. The measured and estimated FRFs from route BG are presented in *Figure 8-54* for the SWEV-A and *Figure 8-55* for the SWEV-B at various nominally constant operating speeds. For the return route GB, the measured and estimated FRFs are given in *Figure 8-56* for the SWEV-A and *Figure 8-57* for the SWEV-B. From the estimated FRFs, there is an increased difference observed from the measured FRFs compared to the first approach (Hilbert Domain). In some cases, the estimated FRF is in good agreement with the measured FRF, in others there is noticeable frequency-shifting of the sprung mass mode characteristics. The process for establishing the FRF by scaling is far more straightforward, overall the estimated FRFs do not correspond as well as the first approach.

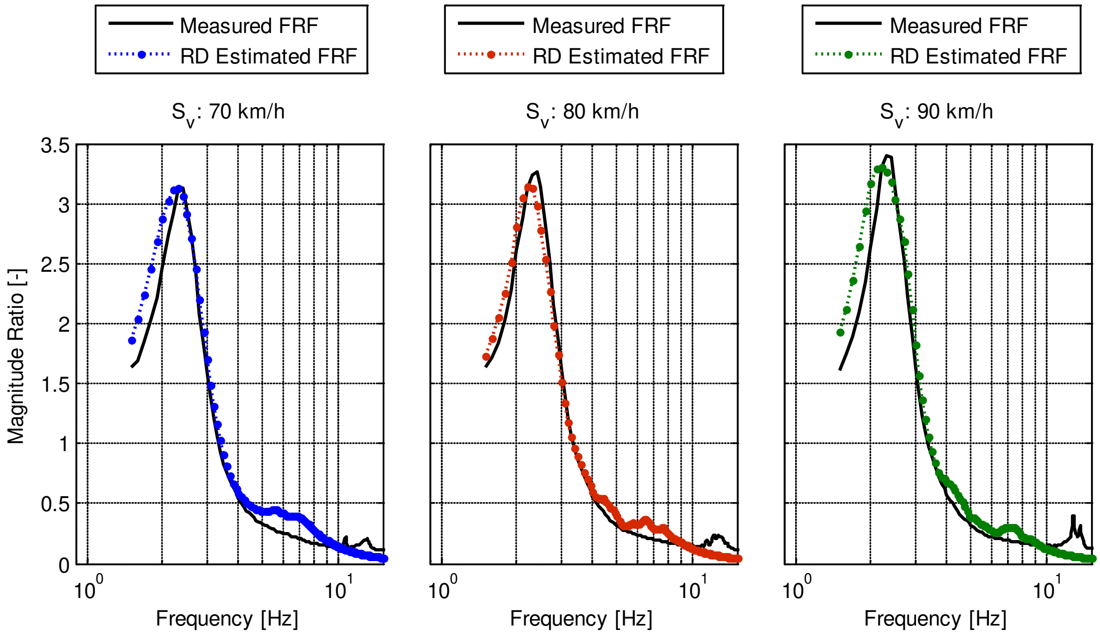

Figure 8-54: Measured and estimated (random decrement – Frequency Domain) transmissibility FRFs of the SWEV-A (50 kg) travelling over route BG at nominally constant operating speeds of 70, 80 and 90 km/h.

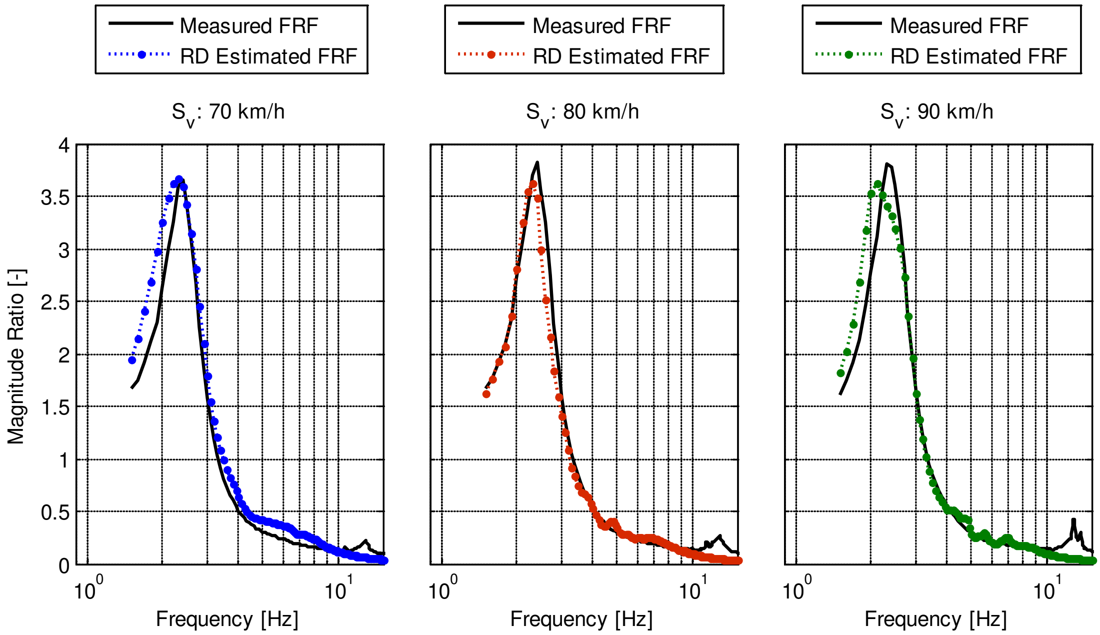

Figure 8-55: Measured and estimated (random decrement – Frequency Domain) transmissibility FRFs of the SWEV-B (50 kg) travelling over route BG at nominally constant operating speeds of 70, 80 and 90 km/h.

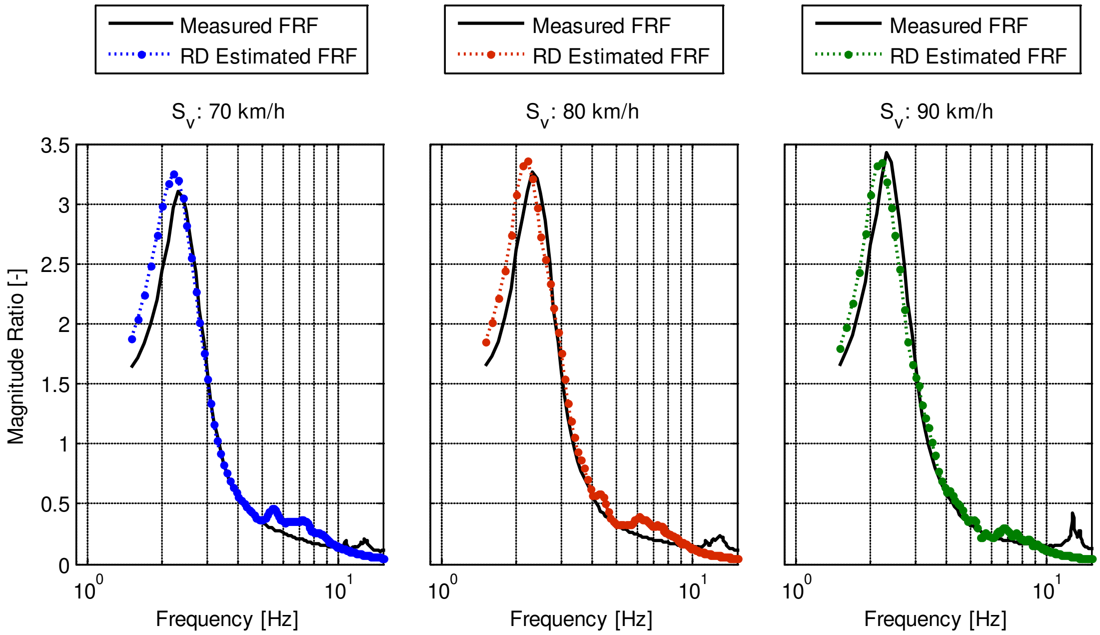

Figure 8-56: Measured and estimated (random decrement – Frequency Domain) transmissibility FRFs of the SWEV-A (50 kg) travelling over route GB at nominally constant operating speeds of 70, 80 and 90 km/h.

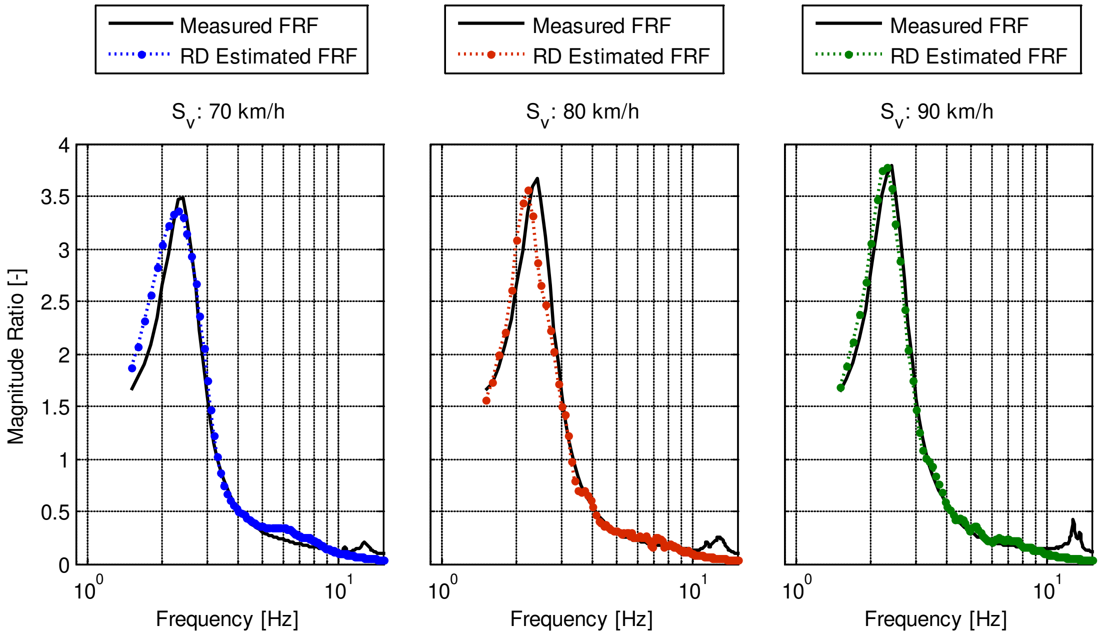

Figure 8-57: Measured and estimated (random decrement – Frequency Domain) transmissibility FRFs of the SWEV-B (50 kg) travelling over route GB at nominally constant operating speeds of 70, 80 and 90 km/h.

8.4.2 Routes SR and RS

The measured sprung mass acceleration response data of the SWEV-A and SWEV-B (50 kg) travelling over routes SR and RS were also analysed to obtain the random decrement signature using both approaches (Hilbert and Frequency Domains) to estimate the sprung mass dynamic characteristics.

8.4.2.1 Estimation of the Sprung Mass Dynamic Characteristics (Hilbert Domain)

The dynamic characteristics of the SWEV sprung mass mode travelling over routes SR and RS are estimated using the random decrement technique (Hilbert Domain). The established random decrement signatures from routes SR and RS are presented in *Figure 8-58* for the SWEV-A and *Figure 8-59* for the SWEV-B.

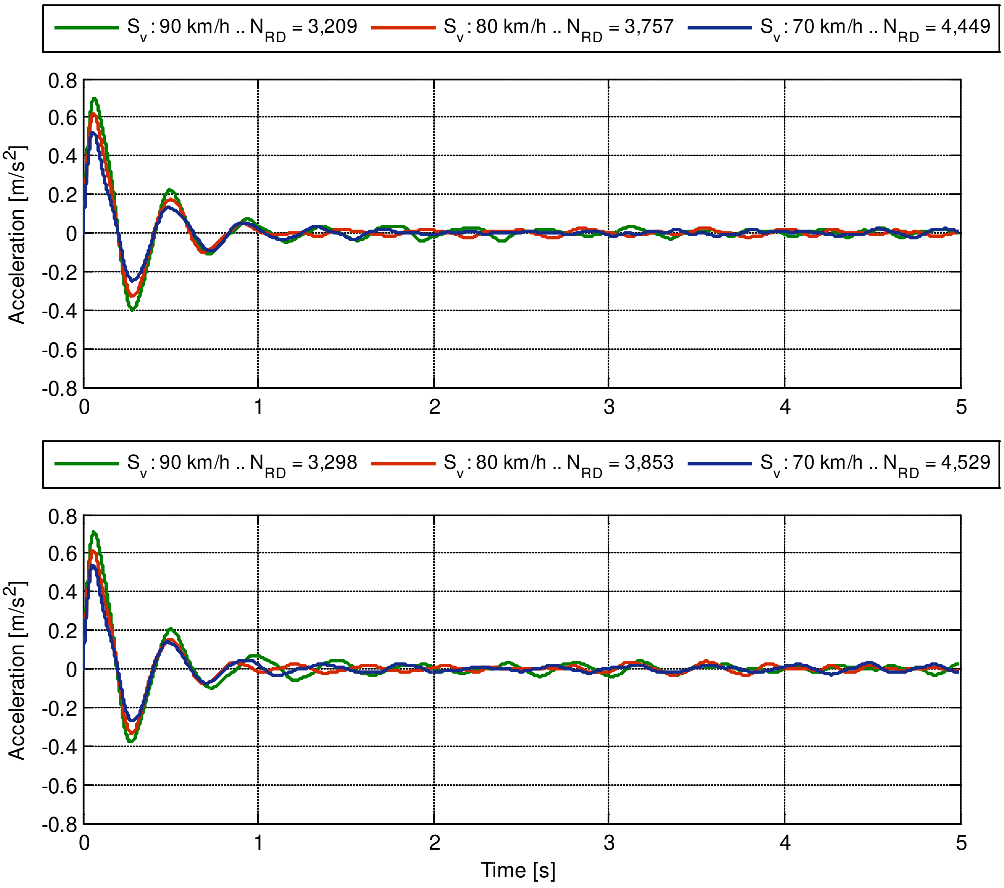

Figure 8-58: Established random decrement signatures from the sprung mass acceleration of the SWEV-A (50 kg) travelling over routes SR (top) and RS (bottom) for various nominally constant operating speeds.

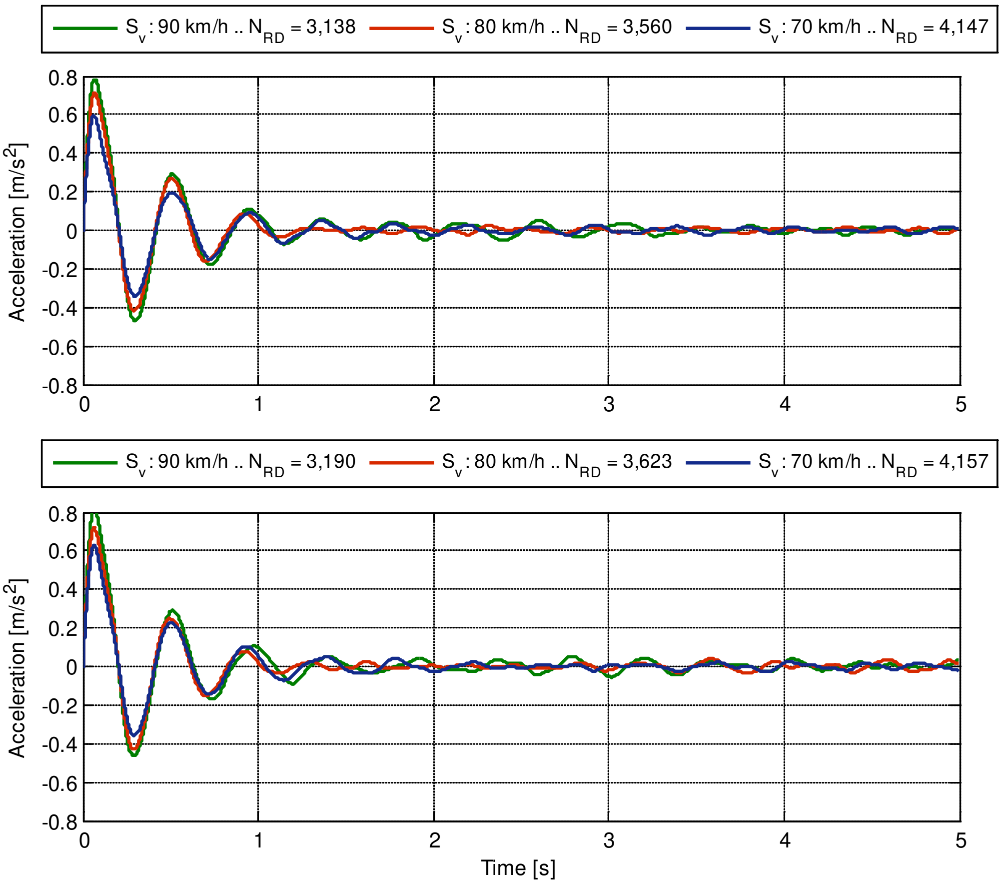

Figure 8-59: Established random decrement signatures from the sprung mass acceleration of the SWEV-B (50 kg) travelling over routes SR (top) and RS (bottom) for various nominally constant operating speeds.

The established random decrement signatures were analysed using the Hilbert Transform to estimate the dynamic characteristics of the SWEV sprung mass mode (damped natural frequency and damping ratio). A typical example of the unwrapped instantaneous phase and Hilbert envelope from the random decrement signature established for the SWEV-A travelling over route RS at 70 km/h is presented in *Figure 8-60*. *Table 8-Q* and *Table 8-R* present the measured and estimated dynamic characteristics of the sprung mass mode of the SWEV-A and SWEV-B over routes SR and RS, respectively.

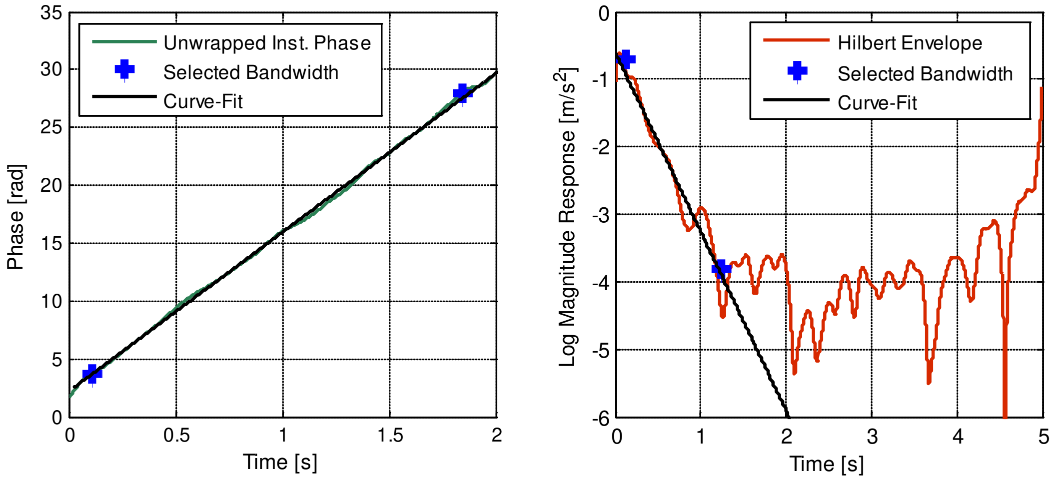

Figure 8-60: Typical example of the obtained unwrapped instantaneous phase (left) and the Hilbert envelope (right), shown for the SWEV-A (50 kg) travelling over route RS at a nominally constant operating speed of 70 km/h.

Table 8-Q: The average nominal operating speed and the estimated and measured dynamic characteristics of the SWEV-A (50 kg) sprung mass mode travelling over routes SR and RS.

	FRF Curve-Fit		**Random Decrement**	
Nominal Operating Speed [km/h]	**Natural Frequency f_{sn} [Hz]**	**Damping Ratio ζ_s [-]**	**Natural Frequency f_{sn} [Hz]**	**Damping Ratio ζ_s [-]**
Route SR				
70	2.49	0.196	2.49	0.195
80	2.49	0.183	2.47	0.182
90	2.47	0.169	2.48	0.171
Route RS				
70	2.49	0.187	2.46	0.186
80	2.52	0.179	2.53	0.182
90	2.49	0.168	2.46	0.162

Table 8-R: The average nominal operating speed and the estimated and measured dynamic characteristics of the SWEV-B (50 kg) sprung mass mode travelling over routes SR and RS.

	FRF Curve-Fit		**Random Decrement**	
Nominal Operating Speed [km/h]	**Natural Frequency f_{sn} [Hz]**	**Damping Ratio ζ_s [-]**	**Natural Frequency f_{sn} [Hz]**	**Damping Ratio ζ_s [-]**
Route SR				
70	2.46	0.162	2.47	0.169
80	2.47	0.148	2.47	0.153
90	2.46	0.144	2.44	0.149
Route RS				
70	2.46	0.151	2.45	0.149
80	2.49	0.144	2.46	0.149
90	2.46	0.140	2.43	0.137

From the measured and estimated dynamic characteristics of the SWEV-A there is some slight variation between the sprung mass natural frequency and damping ratio, however the differences are quite small. The estimated dynamic characteristics of the SWEV-B are all fairly consistent with the measured values. The estimated dynamic characteristics of the sprung mass are combined with the SDoF transmissibility FRF model (Equation 3-53). The measured and estimated FRFs for route SR are presented in *Figure 8-61* for the SWEV-A and *Figure 8-62* for the SWEV-B. The measured and estimated FRFs for the return route RS are presented in *Figure 8-63* and *Figure 8-64* for the SWEV-A and SWEV-B, respectively. Overall, there is good agreement between the measured and estimated FRFs for both configurations of the SWEV. There are some cases, such as the SWEV-A travelling over route SR at an operating speed of 80 km/h, where the estimated resonant frequency is slightly shifted.

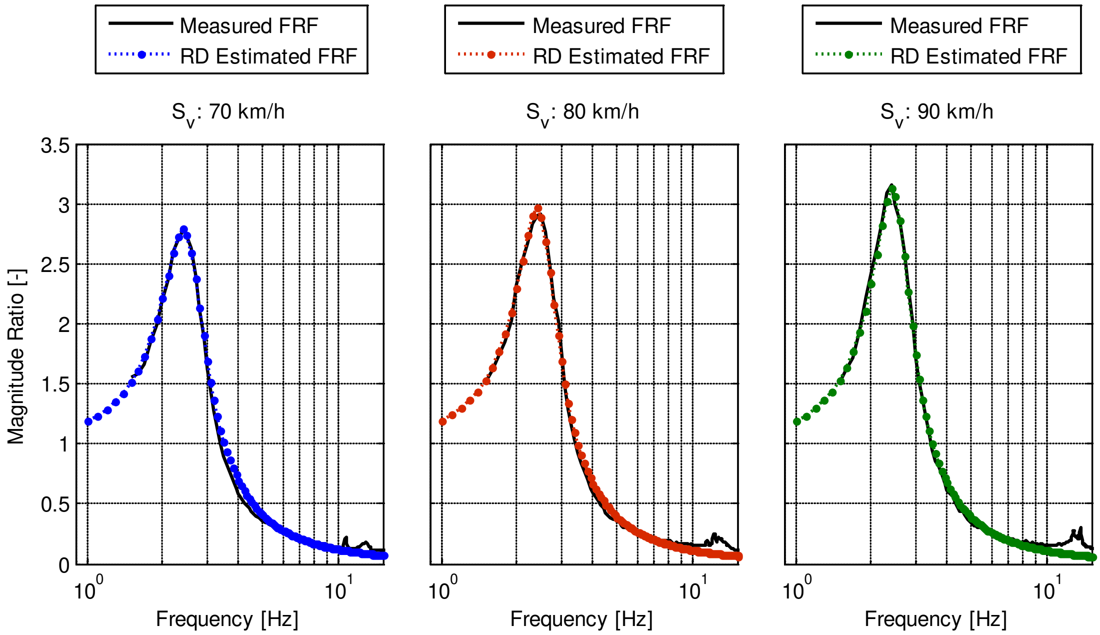

Figure 8-61: Measured and estimated (random decrement – Hilbert Domain) transmissibility FRFs of the SWEV-A (50 kg) travelling over route SR at nominally constant operating speeds of 70, 80 and 90 km/h.

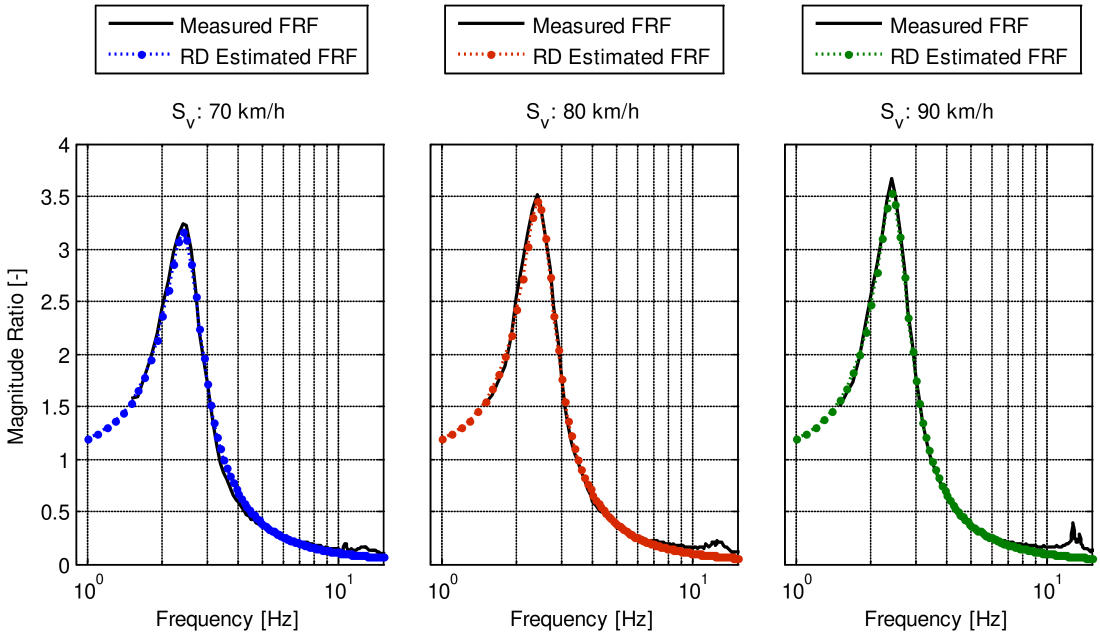

Figure 8-62: Measured and estimated (random decrement – Hilbert Domain) transmissibility FRFs of the SWEV-B (50 kg) travelling over route SR at nominally constant operating speeds of 70, 80 and 90 km/h.

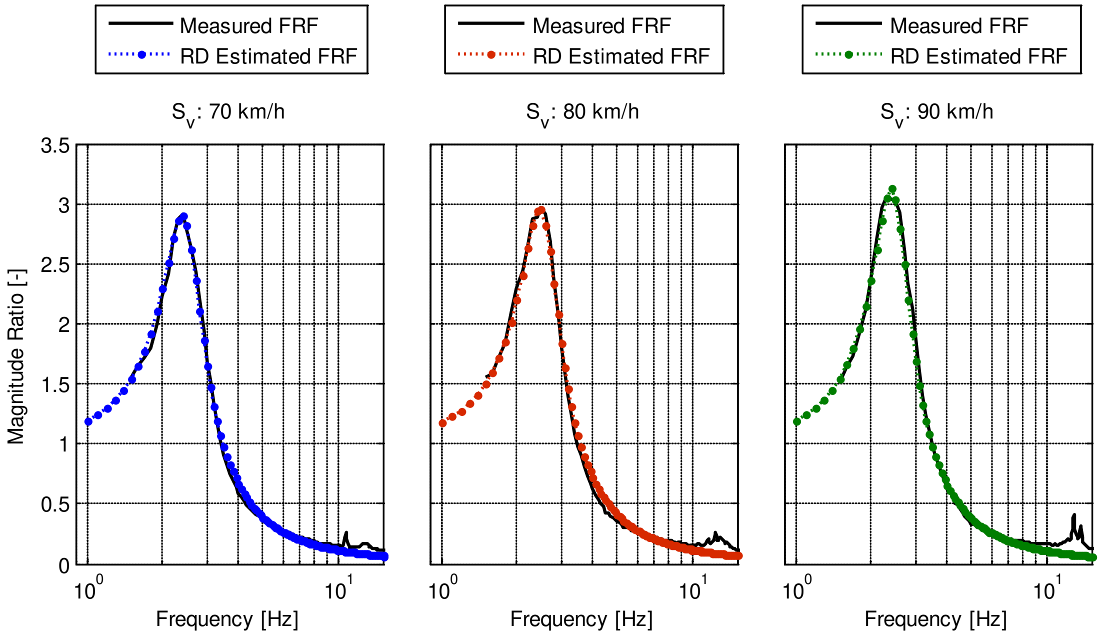

Figure 8-63: Measured and estimated (random decrement – Hilbert Domain) transmissibility FRFs of the SWEV-A (50 kg) travelling over route RS at nominally constant operating speeds of 70, 80 and 90 km/h.

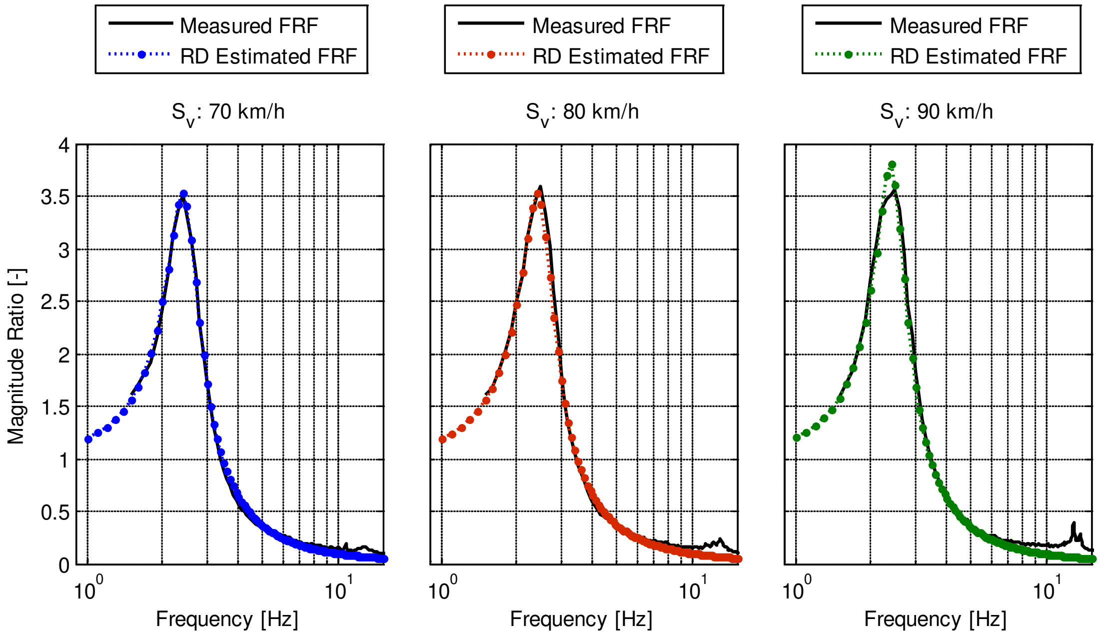

Figure 8-64: Measured and estimated (random decrement – Hilbert Domain) transmissibility FRFs of the SWEV-B (50 kg) travelling over route RS at nominally constant operating speeds of 70, 80 and 90 km/h.

8.4.2.2 Estimation of the Frequency Response Function (Frequency Domain)

The second random decrement approach (Frequency Domain) to estimate the FRF was used to analyse the measured response data for both configurations of the SWEV travelling over routes SR and RS. The random decrement signatures established for each of the experimental runs over routes SR and RS are presented in *Figure 8-65* for the SWEV-A and *Figure 8-66* for the SWEV-B.

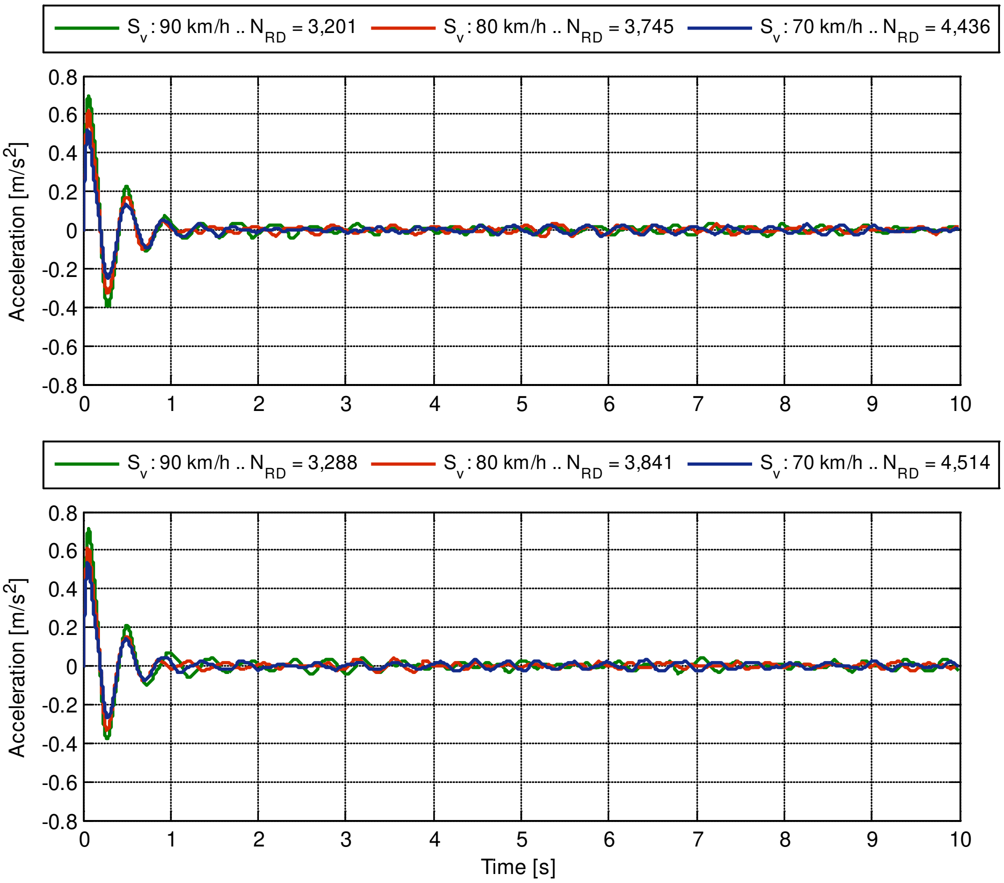

Figure 8-65: Established random decrement signatures from the sprung mass acceleration of the SWEV-A (50 kg) travelling over routes SR (top) and RS (bottom) for various nominally constant operating speeds.

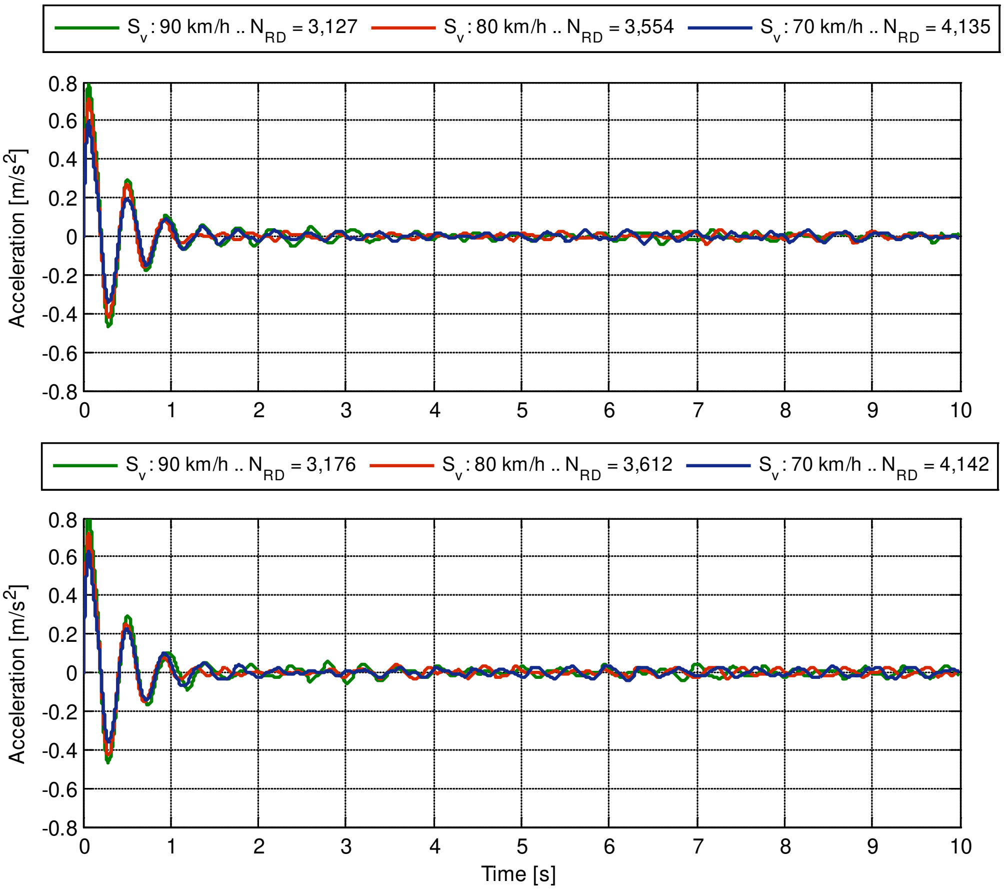

Figure 8-66: Established random decrement signatures from the sprung mass acceleration of the SWEV-B (50 kg) travelling over routes SR (top) and RS (bottom) for various nominally constant operating speeds.

The random decrement signatures were analysed using the FFT to establish an estimate of the unscaled FRF, which were then scaled to approach one at low frequency. The measured and estimated FRFs from route SR are presented in *Figure 8-67* for the SWEV-A and *Figure 8-68* for the SWEV-B. For the return route RS, the measured and estimated (random decrement) FRFs are presented in *Figure 8-69* and *Figure 8-70* for the SWEV-A and SWEV-B, respectively. The estimated FRFs are all fairly consistent with the measured FRFs, with some minor variation in the natural frequency and level of damping. It was also observed that some of the peaks around the resonant frequency for the SWEV-A estimated FRFs are wider than the measured FRF. This was also observed in the SWEV-B estimated FRFs, but is not as significant.

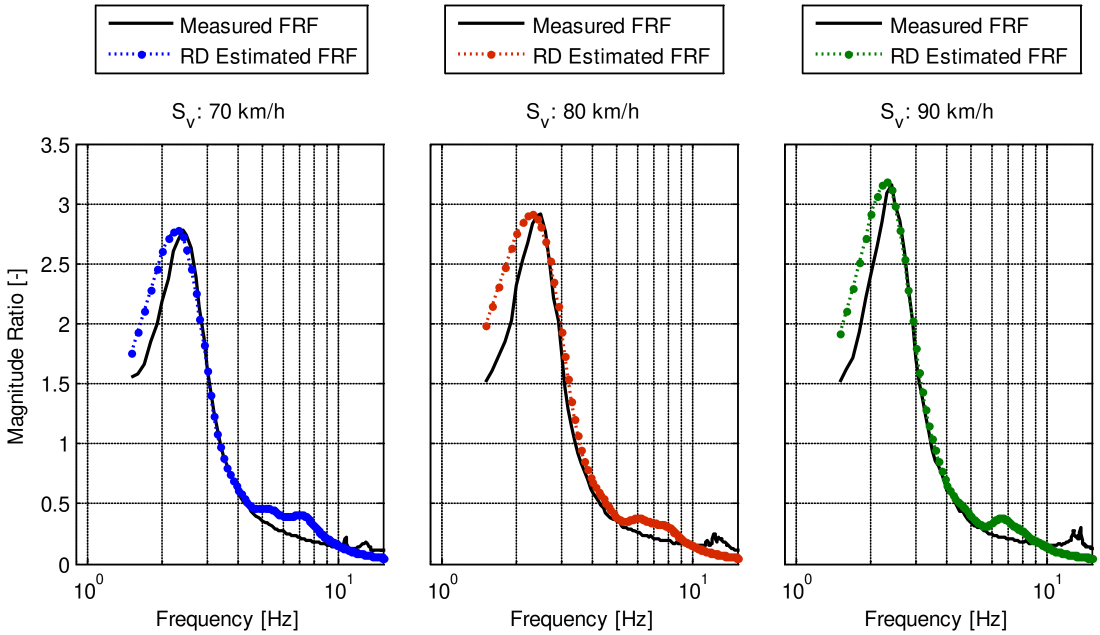

Figure 8-67: Measured and estimated (random decrement – Frequency Domain) transmissibility FRFs of the SWEV-A (50 kg) travelling over route SR at nominally constant operating speeds of 70, 80 and 90 km/h.

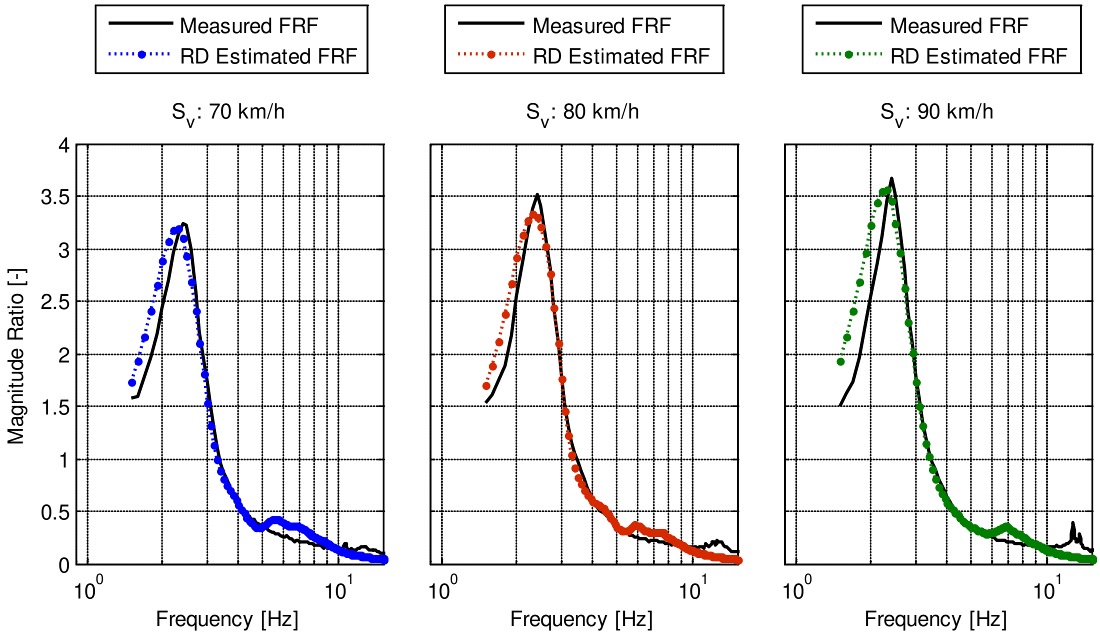

Figure 8-68: Measured and estimated (random decrement – Frequency Domain) transmissibility FRFs of the SWEV-B (50 kg) travelling over route SR at nominally constant operating speeds of 70, 80 and 90 km/h.

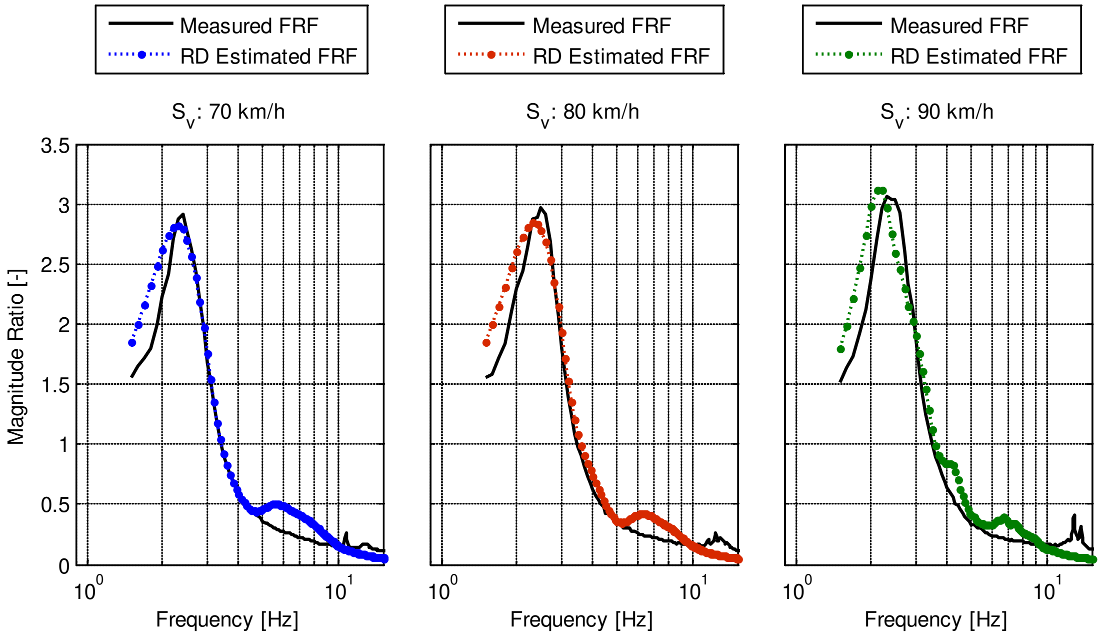

Figure 8-69: Measured and estimated (random decrement – Frequency Domain) transmissibility FRFs of the SWEV-A (50 kg) travelling over route RS at nominally constant operating speeds of 70, 80 and 90 km/h.

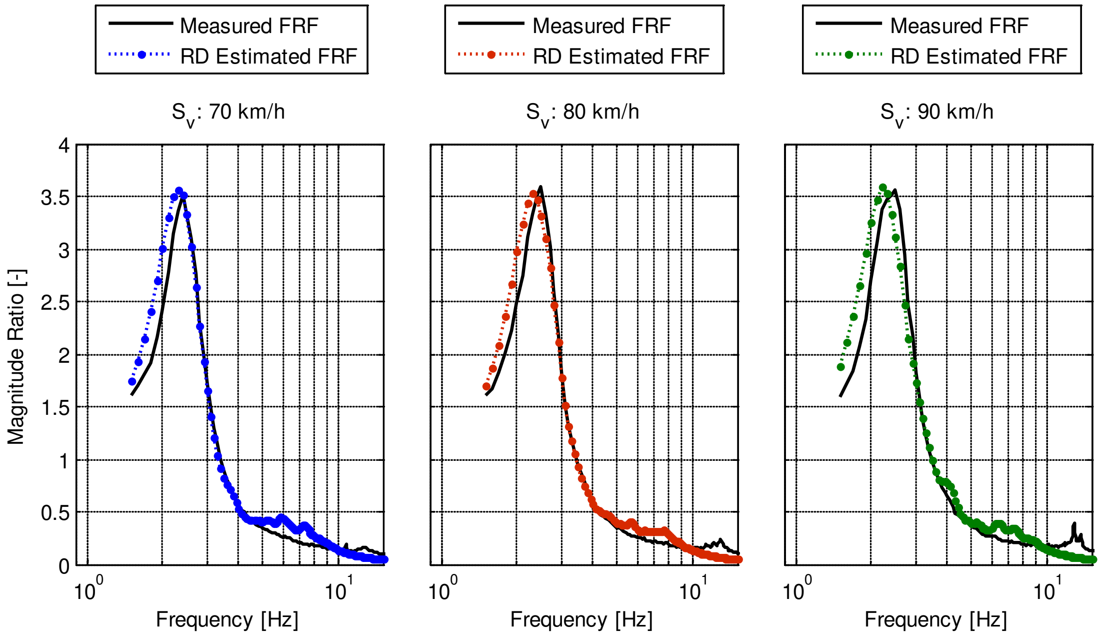

Figure 8-70: Measured and estimated (random decrement – Frequency Domain) transmissibility FRFs of the SWEV-B (50 kg) travelling over route RS at nominally constant operating speeds of 70, 80 and 90 km/h.

8.4.3 Comparison of Random Decrement Approaches

Two approaches based on the random decrement technique were used to estimate the transmissibility FRF of the two configurations of the SWEV travelling over two different roads (four routes in total). When comparing the two approaches, there are two considerations to be taken into account. The first factor to consider is the subjectivity of estimating the dynamic characteristics. It is straightforward to scale the magnitude spectrum (unscaled FRF) using the second approach compared to the first approach, which requires careful consideration when selecting the bandwidth for estimation of the damped natural frequency and damping ratio using the unwrapped instantaneous phase and Hilbert envelope, respectively. The second consideration is the agreement between the measured and estimated FRFs. The estimated FRFs using the first approach were found to agree better with the measured FRFs than the second approach. While both approaches could be used to estimate the FRF reasonably well, care must be exercised when selecting the most appropriate method. Finally, one drawback of both the random decrement approaches is that they are limited to the sprung mass mode, requiring further work to compensate for the unsprung mass mode.

8.5 INFLUENCE OF RECORD LENGTH

As outlined the hypothesis (Chapter 4), the question arises of how long a vibration record, or pavement length, is required in order to achieve a sufficiently accurate estimate of a vehicle’s FRF. An investigation was undertaken to provide some initial insights into the minimum pavement length required to establish sufficient estimates of the response PSD functions and the random decrement signatures of the SWEV. The measured response spectra and the established random decrement signatures were evaluated against the entire road length response spectra and random decrement signatures. For the in-service experiments, one consideration was to select a sufficiently long road in order to allow the pavement to converge towards the ISO 8608 (1995) spectral model. For the in-service experiments described above, it was anticipated that the length of the first road (routes BG and GB) would be long enough to allow for convergence to occur. The characteristics of the pavement elevation profile also play an important role and are dependent on the stationarity of the pavement under investigation. Nonstationarity of a pavement is manifested in two ways; the first is a change in the level of roughness experienced (rms) and the second is a change in the frequency structure (shape).

Investigating the length of road required is subject to two considerations. The first consideration is the selection of the length of the road and has already been discussed. The second consideration is where to begin the measurement along the road. For this, it was assumed that the road was circular, where the beginning and end of each route are at the same position. To undertake this investigation, various pavement length ratios were selected and a Monte Carlo simulation was employed to randomly determine the starting point of the measurement.

The statistical distribution used for the Monte Carlo simulation was a uniform distribution in order to provide equal opportunity to start anywhere along the road. The pavement length investigation was undertaken using the SWEV-B (50 kg) configuration travelling over routes BG and SR at nominally constant operating speeds of 70, 80 and 90 km/h. The various pavement length ratios and the actual section lengths for both routes investigated using the Monte Carlo simulation are presented in *Table 8-S*.

Table 8-S: Pavement length ratios and actual lengths of routes BG and SR.

Pavement Length Ratio [-]	**Actual Pavement Length [km]**	
	Route BG	**Route SR**
1	40	26
1/2	20	13
1/4	10	6.5
1/8	5	3.25
1/16	2.5	1.625
1/32	1.25	0.8125

To evaluate various lengths of vibration records, some authors have used the rms ratio or the rms error. The principal shortcoming of this approach is that it does not take into account any frequency shifting, or distortion of the frequency response. The Mean Squared Error (MSE) is used to evaluate the length of pavement as it takes into account any frequency shifting. The average and standard deviation of the MSE for the 1,000 iterations are calculated using the response spectrum or random decrement signature established from the full length of the road. A preliminary investigation into the Monte Carlo sample size found that it has negligible impact on the estimates. The only cost incurred by increasing the estimates is additional time required to perform the simulation, and so a sample size of 1,000 was used for completeness.

8.5.1 Response Spectra

The results of the Monte Carlo simulation to evaluate the response spectra in comparison with the spectrum established from the full length of the pavement are presented herein. The comparisons were made between each of the iterations and the full length spectra around the sprung mass mode (frequency band of 1 – 5 Hz). The average and standard deviation of the MSE of the spectra for various pavement length ratios are presented in *Table 8-T* for the SWEV-B travelling at three nominally constant operating speeds over route BG. A typical example of the average MSE (± 1σ) of the established response spectra for the SWEV-B travelling over route BG is presented in *Figure 8-71* for an operating speed of 70 km/h. The average MSE of the established response spectra for the SWEV-B travelling over route BG is presented in *Figure 8-72*, for the three operating speeds of 70, 80 and 90 km/h.

Table 8-T: The average and standard deviation of the MSE of the response spectra for various pavement lengths investigated using the Monte Carlo simulation (1,000 iterations) for the SWEV-B travelling at various operating speeds over route BG.

Pavement Length Ratio [-]	**Average MSE $[(m/s^2)^4/Hz^2]$**			**Standard Deviation MSE $[(m/s^2)^4/Hz^2]$**		
	70 km/h	**80 km/h**	**90 km/h**	**70 km/h**	**80 km/h**	**90 km/h**
1/2	0.0019	0.0064	0.0067	0.0013	0.0042	0.0042
1/4	0.0030	0.0128	0.0195	0.0023	0.0260	0.0302
1/8	0.0074	0.0316	0.0426	0.0115	0.0810	0.0795
1/16	0.0153	0.0579	0.0662	0.0243	0.1824	0.1299
1/32	0.0336	0.0846	0.1299	0.0847	0.3294	0.3128

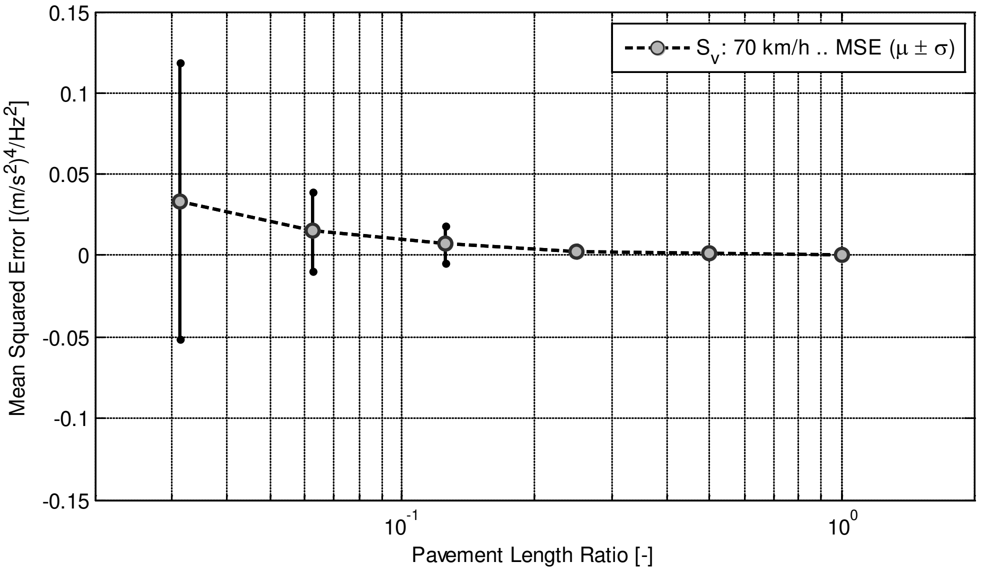

Figure 8-71: Typical example of the average MSE (± 1σ) of the response spectra for various pavement length ratios using a Monte Carlo simulation (1,000 iterations) for the SWEV-B travelling over route BG at 70 km/h.

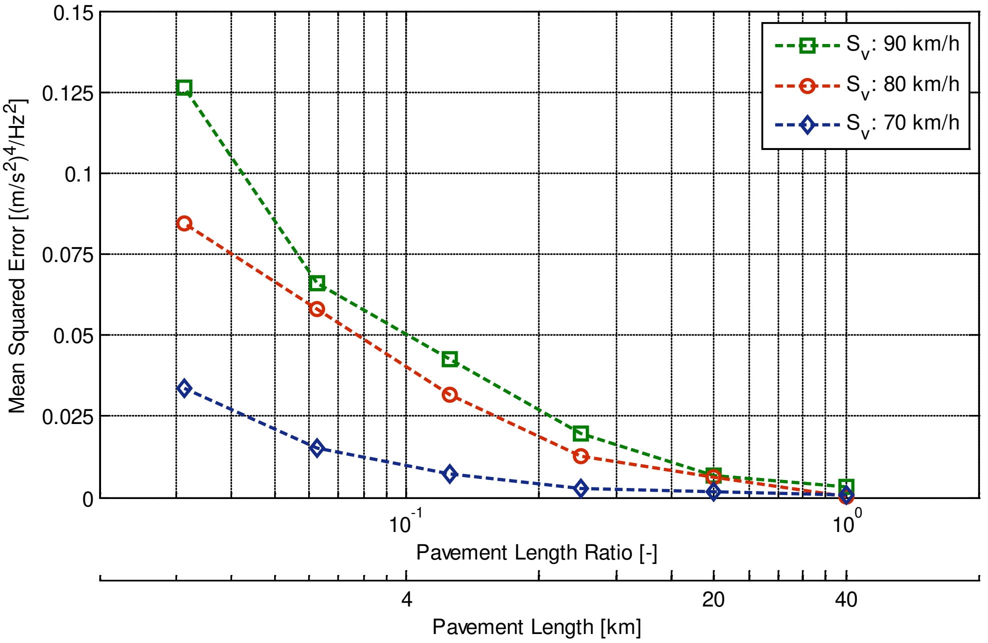

Figure 8-72: The average MSE of the response spectra for various pavement length ratios using a Monte Carlo simulation (1,000 iterations) for the SWEV-B travelling over route BG at 70, 80 and 90 km/h.

From the results, both the average and standard deviation of the MSE increase as the pavement length is decreased. It is also dependent on the operating speed of the vehicle, since for a given road length the duration of the measurement decreases for an increased operating speed. For any of the three operating speeds selected, a sufficient estimate of the response spectrum is obtained for a pavement length of approximately 10 km.

The Monte Carlo simulation was repeated using the measured data from the SWEV-B travelling over route SR. *Table 8-U* presents the average and standard deviation of the MSE of the response spectra for the pavement length ratios. The average MSE of the established response spectra for the SWEV-B travelling over route SR at 70, 80 and 90 km/h is presented in *Figure 8-73*. A pavement length of 10 km provides an adequate estimate of the response spectrum regardless of the operating speed.

Table 8-U: The average and standard deviation of the MSE of the response spectra for various pavement lengths investigated using the Monte Carlo simulation (1,000 iterations) for the SWEV-B travelling at various operating speeds over route SR.

Pavement Length Ratio [-]	Average MSE $[(m/s^2)^4/Hz^2]$			Standard Deviation MSE $[(m/s^2)^4/Hz^2]$		
	70 km/h	80 km/h	90 km/h	70 km/h	80 km/h	90 km/h
1/2	0.0040	0.0158	0.0633	0.0022	0.0083	0.0440
1/4	0.0144	0.0384	0.1825	0.0116	0.0368	0.2418
1/8	0.0255	0.0782	0.3155	0.0248	0.1177	0.6188
1/16	0.0401	0.1228	0.3493	0.0590	0.2215	0.9768
1/32	0.0759	0.1607	0.3795	0.1627	0.4867	1.6879

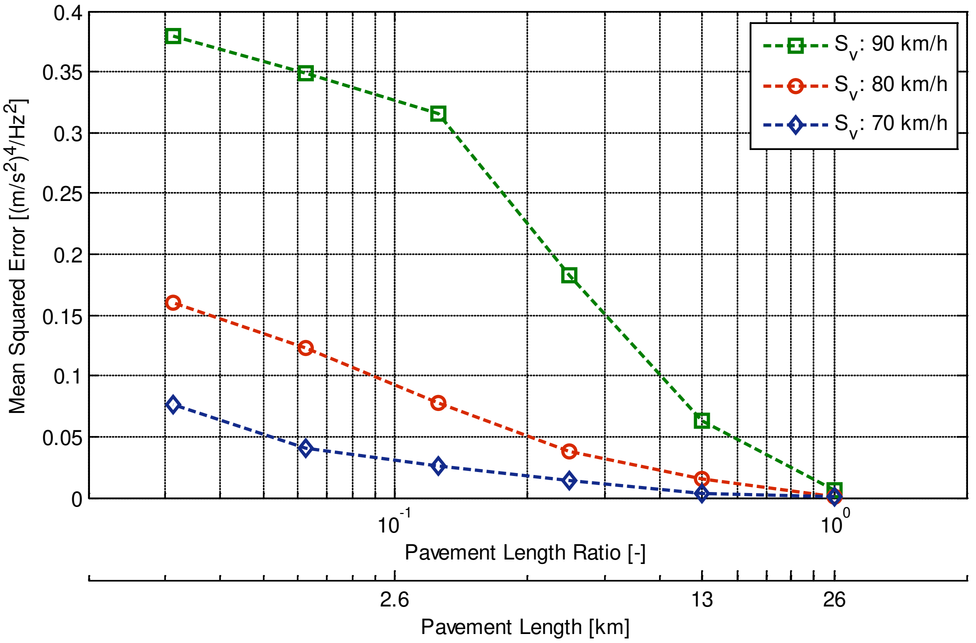

Figure 8-73: The average MSE of the response spectra for various pavement length ratios using a Monte Carlo simulation (1,000 iterations) for the SWEV-B travelling over route SR at 70, 80 and 90 km/h.

8.5.2 Random Decrement Signatures

The evaluation of the established random decrement signatures using a Monte Carlo simulation for various pavement lengths is presented herein. The average and standard deviation of the MSE of the random decrement signatures established from the Monte Carlo simulation for the SWEV-B over route BG are listed in *Table 8-V*. A typical example of the average MSE (± 1σ) of the established random decrement signatures of the SWEV-B travelling at 70 km/h over route BG is presented in *Figure 8-74*. The average MSE (± 1σ) of the random decrement signatures for the SWEV-B travelling over route SR is presented in *Figure 8-75* for the three operating speeds of 70, 80 and 90 km/h. Similar to the evaluation of the response spectra, adequate random decrement signatures are established for a pavement length of around 10 km, for any of the operating speeds investigated. For road lengths shorter than 10 km, the average and standard deviation of the MSE increase significantly.

Table 8-V: The average and standard deviation of the MSE of the random decrement signatures for various pavement lengths investigated using the Monte Carlo simulation (1,000 iterations) for the SWEV-B travelling at various operating speeds over route BG.

Pavement	**Average MSE $[(m/s^2)^2]$**			**Standard Deviation MSE $[(m/s^2)^2]$**		
Length Ratio [-]	**70 km/h**	**80 km/h**	**90 km/h**	**70 km/h**	**80 km/h**	**90 km/h**
1/2	0.0004	0.0005	0.0005	0.0001	0.0001	0.0001
1/4	0.0007	0.0011	0.0014	0.0002	0.0008	0.0010
1/8	0.0014	0.0026	0.0023	0.0005	0.0023	0.0025
1/16	0.0029	0.0052	0.0063	0.0012	0.0044	0.0043
1/32	0.0060	0.0091	0.0117	0.0036	0.0071	0.0081

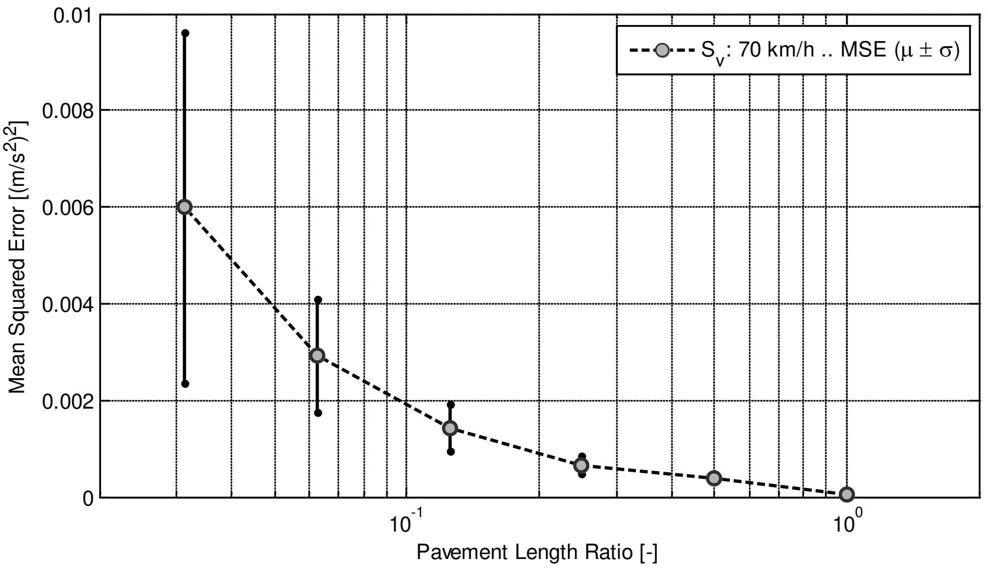

Figure 8-74: A typical example of the average MSE (± 1σ) of the random decrement signatures obtained for various pavement length ratios using a Monte Carlo simulation (1,000 iterations) for the SWEV-B travelling over route BG at 70 km/h.

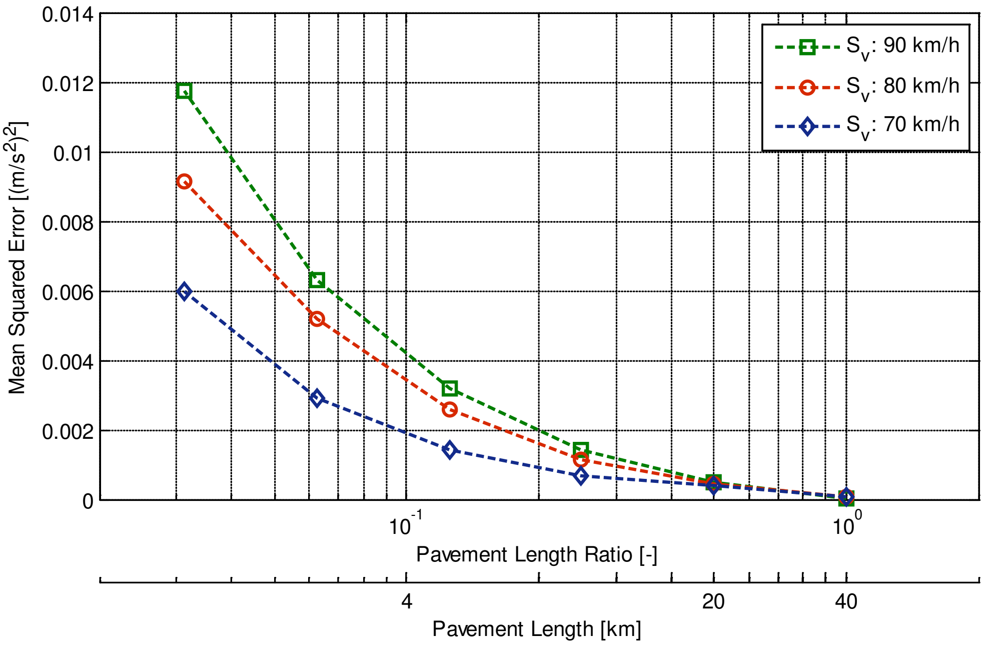

Figure 8-75: The average MSE of the random decrement signatures for various pavement length ratios using a Monte Carlo simulation (1,000 iterations) for the SWEV-B travelling over route BG at 70, 80 and 90 km/h.

The Monte Carlo simulation was repeated for the SWEV-B travelling over route SR. *Table 8-W* presents the values of the average and standard deviation of the MSE of the random decrement signatures for various pavement length ratios. The average MSE of the established random decrement signatures for the SWEV-B configuration travelling over route SR at 70, 80 and 90 km/h are presented in *Figure 8-76*.

The results indicate that a pavement length of 10 km establishes a reasonable estimate of the random decrement signature for all operating speeds investigated. One of the main requirements for the development of an approach to estimate the dynamic characteristics using only response data is for the approach to be practical. As an initial investigation it was found that, provided the road is spectrally rich and relatively stationary, a sufficient estimate of the response spectrum or the random decrement signature may be obtained for a minimum pavement length of 10 km.

Table 8-W: The average and standard deviation of the MSE of the random decrement signatures for various pavement lengths investigated using the Monte Carlo simulation (1,000 iterations) for the SWEV-B travelling at various operating speeds over route SR.

Pavement Length Ratio [-]	**Average MSE $[(m/s^2)^2]$** 70 km/h	80 km/h	90 km/h	**Standard Deviation MSE $[(m/s^2)^2]$** 70 km/h	80 km/h	90 km/h
1/2	0.0004	0.0008	0.0012	0.0002	0.0004	0.0004
1/4	0.0011	0.0021	0.0035	0.0005	0.0010	0.0021
1/8	0.0023	0.0039	0.0073	0.0012	0.0024	0.0072
1/16	0.0041	0.0070	0.0134	0.0026	0.0056	0.0186
1/32	0.0073	0.0112	0.0181	0.0063	0.0107	0.0274

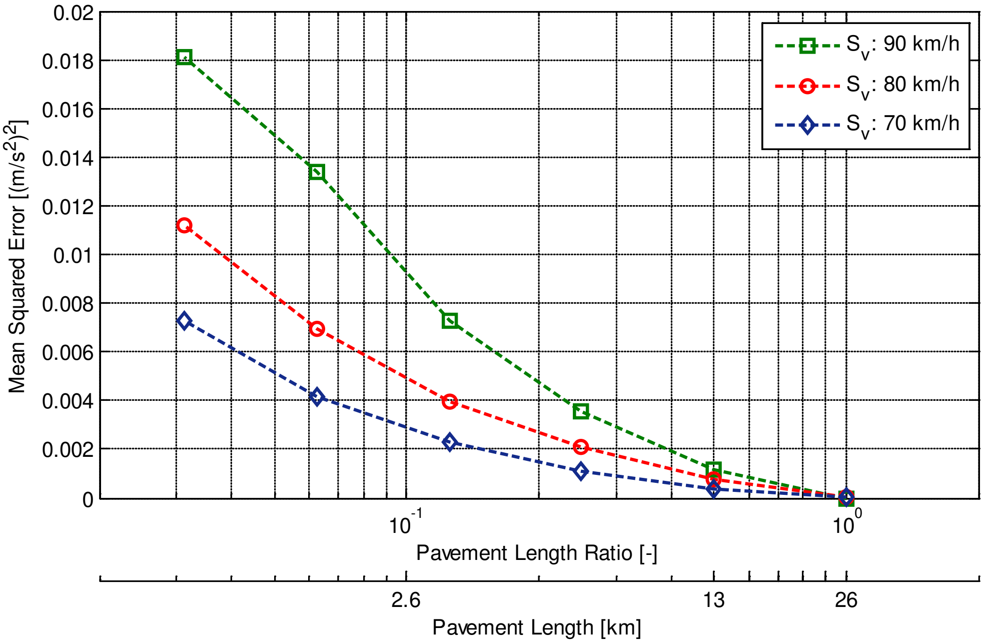

Figure 8-76: The average MSE of the random decrement signatures for various pavement length ratios using a Monte Carlo simulation (1,000 iterations) for the SWEV-B travelling over route SR at 70, 80 and 90 km/h.

8.6 REAL VEHICLE IN-SERVICE EXPERIMENTS

Having established the random decrement technique to estimate the sprung mass mode of the SWEV, the final section of this Chapter describes a series of in-service experiments undertaken using actual transport vehicles. Two transport vehicles were instrumented and driven across two different routes at various nominally constant operating speeds whilst simultaneously measuring the vertical acceleration vibration response. Only the first random decrement approach (Hilbert Domain) was used to analyse the response data. The use of real vehicles introduces numerous complexities into the interaction, such as multiple sources of excitation (via the wheels) and intricate suspension systems. To provide a comparison with the dynamic characteristics estimated using in-service response data, the vehicles were subjected to the CEU (1996) ramp test.

8.6.1 Vehicle Configurations

Two vehicles were selected to undertake the in-service experiments; a light truck and a heavy truck, shown in *Figure 8-77* and *Figure 8-78*, respectively. A list of the specifications of the two vehicles is presented in *Table 8-X*. All vehicles were mounted with a sensor at the rear to measure the vertical acceleration vibration response of the sprung mass (body). The light and heavy trucks were both instrumented with a Lansmont 9X30 SAVER unit to measure the vertical acceleration response of the sprung mass and operating speed (using a GPS sensor). As an example, the location of the vibration sensor in the heavy truck is shown in *Figure 8-79*.

Figure 8-77: Photographs of the side (left) and front (right) of the light truck used for the in-service experiments (Mercedes Sprinter 511 CDI 109CV).

Figure 8-78: Photographs of the side (left) and front (right) of the heavy truck used for the in-service experiments (Renault 180 Midlum).

Table 8-X: The specifications of the vehicles used to undertake the in-service experiments.

Light Truck	
Vehicle Type	Mercedes Sprinter 511 CDI 109CV
Tare / Max Gross Vehicle Mass	2,650 kg / 3,500 kg
Gross Vehicle Mass	2,650 kg (No Load)
Vibration Sensor	Lansmont SAVER 9X30 (GPS)
Heavy Truck	
Vehicle Type	Renault Midlum 180 dci
Tare / Max Gross Vehicle Mass	6,560 kg / 10,000 kg
Gross Vehicle Mass	6,560 kg (No Load)
Vibration Sensor	Lansmont SAVER 9X30 (GPS)

Figure 8-79: The location of the accelerometer and GPS antenna in the rear of the heavy truck.

8.6.2 Route Selection

The criteria for route selection have already been discussed and will not be described further. The route selected was the Autovía del Mediterráneo (Mediterranean Highway), shown in *Figure 8-80*, and the two vehicles were driven along the highway route A-7 between the Valencian towns of Paterna and Almussafes, with the first route designated PA and the return route AP.

Figure 8-80: Route A-7 (between Paterna and Almussafes) highlighted on the map of Valencia, Spain.

8.6.3 In-Service Experimental Procedure

The in-service experiments were undertaken using the light truck and the heavy truck travelling along the routes PA and AP. Both vehicles were operated with no additional load and the sprung mass vertical vibration acceleration was measured for three trips along the routes at nominally constant operating speeds of 70, 80 and 90 km/h. The Lansmont 9X30 SAVER was set to record prior to undertaking the experiments (sampling frequency of 500 Hz) and the GPS capabilities enables the location and speed of the vehicle to be measured throughout the trip and only the relevant data was used for analysis. In some cases during these experiments an occasional lane change was required due to traffic, and the driver of the vehicle increased or decreased speed so that this data could be easily identified and excluded from the analysis.

8.6.4 Light Truck Experimental Results

The filtered response PSD functions of the acceleration response of the light truck sprung mass from both routes PA and AP are presented in *Figure 8-81*. The increased complexity of the light truck over the SWEV is evident in the measured response PSD functions (particularly beyond the sprung mass); however the sprung mass mode is clearly identifiable.

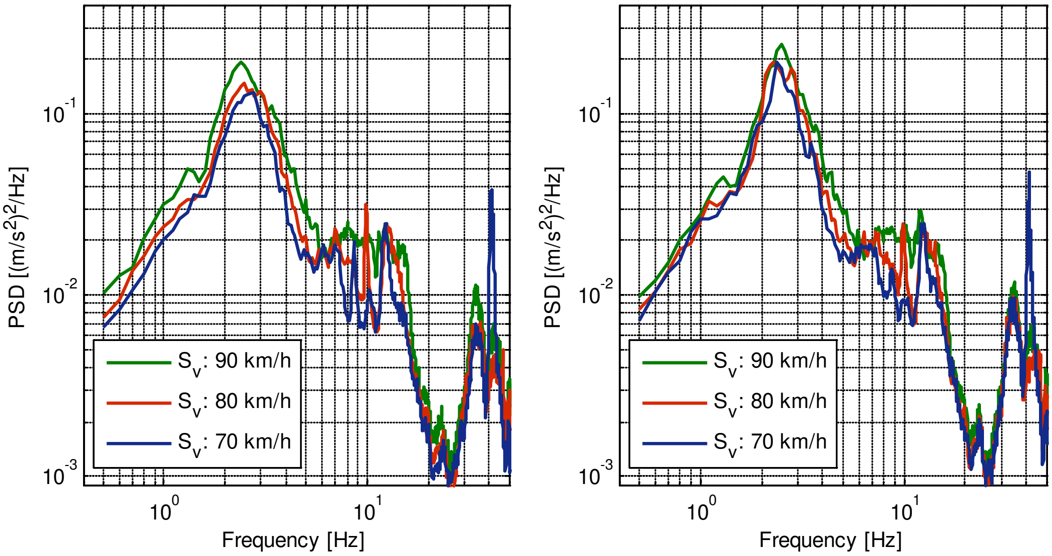

Figure 8-81: The response PSD functions of the light truck sprung mass travelling over routes PA (left) and AP (right) at various nominally constant operating speeds (Δf = 0.1 Hz).

The random decrement signatures for the light truck travelling over routes PA and AP are presented in *Figure 8-82*. Note that the number of averages obtained for each signature do not vary significantly, as during each experimental run some sections were omitted due to significant changes in speed below or above the desired operating speed. The random decrement signatures established are consistent in shape for the various operating speeds, but appear to possess a higher level of damping compared to the SWEV and may be due to the truck having no additional loading.

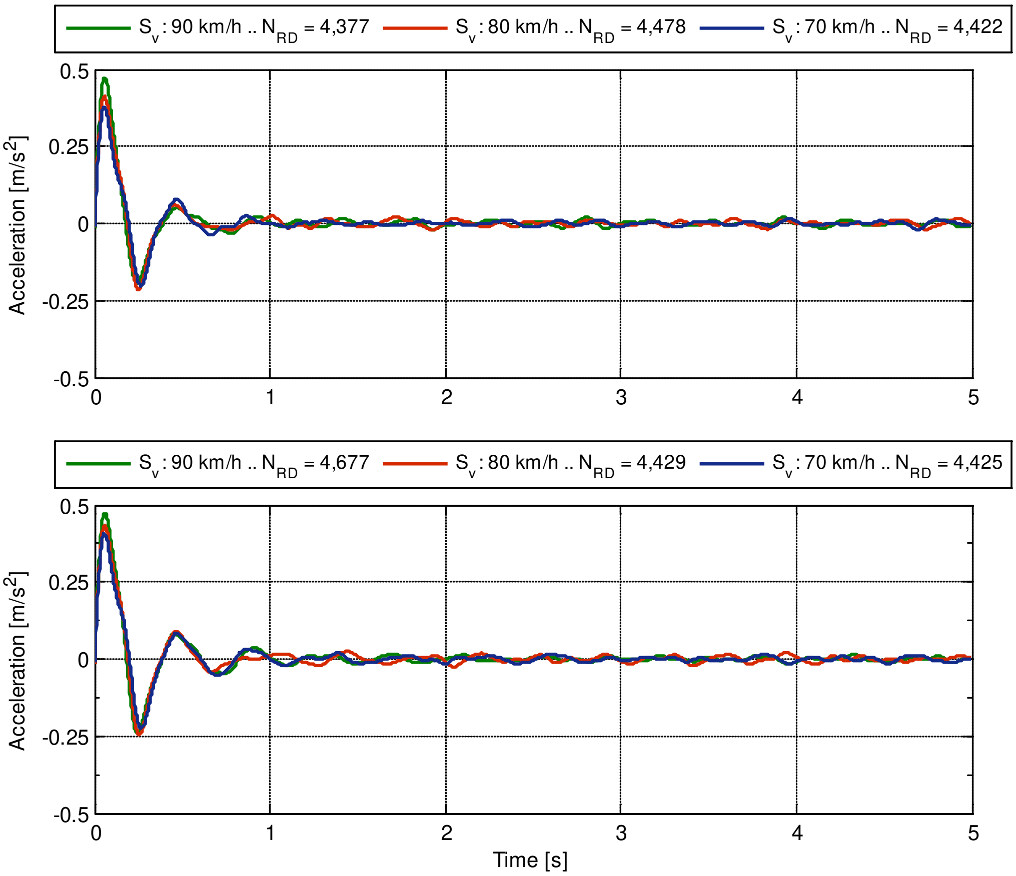

Figure 8-82: Established random decrement signatures from the sprung mass acceleration of the light truck travelling over routes PA (top) and AP (bottom) for various nominally constant operating speeds.

The random decrement signatures were analysed using the unwrapped instantaneous phase to estimate the damped natural frequency and the Hilbert envelope to estimate the damping ratio. A typical example of the unwrapped instantaneous phase and Hilbert envelope for the light truck travelling over route AP at an operating speed of 70 km/h is presented in *Figure 8-83*. The estimated dynamic characteristics of the light truck sprung mass are given in *Table 8-Y*. The estimates of the sprung mass dynamic characteristics are fairly consistent and do not considerably vary due to the vehicle's operating speed.

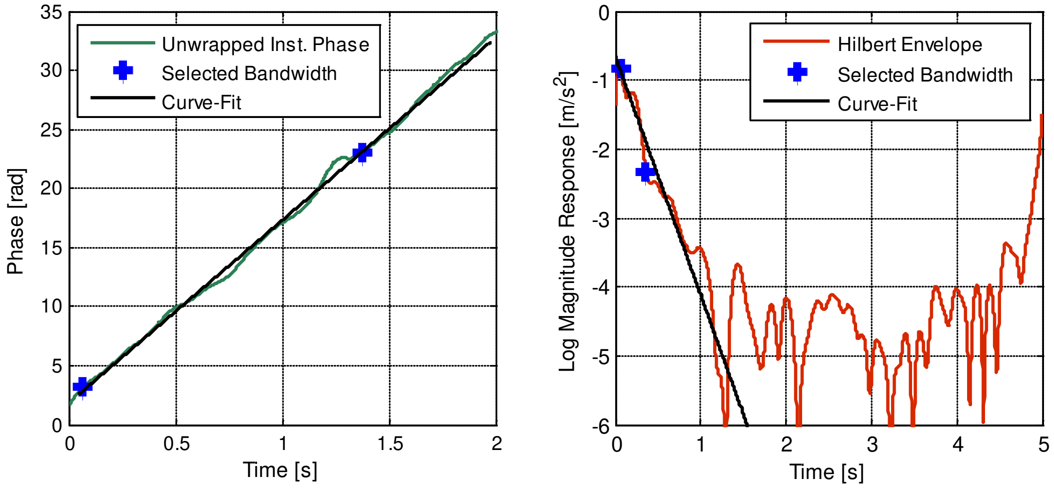

Figure 8-83: Typical example of the obtained unwrapped instantaneous phase (left) and the Hilbert envelope (right) from the response of the light truck travelling over route AP (speed of 70 km/h).

Table 8-Y: The estimated dynamic characteristics of the sprung mass of the light truck using the random decrement approach travelling over routes PA and AP.

Nominal Operating Speed [km/h]	**Natural Frequency f_{sn} [Hz]**	**Damping Ratio ζ_s [-]**
Route PA		
70	2.35	0.220
80	2.40	0.218
90	2.26	0.210
Route AP		
70	2.42	0.225
80	2.44	0.220
90	2.42	0.212

To provide a comparison with the in-service response estimates, the light truck was subjected to the CEU (1996) ramp test. A total of five experimental runs of the ramp test were undertaken, however the fifth run measured data was unusable due to slow vehicle speed. A typical example of the filtered time response of the light truck is presented in *Figure 8-84* of a run from the ramp test. *Figure 8-85* shows a typical example of the unwrapped instantaneous phase and Hilbert envelope from the second run of the ramp test. The estimated natural frequency and damping ratio for each of the ramp test runs are given in *Table 8-Z.*

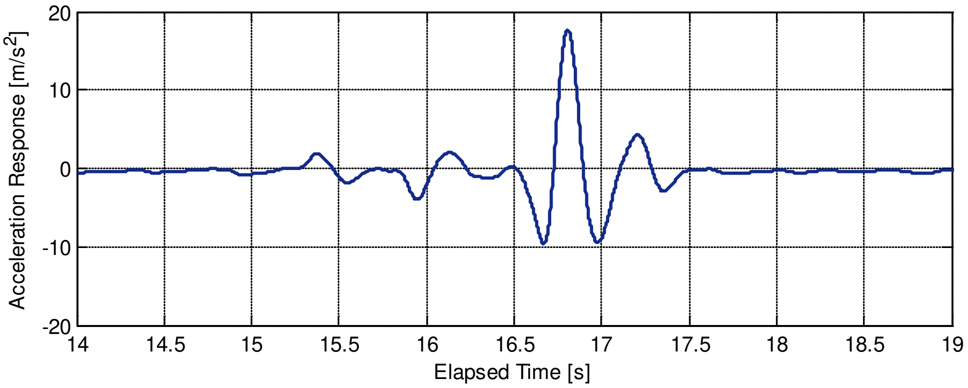

Figure 8-84: Typical filtered time response of the light truck from the ramp test (run 2).

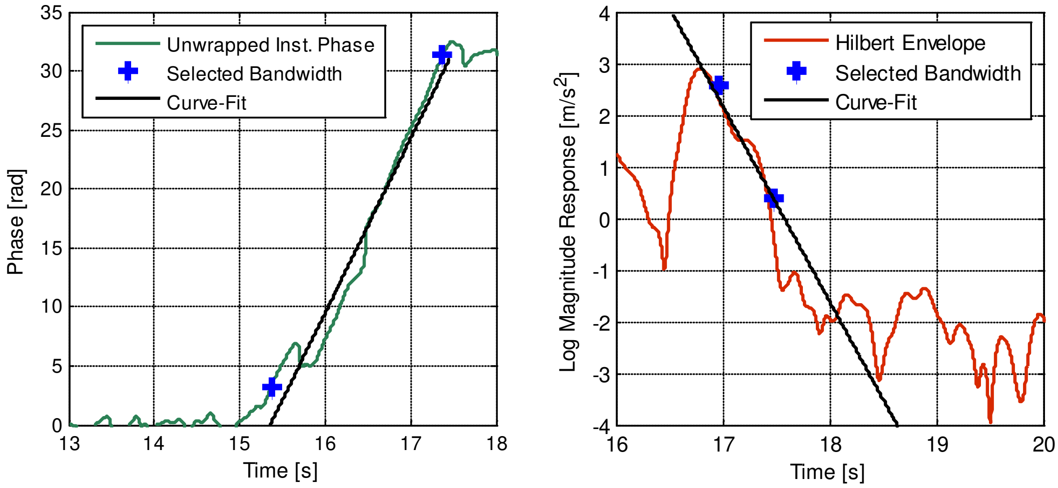

Figure 8-85: Typical example of the obtained unwrapped instantaneous phase (left) and the Hilbert envelope (right) from the response of the light truck during the ramp test (run 2).

Table 8-Z: The estimated dynamic characteristics of the light truck sprung mass mode from the various runs of the ramp test.

Ramp Test	**Natural Frequency** f_{sn} **[Hz]**	**Damping Ratio** ζ_s **[-]**
Run 1	2.68	0.211
Run 2	2.75	0.212
Run 3	2.69	0.208
Run 4	2.69	0.218

Note: Run 5 was not completed at correct speed and omitted.

Compared to the estimates obtained from the in-service experiments, the sprung mass natural frequency is higher and the damping ratio estimates are lower. The difference between the estimates provides further evidence of the lack of relevance between the ramp tests and the behaviour of vehicles during normal operation.

8.6.5 Heavy Truck Experimental Results

To provide a preliminary inspection of the measured response data, the filtered response PSD functions of the sprung mass of the heavy truck were computed and presented in *Figure 8-86* from routes PA and AP. From the measured response PSD functions, it is clear that the sprung mass mode is either very broad in frequency or another mode is present around the same frequency. There is a possibility that the accelerometer measured a strong pitch response from the vehicle due to the location of the sensor.

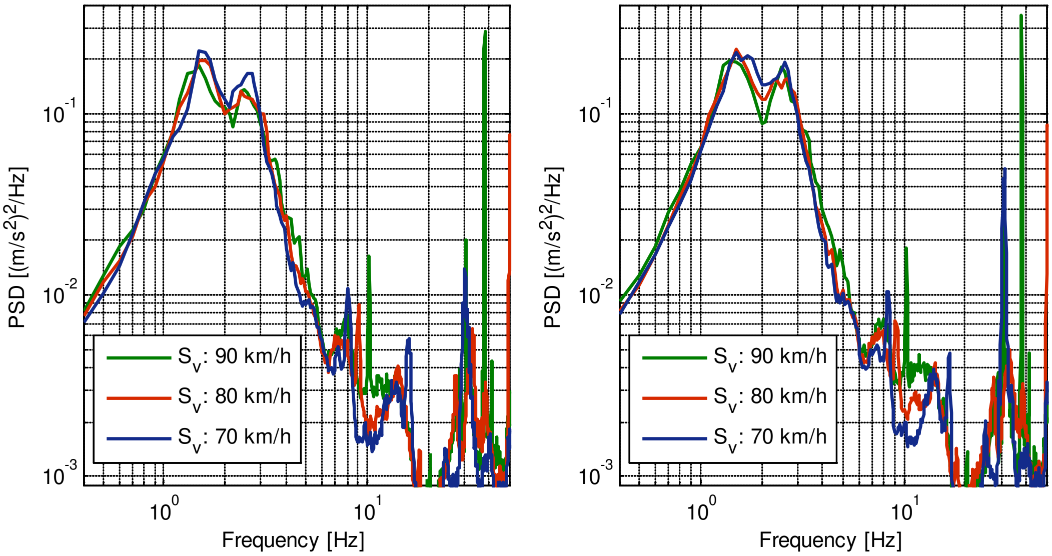

Figure 8-86: The response PSD functions of the heavy truck sprung mass travelling over routes PA (left) and AP (right) at various nominally constant operating speeds (Δf = 0.1 Hz).

As noted for the light truck random decrement signatures, the number of averages are not only dependent on the duration of data, but also some sections were omitted due to a change in speed below or above the desired operating speed. The random decrement signatures obtained from the response of the heavy truck over both routes PA and AP are presented in *Figure 8-87*. As noted for the light truck signatures, the random decrement signatures established for the heavy truck are consistent in shape between the various operating speeds, but their shape is rather unusual and possibly due to the pitch response of the vehicle.

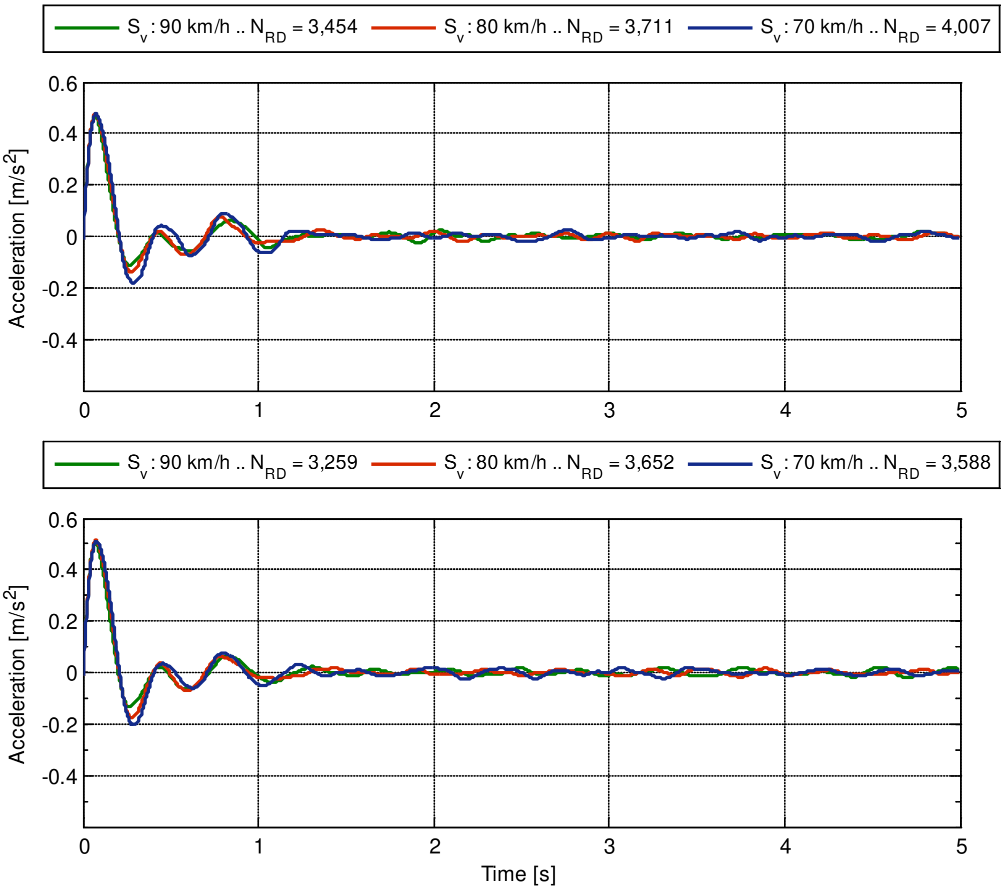

Figure 8-87: Established random decrement signatures from the sprung mass acceleration of the heavy truck travelling over routes PA (top) and AP (bottom) for various nominally constant operating speeds.

Once the random decrement signatures were established they were then analysed using the unwrapped instantaneous phase to estimate the damped natural frequency and the Hilbert envelope to estimate the damping ratio. A typical example of the unwrapped instantaneous phase and Hilbert envelope for the heavy truck travelling over route AP at an operating speed of 70 km/h is presented in *Figure 8-88*. The estimated dynamic characteristics of the heavy truck sprung mass mode are listed in *Table 8-AA*.

From the results, it is evident that the multiple peaks significantly affect the estimates of the damped natural frequency. It is difficult to justify the selection of a single natural frequency of the sprung mass mode. This illustrates the difficulty associated with estimating the dynamic characteristics of vehicles due to their numerous complexities. Overall, the estimates of the natural frequency and damping ratio are consistent for the different operating speeds and routes.

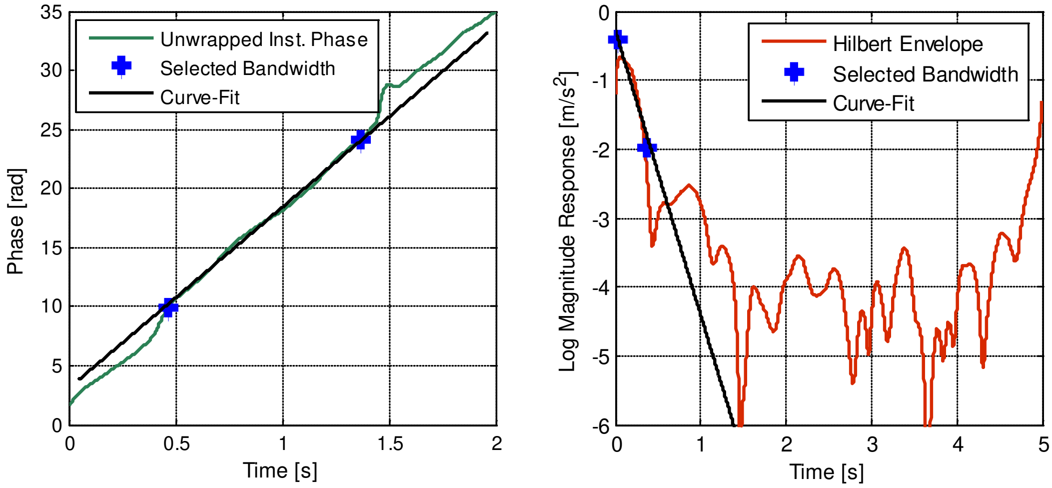

Figure 8-88: Typical example of the obtained unwrapped instantaneous phase (left) and the Hilbert envelope (right) from the response of the heavy truck travelling over route AP (speed of 70 km/h).

Table 8-AA: The estimated dynamic characteristics of the sprung mass mode of the heavy truck using the random decrement approach travelling over routes PA and AP.

Nominal Operating Speed [km/h]	**Natural Frequency f_{sn} [Hz]**	**Damping Ratio ζ_s [-]**
Route PA		
70	2.04	0.223
80	2.19	0.233
90	2.32	0.241
Route AP		
70	2.11	0.240
80	2.06	0.232
90	2.08	0.242

To compare the in-service estimated dynamic characteristics, the heavy truck was also subjected to the CEU (1996) ramp test (five experimental runs). A typical example of the filtered time response of the light truck is presented in *Figure 8-89* from one of the experimental runs of the ramp test. A typical example of the obtained unwrapped instantaneous phase and Hilbert envelope from the third run of the ramp test is shown in *Figure 8-90*. The estimates of the natural frequency and damping ratio from each run of the ramp test are presented in *Table 8-BB*.

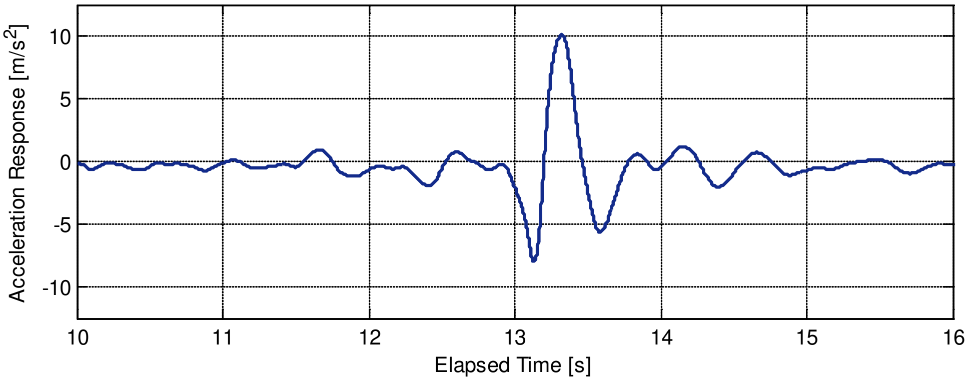

Figure 8-89: Typical filtered time response of the heavy truck from the ramp test (run 3).

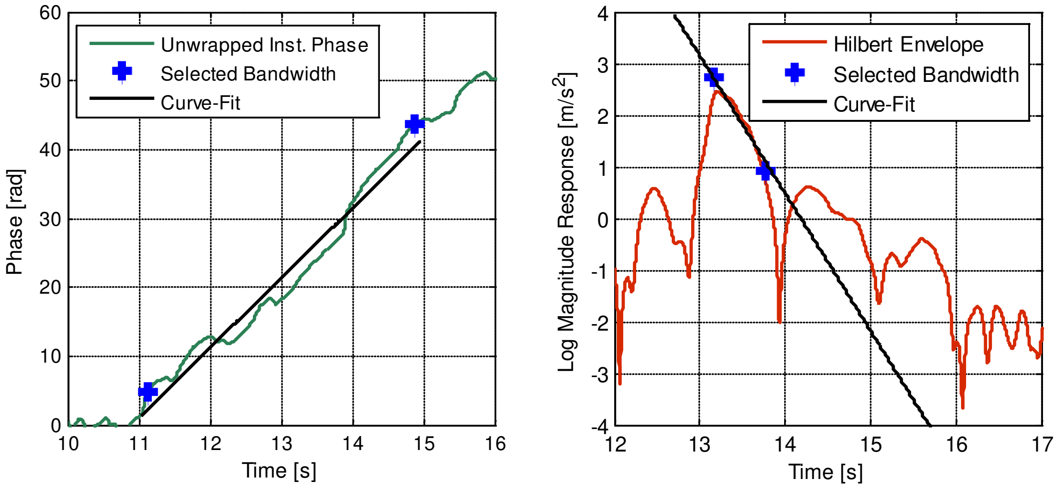

Figure 8-90: Typical example of the obtained unwrapped instantaneous phase (left) and the Hilbert envelope (right) from the response of the heavy truck during the ramp test (run 3).

Table 8-BB: The estimated dynamic characteristics of the sprung mass of the heavy truck from the ramp test.

Ramp Test	**Natural Frequency** f_{sn} **[Hz]**	**Damping Ratio** ζ_s **[-]**
Run 1	1.87	0.234
Run 2	1.86	0.246
Run 3	1.89	0.268
Run 4	1.86	0.252
Run 5	1.92	0.244

The estimates obtained from the ramp test are significantly different to those established using the in-service response data. The closely-spaced peaks around the sprung mass mode cause difficulty in estimating the sprung mass natural frequency and results in significantly different estimates. Both the natural frequency and damping ratio are different to the estimates obtained from the in-service response data. Again, further evidence is provided to highlight the difficulty in justifying the use of other methods to estimate the dynamic characteristics of vehicles.

8.7 CHAPTER SUMMARY

This Chapter described a series of in-service experiments, the focus of which was on the validation of the two techniques using the idealised SWEV. The first series of in-service experiments were undertaken with the SWEV loaded with 100 kg of dead weight over a 40 km route at three different nominally constant operating speeds. Only the sprung mass acceleration response was measured during these experiments. The first approach (assuming the excitation can be approximated using the ISO 8608 spectral model) attempted to estimate the spectral exponent; however there was no consistency between the estimates. This prompted an investigation into the actual pavement profile and the left and right wheel tracks were obtained from a local road authority and used to provide a comparison with the FRFs obtained from the excitation-response experiments (using a vibration table).

The comparison FRFs were re-examined using linear scales and found that, regardless of the predicted spectral exponent used for the excitation, the FRF of only the sprung mass resonant frequency could be reasonably approximated using only in-service response data. However, an inconsistency in the analysis remained, as the actual pavement elevation profile traversed by the SWEV is between the left and right wheel tracks and may vary between experimental runs. To validate the approaches, the SWEV was instrumented and calibrated to operate as an inertial profilometer.

The second series of in-service experiments were undertaken with the SWEV, measuring both the excitation and response. The SWEV was loaded with 50 kg of dead weight and driven across two roads (approximately 40 km and 26 km in length). The actual excitation spectra were established and curve-fitted to obtain the spectral properties of the pavement. The established values of the spectral exponent were found to vary between runs, which is a cause of the failure for the spectral exponent to be accurately estimated. The measured FRFs from the in-service experiments were compared with those established in the laboratory using a vibration table and found that there is a difference, particularly for the unsprung mass mode, between the FRFs measured in the laboratory (excitation-response) and those measured in-service.

Measuring the actual transmissibility FRFs of the SWEV-A and SWEV-B (50 kg) allowed for the random decrement technique to be validated. Two approaches were developed in Chapter 7 to estimate the dynamic characteristics using only in-service response data. The first approach estimates the dynamic characteristics of the sprung mass (Hilbert Domain), while the second estimates the FRF of the vehicle directly from the random decrement signature (Frequency Domain). While both approaches using the random decrement technique provide good estimates of the SWEV's FRF, the first approach provides the better agreement. Both approaches are limited to the sprung mass mode.

Having established the two techniques, an investigation was undertaken into the length of pavement required to obtain a sufficient estimate of the response spectrum and random decrement signature. The investigation was undertaken using a Monte Carlo simulation (1,000 iterations) to randomly select a starting point along the road for a variety of selected pavement length ratios. The average and standard deviation of the MSE from each of the iterations was determined and compared with the estimate obtained from the full length of the pavement. The measured response of the SWEV-B (50 kg) configuration over routes BG and SR were evaluated using the Monte Carlo simulation for all three operating speeds. While only indicative, the results of the simulation suggest that a minimum road length of 10 km is required to establish a sufficient estimate of the response spectrum or random decrement signature (from which the dynamic characteristics, or FRF, are estimated).

To conclude the research, a series of in-service experiments were undertaken using two transport vehicles; a light truck and a heavy truck. The random decrement technique (Hilbert Domain) was used to establish the random decrement signatures to estimate the dynamic characteristics of the sprung mass. For comparison, the two trucks were also subjected to the ramp test. The dynamic characteristics were able to be consistently estimated between runs (different operating speeds); however there was a difference between those estimated using the in-service response data to those estimated from the ramp test. This provides further evidence supporting the use of in-service experiments, which do not remove the vehicle from normal use, and provide an improved representation of the vehicle's dynamic characteristics during operation.

Chapter 9

CONCLUSIONS

The development of a practical technique to estimate the dynamic characteristics of road vehicles is important for many applications. The environmental and economic costs associated with protective packaging are becoming increasingly significant in the modern world. The need to effectively and efficiently deliver products and equipment via road transport is dependent on the optimisation of protective packaging. The current methods to optimise protective packaging in the laboratory involve the use of either generic vibration spectra (cheap and easily accessible) or measured vibration spectra (expensive and resource intensive).

An approach is currently being developed to improve transportation vibration simulations by utilising publicly available information on road roughness, vehicle FRFs and trip schedules (speed and duration over each road). While generic FRFs can be used, they do not represent the dynamic behavior of the particular vehicle used, and so developing a practical method to estimate the FRF of a vehicle is an important aspect of the approach. Another area of importance for the estimation of the dynamic characteristics of vehicles includes assessing the road-damaging potential of heavy vehicles, commonly evaluated by establishing the vehicle's sprung mass mode dynamic characteristics.

The research presented in this thesis has culminated in the development of a practical approach to estimate the dynamic characteristics of road vehicles using only in-service response data measured during normal operation. From the broad literature review, one of the main outcomes was that the various techniques currently available to estimate the dynamic characteristics of road vehicles each have their limitations and no comparative evaluation has been undertaken to assess their accuracy and repeatability. Furthermore, they all require the vehicle to be taken out of normal operation.

As part of the methodology, the requirements for an idealised quarter car vehicle to be used as a tool to validate the experiments were discussed. A critical evaluation of the experimental methods currently available was undertaken using the idealised quarter car vehicle, known as the SWEV (of which there were two configurations). One of the aims of the critical evaluation was to determine if one single, true, estimate of the vehicles dynamic characteristics exist, and if so, which method(s) provided the best estimate. For both configurations of the vehicle, it was found that the estimates of the dynamic characteristics varied depending on the excitation type and level and it is unclear which method establishes the true FRF of the vehicle or their relevance to the in-service performance of the vehicle.

The development of two practical techniques to analyse the in-service vibration response data of vehicles during normal operation to estimate the dynamic characteristics was described in Chapter 7. Various techniques were investigated and considered, but only two were selected. The first technique assumes that the excitation (road elevation profile) can be adequately approximated using a predefined spectral model with only two parameters. If the response of a vehicle travelling over the same pavement at two nominally constant operating speeds is the same, such that the vehicle is linear, then the measured response can be used to estimate one of the parameters of the pavement spectral model. The remaining parameter of the pavement model is the roughness constant, which translates the spectrum vertically and so the value is adjusted until the transmissibility FRF of the vehicle approaches unity at low frequency. This enables for not only an estimate of the vehicle’s FRF, but also the pavement spectral properties.

The next technique involves the use of the random decrement method to establish the random decrement signature (estimate of the vehicle’s impulse response) from the measured vibration response of a vehicle travelling over irregular road surfaces. Two different approaches were evaluated using the random decrement method; the first is to estimate the damped natural frequency and damping ratio of the sprung mass mode using the Hilbert Transform, while the second approach aims to estimate the FRF directly from the random decrement signature (using the FFT). An experimental investigation into the optimum parameters for both approaches using the random decrement technique was also undertaken. The only difference between the two sets of parameters was the length of the random decrement signature. Some potential pitfalls that were expected to be encountered for the first technique was the inability of the spectral exponent of the pavement spectrum to be estimated accurately if the pavement travelled over by the vehicle varied between experimental runs. While the second random decrement approach (directly estimate the FRF from the signature) was able to identify the unsprung mass mode, it was always slightly underestimated in terms of the magnitude ratio.

The first series of in-service experiments were undertaken without any knowledge of the actual longitudinal pavement profiles driven over by the SWEV. The sprung mass acceleration response of both configurations of the SWEV was measured while driven over a rural road. The PSD functions of the measured response data were combined with the ISO spectral model (corresponding to violet noise acceleration) and the two parameters were adjusted and compared with the FRFs measured in the laboratory using a vibration table. It was found that the ISO recommended value for the spectral exponent did not provide the best agreement with the FRFs measured in the laboratory. The spectral exponent was then estimated using only the measured response data and the estimates were found to be inconsistent and the actual spectral properties of the pavement remained unknown.

The longitudinal pavement elevation profiles of the left and right wheel tracks were obtained from a local authority and analysed to compute the elevation PSD function. The PSD function of the left wheel track was further investigated to estimate the spectral properties of the pavement. The pavement spectrum was then combined with the measured in-service response data to compute the FRF of the SWEV and again compared with the vibration table FRFs measured in the laboratory. Despite the use of the measured pavement elevation profile, a significant difference remained between the two sets of FRFs. It is also likely that the pavement elevation profile traversed by the SWEV is different to the obtained elevation profiles (as it travels between the wheel tracks).

A second series of in-service experiments were undertaken over two roads using the two configurations of the SWEV. The vehicle was instrumented to not only measure the sprung mass acceleration response, but also the longitudinal pavement elevation profile travelled by the SWEV. The in-service measured transmissibility FRFs were compared with those established in the laboratory (using a vibration table) and found significant differences, particularly in the level of damping for sprung mass mode. The comparison of the FRFs revealed that the vehicle has significantly different characteristics during operation (particularly the unsprung mass mode), demonstrating the importance of using in-service response data to estimate the FRF.

Both of the approaches based on the random decrement technique were evaluated using the measured transmissibility FRFs for validation (from the second series of in-service experiments). The first random decrement approach (Hilbert Domain) was limited to the sprung mass mode, while the second approach (Frequency Domain) to directly estimate the FRF from the random decrement signature was able to identify the location of the unsprung mass, but was significantly overestimated in the magnitude ratio. Both random decrement approaches were able to estimate the dynamic characteristics of the vehicle's sprung mass mode for almost all cases. The first approach was found, overall, to consistently obtain accurate estimates of the dynamic characteristics of the sprung mass mode of the vehicle.

An investigation into the minimum length of pavement required was undertaken using a Monte Carlo simulation. The measured response spectra and random decrement signatures were compared with those established using the full pavement length. Several pavement length ratios (such as a half of the actual pavement length) were selected and the Monte Carlo simulation was used to randomly select the starting points. While only an indication (and dependent on the stationarity of the road), the results found that, regardless of the operating speed, a minimum road length of 10 km is sufficient to provides an accurate estimate of the response spectrum or random decrement signature.

Having established the random decrement technique, a final series of in-service experiments were undertaken using two transport vehicles. A light truck and heavy truck were driven along a road at three nominally constant operating speeds and the dynamic characteristics of the sprung mass estimated. To provide a comparison with the in-service experimental results, the trucks were subjected to the ramp test to estimate the dynamic characteristics of the sprung mass mode. The approach was shown to yield consistent estimates of the sprung mass mode of the two transport vehicles. The results also found that the estimated dynamic characteristics using in-service response data differed to those estimated using the ramp test. This further reinforces the need to estimate the dynamic characteristics of vehicles using in-service response data.

The analysis technique based on the random decrement method is able to accurately estimate the dynamic characteristics of a vehicle (limited to the sprung mass mode) and can be used to provide realistic vibration simulations in the laboratory without the need to undertake significant vibration surveys. As a practical tool, a vehicle can be instrumented to measure the sprung mass vibration acceleration and the speed (using GPS) and driven at ambient speeds (normal operating conditions). Provided that at least 10 km of response data is obtained at a nominally constant operating speed, the response data can be carefully concatenated and used to estimate the dynamic characteristics of the vehicle.

9.1 FUTURE WORK

Since the research presented in this thesis is the initial stage of a broader effort, there are numerous avenues for further work and investigation. The random decrement technique is the most promising approach investigated for the estimation of a vehicle's FRF, however it is limited to the sprung mass mode. Further work should be undertaken to estimate the unsprung mass mode of vehicles as well in order to provide an improved representation of the vehicle's dynamic characteristics. The second approach, which estimates the FRF directly from the random decrement signature, was found to significantly overestimate the unsprung mass mode and is likely due to the non-white noise excitation. As the pavement excitation approaches a violet noise spectrum in the acceleration domain, it may be beneficial to measure the velocity (or integrate the acceleration) response of the vehicle and establish the random decrement signature. The first random decrement approach (Hilbert Domain) employed the use of a numerical SDoF model of the transmissibility FRF and so the development of a more complex model incorporating the unsprung mass mode may be a viable approach.

The effect of speed variation on estimating the dynamic characteristics is another area that requires further investigation. The sensitivity of variations in the operating speed should be established to improve the understanding of their influence on estimating the dynamic characteristics. The influence of large transient events, such as potholes or train tracks, and significantly nonstationary pavements is another avenue that requires attention.

Any comparisons made in the future should use the FRFs measured during in-service operation, as there is a clear difference between estimating the FRF in the laboratory using a vibration table. In general, the techniques are well enough established, and the majority of the research going forward should be concerned with the use of real transport vehicles. It is strongly recommended that for any future work involving the use of transport vehicles, the actual longitudinal pavement profile of the left and right wheel tracks be simultaneously measured for validation. The results presented in this research found that the longitudinal pavement elevation profile varies between experimental runs and data provided by local road authorities, and is inadequate for establishing the actual pavement elevation profiles traversed by the vehicle. Also, the focus of this thesis was limited to only the vertical mode of vibration, which is dominant mode exhibited by vehicles. However, it is not the only type of vibration, and characterising other motions, notably the pitch and roll of a vehicle, should also be undertaken.

REFERENCES

Alam, M., Sedaghati, R., Soucy, Y. & Bhat, R.B. 2009, *Analytical and Experimental Study Using Output-Only Modal Testing for On-Orbit Satellite Appendages*, Advances in Acoustics and Vibration, vol. 2009, pp. 1-10.

Andren, P. 2006, *Power Spectral Density Approximations of Longitudinal Road Profiles*, International Journal of Vehicle Design, vol. 40, no. 1-3, pp. 2-14.

APC 2011, *The Australian Packaging Covenant 2011 Annual Report*, Australian Packaging Covenant, Sydney.

AASHO 1962a, *The AASHO Road Test, Report 5, Pavement Research*, Highway Research Board, Special Report 61E.

AASHO 1962b, *The AASHO Road Test, Report 6, Special Studies*, Highway Research Board, Special Report 61F.

Asmussen, J.C. 1997, *Modal Analysis Based on the Random Decrement Technique – Application to Civil Engineering Structures*, PhD Thesis, University of Aalborg.

Asmussen, J.C. & Brincker, R. 1996, *Estimation of Frequency Response Functions by Random Decrement*, Proceedings of the 14th International Modal Analysis Conference, 12-15th February, Michigan, USA.

ASTM 2005, *Terminology Relating to Vehicle-Pavement Systems*, E867-02a, American Society of Testing and Materials, ASTM Standards on disk: Standards Worldwide, vol. 04.03, ASTM, West Conshohocken.

ASTM 2009, *Standard Practice for Performance Testing of Shipping Containers and Systems: D4169-08*, American Society of Testing and Materials, ASTM Standards on disk: Standards Worldwide, vol. 15.10, ASTM, West Conshohocken.

Austroads 2005, *RoadFacts 2005, An Overview of the Australian and New Zealand Road Systems*, AP-G18/05, Austroads, Sydney, Australia.

Avitabile, P. 1999, *Which Shaker Excitation is best?*, SEM Experimental Techniques, vol. 23, no. 1, pp. 13-14.

Bendat, J.S. & Piersol, A.G. 1980, *Engineering Applications of Correlation and Spectral Analysis*, Wiley Interscience, New York, USA.

Bendat, J.S. & Piersol, A.G. 2000, *Random Data: Analysis and Measurement Procedures*, 3rd edn, Wiley, New York, USA.

Blanksby, C., George, R., Germanchev, A., Patrick, S. & Marsh, F. 2006, *An In-Service Survey of Heavy Vehicle Suspensions*, Report No. VC71235-01-01, Road and Traffic Authority of NSW, Sydney.

Bogsjo, K. 2007, *Evaluation of Stochastic Models of Parallel Road Tracks*, Probabilistic Engineering Mechanics, vol. 22, no. 4, pp. 362-370.

Brincker, R. & Asmussen, J.C. 1997, *Random Decrement Based FRF Estimation*, Proceedings of the 15th International Modal Analysis Conference, Orlando, Florida.

Bruscella, B. 1997, *The Analysis and Simulation of the Spectral and Statistical Properties of Road Roughness for Package Performance Testing*, M.Eng Thesis, Victoria University.

Bruscella, B., Rouillard, V. & Sek, M. 1999, *Analysis of Road Surface Profiles*, Journal of Transportation Engineering, vol. 125, no. 1, pp. 55-59.

Caldicott, P.J. 1991, *Distribution Testing – Sine or Random?*, Journal of Packaging Technology and Science, vol. 4, no. 5, pp. 287-291.

Cebon, D. 1993, *Interaction Between Heavy Vehicles and Roads,* Paper presented at the 39th L Ray Buckendale Lecture.

Cebon, D. 1999, *Handbook of Vehicle-Road Interaction*, Swets & Zeitlinger B.V., Lisse, Netherlands.

Cebon, D. & Newland, E.D. 1983, *The Artificial Generation of Road Surface Topography by the Inverse FFT Method*, Proceedings of the 8th IASVD Symposium on Dynamics of Vehicles on Roads and on Railway Tracks, Cambridge.

CEU 1994, *Council Directive 94/62/EC*, The Council of European Communities, Brussels.

CEU 1996, *Council Directive 96/53/EC*, The Council of European Communities, Brussels.

Chaika, M., Gorsich, D. & Sun, T.C. 2004, *Some Statistical Tests in the Study of Terrain Modelling*, International Journal of Vehicle Design, vol. 36, no. 2-3, pp. 132-148.

Chang, C.S. 1975, *Study of Dynamic Characteristics of Aeroelastic Systems Utilizing Randomdec Signatures*, NASA CE-132563.

Charles, D. 1993, *Derivation of Environment Descriptions and Test Severities from Measured Road Transportation Data*, Journal of the Institute of Environmental Sciences, vol. 36, no. 1, pp. 37-42.

Chemistruck, H.M., Detweiler, Z.R., Ferris, J.B., Reid, A.A. & Gorsich, D.J. 2009, *Review of Current Developments in Terrain Characterisation and Modeling*, Proceedings of SPIE, International Society for Optical Engineering, Bellingham, Washington.

Cole, D.J. & Cebon, D. 1991, *Assessing the Road-Damaging Potential of Heavy Vehicles*, Proceedings of the Institution of Mechanical Engineers, Part D: Journal of Automobile Engineering, vol. 205, no. 4, pp. 223-232.

Cole, H.A. 1968, *On-The-Line Analysis of Random Vibrations*, Journal of the American Institute of Aeronautics and Astronautics, Paper no. 68-288.

Cole, H.A. 1973, *On-Line Failure Detection and Damping Measurements of Aerospace Structures by Random Decrement Signature*, NASA CR-2205.

Cooley, J.W. & Tukey, J.W. 1965, *An Algorithm for the Machine Calculation of Complex Fourier Series*, Mathematics of Computation, vol. 19, pp. 297-301.

Davis, L. & Sack, R. 2004, *Analysis of Heavy Vehicle Suspension Dynamics Using an On-Board Mass Measurement System*, Proceedings of the 27th Australasian Transport Research Forum, Adelaide, Australia, 29th Sep – 1st Oct.

Davis, L., Kel, S. & Sack, R. 2007, *Further Development of In-Service Suspension Testing for Heavy Vehicles*, Proceedings of the 30th Australasian Transport Research Forum, Melbourne, Australia.

De Pont, J. 1992, *Using Servo-Hydraulics to Assess Heavy Vehicle Suspensions for Road Wear*, Heavy Vehicles and Roads: Technology, Safety and Policy, pp. 252-259.

De Pont, J. 1996, *Experiences with Simulating On-Road Heavy Vehicle Suspension Behaviour Using Servo-Hydraulics*, International Journal of Heavy Vehicle Systems, vol. 3, No. 1-4, pp. 127-139.

De Pont, J. 1999, *Suspensions or Whole Vehicles? Rating Road Friendliness*, International Journal of Heavy Vehicle Systems, vol. 6, no. 1-4, pp. 75-98.

Delanne, Y. & Pereira, P.A. 2001, *Advantages and Limits of Different Road Roughness Profile Signal-Processing Procedures Applied in Europe*, Transportation Research Record: Journal of the Transportation Research Board, vol. 1764, no. 1, pp. 254-259.

Department for Transport 2011, *Domestic Activity of GB-Registered Heavy Goods Vehicles*, London.

Dodds, C.J. & Robson, J.D. 1973, *The Description of Road Surface Roughness*, Journal of Sound and Vibration, vol. 31, no. 2, pp. 175-183.

Dodds, C.J. & Robson, J.D. 1975, *Simulation of Dynamic Stresses in Vehicles and Components*, Vehicle System Dynamics: International Journal of Vehicle Mechanics and Mobility, vol. 4, no. 2-3, pp. 130-134.

DoTaRS 2004, *Vehicle Standards Bulletin 11: Certification of Road-Friendly Suspension Systems*, Department of Transport and Regional Services, Canberra.

Eichstädt, T., Carius, A. & Andreas Kraemer, R. 1999, *Producer Responsibility Within Policy Networks: the Case of German Packaging Policy*, Journal of Environmental Policy and Planning, vol. 1, no. 2, pp. 133-153.

Elshafey, A.A., Haddara, M.R. & Marzouk, H. 2009, *Identification of the Excitation and Reaction Forces on Offshore Platforms Using the Random Decrement Technique*, Ocean Engineering, vol. 36, no. 6-7, pp. 521-528.

EURF 2009, *European Road Statistics*, European Union Road Federation and International Road Federation, Brussels.

Ewins, D.J. 1995, *Modal Testing: Theory and Practice*, Research Studies Press, Taunton, UK.

Feldman, M. 2011, *Hilbert Transform Applications in Mechanical Vibration*, John Wiley & Sons, West Sussex, UK.

Garcia, D. 2010, *Robust Smoothing of Gridded Data in One and Higher Dimensions with Missing Values*, Computational Statistics and Data Analysis, vol. 54, no. 4, pp. 1167-178.

Gillespie, T.D. & Sayers, M. 1981, *Role of Road Roughness in Vehicle Ride*, Transportation Research Record, no. 836, pp. 15-20.

Gillespie, T.D. 1985, *Heavy Truck Ride*, SP-607, Society of Automotive Engineers, Warrendale, Pennsylvania.

Gillespie, T.D. 1992a, *Everything You Always Wanted to Know about the IRI, But Were Afraid to Ask!*, Presented at the Road Profile Users Group Meeting, 22nd-24th September, Lincoln, USA.

Gillespie, T.D. 1992b, *Fundamentals of Vehicle Dynamics*, Society of Automotive Engineers, Warrendale.

Gillespie, T.D. & Karamihas, S.M. 1994, *Heavy Truck Properties Significant to Pavement Damage*, ASTM Special Technical Publication 1225, pp. 52-63.

Gonzalez, A., O'Brien, E.J., Li, Y.Y. & Cashell, K. 2008, *The Use of Vehicle Acceleration Measurements to Estimate Road Roughness*, Vehicle System Dynamics, vol. 46, no. 6, pp. 483-499.

Goodwin, D. & Young, D. 2010, *Protective Packaging for Distribution: Design and Development*, DEStech Publishing, PA, USA.

Gyenes, L., Mitchell, C.G.B. & Phillips, S.D. 1992, *Dynamic Pavement Loads and Tests of Road-Friendliness for Heavy Vehicle Suspensions*, Proceedings of the 3rd International Symposium on Heavy Vehicle Weights and Dimensions, 28th June – 2nd July, Queen's College, Cambridge, UK.

He, J. & Fu, Z.F. 2001, *Modal Analysis*, Butterworth-Heinemann, Oxford, UK.

Heath, A.N. 1987, *Application of the Isotropic Road Roughness Assumption*, Journal of Sound and Vibration, vol. 115, no. 1, pp. 131-144.

Heath, A.N. 1988, *Evaluation of the Isotropic Road Roughness Assumption*, Vehicle System Dynamics, vol. 17, no. 6, pp. 157-160.

Heath, A.N. 1989, *Modelling and Simulation of Road Surface Roughness*, Vehicle System Dynamics, vol. 18, pp. 275-284.

Hickling, R. 2006, *Decibels and Octaves, who needs them?*, Journal of Sound and Vibration, vol. 291, no 3-5, pp. 1202-1207.

Houbolt, J.C., Walls, J.H. & Smiley, R.F 1955, *On Spectral Analysis of Runway Roughness and Loads Developed During Taxiing*, Technical Note 3484, Langley Aeronautical Laboratory, National Advisory Committee for Aeronautics, Langley Field.

Houbolt J.C. 1962, *Runway Roughness Studies in the Aeronautical Field*, Transactions of the American Society of Civil Engineers, vol.127, part IV, pp. 428-447.

Ibrahim, S.R. & Mikulcik, E.C. 1977, *A Method for the Direct Identification of Vibration Parameters from the Free Response*, The Shock and Vibration Bulletin, vol. 47, no. 4, pp. 183-198.

Ibrahim, S.R. 1980, *Limitations on Random Input Forces in Randomdec Computation for Modal Identification*, The Shock and Vibration Bulletin, vol. 50, no. 3, pp. 99-112.

Ibrahim, S.R., Brincker, R. & Asmussen, J.C. 1996, *Modal Parameter Identification From Responses of General Unknown Random Inputs*, Proceedings of the 14th International Modal Analysis Conference, 12-15th February, Michigan, USA.

IMechE 2013, *Global Food: Waste Not, Want Not*, Institution of Mechanical Engineers, London.

IRTU 2009, *Road Transport in the People's Republic of China*, International Road Transport Union, Geneva.

ISO 1995, *International Standard 8608: Mechanical Vibration – Road Surface Profiles – Reporting of Measured Data*, ISO 8608:1995 (E), International Organisation for Standardisation, Geneva.

ISTA 2009, *ISTA Project 4AB*, International Safe Transit Association, East Lansing, MI.

Jazar, R.N. 2009, *Vehicle Dynamics: Theory and Application*, Springer, New York, USA.

Kamash, K.M.A. & Robson, J.D. 1977, *Implications of Isotropy in Random Surfaces*, Journal of Sound and Vibration, vol. 54, no. 1, pp. 131-145.

Kamash, K.M.A. & Robson, J.D. 1978, *The Application of Isotropy in Road Surface Modelling*, Journal of Sound and Vibration, vol. 57, no. 1, pp. 89-100.

Kijewski, T. & Kareem, A. 2000, *Reliability of Random Decrement Technique for Estimates of Structural Damping*, Proceedings of the 8th ASCE Specialty Conference on Probabilistic Mechanics and Structural Probability, 24-26th July, Indiana, USA.

Kipp, W.I. 2008, *Random Vibration Testing of Packaged-Products: Considerations for Methodology Improvement*, Proceedings of the 16th IAPRI World Conference on Packaging, 8-12 June, Bangkok, Thailand.

Kropac, O. & Mucka, P. 2004, *Non-Standard Longitudinal Profiles of Roads and Indicators for Their Characterisation*, International Journal of Vehicle Design, vol. 36, no. 2-3, pp. 149-172.

Kropac, O. & Mucka, P. 2008, *Indicators of Longitudinal Unevenness of Roads in the USA*, International Journal of Vehicle Design, vol. 46, no. 4, pp. 393-415.

Kropac, O. & Mucka, P. 2009a, *Classification Scheme for Random Longitudinal Road Unevenness Considering Road Waviness and Vehicle Response*, Journal of Shock and Vibration, vol. 16, no. 3, pp. 273-289.

Kropac, O. & Mucka, P. 2009b, *Non-Uniqueness of Single-Number Indicators of Longitudinal Road Profiles*, Road Materials and Pavement Design, vol. 10, no. 4, pp. 747-766.

La Barre, R.P., Forbes, R.T. & Andrew, S. 1969, *The Measurement and Analysis of Road Surface Roughness*, Technical Report 170/5, Motor Industry Research Association, Lindley, Warwickshire.

Lamb, M., Rouillard, V. & Ainalis, D. 2010, *A Practical Study of Fourier Analysis for Monitoring Fatigue Progression in Elements Subjected to Random Loads*, Proceedings of the 6th Australasian Congress on Applied Mechanics, 12-15th Dec, Perth, Australia.

LeBlanc, P. 1995, *Performance Evaluation of Suspension-Systems vs Vehicle Systems*, Proceedings of the Dynamic Loading of Heavy Vehicles and Road Wear Mid-Term Seminar, 2-3rd February, Sydney, Australia.

Mabbot, N., Foster, G. & McPhee, B. 2001, *Heavy Vehicle Seat Vibration and Driver Fatigue*, Department of Transport and Regional Services Report No. CR 203, ARRB Transport Research Ltd, Canberra.

Macaulay, M.A. 1963, *Measurement of Road Surfaces*, Advances in Automobile Engineering. Proceedings of the Symposium on Vehicle Ride, Vol. 4 of Cranfield International Symposium

Series, Advanced School of Automotive Engineering, Cranfield, England: Pergamon Press, pp. 93-112.

Mann, A.V., McManus, K.J. & Holden, J.C. 1997, *Power Spectral Density Analysis of Road Profiles for Road Defect Assessment*, Road and Transport Research, vol. 6, no. 3, pp. 36-47.

Marcondes, J.A. 1990, *Modeling Vertical Acceleration in Truck Shipments Using the International Roughness Index for Pavements*, PhD Thesis, Michigan State University.

Marcondes, J., Burgess, G., Harichandran, R. & Snyder, M. 1991, *Spectral Analysis of Highway Pavement Roughness*, Journal of Transportation Engineering, vol. 117, no. 5, pp. 540-549.

Milliken, P., De Pont, J., Mueller, T. & Latto, D. 2001, *Assessing Road-Friendly Suspensions*, Transfund Research Report No. 206, Wellington, New Zealand.

Mucka, P. 2004, *Road Waviness and the Dynamic Tyre Force*, International Journal of Vehicle Design, vol. 36, no. 2/3, pp. 216-232.

Mucka, P. 2012, *Longitudinal Road Profile Spectrum Approximation by Split Straight Lines*, Journal of Transportation Engineering, vol. 138, no. 2, pp. 243-251.

Mucka, P. & Granlund, J. 2012, *Comparison of Longitudinal Unevenness of Old and Repaired Highway Lanes*, Journal of Transportation Engineering, vol. 138, no. 3, pp. 371-380.

OECD 1992, *Dynamic Loading of Pavements*, Road Transport Research Programme, Report No. 9264137629, Organisation for Economic Co-operation and Development, Paris.

OECD 1998, *Dynamic Interaction Between Vehicles and Infrastructure Experiment (DIVINE)*, Technical Report No. DSTI/DOT/RTR/IR6(98)1/FINAL, Organisation for Economic Co-operation and Development, Paris.

Ostergaard, S. 1991, *Packaging Goals in Transport Quality*, Proceedings of the 7th IAPRI World Conference on Packaging, Utrecht, Holland.

PCA 2005, *Australian Packaging: Issues and Trends*, Packaging Council of Australia, Melbourne.

Prem, H. 1987, *Road Roughness Influence on Suspension Performance*, Proceedings of the Symposium on Heavy Vehicle Suspension Characteristics, 23rd-25th March, Canberra, Australia.

Popp, K. & Schiehlen, W. 2010, *Ground Vehicle Dynamics*, Springer, Berlin, Germany.

Quinn, B.E. & Zable, J.L. 1966, *Evaluating Highway Elevation Power Spectra from Vehicle Performance*, Highway Research Record 121, Highway Research Board, pp. 15-26.

Randall, R.B. 1987, *Frequency Analysis*, Bruel & Kjaer, Naerum, Denmark.

Rao, S.S. 2005, *Mechanical Vibrations: SI Edition*, Prentice Hall, Singapore.

Reck, S.M. 1990, *The Expanding Environmental Consciousness of Local Government: Municipalities that Have Banned Styrofoam and the Legal Consequences*, University of Bridgeport Law Review, vol. 11, pp. 127-145.

Robson, J.D. & Dodds, C.J. 1976, *Stochastic Road Inputs and Vehicle Response*, Vehicle System Dynamics: International Journal of Vehicle Mechanics and Mobility, vol. 5, no. 1-2, pp. 1-13.

Robson, J.D. 1979, *Road Surface Description and Vehicle Response*, International Journal of Vehicle Design, vol. 1, no. 1, pp. 25-35.

Root, D. 1997, *Six-Step Method For Cushioned Package Development*, Lansmont Corporation, www.lansmont.com.

Rouillard, V., Sek, M.A. & Perry, T. 1996, *Analysis and Simulation of Road Profiles*, Journal of Transportation Engineering, vol. 122, no. 3, pp. 241-245.

Rouillard, V., Bruscella, B. & Sek, M. 2000, *Classification of Road Surface Profiles*, Journal of Transportation Engineering, vol. 126, no. 1, pp. 41-45.

Rouillard, V. & Sek, M. 2000, *Monitoring and Simulating Non-Stationary Vibrations for Package Optimisation*, Journal of Packaging Technology and Science, vol. 13, no. 4, pp. 149-156.

Rouillard, V. 2002, *Excitation Techniques for Resonance Analysis of Packages*, Journal of Packaging Technology and Science, Vol. 15, no. 5, pp. 267-274.

Rouillard, V. & Sek, M. 2002, *A Statistical Model for Longitudinal Road Topography*, Road and Transport Research, vol. 11, no. 3, pp. 17-23.

Rouillard, V. 2008, *Generating Road Vibration Test Schedules from Pavement Profiles for Packaging Optimisation*, Journal of Packaging Technology and Science, vol. 21, no. 8, pp. 501-514.

Rouillard, V. 2009, *Decomposing Pavement Surface Profiles into a Gaussian Sequence*, International Journal of Vehicle Systems Modelling and Testing, vol. 4, no. 4, pp. 288-305.

Rouillard, V. & Sek, M. 2010a, *Synthesising Nonstationary, Non-Gaussian Random Vibrations*, Journal of Packaging Technology and Science, vol. 23, no. 8, pp. 423-439.

Rouillard, V. & Sek, M. 2010b, *A Practical Method for Estimating Ground Vehicle Frequency Response Function from Response Data*, Proceedings of the 6th Australasian Congress on Applied Mechanics, 12-15th Dec, Perth, Australia.

Rouillard, V. & Sek, M. 2013, *Creating Transport Vibration Simulation Profiles from Vehicle and Road Characteristics*, Journal of Packaging Technology and Science, vol. 26, no. 2, pp. 82-95.

Sayers, M.W. 1986, *Characteristic Power Spectral Density Functions for Vertical and Roll Components of Road Roughness*, Symposium on Simulation and Control of Ground Vehicles and Transportation Systems, vol. AMD-Vol. 80, DSC-Vol. 2, Anaheim, CA, pp. 113-139.

Sayers, M.W. 1988, *Dynamic Terrain Inputs to Predict Structural Integrity of Ground Vehicles*, University of Michigan, Transportation Research Institute, UMTRI-88-16.

Sayers, M.W. & Karamihas, S.M. 1998, *The Little Book of Profiling: Basic Information about Measuring and Interpreting Road Profiles*, University of Michigan Transportation Research Institute.

Sek, M.A. 2001, *Optimisation of Packaging Design Through an Integrated Approach to the Measurement and Laboratory Simulation of Transportation Hazards*, Proceedings of the 12th International Conference on Packaging, Warsaw, Poland.

Semmlow, J. 2005, *Circuits, Signals and Systems for Bioengineers: A Matlab Based Introduction*, Elsevier Academic Press, USA.

Shires, D. 2011, *On the Time Compression (Test Acceleration) of Broadband Random Vibration Tests*, Journal of Packaging Technology and Science, vol. 24, no. 2, pp. 75-87.

Siviter, R. & Pollard, M.G. 1985, *Measurement of Railway Vehicle Kinematic Behaviour Using the Random Decrement Technique*, The Shock and Vibration Bulletin, vol. 55, no. 3, pp. 57-66.

Sweatman, P.F., McFarlane, S., Ackerman, C. & George, R.M. 1994, *Ranking of the Road Friendliness of Heavy Vehicle Suspensions: Low Frequency Dynamics*, Technical Working Paper No. 13, National Road Transport Commission.

Sweatman, P.F., McFarlance, S., Komadina, J. & Cebon, D. 2000, *In-Service Assessment of Road-Friendly Suspensions*, Roaduser International Pty Ltd, Melbourne.

Thrane, N. 1984, *The Hilbert Transform*, Bruel & Kjaer Technical Review No. 3, Naerum, Denmark.

U.S. DoT 2008, *American Industry Shipped 13 Billion Tons of Goods in 2007*, Brief BTS 58-08, Research and Innovative Technology Administration, Bureau of Transportation Statistics, U.S. Department of Transportation, Washington.

U.S. DoT 2010, *Freight Transportation: Global Highlights*, Research and Innovative Technology Administration, Bureau of Transportation Statistics, U.S. Department of Transportation, Washington.

Vandiver, J.K., Dunwoody, A.B., Campbell, R.B. & Cook, M.F. 1982, *A Mathematical Basis for the Random Decrement Vibration Signature Analysis Technique*, Journal of Mechanical Design, vol. 104, no. 2, pp. 307-313.

Virchis, V.J. & Robson, J.D. 1971, *Response of an Accelerating Vehicle to Random Road Undulation*, Journal of Sound and Vibration, vol. 18, no. 3, pp. 423-427.

Vogel, W. 1965, *Distribution of Wavelengths and Heights of Various Road Surfaces*, Automobile Technische Zeitschrift, vol. 67, pp. 7-11.

Weeks, M. 2007, *Digital Signal Processing using Matlab and Wavelets*, Infinity Science Press, Hingham, USA.

WPO 2008, *Market Statistics and Future Trends in Global Packaging*, World Packaging Organisation, Illinois.

Woodrooffe, J.H.F. 1995, *Heavy Truck Suspension Damper Performance for Improved Road Friendliness and Ride Quality*, SAE Technical Paper 952636.

Woodrooffe, J. 1996, *Heavy Truck Suspension Dynamics: Methods for Evaluating Suspension Road-Friendliness and Ride Quality*, SAE Technical Paper 962152.

Xu, D.M., Mohamed, A.M.O., Yong, R.N. & Caporuscio, F. 1992, *Development of a Criterion for Road Surface Roughness Based on Power Spectral Density Function*, Journal of Terramechanics, vol. 29, no. 4/5, pp. 277-486.

Appendix A

COLOURS OF NOISE

In many applications, it is useful to characterise random noise by computing the PSD function. Many random processes that occur in a wide variety of fields are able to be described by the colour of the noise. In general, the PSD of the noise is proportional to the frequency:

$$PSD(f)\,\alpha\, f^{\beta} \tag{A-1}$$

where β is an integer.

From Equation A-1, the value of the integer β will determine how the PSD function varies with frequency. The various colours of noise and the respective spectra proportional to frequency is presented *Table A-A*.

Table A-A: The noise colour, value of the integer β and a description of its spectral model.

β [-]	**General PSD Model [units^2/Hz]**	**Noise Colour**
-2	$PSD(f) = Cf^{-2}$	Brown / Red
-1	$PSD(f) = Cf^{-1}$	Pink
0	$PSD(f) = Cf^{0}$	White
1	$PSD(f) = Cf^{1}$	Blue
2	$PSD(f) = Cf^{2}$	Violet

From *Table A-A*, it is evident that brown noise decreases at a rate of two octaves in the spectrum for every octave in the frequency. White noise, arguably the most common spectral model used, has equal energy across the frequency band. The various spectra of the colours of noise are presented below. *Figure A-1* presents the spectrum for brown noise, *Figure A-2* presents the spectrum for pink noise, *Figure A-3* presents a white noise spectrum and *Figure A-4* and *Figure A-5* present the spectra for blue and violet noise, respectively. It is also important to remember that the integration or differentiation of the PSD function transforms the noise colour by a factor of 2. For instance, integrating violet noise will result in a white noise spectrum, and another integration of the spectrum would result in a brown noise spectrum.

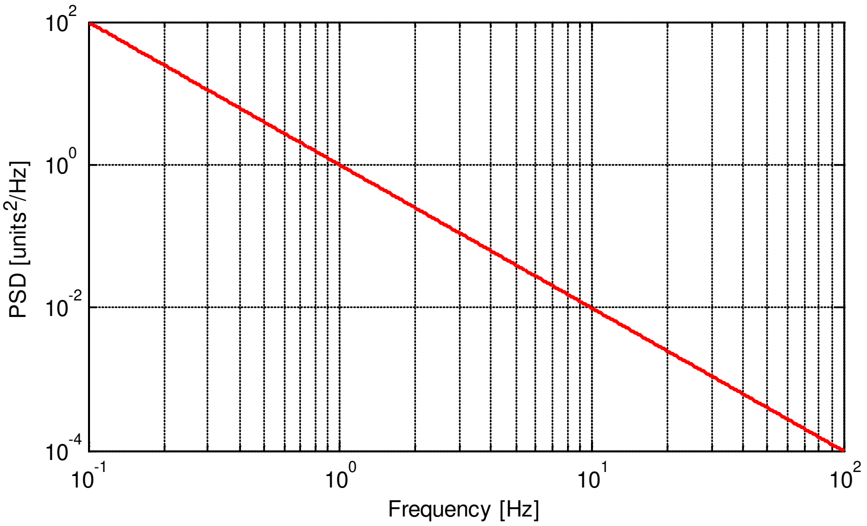

Figure A-1: Example of a brown (or red) noise spectrum.

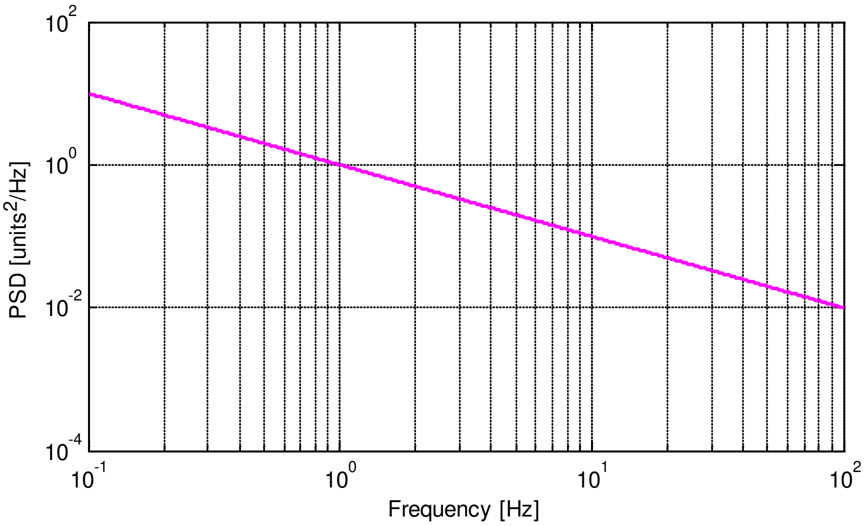

Figure A-2: Example of a pink noise spectrum.

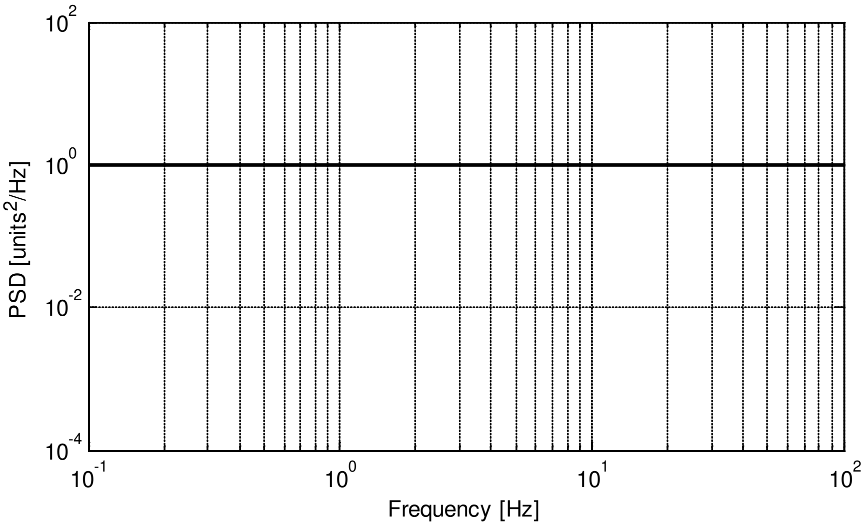

Figure A-3: Example of a white noise spectrum.

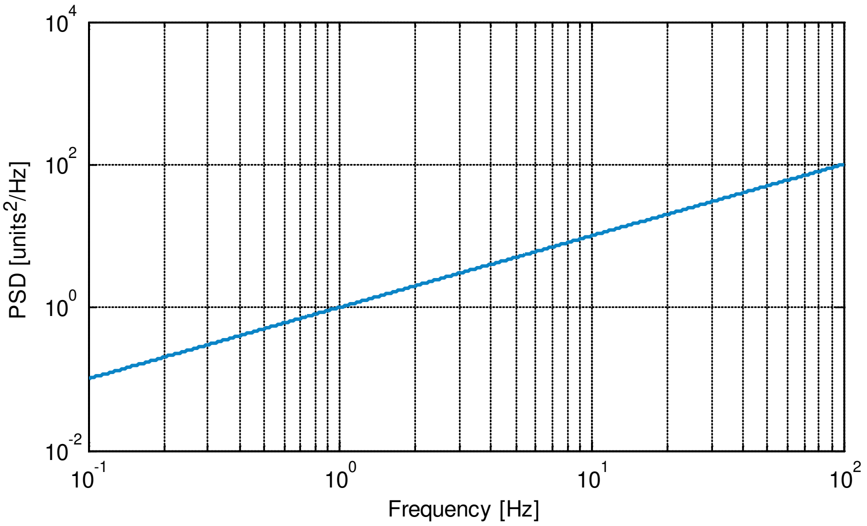

Figure A-4: Example of a blue noise spectrum.

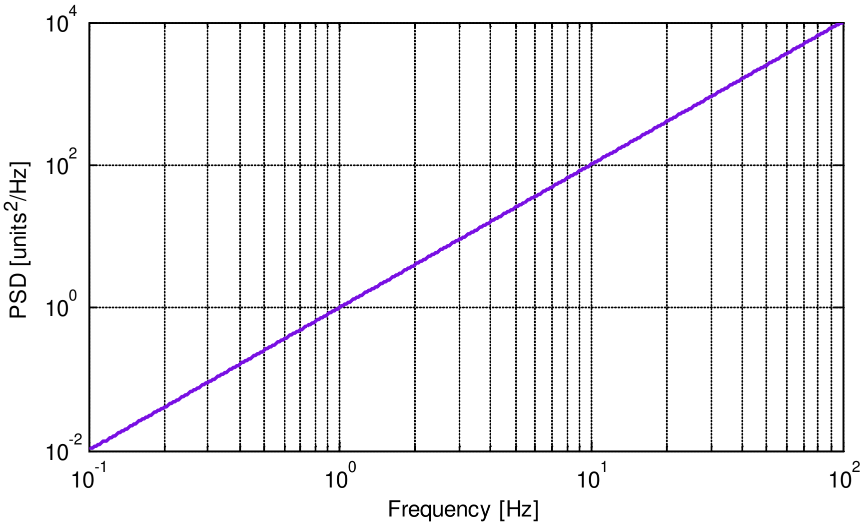

Figure A-5: Example of a violet noise spectrum.

While band-limited white noise acceleration is one of the most commonly used spectral shapes, it does not always provide a realistic representation of the environment. In practice, modern vibration controllers can be programmed to use almost any type of spectrum to excite a system, whether it is defined by the operator or measured in the field. For the simulation of a typical longitudinal pavement elevation profile, the spectral model outlined under ISO standard 8608 (1995) is often used. The ISO 8608 spectral model, described in terms of the colours of noise is:

- Pavement displacement PSD function – brown noise.
- Pavement velocity PSD function – white noise.
- Pavement acceleration PSD function – violet noise.

Appendix B

SHOCK ABSORBER CHARACTERISATION

The experimental results presented in Chapter 6 revealed that the SWEV-A (original configuration) exhibits significant nonlinear characteristics. The vehicle was dismantled and the spring and original factory-fitted shock absorber were individually evaluated. The spring was found to be near-linear within the expected range of operation (r^2 = 0.999), isolating the shock absorber as the primary candidate for the nonlinear behaviour. The factory-fitted shock absorber was subjected to a range of excitations to evaluate and identify any nonlinear characteristics. The nominally linear shock absorber in the SWEV-B configuration was also subjected the same series of tests for comparison.

B.1 EXPERIMENTAL PROCEDURE

Considering the shock absorber's role and operation, there are at least four parameters of the motion of the shock absorber that require consideration – direction of stroke (compression and extension), displacement, velocity and frequency. With a universal testing machine available, it was decided to mount the shock absorbers (one at a time) into the machine and subject them to various excitations (whilst simultaneously measuring the force and displacement using in-built transducers) to investigate the effect of the various parameters on the two shock absorbers. One important consideration is the shock absorber temperature during testing. Previous studies have suggested that shock absorber temperature "appears to have only a small effect on the shock absorber effectiveness as measured by a dynamometer" (Sweatman *et al.* 2000). The effect of temperature was investigated using a surface temperature sensor and it was found that the change in temperature experienced during laboratory and in-service experiments was negligible. For each test, the shock absorber began at mid-stroke and the velocity was limited by the universal testing machine (approximately 400 mm/s).The experimental arrangement of the shock absorber tests (for both shock absorbers) is presented in *Figure B-1*, with the shock absorber A shown mounted in the universal testing machine.

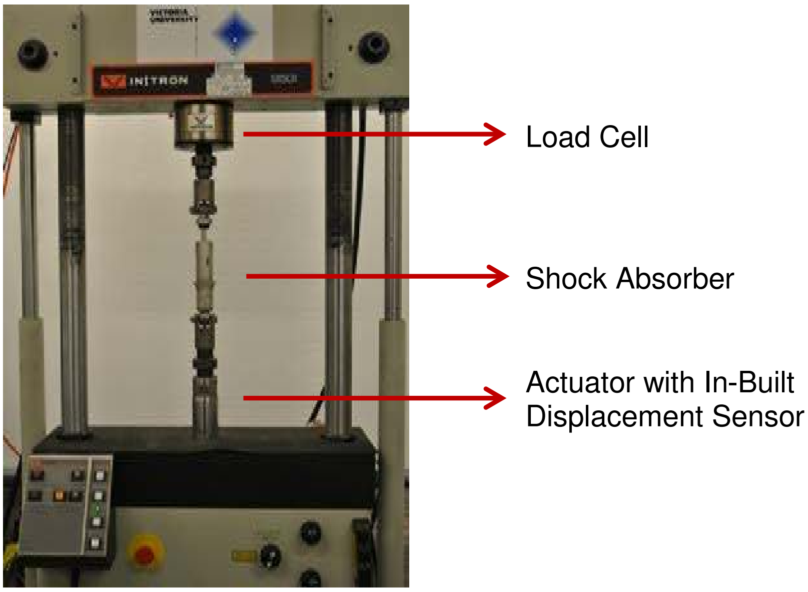

Figure B-1: Experimental arrangement of the shock absorber characterisation tests, shown with the factory-fitted shock absorber mounted in the universal testing machine.

A range of excitation functions and parameters were used in an attempt to reveal the behaviour of the shock absorber under various operational conditions. The first excitation was a triangular displacement waveform, or constant-velocity actuation, at an arbitrary frequency of 5 Hz. The sustained compression and extension amplitudes used were 2, 4, 6, 8 and 10 mm and each test was undertaken for duration of 20 seconds. The measured force was filtered using a 5th order Butterworth low-pass filter with a cutoff frequency of 80 Hz. To establish the velocity, the displacement signal was differentiated to obtain the velocity and the measured force is divided by the velocity to obtain the damping coefficient. The shock absorber was then subjected to sinusoidal displacement at an arbitrary frequency of 5 Hz and various amplitudes of 1, 2, 4, 6, 8 and 10 mm were used over a short period of time to prevent a significant temperature change in the shock absorber (total duration of 30 seconds for each excitation).

Finally, the shock absorber was subjected to three displacement sinusoids with different frequency and amplitude combinations to investigate the damping coefficient over the same velocity range. The frequencies and amplitudes investigated were 6 Hz and 10 mm, 12 Hz and 5 mm and finally 30 Hz and 2 mm. These tests were also undertaken for a total duration of 30 seconds. For the sinusoidal displacement excitations, the damping coefficient was computed as a function of velocity by computing the Secant slope of the force-velocity relationship. The final test was to subject the shock absorber to a band-limited violet noise acceleration excitation (band-limited between 0.5 – 50 Hz) at various excitation intensities and the results presented are for an rms intensity of 2.5 m/s^2 and 3.0 m/s^2 for shock absorber A and B, respectively.

B.2 EXPERIMENTAL CHARACTERISATION

The experimental characterisation results for both the original factory-fitted (A) and third party, nominally linear shock absorbers (B) are presented herein.

B.2.1 Constant-Velocity Actuation

The first test undertaken was to subject the shock absorber to constant-velocity actuation for various displacement amplitudes at an arbitrarily chosen frequency of 5 Hz. *Figure B-2* shows the time-history of the displacement excitation and force response of shock absorber A during the triangular displacement test (2 mm amplitude). The triangular displacement waveform applies a constant velocity during both compression and extension of the shock absorber. For each constant-velocity test, the damping coefficients were calculated for both the extension and compression strokes and are compiled in *Figure B-3*. This figure illustrates the inherently nonlinear nature of shock A, and indicates that the damping produced varies significantly depending on not only the velocity but also the direction of travel or motion. The damping produced by shock B is, as expected, far more consistent and is largely unaffected by the direction of stroke or the velocity.

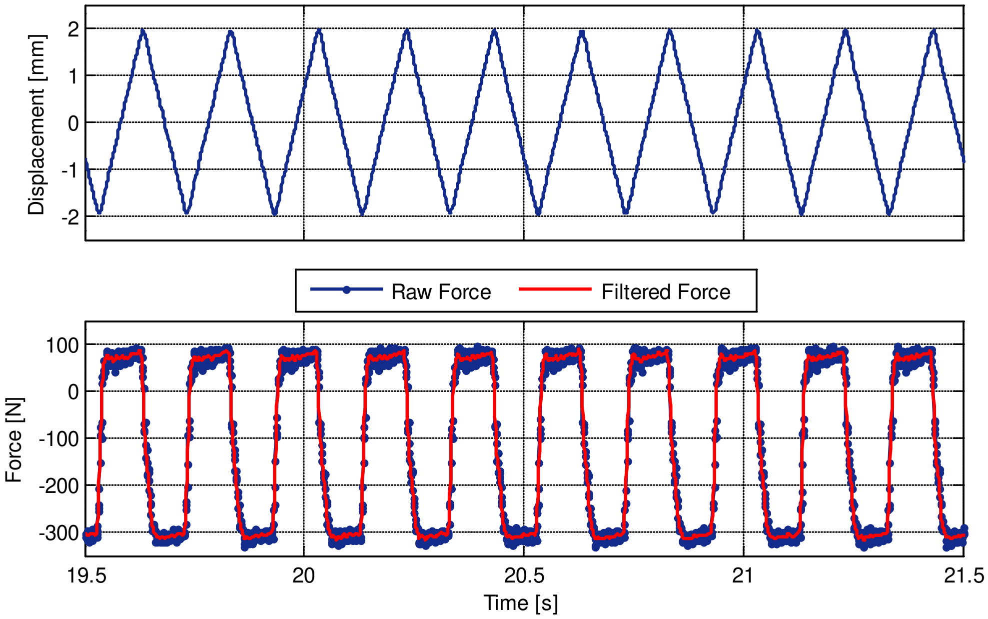

Figure B-2: Sample time-history of the measured displacement (top) and the raw and filtered force (bottom) from shock absorber A subjected to a constant-velocity actuation (frequency 5 Hz, amplitude 2 mm).

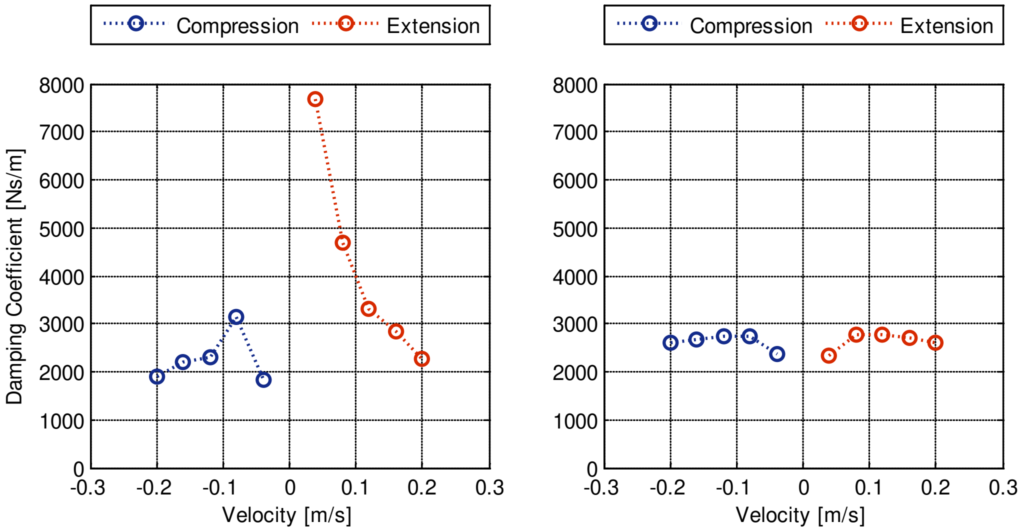

Figure B-3: Damping-velocity relationship for shock absorbers A (left) and B (right) subjected to various constant-velocity actuations (frequency 5 Hz).

B.2.2 Sinusoidal Displacement: Fixed Frequency at Various Amplitudes

The next excitation was a sinusoidal displacement (frequency of 5 Hz) at amplitudes of 1, 2, 4, 6, 8 and 10 mm to investigate the effect of the maximum displacement from mid-stroke. The measured force-velocity for a single compression and extension stroke of each shock absorber at each excitation amplitude are shown in *Figure B-4*. There is a significant difference in the slope of the force-velocity curves for shock absorber A, but the results from shock B are much more consistent in their slope. It is important to note that when calculating the damping coefficient from the force-velocity measurements, the slope from the origin (Secant) is used.

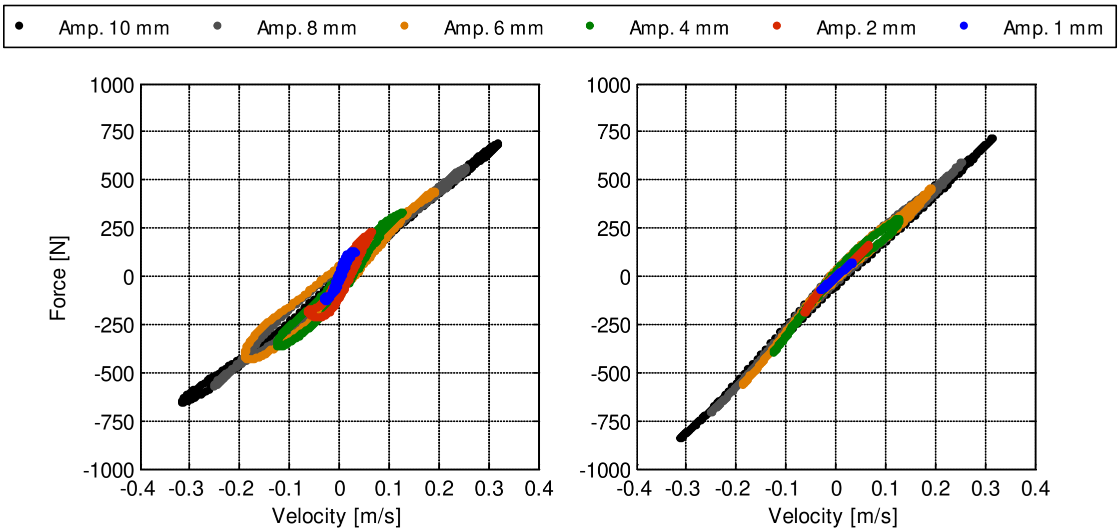

Figure B-4: The force-velocity relationship over a stroke of compression and extension for shock absorbers A (left) and B (right) subjected to sinusoidal displacement at various amplitudes (frequency 5 Hz).

The calculated damping-velocity relationships for both of the shock absorbers are presented in *Figure B-5*. Around the low velocity region there is some expected variation, however it is clear that the linear shock absorber B could be modelled with an equivalent value of 2500 Ns/m for all excitation amplitudes. The same is not possible for shock absorber A, providing another illustration of its inherent nonlinear nature. While the damping coefficient approaches extremely high values as the velocity approaches zero, the actual force produced by the shock absorbers at these low velocities are much less than what is produced at higher velocities.

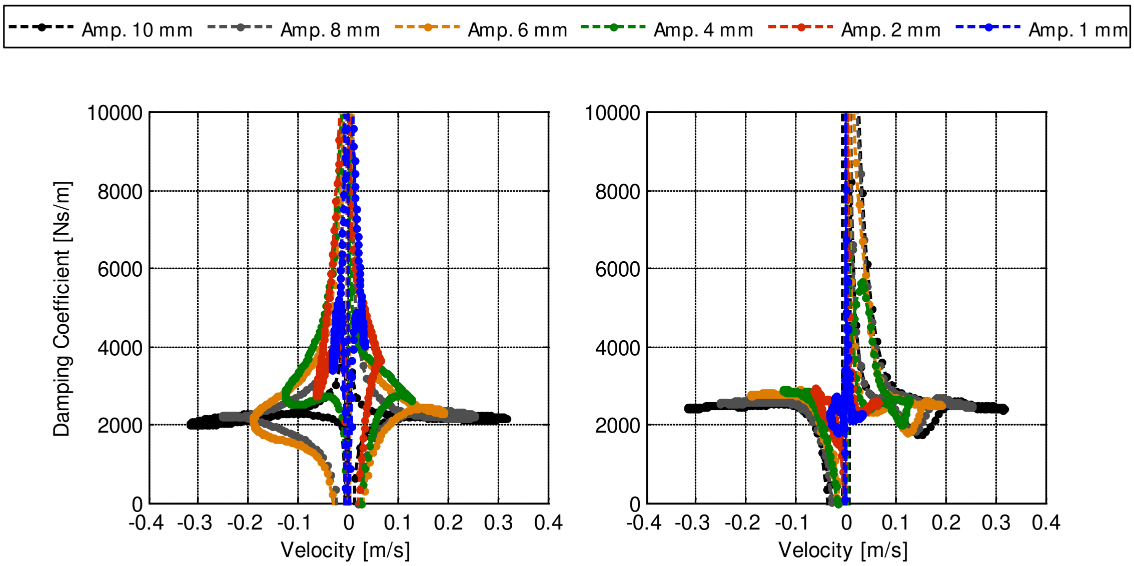

Figure B-5: Damping-velocity relationship for shock absorbers A (left) and B (right) subjected to sinusoidal displacement at various amplitudes (frequency 5 Hz).

B.2.3 Sinusoidal Displacement: Various Frequency-Amplitude Combinations

The next test was to subject the shock absorbers to three sinusoidal displacements with differing frequency-amplitude combinations to cover the same velocity range. *Figure B-6* shows the force-velocity for a single stroke of compression and extension for both shock absorbers A and B for the three sinusoidal displacements with varying frequency-amplitude combinations. Both shock absorbers show some variation between the measured force and the 30 Hz, 2 mm amplitude excitation for shock absorber A significantly changes shape compared to the other two excitations.

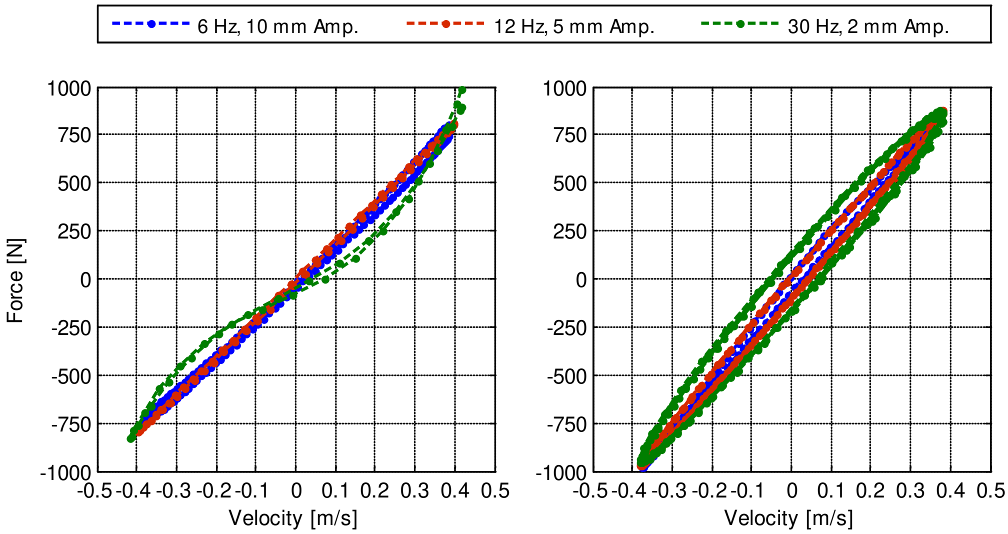

Figure B-6: The force-velocity relationship over a stroke of compression and extension for shock absorbers A (left) and B (right) subjected to sinusoidal displacement for various frequency-amplitudes combinations.

The damping-velocity relationships for both shock absorbers calculated from *Figure B-6*, are presented in *Figure B-7*. While the considerably nonlinear nature of shock absorber A is evident in this figure, it is interesting to note that the third-party, nominally linear shock absorber B also exhibits significant variation in the estimated damping. This also indicates that both of the shock absorbers are dependent on the frequency applied, not only the velocity and displacement.

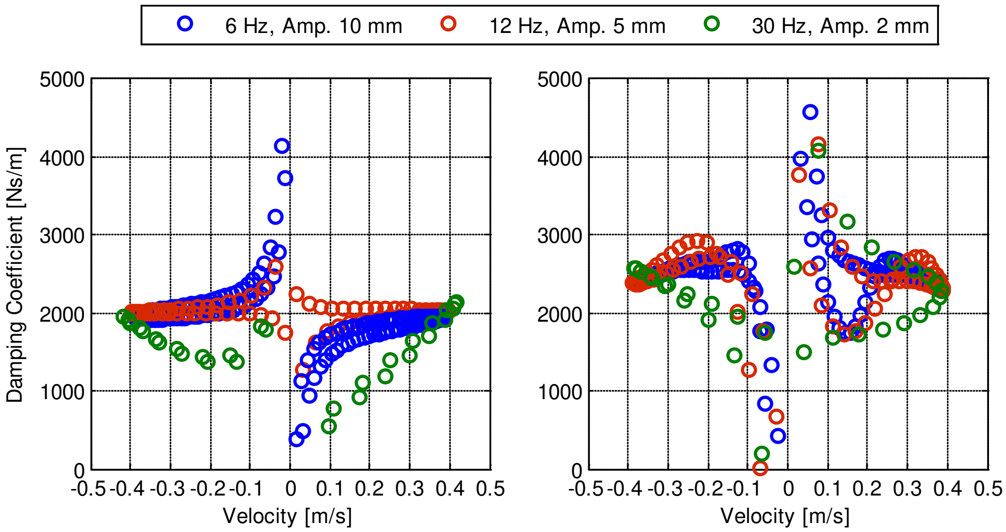

Figure B-7: The damping-velocity relationship for shock absorbers A (left) and B (right) subjected to sinusoidal displacement for various frequency-amplitudes combinations.

B.2.4 Random Vibration Excitation

The final test was to subject the shock absorber to random vibration, specifically violet noise acceleration (representative of longitudinal pavement profiles). These tests were aimed at investigating the statistical nature of the response of the force produced by the shock absorbers. The tests for both shock absorbers were undertaken at different times and the rms intensities were different. All the results produced similar results and so for comparison only the force response from one excitation rms intensity for each shock absorber is presented. The measured force PDFs of the shock absorbers A and B subjected to an excitation rms intensity of 2.00 m/s^2 and 3.00 m/s^2, respectively, are shown along with the best Gaussian fits in *Figure B-8*. While the excitation applied to the shock absorber was Gaussian, the response for shock absorber A is clearly not Gaussian. The shape of the distribution is bimodal; indicating the compression and extension strokes of shock absorber A. The statistical response of shock absorber B approaches a Gaussian distribution.

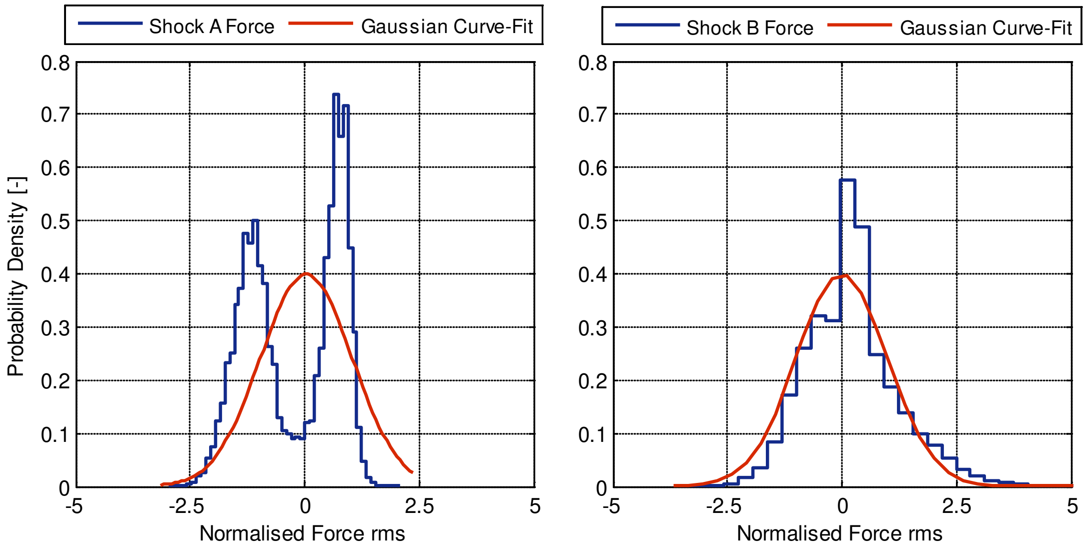

Figure B-8: PDFs of the force response of shock absorbers A (left) and B (right) subjected to random vibration acceleration (violet noise) at rms intensities of 2.5 m/s^2 and 3.0 m/s^2, respectively.

The custom-made nominally linear shock absorber exhibited marginal nonlinear behaviour compared to the original factory-fitted shock absorber. The results presented illustrate the difficulties in accurately modelling the behaviour of shock absorbers and further work is required to be able to adequately characterise shock absorbers for use in numerical simulations by accounting for displacement, velocity, frequency and stroke direction dependence. These tests also serve to demonstrate the implications of using a nonlinear shock absorber to establish a single, or true, estimate of the dynamic characteristics.

B.3 STATISTICAL NATURE OF SHOCK ABSORBER VELOCITY

A further investigation into the statistical nature of the shock absorbers was undertaken during a series of vibration table experiments (excitation-response), where the actual velocity of the shock absorber was measured. The dynamic motion of the shock absorber was measured using two accelerometers; one at the top and one at the base of the shock-spring. The relative velocity was measured for both shock absorbers as the SWEV was subjected to violet noise acceleration at rms intensities of 3.00, 6.00 and 9.00 m/s^2. The time-histories and PDFs of the relative velocity of the factory-fitted shock absorber, part of the SWEV-A configuration, measured during the experiments are presented in *Figure B-9*, *Figure B-10* and *Figure B-11* for rms intensities of 3.00, 6.00 and 9.00 m/s^2, respectively.

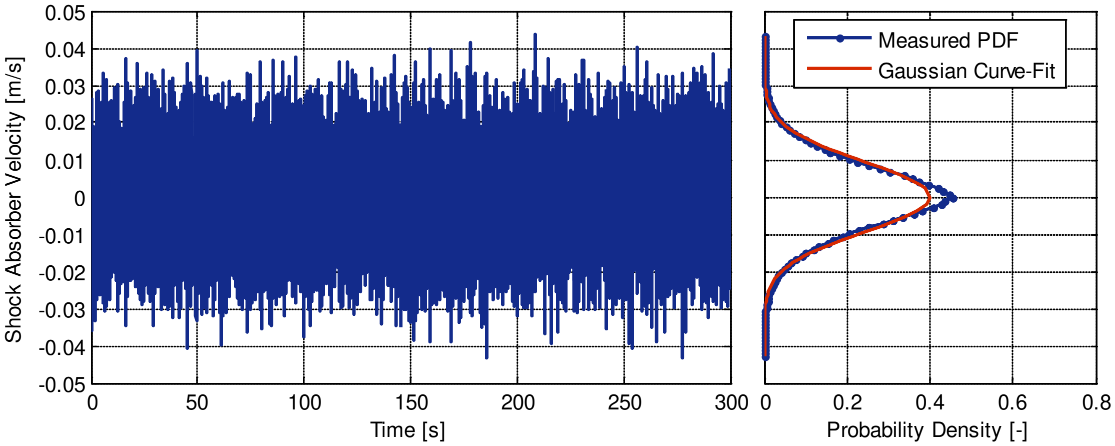

Figure B-9: The relative velocity of the factory-fitted shock absorber in the SWEV-A measured during the laboratory experiments (Excitation: violet noise 3.00 m/s^2 rms).

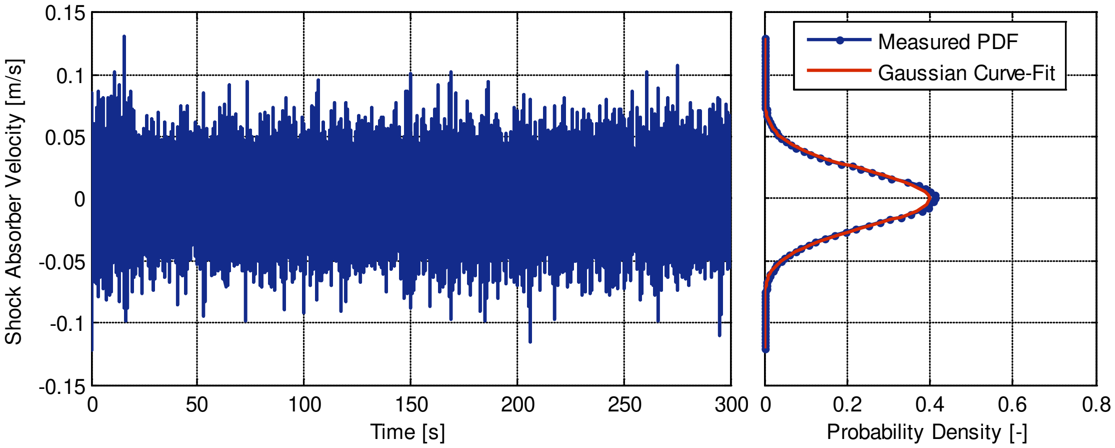

Figure B-10: The relative velocity of the factory-fitted shock absorber in the SWEV-A measured during the laboratory experiments (Excitation: violet noise 6.00 m/s^2 rms).

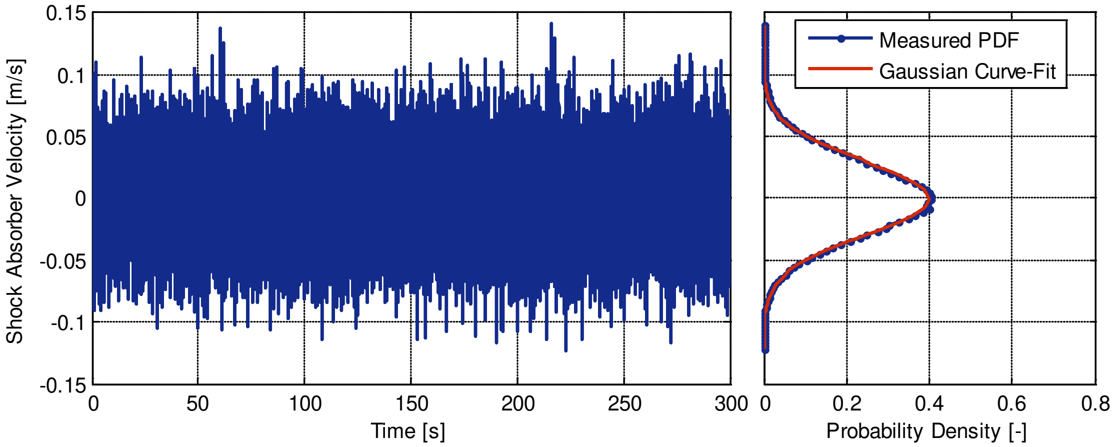

Figure B-11: The relative velocity of the factory-fitted shock absorber in the SWEV-A measured during the laboratory experiments (Excitation: violet noise 9.00 m/s^2 rms).

The established PDFs of the velocity of shock absorber A do not reveal any unusual behaviour in its operation. For the custom-made, nominally linear shock absorber, the time-history and PDF of the relative velocity are presented in *Figure B-12*, *Figure B-13* and *Figure B-14* for the different rms intensities of 3.00, 6.00 and 9.00 m/s^2, respectively. Unlike the factory-fitted shock, there is an interesting characteristic of the established PDFs for shock absorber B. At zero-velocity, there are a significantly greater number of occurrences and may be due to the shock absorber having difficulty changing the direction of stroke.

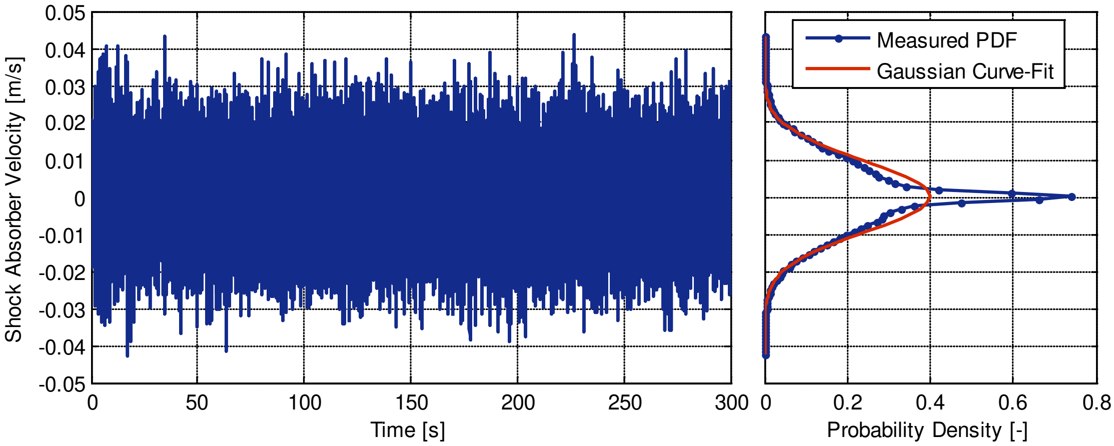

Figure B-12: The relative velocity of the nominally linear shock absorber in the SWEV-B measured during the laboratory experiments (Excitation: violet noise 3.00 m/s^2 rms).

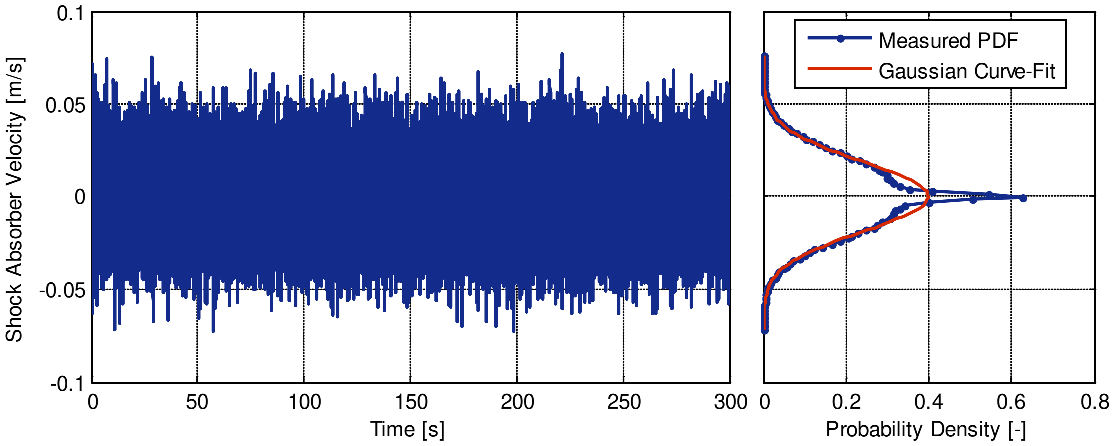

Figure B-13: The relative velocity of the nominally linear shock absorber in the SWEV-B measured during the laboratory experiments (Excitation: violet noise 6.00 m/s^2 rms).

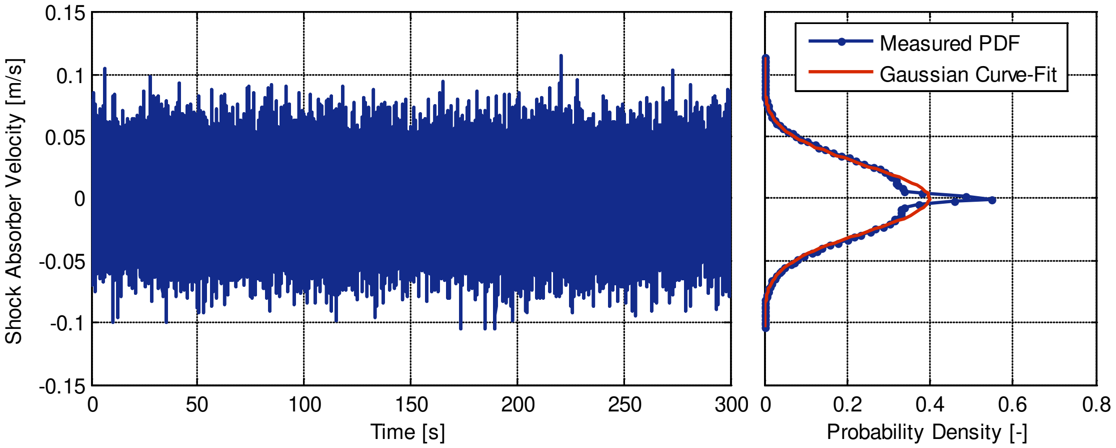

Figure B-14: The relative velocity of the nominally linear shock absorber in the SWEV-B measured during the laboratory experiments (Excitation: violet noise 9.00 m/s^2 rms).

The various characterisation and investigation tests undertaken demonstrate the significant differences in the behaviour of the factory-fitted shock absorber A and the custom-designed nominally linear shock absorber B. The dependency of the shock absorbers on frequency, velocity and direction of stroke illustrate their complex behaviour is not easily characterised. The custom-made nominally linear shock absorber, while easier to characterise than the factory-fitted shock absorber, is still complex in its operation, as shown in the established relative velocity PDFs. The nonlinear behaviour of the factory-fitted shock absorber makes it difficult to obtain a single estimate of the vehicle's FRF, let alone predicting the response of the component itself.

B.4 SHOCK ABSORBER PUMPING AND FRF ESTIMATES

For the second series of in-service experiments, the FRFs of the SWEV-A and SWEV-B configurations loaded with 50 kg of dead weight were established. The vehicles were excited with a violet noise acceleration spectrum at various rms intensities. During these experiments, it was found that the condition of the shock absorber plays an integral role in the level of damping. If the shock absorber is left unused for a significant period of time, it is widely acknowledged that it should be pumped up prior to use. Both of the shock absorbers were removed from the vehicle and left for a period of time and were then installed on the vehicle (one at a time) and the FRFs were established. After a second period of inactivity for the shock absorbers, they were then manually pumped prior to their installation and the FRFs were again established.

The FRFs established for SWEV-A (50 kg) excited with violet noise at various intensities with and without pumping prior to the measurements are presented in *Figure B-15*. From the figure it is interesting to note that the rms intensity of 3.00 m/s^2 does not produce a significant response around the sprung mass resonance frequency compared to the other two excitations. This may be due to the decreased mass loading compared to previous FRFs establish or the low level of excitation The FRF established from the 6.00 m/s^2 rms excitation exhibits far less damping than the 9.00 m/s^2 rms excitation, despite what was to be expected from the previous FRFs established (SWEV configuration loaded with 100 kg). It was believed that the cause of these unexpected FRFs was that the shock required pumping to remove any air pockets and allow the fluid to flow in order to operate correctly. After pumping the shock absorber, it was noted that FRF established from the 3.00 m/s^2 rms excitation is again significantly different to the FRFs established from the 6.00 and 9.00 m/s^2 rms excitations.

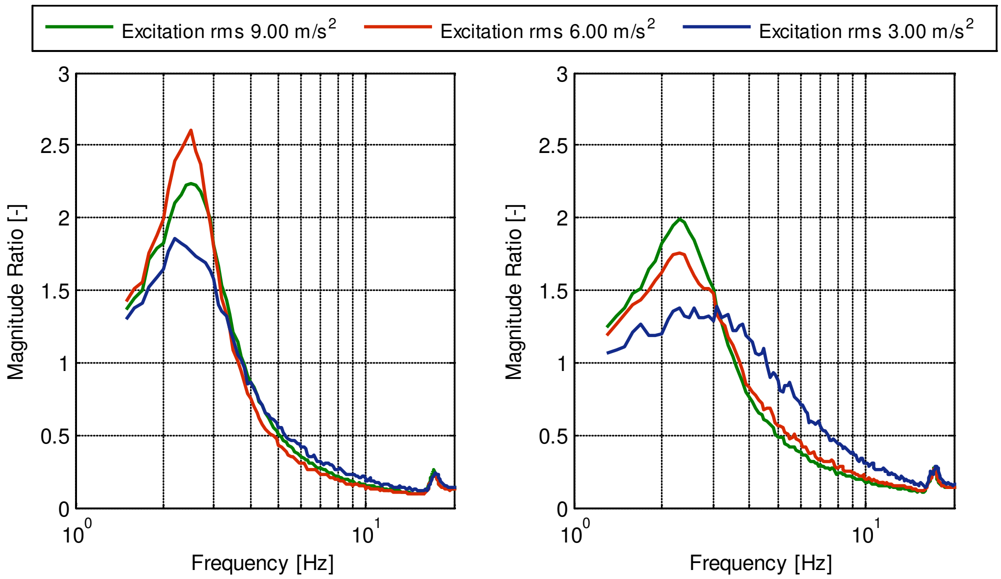

Figure B-15: The established FRFs for the SWEV-A (50 kg) without (left) and with (right) pumping of the shock absorber prior to testing, subjected to violet noise excitation at various rms intensities.

The same procedure was repeated for the nominally linear shock absorber. The FRFs established with and without pumping the shock absorber for SWEV-B (50 kg) are presented in *Figure B-16*. As with the SWEV-A, the FRF established from the 3.00 m/s^2 rms excitation exhibits a significantly higher damping ratio than the FRFs from the 6.00 and 9.00 m/s^2 rms excitations.

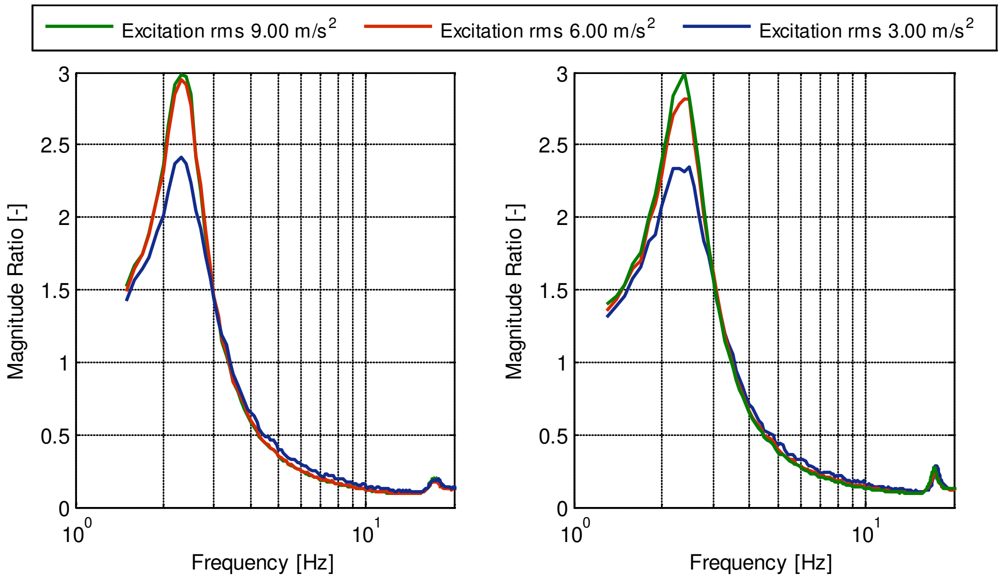

Figure B-16: The established FRFs for the SWEV-B (50 kg) without (left) and with (right) pumping of the shock absorber prior to testing, subjected to violet noise excitation at various rms intensities.

The estimated FRFs do not significantly vary before and after pumping for the SWEV-B configuration compared to the changes observed from the SWEV-A. While pumping the nominally linear shock absorber in SWEV-B yielded no significant change in the established FRFs, the factory-fitted shock absorber in the SWEV-A produced significantly different FRFs. These tests serve to illustrate the difficulty in obtaining consistent estimates of the dynamic characteristics of road vehicles with shock absorbers that are often complex in nature. If a vehicle was evaluated with shock absorbers that performed similarly to the factory-fitted shock in SWEV-A, a different FRF may be established depending on a variety of factors such as whether the vehicle was driven prior to the experiments, or if the shock absorbers were pumped prior to their installation.

Appendix C

INERTIAL PROFILOMETER CONFIGURATION AND CALIBRATION

This appendix is concerned with the development of an in-built inertial profilometer on the SWEV to measure the pavement profile during the in-service experiments. Despite road authorities measuring road profiles on a regular basis, the SWEV travels between the left and right wheel tracks that are measured. The SWEV must be able to measure the longitudinal pavement elevation profile along the actual wheel track during the in-service experiments.

C.1 THE SWEV INERTIAL PROFILOMETER

During the initial design and conception stage of the SWEV, it was anticipated that the use of a profilometer system mounted onto the vehicle may be beneficial for the in-service experiments to measure not only the actual excitation but also to establish the actual vehicle transmissibility for each experimental run. The SWEV was designed with the potential to simultaneously operate as an inertial profilometer, capable of measuring the excitation applied to the SWEV during the in-service experiments. In order to operate as an inertial profilometer, the SWEV is equipped with three additional sensors:

1) Laser displacement sensor.
2) Accelerometer mounted on the laser.
3) Wheel encoder to measure the cumulative displacement of the vehicle.

An illustration of the three sensors mounted onto the SWEV is presented in *Figure C-1*.

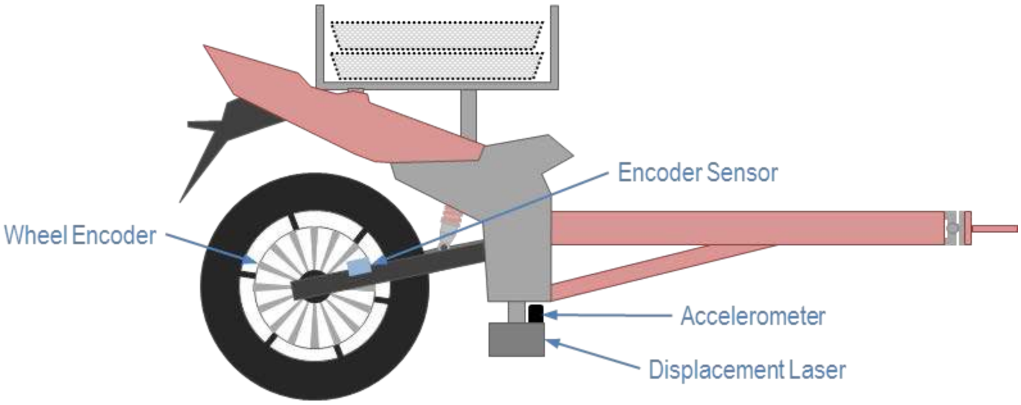

Figure C-1: The SWEV with the profilometry sensors labelled.

High speed inertial profilometers are widely-used for numerous applications and it is important to establish their accuracy. While ASTM E950-98 is the most widely used method to rate the repeatability and accuracy of a profilometer, the gain, or transfer function, of the system can also be used to evaluate the accuracy of the profilometer.

C.2 PROFILOMETER CALIBRATION METHODOLOGY

The main operational limitation of the profilometer is the frequency range, which is 1 – 50 Hz. In order to test and calibrate the inertial profilometer system on the SWEV, three steps must be undertaken.

1) Calibration of Equipment.

The first step is to calibrate each of the individual sensors used as part of the profilometer system, along with the reference measurement sensors. First, the laser displacement sensor on the SWEV is calibrated, then the DCDT displacement sensor in-built into a large-scale vibration table is calibrated as it will be used to measure the actual profile during the profilometer calibration tests. The DCDT displacement sensor will be calibrated using the laser displacement sensor on the SWEV. The two accelerometers (one to measure the sprung mass acceleration and the other to measure the acceleration of the laser displacement sensor) also require calibration. The accelerometers are calibrated by mounting the accelerometers on a vibration table along with a calibration accelerometer with a known sensitivity (independently calculated) and excite the table with random vibration. Computing the FRF of the two accelerometers, provided their calibration factors are correct, will yield a magnitude of one (1) across the relevant frequency bandwidth. Any deviation from one is due to an incorrect sensitivity and is adjusted until the magnitude is one to find the calibrated value of the sensitivity.

2) Simple Profilometer Tests.

Once the various sensors have been calibrated, the profilometer will be subjected to two basic tests as an initial evaluation of the profilometer. If the profilometer is unable to successfully replicate these two tests, then the complex measurement of a pavement profile will not be possible. The first test undertaken is designed to test the laser displacement sensor by sliding a geometric obstacle along the floor underneath the laser, and therefore the profile obtained is expected to take the same shape as the geometric obstacle. The second test is to induce a series of slow vibration into the SWEV to test both the laser displacement sensor and the accelerometer, with the resulting profile expected to be level with no undulations.

3) Advanced Profilometer Tests.

The profilometer will be calibrated using a large-scale servo-hydraulic vibration table and the DCDT displacement sensor built into the table will be measured to obtain the actual profile for reference. The ability of the profilometer to measure both sine-sweep and random vibration excitations will be evaluated. The random vibration spectrum to be used is violet noise acceleration at different rms intensities.

4) Calibration of the Wheel Encoder.

Finally, the wheel encoder must be calibrated to measure the cumulative distance over the elevation measurements during operating. To calibrate the wheel encoder, an exact distance along a road is measured and identified by placing two small obstacles at either end (so the laser of the profilometer can detect the beginning and end). The profilometer is then driven along the road whilst simultaneously measuring the wheel encoder pulses and laser displacement, from which the dynamic radius of the tyre can be calculated.

C.3 PROFILOMETER EXPERIMENTAL CALIBRATION

This section describes the experimental calibration of the various sensors and the profilometer tests to measure known excitations.

C.3.1 Individual Sensor Calibration

First, the individual sensors require calibration to establish their sensitivities. The sensors to be calibrated are:

- M5L laser displacement sensor (on the SWEV).
- DCDT displacement sensor (built into a large-scale vibration table).
- Two SD 2260 accelerometers.

The calibration of the M5L laser displacement sensor was undertaken first. Once the location of zero voltage has been found, the relative displacement and voltage between ± 10 V is measured. The zero voltage was found to be at a distance of 206 mm; which is the distance that the sensor must be positioned from the ground in the SWEV. The calibration chart in *Figure C-2* shows the relationship between the relative displacement and the voltage output by the M5L laser displacement sensor.

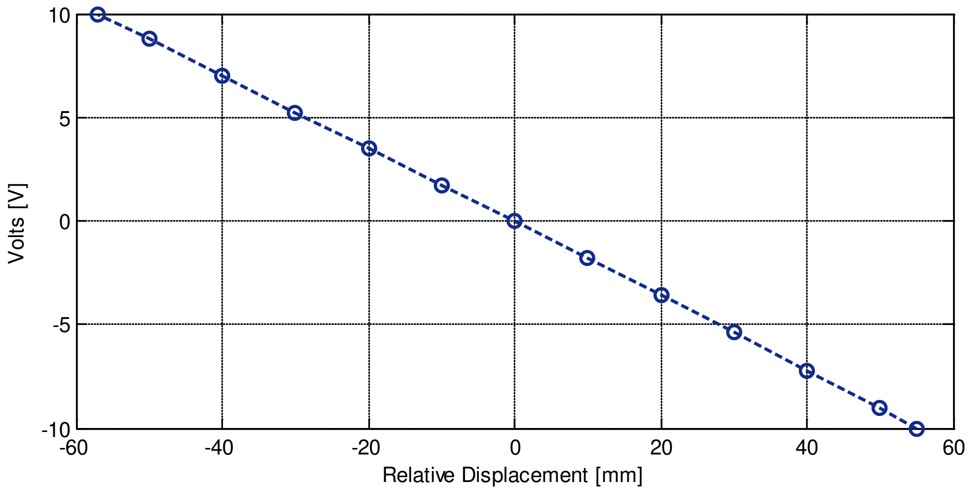

Figure C-2: The relationship between the relative displacement and the output voltage from the M5L laser displacement sensor.

Next, the DCDT displacement sensor in the vibration table (which will be used to measure the actual elevation profile for calibration of the profilometer system) must be calibrated using the calibrated laser displacement sensor. The calibration chart for the DCDT laser displacement sensor is presented in *Figure C-3*.

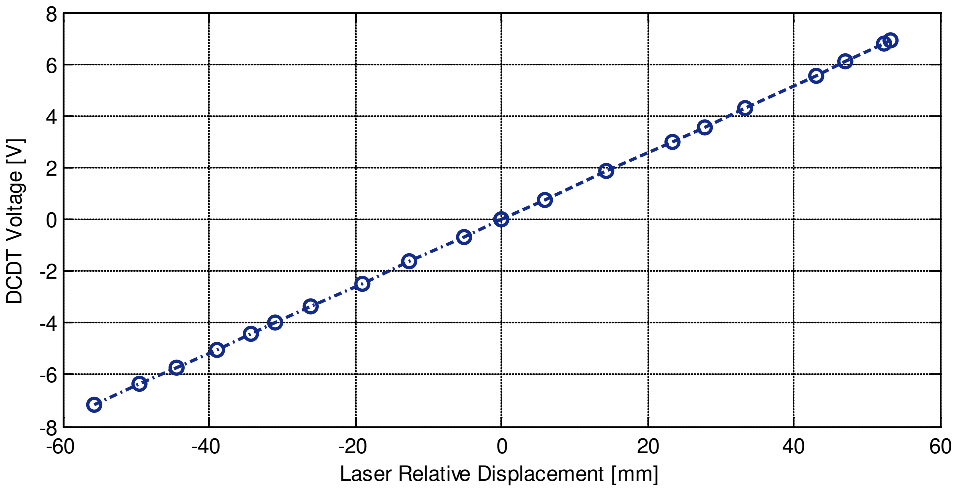

Figure C-3: The relationship between relative displacement and the output voltage from the DCDT displacement sensor in the vibration table.

The final sensors to be calibrated are the two SD 2260 accelerometers (1661 and 1696). During the in-service experiments the 1661 measures the sprung mass vibration, while the 1696 is mounted onto the laser displacement sensor for the profilometer. The accelerometers were subjected to band-limited white noise and a calibration accelerometer was used for reference. The FRFs of the calibration accelerometer to the 1661 and the 1696 accelerometers were computed. Both accelerometers were calibrated between the profilometer operational frequency range of 1 – 50 Hz. The final calibrated sensitivities of the sensors are presented in *Table C-A*.

Table C-A: The calibrated sensitivities of the various sensors.

Sensor	**Sensitivity**
M5L Laser Displacement Sensor	5.614 mm/V
DCDT Displacement Sensor	7.768 mm/V
SD 2260 Accelerometer (1661)	0.4117 V/g
SD 2260 Accelerometer (1696)	0.3875 V/g

C.3.2 Profilometer Calibration

The first test undertaken is to simply slide a geometric object (wood block) back and forth along the ground underneath the laser displacement sensor attached to the SWEV. This preliminary test will ensure that the laser and accelerometer operate correctly; if the estimated profile of the block of wood is unable to be measured then there is no point continuing with further tests. The black of wood was slid along the floor underneath the laser twice and the estimated profile is shown in *Figure C-4*. From the figure, it is evident that the laser and accelerometer function reasonably well; the profile of the block of wood is easily identified. One side of the block of wood was quite coarse and resulted in some distortion in the estimated profile.

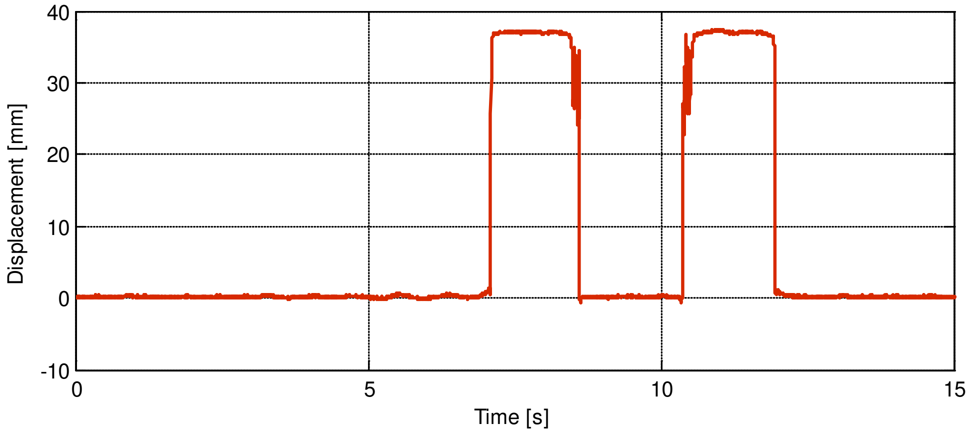

Figure C-4: Displacement from the block-slide test of the vibration table displacement (blue) and profilometer laser (red).

The second test involves inducing a series of vibration (by the operator) into the sprung mass of the vehicle. This test will indicate the ability of the laser and accelerometer to reconcile with the actual profile (flat line). The time history of the actual and estimated profiles from the slow vibration test is shown in *Figure C-5*. The estimated profile appears to match the actual profile reasonably well, although there is some slight distortion in the displacement, particularly between 2 - 5 s, with the rms error 0.289 mm.

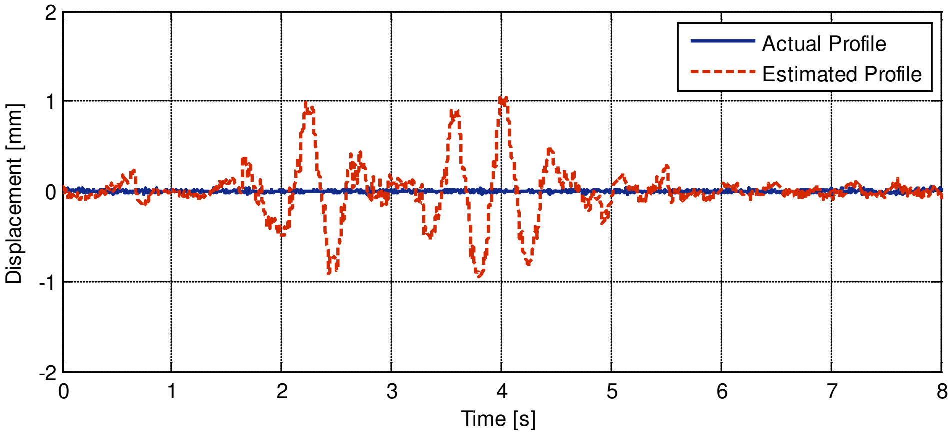

Figure C-5: Displacement from the slow-vibration test of the vibration table displacement (blue) and profilometer laser (red).

With the profilometer able to replicate the actual profile for the two simple tests reasonably well, the SWEV was placed on a large-scale vibration table and subjected to a sine-sweep between 2 – 50 Hz. A sample time history of the actual and estimated profiles from the sine-sweep excitation is presented in *Figure C-6*. The error of the estimated profile was then calculated, shown in *Figure C-7*, and never exceeds 1 mm. The rms error between the actual and estimated profiles is 0.191 mm, which is an improvement compared to the rms error from the slow vibration test.

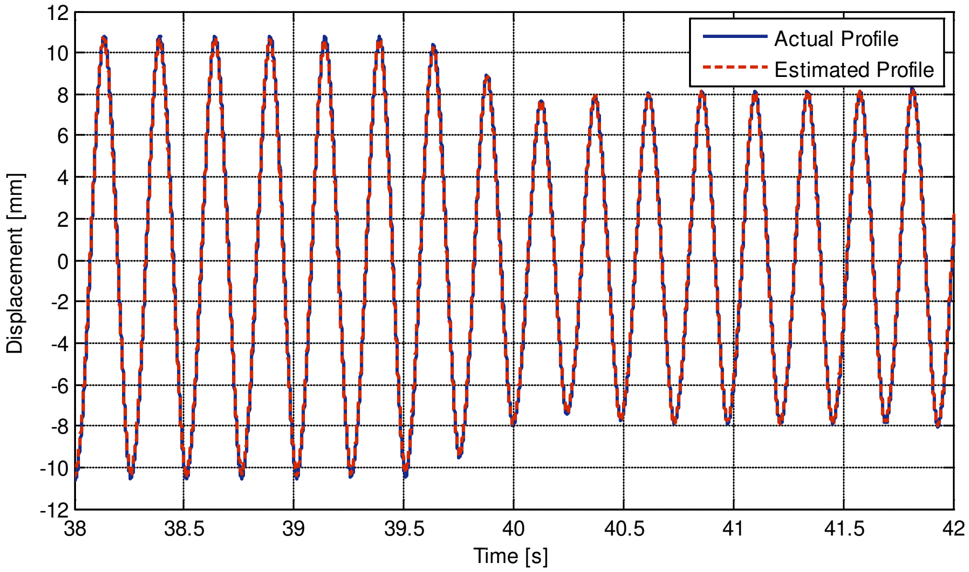

Figure C-6: Sample time history of the actual (blue) and estimated (red) profiles for a swept-sine excitation from 2 – 50 Hz.

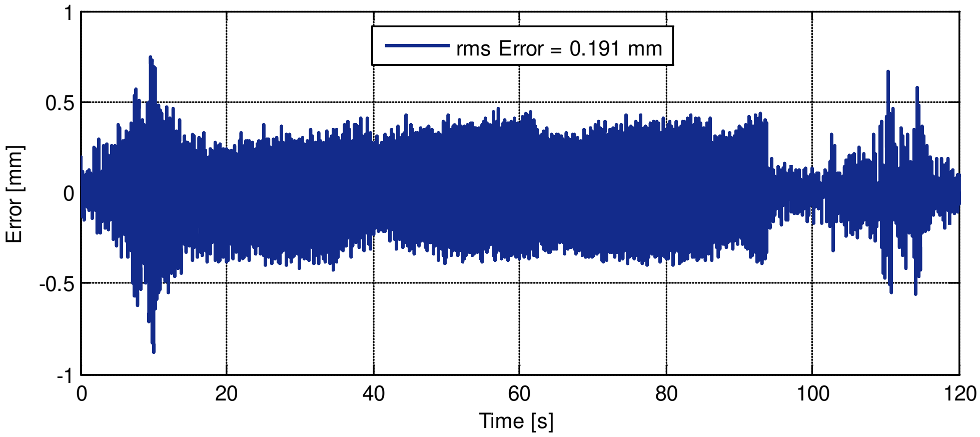

Figure C-7: Time history of the error between the actual and estimated profiles for a swept-sine excitation from 2 – 50 Hz.

The final test for the evaluation of the profilometer system is to subject the vehicle to random vibration, specifically a violet noise acceleration spectrum at two distinct rms intensities of 1 and 2 g (frequency range: 1 – 50 Hz). The excitation rms of 1 g is first examined; a sample of the time history of the displacement of the actual and estimated profiles given in *Figure C-8*.

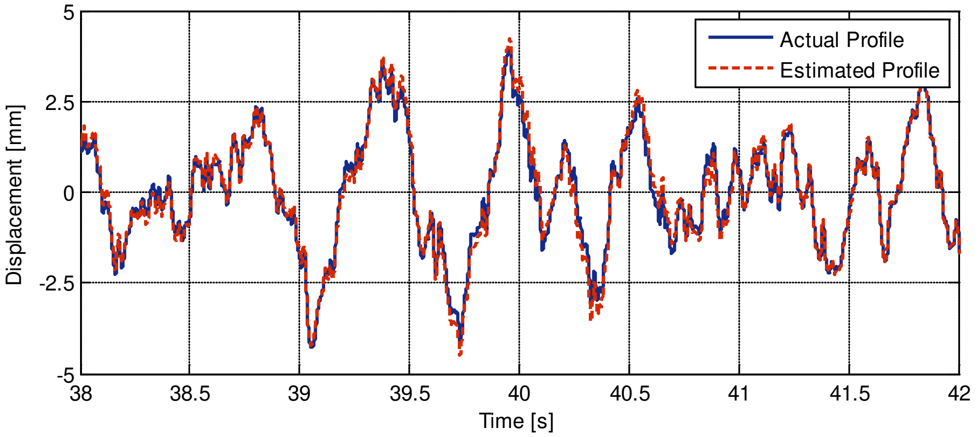

Figure C-8: Sample time history of the actual (blue) and estimated (red) profiles for violet noise excitation at an rms of 1 g.

From the measured displacement profiles, the actual and estimated PSD functions were computed and are presented in *Figure C-9*. The PSD functions of the estimated and actual profiles are quite similar in shape, with only minor variation at the lower and upper frequency bands. The calculated rms values of the spectra are also quite similar, with the estimated profile rms slightly higher than the actual profile rms.

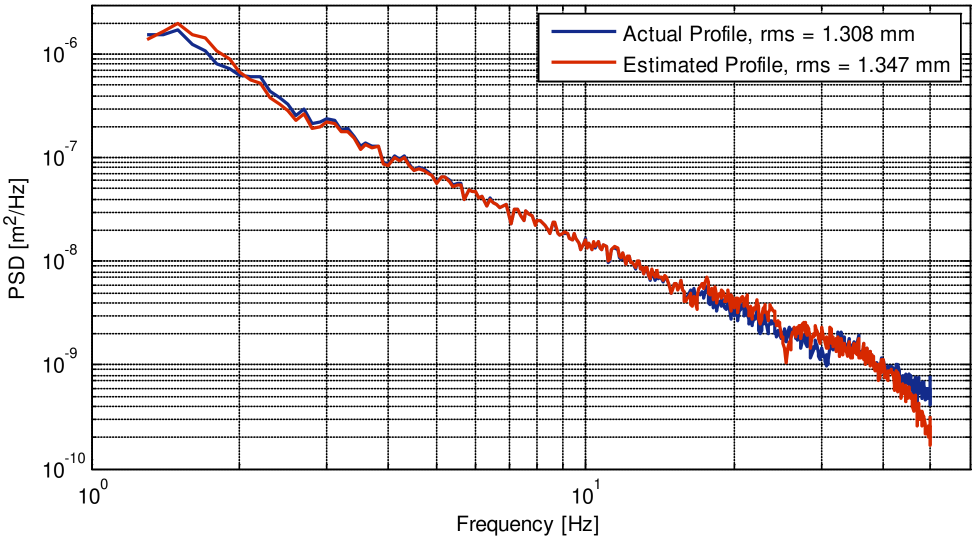

Figure C-9: Estimated PSD functions of the actual (blue) and estimated (red) profiles for violet noise excitation at an rms of 1 g.

The time history and PDF of the error of the estimated profile are shown in *Figure C-10* and it is observed that the error of the estimated profile during the test (violet noise 1 g rms) never exceeds 0.70 mm.

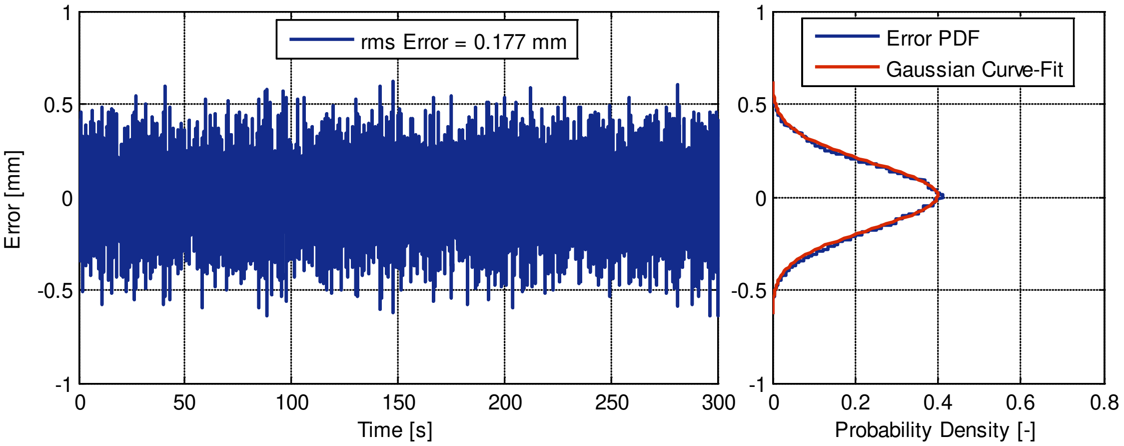

Figure C-10: Time history (left) and PDF (right) of the displacement error of the estimated profile from the violet noise excitation at an rms of 1 g.

Next, the results for the violet noise excitation at an rms level of 2 g are presented. A sample time history of the measured actual and estimated profiles is presented in *Figure C-11*. From the time history, there is little observable difference between the actual and estimated elevation profiles. The elevation PSD functions were computed for both the actual and estimated profiles and are presented in *Figure C-12*.

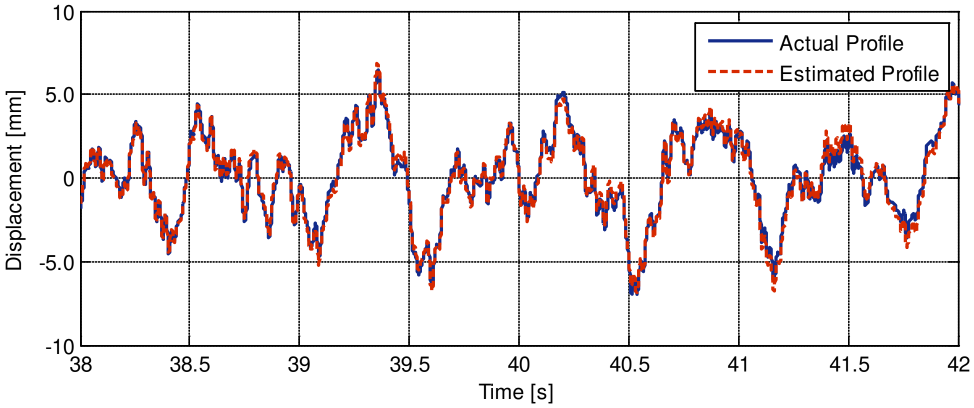

Figure C-11: Sample time history of the actual (blue) and estimated (red) profiles for violet noise excitation at an rms of 2 g.

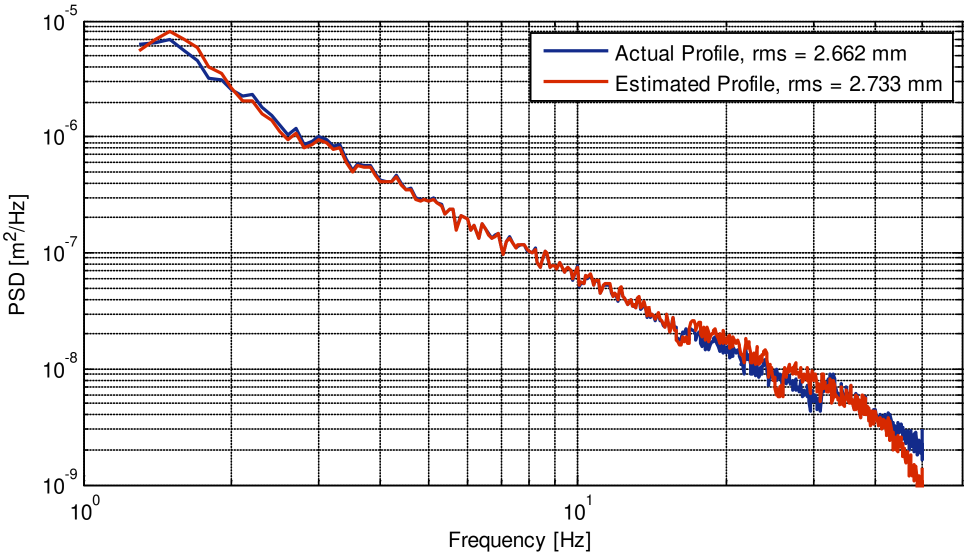

Figure C-12: Estimated PSD functions of the actual (blue) and estimated (red) profiles for violet noise excitation at an rms of 2 g.

The error between the actual and estimated profiles was calculated and a time history of the error, along with the error PDF, is presented in *Figure C-13*. In comparison to the 1 g rms excitation, the rms error of the estimated profile from the 2 g rms excitation is slightly greater.

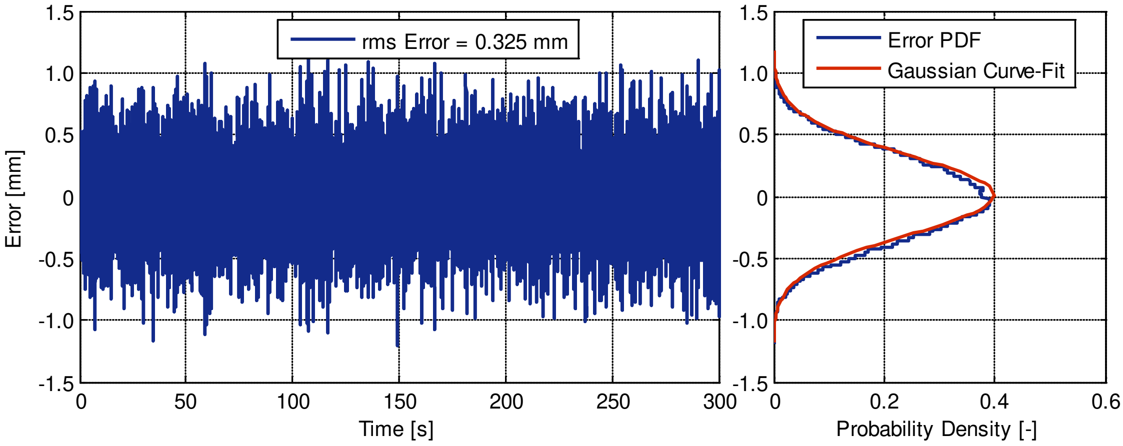

Figure C-13: Time history (left) and PDF (right) of the displacement error of the estimated profile from the violet noise excitation at an rms of 2 g.

To evaluate the performance of the profilometer, the transfer function (or gain) of the profilometer was established using the actual and estimated profiles. The established transfer functions of the SWEV profilometer from both violet noise excitations are presented in *Figure C-14*. From the figure, the transfer function of the profilometer is not completely flat (as would be expected for an ideal profilometer system). *Table C-B* presents a comparison of the error of the profilometer gain and rms error from both violet noise acceleration excitations. The gain error is considerably small across the frequency range (less than 1 % for both excitation intensities) and indicates that the SWEV can be used as a profilometer to measure the longitudinal pavement elevation profile.

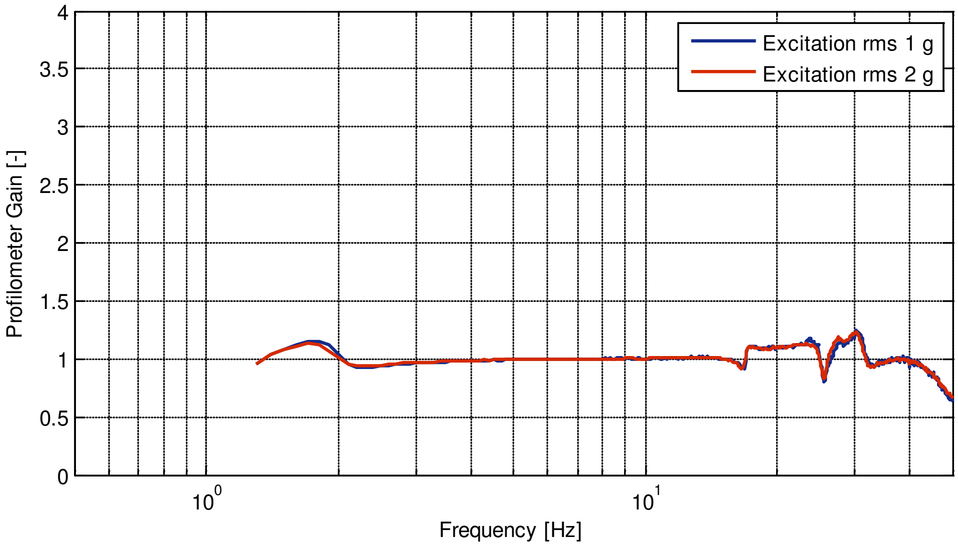

Figure C-14: The gain of the SWEV profilometer from the violet noise excitation at two rms intensities.

Table C-B: The rms error and gain error of the SWEV profilometer from the violet noise excitations.

Excitation	rms Error [mm]	Gain Error [%]
Violet Noise rms 1 g	0.177	0.64
Violet Noise rms 2 g	0.325	0.37

C.3.3 Wheel Encoder Calibration

The last component that requires calibration is the wheel encoder. The encoder wheel is made up of 144 strips (72 clear and 72 reflective strips at 2.5° per strip) and pulses are measured only across the reflective strips. As a preliminary test, the wheel was rotated manually and the encoder was able to identify the pulses. Prior to undertaking the test, the vehicle must be driven for a reasonable amount of time to allow the temperature of the tyre to warm up and stabilise. The tyre, prior to all experiments, was pumped to 32 psi. To determine the cumulative distance of each reflective strip along the wheel encoder, the dynamic radius of the tyre must be established.

A distance of 929.03 m (3048 ft) was measured along a remote road with little to no traffic and small wooden planks were positioned at the beginning and end of the section. The profilometer system was towed along the road at a speed of 60 km/h while simultaneously recording the laser displacement and the wheel encoder pulses. The last displacement sensor was able to identify the planks of the wood and the corresponding times were used to compute the number of pulses recorded by the encoder. The dynamic radius of the tyre was calculated to be 293.40 mm. From the dynamic radius (and the number of pulses in one revolution of the tyre), the distance between each pulse is calculated to be 25.60 mm.